A NUMERICAL MODELLING AND OBSERVATIONAL EFFORT TO DEVELOP THE CAPABILITY TO PREDICT THE CURRENTS IN THE GULF OF MEXICO FOR USE IN POLLUTANT TRAJECTORY COMPUTATION

A FINAL REPORT SUBMITTED TO
THE BUREAU OF LAND MANAGEMENT
UNDER
BLM INTERAGENCY AGREEMENT 08550-IA5-26

MODEL STUDIES OF THE CIRCULATION IN THE GULF OF MEXICO

May 1976

Robert L. Molinari
David W. Behringer
John F. Festa

National Oceanic and Atmospheric Administration
Atlantic Oceanographic and Meteorological Laboratories
Miami, Florida

A NUMERICAL MODELLING AND OBSERVATIONAL EFFORT TO DEVELOP THE CAPABILITY TO PREDICT THE CURRENTS IN THE GULF OF MEXICO FOR USE IN POLLUTANT TRAJECTORY COMPUTATION

A FINAL REPORT SUBMITTED TO
THE BUREAU OF LAND MANAGEMENT
UNDER
BLM INTERAGENCY AGREEMENT 08550-IA5-26

MODEL STUDIES OF THE CIRCULATION IN THE GULF OF MEXICO

May 1976

Robert L. Molinari
David W. Behringer
John F. Festa

National Oceanic and Atmospheric Administration
Atlantic Oceanographic and Meteorological Laboratories
Miami, Florida

EXECUTIVE SUMMARY

The Atlantic Oceanographic and Meteorological Laboratories of the National Oceanic and Atmospheric Administration have completed the first year of a proposed two-year study for the Bureau of Land Management "to develop the capability to predict the currents in the Gulf of Mexico for use in pollutant trajectory computation". The objectives of the study were:

(1) to modify an existing numerical model for application in the Gulf of Mexico;

(2) to evaluate the ability of the model to simulate the Gulf circulation using various types and distributions of data as input information; and

(3) to describe the Gulf of Mexico circulation using the results of the model.

The formulation of the numerical model and the modifications made are given in the portion of this report entitled "A Guide to a General Circulation Model of the Gulf of Mexico". The data used by the model as interior and boundary conditions were obtained from the National Oceanographic Data Center, and from cruises conducted as part of the present study. The manipulations used to put the data into a form suitable for input to the model are described in the section called "Model Studies of the Circulation in the Gulf of Mexico".

The ability of the numerical model to simulate the observed circulation is demonstrated through a series of comparisons of its solutions with solutions from a geostrophic model. These comparisons are made over a wide range of input and boundary conditions. Therefore, the use of the numerical model results to describe the currents of the region is justified.

The circulation of the Gulf of Mexico at monthly increments is simulated by both models. The solutions are consistent with the results of previous investigations in regard to such large-scale features as the Loop Current, and a gyre in the western Gulf. In addition, the temporal variability of circulation features on the west Florida, MAFLA, and Texas-Louisiana Shelfs are described in detail for the first time.

The results of the monthly increment experiments suggest that significant interactions may occur between the sub-regions of the Gulf. The study of these interactions through the use of the model in a prognostic mode is planned for the second year of the program. The effect of the wind field, and other motion-inducing factors on the circulation will also be evaluated. In addition, the ability of the numerical model to perform in a prognostic mode with input of real-time data is to be tested. The refinement of the data handling techniques is a necessary step in order to meet these objectives, and is planned for next year's effort.

TABLE OF CONTENTS

I. INTRODUCTION

This portion of the final report to the Bureau of Land Management, under BLM Interagency Agreement 08550-IA5-26 with the Environmental Research Laboratories of NOAA, presents the results of "Model Studies of the Circulation in the Gulf of Mexico". The format of this report is as follows.

First, a review of the literature on the subject is presented to set the framework for the following discussions. The review will show that most of the experiments to date have been descriptive studies of the eastern Gulf of Mexico. The major current in this region, the Loop Current, has been shown to possess, at least climatologically, an annual cycle. The cycle is characterized by a variable intrusion of the Loop into the Gulf, and eddy separations from this current.

Most investigators have accepted the contention that the flow in the eastern Gulf is driven by the mass transport through the Yucatan Straits. The flow in the western Gulf was assumed to be driven by eddies which detached from the Loop Current and drifted towards the west. However, recent studies of the Gulf circulation suggest that the dynamics of the region are more complex, with local forcing effects, such as wind, as important as the

external forcing functions, such as the mass transport through the Yucatan Straits.

The assumptions used in the geostrophic model, and the applicability of this approach are then considered. The primitive equation model has been described in the accompanying Guide. However, the limitations of that model will be outlined here also.

The geostrophic and primitive equation models are limited in their ability to reproduce the actual currents by the assumptions used in their derivation. In addition, the quality and quantity of the data available, and the data preparation techniques used are as important as the model assumptions in determining the usefulness of the results. The data preparation methods will be described, as well as the weaknesses of these techniques.

The circulation patterns are presented next. Both models were used to calculate currents from climatological (annual, semi-annual, and monthly) and synoptic (February-March 1962; June- July 1967; August-September 1971; and June 1975) data-sets of temperature and salinity. The results of the two models will be compared,both to describe the circulation and to examine the consistency of the two approaches. In addition drift bottle data available on the MAFLA Shelf have been reanalyzed. These data also will be used for circulation description, and for model verification.

The final section outlines the work to be done during the second year of this program. The inadequacies of the data preparation methods require that more refined techniques than those used in the diagnostic modelling runs be developed to obtain initial and boundary conditions for the prognostic modelling tests. The development of these techniques will necessitate additional work during the second year beyond that initially planned when the original proposal was written.

II. REVIEW OF HISTORICAL LITERATURE

Historically the distribution of water masses and currents of the Gulf of Mexico has been studied in the context of regional experiments concerned with limited portions of the Gulf. Little consideration has been given to the interaction between regions in these studies. The Yucatan Straits, the deep basin in the eastern Gulf, and the Straits of Florida have been studied intensively because of the strong currents located in these regions. But, the effects of these currents on the circulation of the Florida Shelf or the western Gulf, have received little attention.

The following review of the historical literature will reflect the regional approach established by past investigators. Those studies which attempt to describe the Gulf as one system will be considered in a concluding section.

Usually, the eastern Gulf of Mexico is considered to be the region east of 90°W longitude. The Yucatan Straits and the Straits of Florida both are located in the eastern Gulf. A considerable portion of the eastern basin is continental shelf with depths less than 200m (see Figure 1) The Campeche Bank, Florida Shelf, and Mississippi-Alabama-Florida-(MAFLA)-Louisiana Shelf are wide, and are rimmed by steep escarpments. The De Soto Canyon is located on the MAFLA shelf.

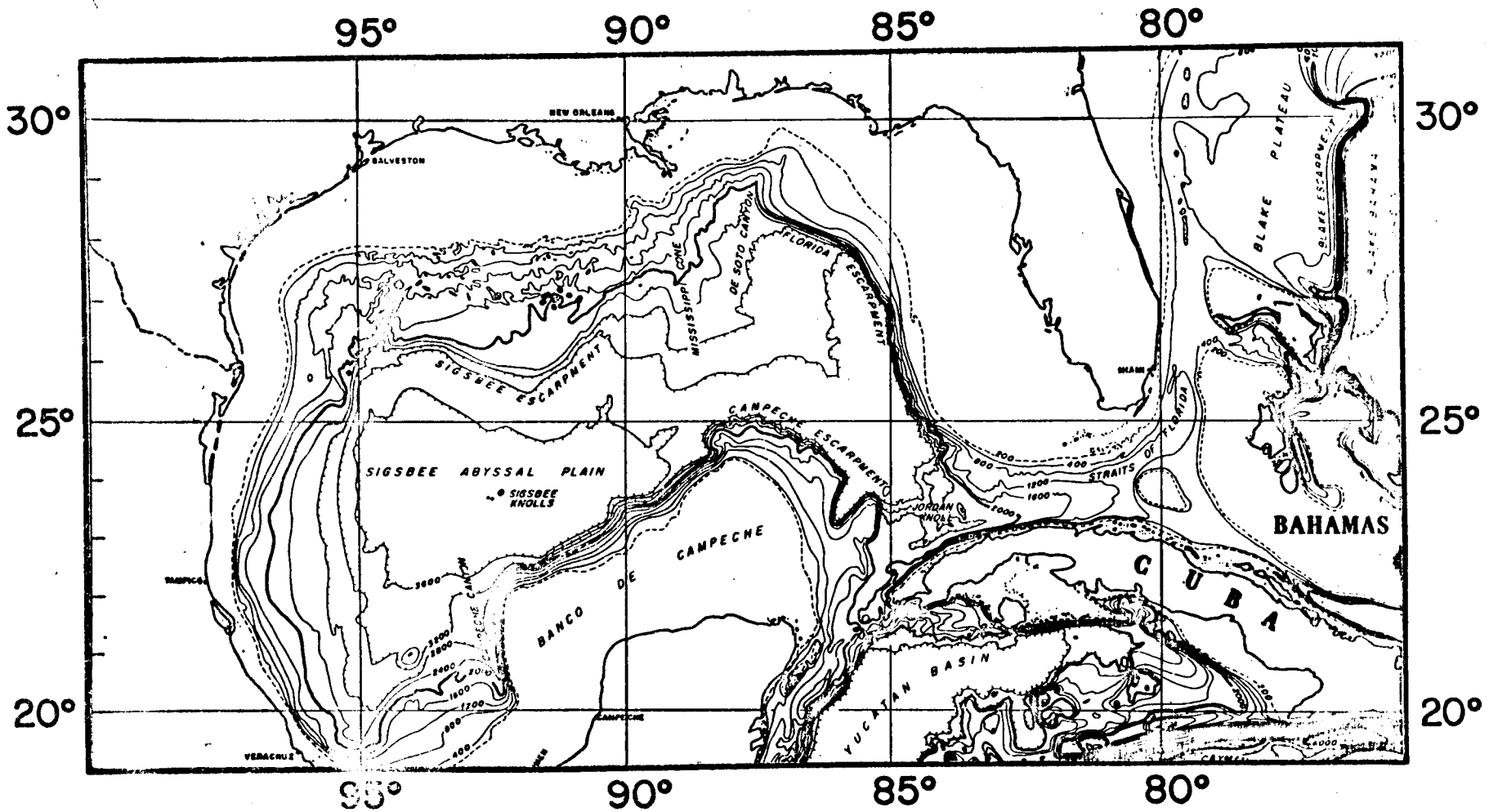

Figure 1. The bottom topography of the Gulf of Mexico as given by Uchupi (1971). Depths are in meters.

The Sigsbee Abyssal Plain, the deepest portion of the Gulf, is found in the western Gulf. Wide shelves are found off the coasts of Texas and the western Yucatan Peninsula, while a narrower shelf extends off the east coast of Mexico. The Bay of Campeche is separated from the eastern Gulf of Mexico by the Yucatan Peninsula.

The major currents of the Gulf of Mexico are shown in Figure 2. The surface geostrophic currents computed from 1^{o} squares, annual averages of dynamic height are calculated relative to 1000 db. The Yucatan Current (denoted by the letters YC on Figure 2) enters the eastern Gulf through the Yucatan Straits and follows the Campeche Bank until it separates at about 24^{o}N. North of the Bank in the central basin, the flow is called the Loop Current (LC). The current along the western edge of the Florida Shelf has been called the West Florida Current (WFC) by Cochrane (1972). Finally, the Florida Current (FC) transports mass out of the Gulf through the Straits of Florida.

Recently, Sturges and Blaha (1976) have proposed that the flow along the central east coast of Mexico be called the Mexican Current (MC). No other currents in the western Gulf have been named, although there is evidence of additional permanent circulation features. The anticyclonic (clockwise circulation) eddy centered at approximately 23.5^{o}N, and 96^{o}W, and a cyclonic (counterclockwise circulation) gyre in the Bay of Campeche are two examples of such features (Nowlin, 1972).

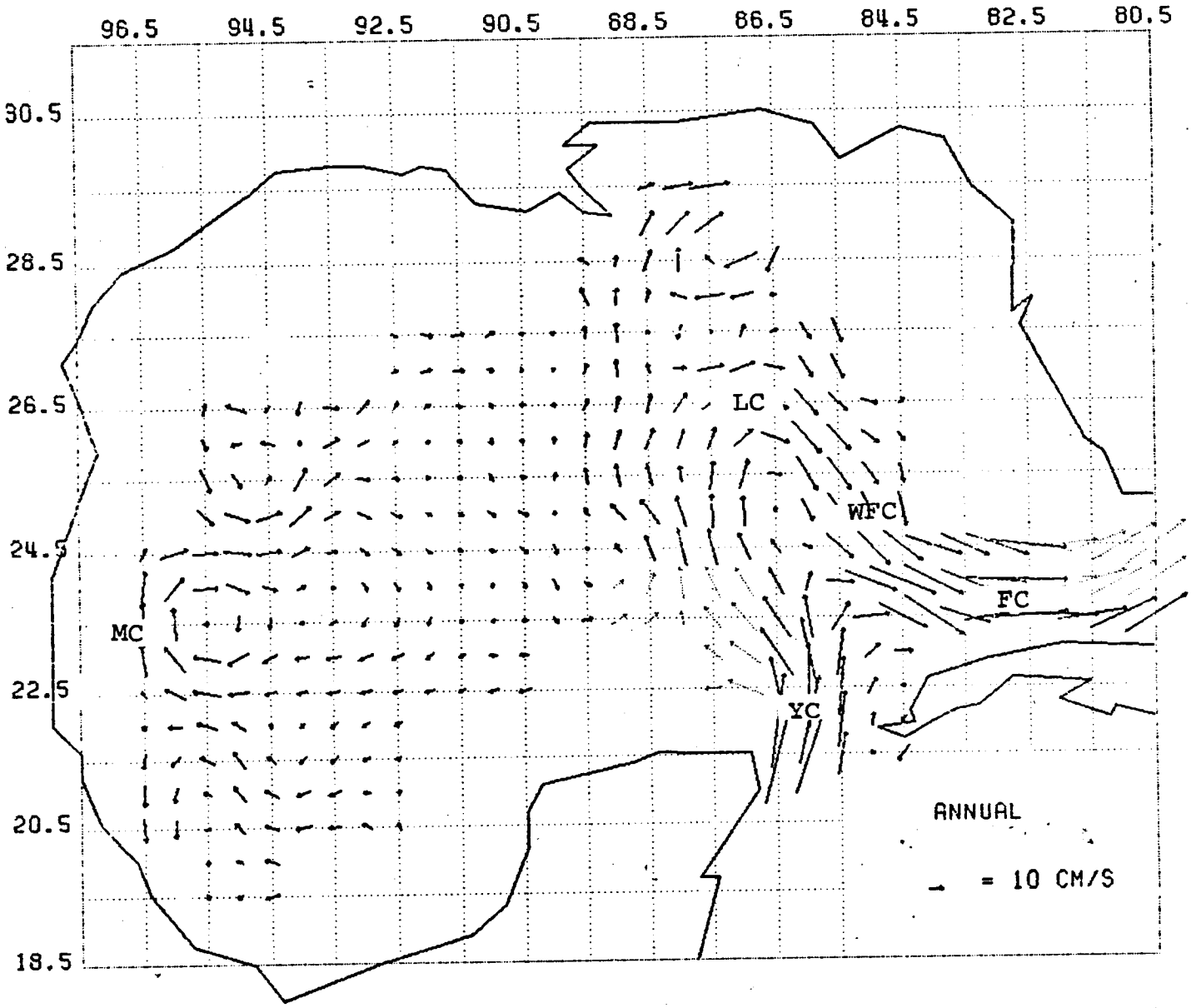

Figure 2. Geostrophic surface currents of the Gulf of Mexico computed from 1° square, annual dynamic height averages computed relative to 1000 db. The data have been interpolated to a 1/2° square grid. The abbreviations given on the figure represent the following currents: YC - the Yucatan Current; LC - the Loop Current; WFC - the west Florida Shelf Current; FC - the Florida Current; and MC - the Mexican Current. Lighter arrows indicate speeds computed from interpolated data.

The distribution of water masses in the Gulf of Mexico is a function of the distribution of currents. Therefore, in the following sections both water masses and circulation will be discussed. To illustrate the findings of some investigators, figures showing the distribution of the depth of the 20°C isotherm will be used. These figures are from a report submitted to BLM under BLM Contract No. 08550-CT4-15 administered by the State University System of Florida Institute of Oceanography (SUSIO , 1975).

1) Yucatan Straits

Cochrane (1963, 1966, 1967, 1968, 1969) has reported extensively on the Yucatan Current. He suggested an annual cycle for the intensity of the flow through the Straits. The surface currents appear to be strongest in May and June, and weakest in November. A sharp drop in current speeds occurs in September and October on the climatological current charts he considered. These charts are deduced from ship drift reports. When the current is strong it may be topographically steered, in the sense that the current axis is constrained to flow along a constant isobath (Molinari and Cochrane, 1972). This steering has not been observed when the current is weakest.

Recent observations suggest that beneath the northward flowing surface current there is a southward flow out

of the Gulf. The progressive vector diagram in Figure 3 is based on the record from a current meter placed at the bottom of the Yucatan Straits (Hansen,1972). This record clearly shows a net flow to the south. Schlitz (1973) noted that the geostrophic flow below 700 m (computed relative to a level near the bottom) was directed out of the Gulf in April 1970. Molinari and Yager (1976) observed a similar result in May 1972 for geostrophic flows computed relative to directly measured surface currents.

There are only a few reported transport measurements through the Straits. Schlitz (1973) found an average geostrophic volume transport of $30 \times 10^6 m^3/sec$, relative to the ocean bottom for three April 1970 transects. Molinari and Yager (1976) found the geostrophic transport above 700 db, referenced to directly measured surface currents, to be 25×10^6 m^3/sec.

The water masses at the Yucatan Strait were identified by Wust (1964). The average T-S relation for the Straits, shown in Figure 4, was obtained from historical data on file at NODC. The T-S relation was calculated by averaging all salinity values for a particular temperature range, regardless of position within the Straits. Beneath the surface waters is found the Subtropical Underwater (SUW) which is characterized by an average salinity maximum of approximately 36.63 $^{o}/oo$ at 22.5^{o}C. The straight line

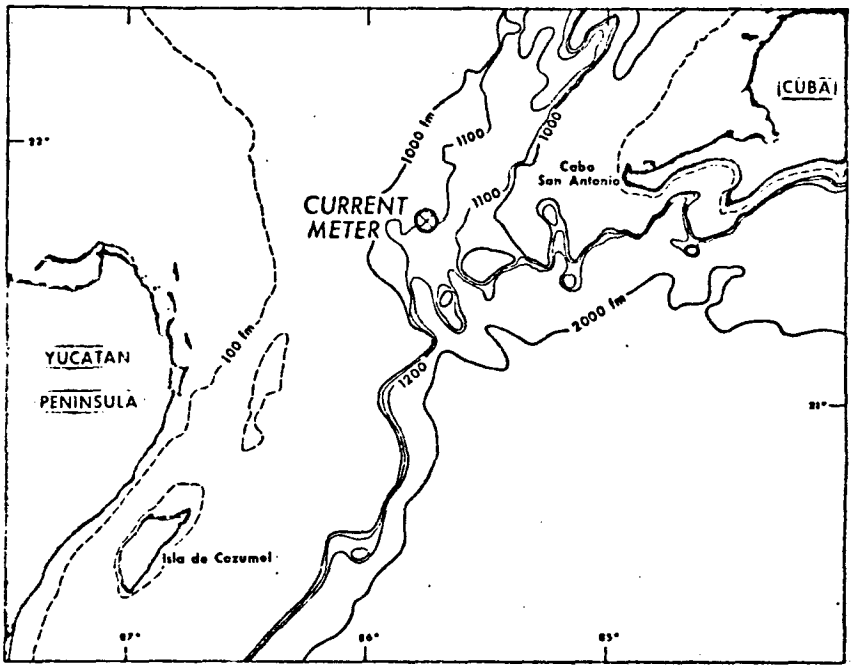

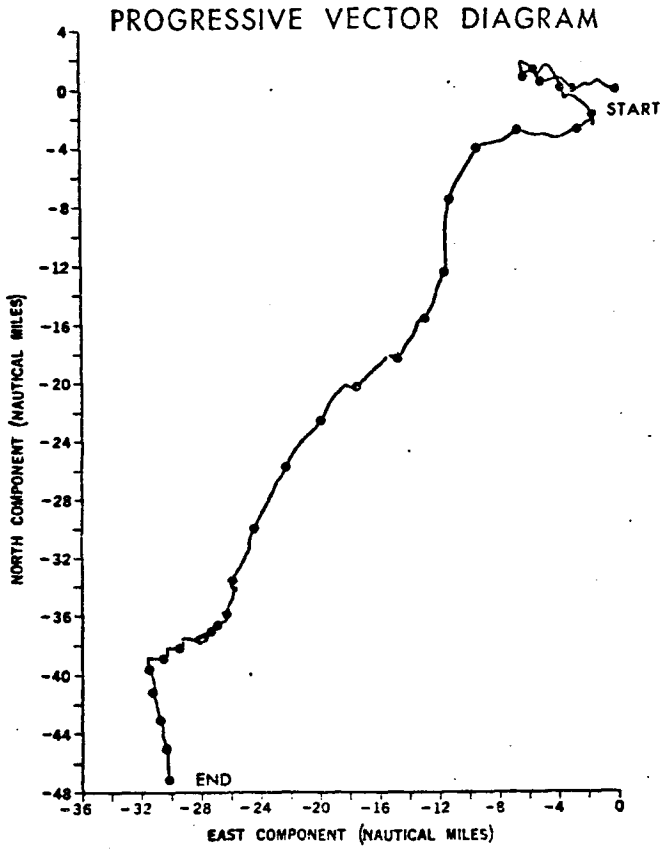

Figure 3. Upper panel. The location of a current meter planted in the Yucatan Straits in October 1970. Lower panel. A progressive vector diagram computed from the current meter record. The dots on the curve represent daily increments.

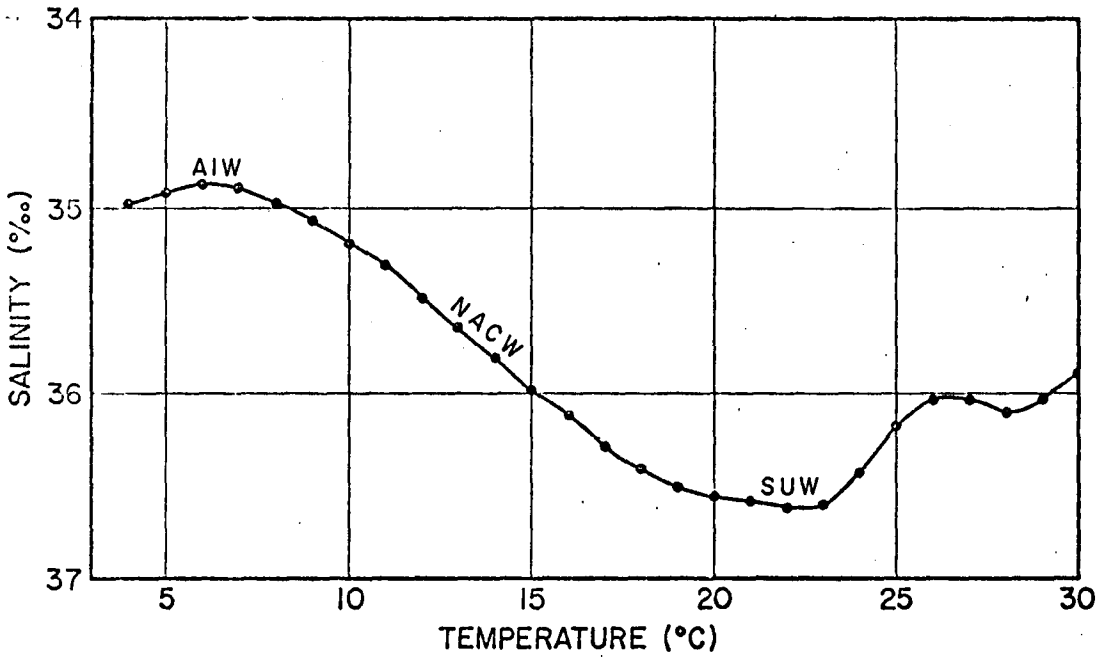

Figure 4. The average T-S relation computed from a historical data-set collected at the Yucatan Straits. All salinity values within a 1°C temperature range are averaged to obtain a mean salinity for the temperature at the center of the interval. The water masses noted on the figure are SUW, Subtropical Underwater; NACW, North Atlantic Central Water, and AIW, Antarctic Intermediate Water.

portion of the curve between approximately 10°C and 17°C is North Atlantic Central Water (NACW). Although found over a large temperature range, this water normally is limited to layers some 200 to 300 m thick. The salinity minimum at 6°C (34.86 °/oo) is a remnant of the Antarctic Intermediate Water (AIW) formed at the Antarctic Convergence Zone. The higher salinity waters with temperatures lower than 5°C could be remnants of Mediterranean or North Atlantic Deep Water (Ichiye and Sudo, 1971).

2) Central Eastern Gulf of Mexico

The northern extension of the Yucatan Current has been named the Loop Current, because of its loop-like path over the eastern Gulf basin. Leipper's (1970) description of a sequence of current patterns in the eastern Gulf is the basis for the hypothesis of an annual cycle for the intrusion of the Loop Current. Leipper characterized the Loop Current cycle by a spring intrusion of the current northward into the Gulf, and a fall spreading of the current toward the west.

A map of the distribution of the depth of the 20°C isotherm during 1965 and 1966, years considered by Leipper in his analysis, is presented in Figure 5. (Leipper used the depth of the 22°C isotherm to portray surface features, but as noted in SUSIO (1975) the 20°C topography also correlates well with the patterns of circulation.) The spring intrusion is observed from December 1965 to August 1966 as the maximum slope in the 20°C surface

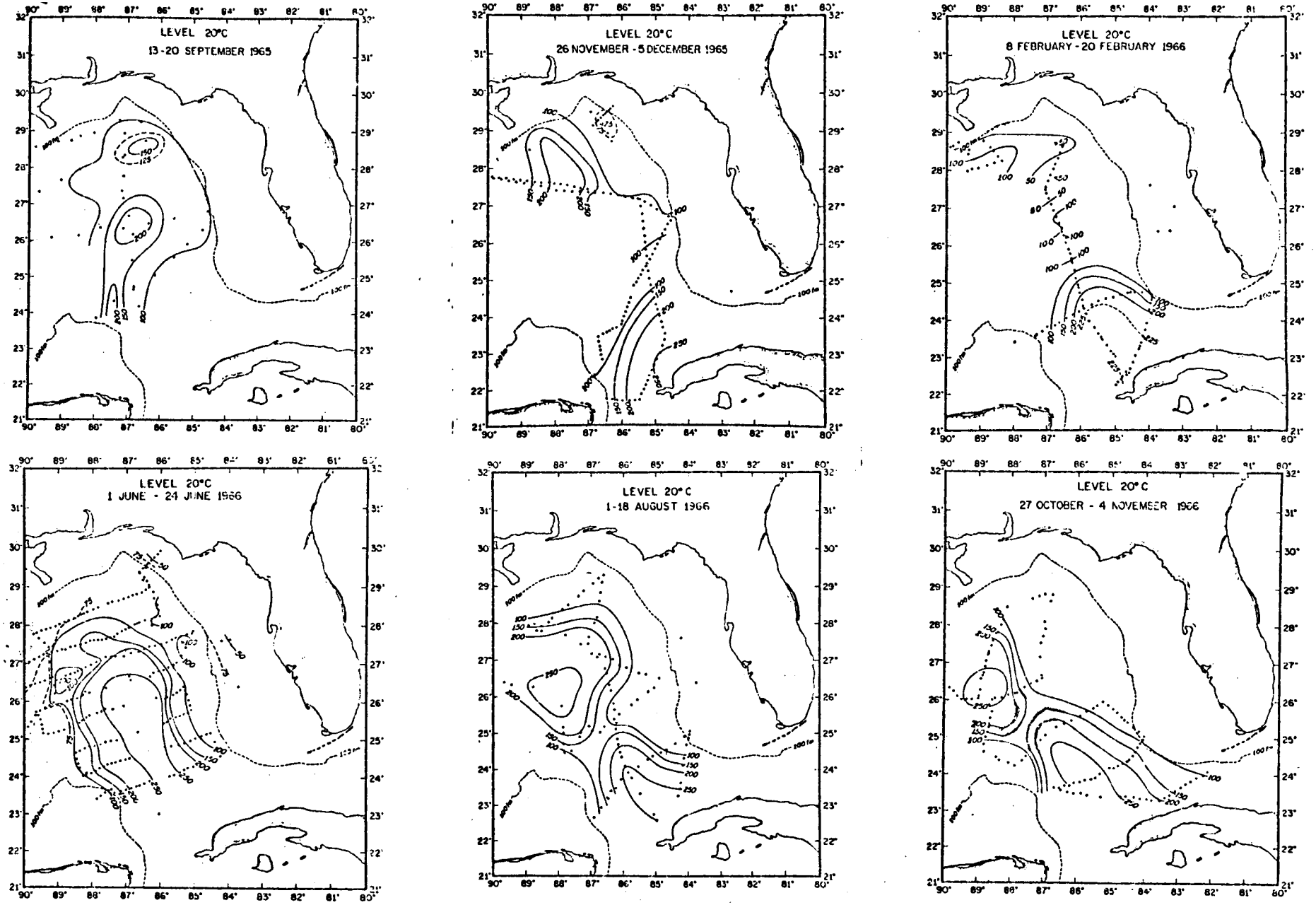

Figure 5. A portion of the data-set considered by Leipper (1970) to demonstrate the intrusion of the Loop Current during 1965-1966. The 150 m isopleth of the 20°C topography coincides closely with both the core of the Loop Current, and the detached eddies (SUSIO, 1975).

moves northward. Leipper found that the greatest rate of intrusion, 150 km/month, occured in late winter and early spring. The fall spreading is observed in August and October-November 1966 as the eddy-Loop system shifts toward the west.

Whitaker (1971), using monthly climatological temperature data averaged over one-degree squares, found that the 150 m isopleth of the 22° C surface progresses north into the Gulf from January to June, and recedes south from August to December. This cycle is evident in the climatological temperature data presented by Robinson (1973). Maul (1975) obtained a fourteen month time history of the Loop Current from August 1972 to September 1973. His results are summarized in Figure 6 which shows the 150 m isopleth of the 20° surface for the months surveyed. The spring intrusion, as defined by Leipper, occurred from December 1972 to July 1973. The fall spreading is not evident in this data-set. The year-to-year variability in the position of the Loop is apparent in the comparison between the August isopleth for 1972 and 1973.

The greatest variability in the surface circulation appears to occur in the summer; however, this may be a result of the large number of Gulf cruises that occurred during this season. A dramatic example of two different summer patterns is given by Nowlin and Hubertz (1972). In June 1966 a well developed Loop extended far into the Gulf (Figure 5), but in June 1967 an eddy had separated

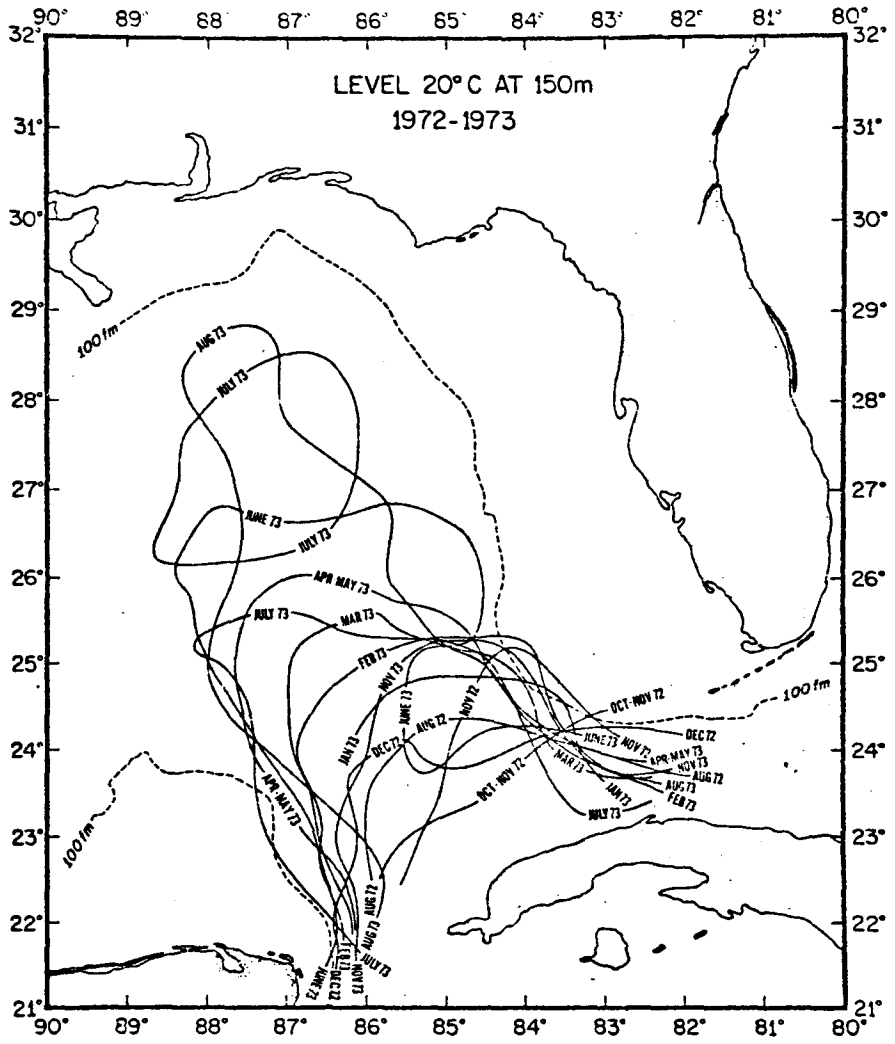

Figure 6. The 1972 - 1973 positions of the 150 m isopleth of the 20°C topography as observed by Maul (1975).

from the main flow, and the Loop Current extended to only 26.5°N (Figure 7).

Cochrane (1972) documented an eddy separation event which occurred in May 1969. He shows that the separation apparently takes place when a meander,formed on the west Florida Shelf,joins with a meander on the Campeche Bank to form a ridge between the main flow and the eddy. Figure 8 demonstrates the evolution of the ridge between the two circulation features. Cochrane (1972) noted that separation also occurred in June 1967, and August 1965 near the shortest distance between the 100 fm isobaths of the Florida and Campeche Banks. Additional eddy separations were observed in November 1970, July-August 1971, May 1972, and July 1973 (Maul, 1975). Leipper, Cochrane,and Hewitt (1972) described a bisection of the August 1965 eddy after the passage of a hurricane through the region.

Direct surface current measurements have been made in the central Gulf using the Geomagnetic Electrokinetograph (GEK), and surface drifters. The maximum GEK speeds given by Nowlin and Hubertz (1972) for the Loop Current are about 175 cm/sec, and for the detached eddy 125 cm/sec. Speeds greater than 50 cm/sec exist in a band approximately 80 km wide in the Loop Current, and 50 km wide in the detached eddy.

Chew (1974) in a theoretical and observational study of turning currents found that surface speeds are reduced

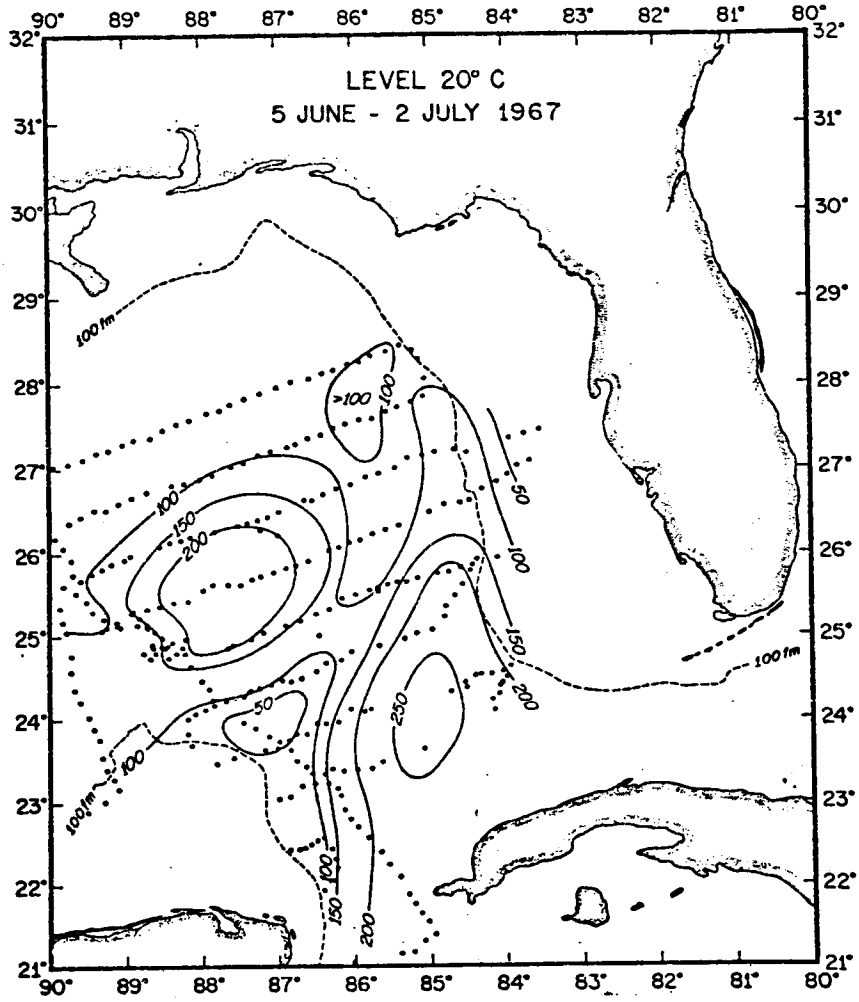

Figure 7. The 20°C topography as determined from data collected in June 1967, and used by Nowlin and Hubertz (1972) to contrast different summer circulation patterns, i.e. June, 1966, Figure 5 and June 1967.

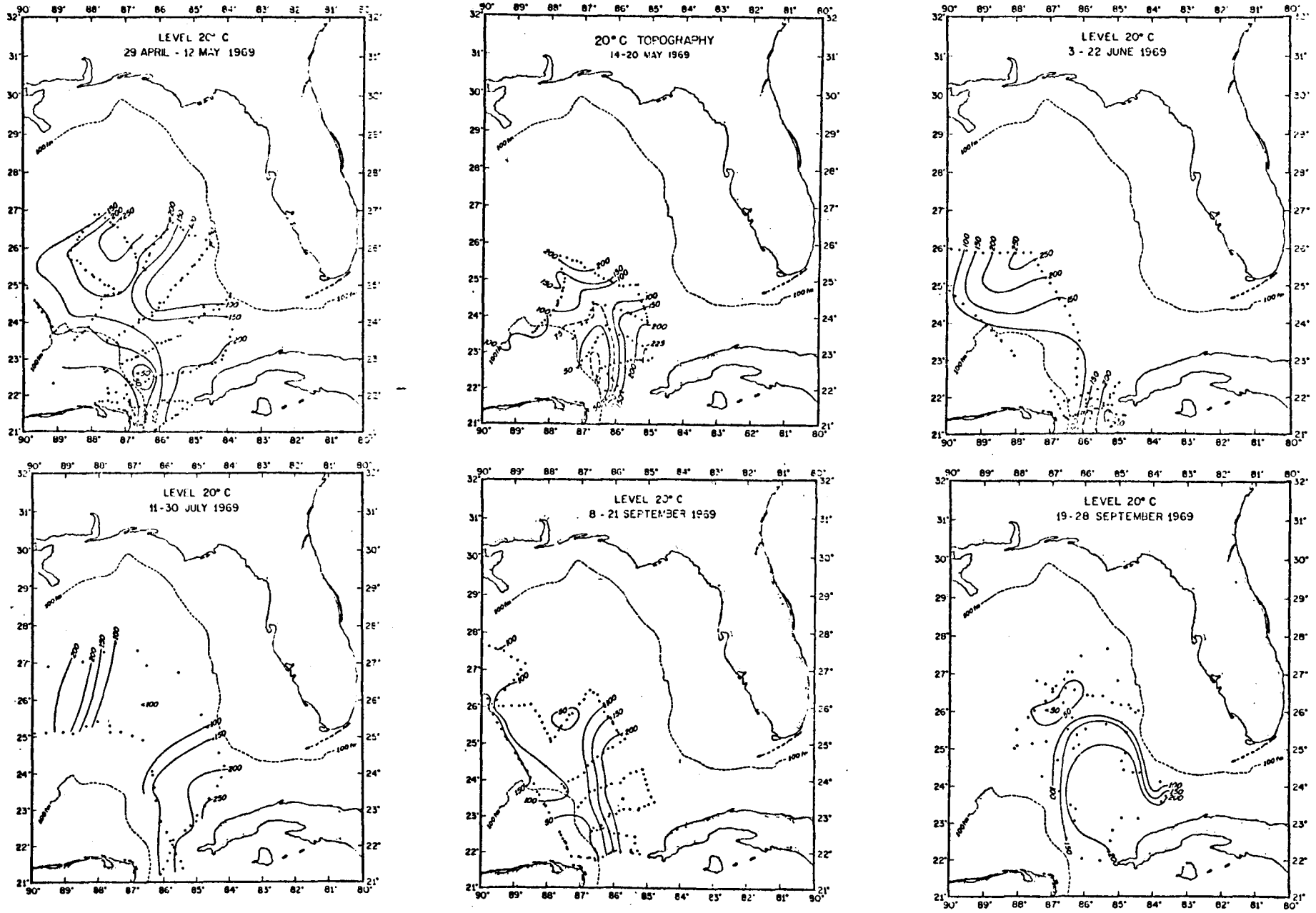

Figure 8. The 20°C topography obtained in 1969, and used by Cochrane (1972) to document an eddy separation event, and subsequent westward drift of the feature.

considerably at the apex of an anticyclonic turn. Surface drifter data obtained in October-November 1970 in the current core (Figure 9) indicate a decrease in buoy speed from 200 cm/sec to 130 cm/sec as a buoy approached the apex of the Loop. Kirwan, McNally, Chang, and Molinari (1975) noted a similar deceleration based on drifter data obtained in June 1973.

Nowlin and Hubertz (1972) computed the Loop Current and detached eddy transports above 1350 m for June 1966 and June 1967. Both systems contain recirculating water; the Loop Current transports exceed 40×10^6 m^3/sec, and the eddy 30×10^6 m^3/sec.

Nowlin and McLellan (1967), and Nowlin (1972) reported on the winter circulation in the eastern Gulf. Nowlin (1972) computed dynamic height topographies relative to 1000 db for January to April 1932, February to April 1935, and February to March 1962. The three topographies are very similar in the eastern Gulf, with the core of the Loop Current extending to approximately 26°N. SUSIO (1975) presented additional data which suggest that the penetration of the Loop Current does not exceed 26°N (Figure 10).

The maximum surface speeds in the central basin, as measured by GEK's, were approximately 150 cm/sec in February and March of 1962 (Nowlin 1972). Little organized geostrophic motion existed between 1500 db and 2000 db over the deep basin, and most flows between 1000 db

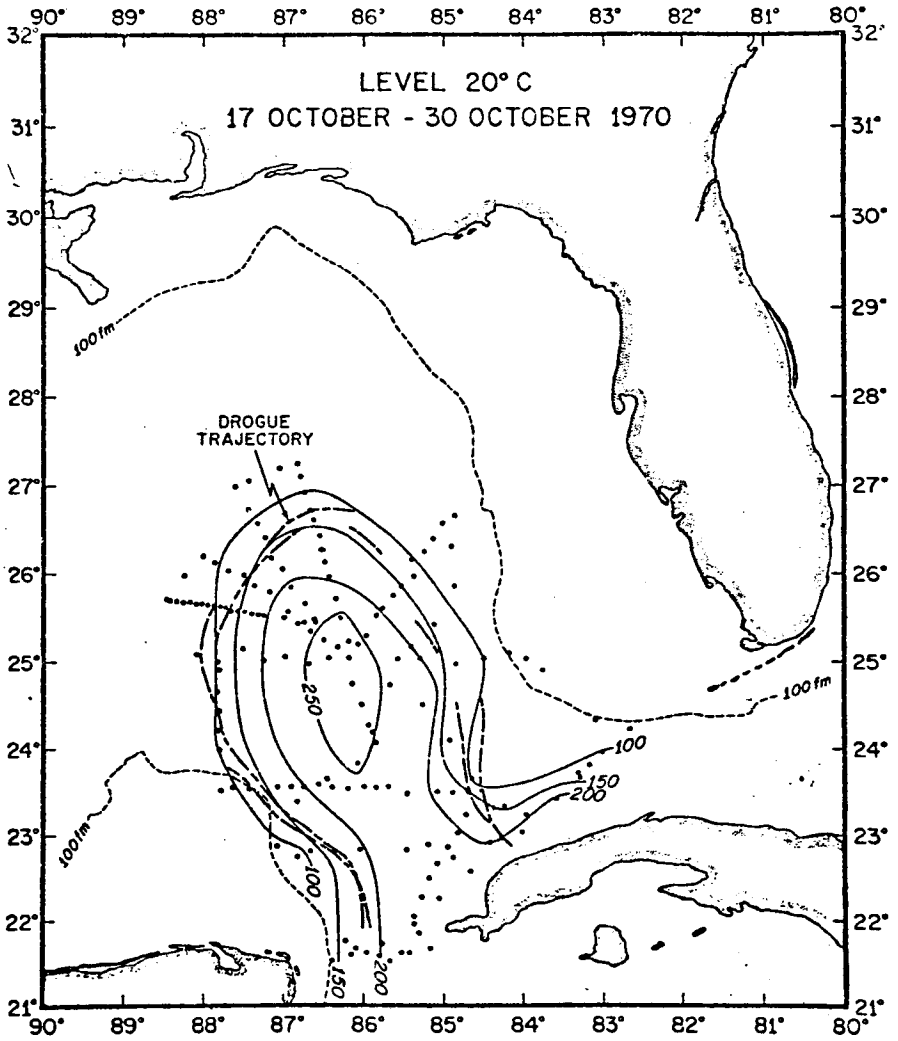

Figure 9. The 20°C topography observed during October 1970. Superimposed on the topography are surface drifter trajectories used by Chew (1974) to describe turning currents.

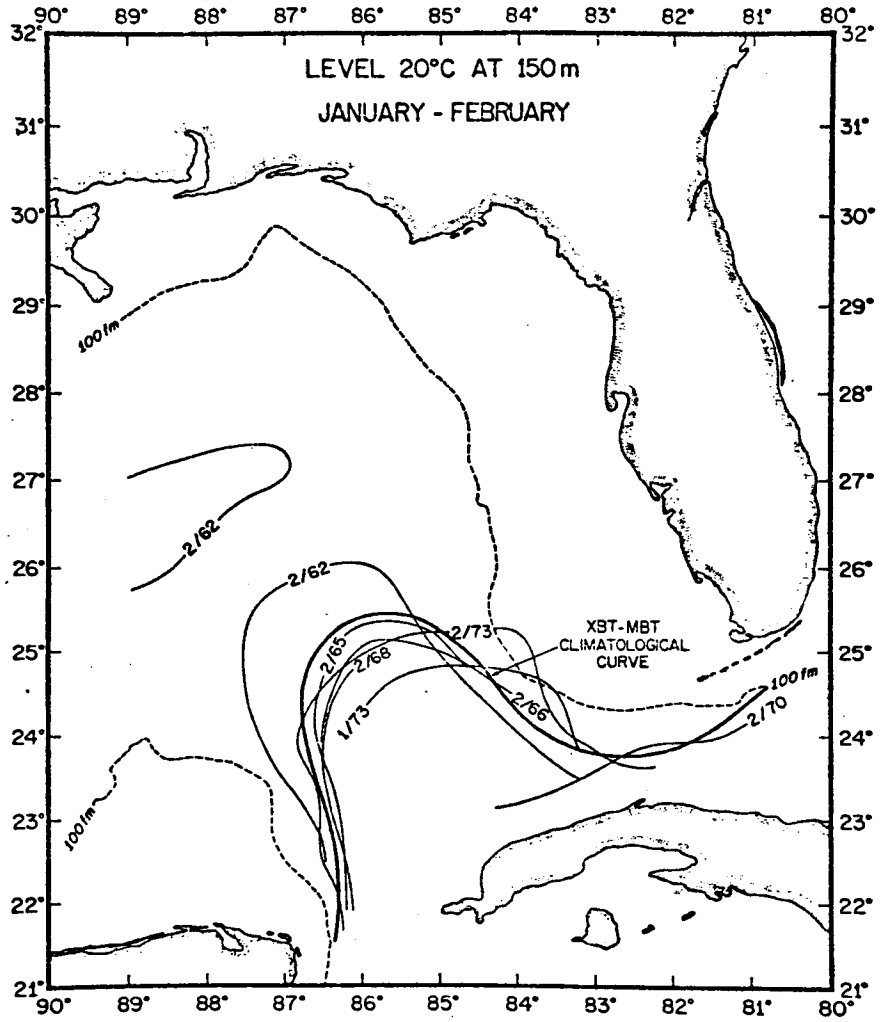

Figure 10. The penetration of the 150 m isopleth of the 20° surface (an indicator of the current core) observed during the months of January and February. The XBT-MBT climatological curve is the mean penetration of the 150 m isopleth determined for these months.

and 1500 db were less than 10 cm/sec. The Loop transport relative to 1000 db was approximately $30 \times 10^6 m^3/sec$.

Many investigators, Wennekens (1959), Grose (1966), Nowlin (1972), Caruthers (1972), for example, have discussed T-S relations for the water masses of the eastern Gulf. The T-S correlation for waters with temperatures less than 17°C exhibits little spatial or temporal variability. The lack of data has hampered the study of the temporal variability of the upper layer T-S relation. However, important spatial variations have been noted.

The T-S relation of the Loop Current waters is identical to the T-S relation observed at the Yucatan Straits indicating the common origin of these waters. However, the maximum salinity of the SUW (Figure 4) is eroded to the left of the current axis looking downstream. This reduction in maximum salinity is frequently used to identify non-Loop waters. For instance, Cochrane (1972) noted that the ridge separating the Loop Current and detached eddy is characterized by these lower salinity values, of the order 36.4 °/oo. Cochrane (1967), and Nowlin (1972) indicated that the erosion of the SUW salinity maximum may be caused by vertical mixing which occurs as the Yucatan Current flows along the Campeche Bank.

3) Straits of Florida

Maul (1975) reported on temperature data which suggest that the position of the Florida Current in the vicinity of

the Marquesas (at 82.1°W in the Straits) is a function of the penetration of the Loop Current. The farther north the Loop is found in the Gulf, the farther south the Florida Current was found at this section.

The surface drifter data given by Chew (1974), collected in the Straits of Florida, in August 1971, show a monotonic acceleration in the Florida Current from 84°W to 82°W . In the vicinity of Key West, the surface speeds approach 200 cm/sec.

Most other studies in the Straits of Florida were conducted further downstream in the vicinity of the Miami-Bimini Island transect, Wunsch, Hansen and Zetler (1969) and Duing (1975). The results of Niiler and Richardson (1973) along this transect bear directly on the present effort. Noting that little water enters the Straits of Florida through the Bahama Channels, they found that the transport out of the Gulf of Mexico has a strong seasonal signal. The mean transport computed from direct velocity measurements is $29.5 \times 10^6 m^3$/sec, and the amplitude of the annual harmonic fitted to the data is $4 \times 10^6 m^3$/sec. The maximum transport occurs in early June. Their results indicate further that the variability for a particular season is as great as the season to season variability.

In a synoptic survey conducted along the Key West-Havana transect, Brooks and Niiler (1975) found the average

transport over a one-month period from the surface to the $27.0\sigma_t$ surface to be $20.2 \times 10^6 m^3/sec$. They also found considerable variability in the transport, $\pm$ $2.3 \times 10^6 m^3/sec$ during this period. The transport through the Yucatan Straits, reported by Molinari and Yager (1976) was obtained concurrently for the same water column and is within 10% of this value.

Wennekens (1959) finds that the water masses of the Straits of Florida are very similar to those of the interior Gulf and Yucatan Straits. He also observes that additional water, with lower salinities than typically found in SUW, has been entrained on the left hand side of the current facing downstream.

4) west Florida Shelf

The hydrology and currents on the west Florida Shelf are affected significantly by its boundaries: the Florida Panhandle to the north, the west coast of Florida to the east, the Florida Keys to the south, the Gulf of Mexico and frequently the Loop Current to the west, and the sea-air interface above.

Although considerable data have been collected on this shelf on such field programs as the Hourglass Study (Florida Department of Natural Resources, 1969), the west Florida Continental Shelf Program (Rinkel, 1974), and the NSF Continental Shelf Dynamics Program (Price and Mooers, 1974 a, b,c, 1975, and Plaisted, Waters, and Niiler, 1975), few scientific results have been reported in the literature.

Jones (1973), in a discussion of drift bottles released during the Hourglass Study, suggested that recovery sites indicate a seasonal circulation pattern. For the region west of the 10-meter and east of the 91-meter isobath, the January, February, and March recoveries indicate a southerly flow. The May, June, July, August, and September recoveries suggest north-northwest flow along 27°35'N, and southerly flow along 26°30'N. The April, October, November, and December recoveries indicate transitional periods with flow both to the north and south observed. In the region shoreward of the 10-meter isobath, the predominant flow was to the north throughout the year. Jones further noted that the observed circulation features are dependent on other factors in addition to the wind stress field.

Mooers and Price (1975) presented some preliminary results on spatial and temporal scales obtained during the NSF Shelf Dynamics Program conducted on the west Florida Shelf. The vertical motions are correlated over 50 m intervals, the alongshore motions over 100 kilometers, and the crossshelf motions over 20 kilometers. The motions are correlated in time for periods of about 5 days. They suggest that these correlations, indicative of slowly varying flow, are directly related to particle displacements in the sense that high frequency motions, such as tides and inertial flows, do not produce large net particle displacements. Their analysis does not permit identification of

the forces which produce these low frequency motions; however, evidence exists suggesting the importance of the Loop Current and atmospheric disturbances as forcing mechanisms.

SUSIO (1975) provides some additional evidence for the importance of the Loop Current to shelf circulation. Vertical sections show isolated cells of high salinity Loop Current water on the Shelf (Figure 11). These features can extend throughout the water column, or may be confined to the bottom layers. They range in size from 60 to 100 km. These eddies transfer momentum as well as water from the Loop Current onto the Shelf. Maul (1975) observed Loop Current eddies approximately 20 km in diameter on the west Florida Shelf.

The meander found off the west Florida Shelf has been discussed in relation to the eddy separation phenomenon (Figure 8). In addition, the meander and the subsequent eddy detachments tend to transport shelf water out into the deep basin (Cochrane, 1972).

5) MAFLA SHELF

Hydrographic and circulation studies on the MAFLA Shelf indicate that the circulation patterns on this shelf are also complicated by wind drift, geostrophic flow,

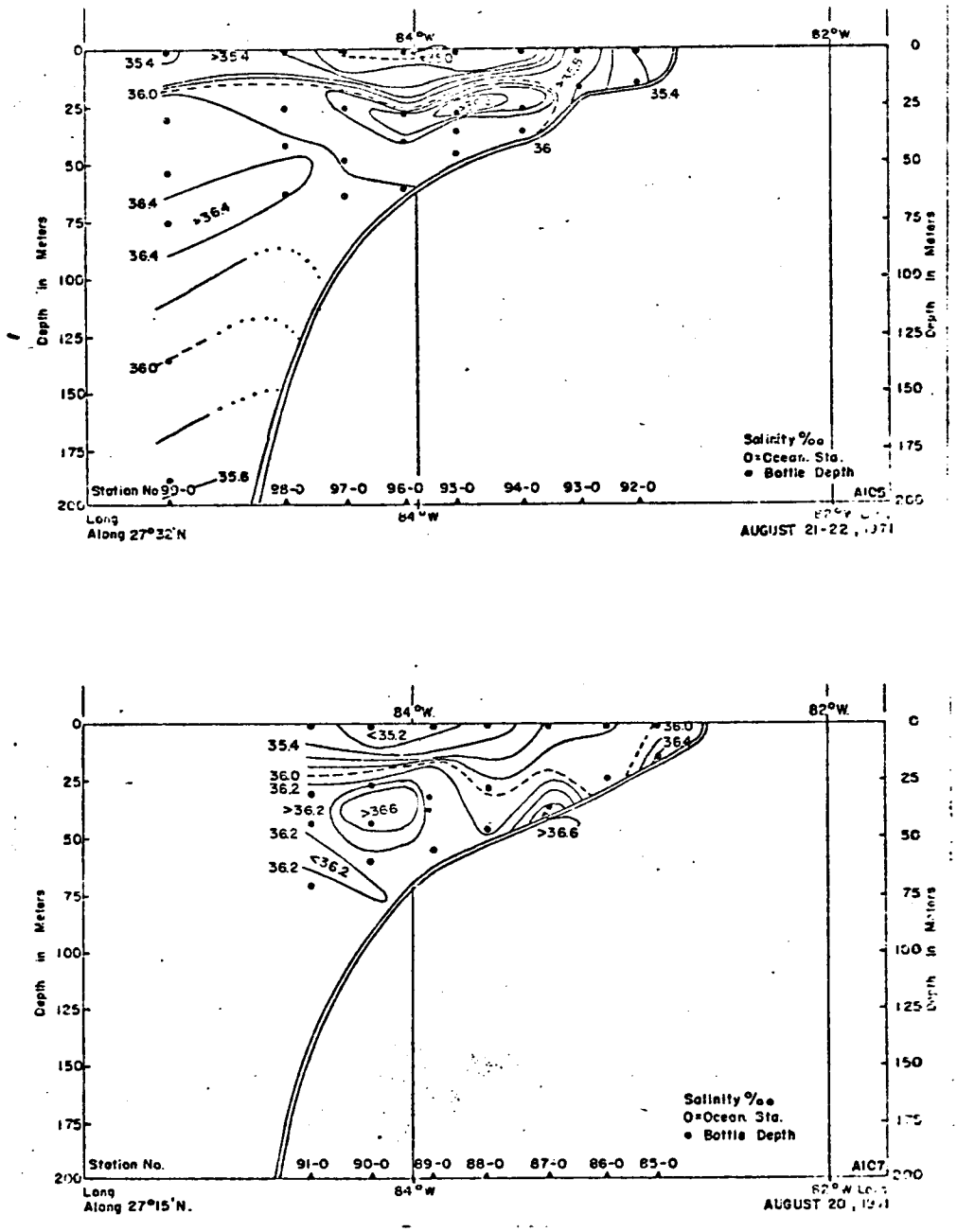

Figure 11. Upper panel. Vertical section of salinity observed during August, 1971 along 27°32'N which shows a mid-level high salinity cell indicative of Loop Current water. Lower panel. Vertical section of salinity observed during August, 1971 along 27°15'N which shows a bottom high salinity cell.

tidal currents, and motions induced by shelf waves and eddies. Drift bottle data given by Gaul (1964, 1965, 1966, 1967); Chew, Drennan, and Demoran (1962): Drennan (1963); and Tolbert and Salsman (1964), have been reanalyzed and will be considered in a subsequent section.

Gaul (1964, 1965, 1966, 1967) and Drennan (1968) considered the hydrographic conditions on this shelf. Mississippi river run-off and Loop Current waters have significant influence on the water mass distribution here. These effects are superimposed on the seasonal variability associated with atmospheric conditions,and therefore,these anomalies can be used to indicate circulation.

In the absence of Loop waters or river run-off, Gaul (1967) shows a smooth transition toward lower salinity values in the SUW as one proceeds north from the Loop Current. SUSIO (1975) presents annual salinity curves for the area off the Mississippi Delta. Salinities in this region depend directly on the phase of Mississippi run-off with lowest salinities occuring in the spring during time of maximum runoff.

Low salinity surface water, originating from the Mississippi River, moved east along the 100 fm curve from April through July 1964 (Drennan, 1968). A lens of low salinity water also has been observed, and tracked to the Straits of Florida in the summer of 1973 (Maul, 1975). Unpublished data collected in the early summer of 1975,

as part of the present BLM effort, show a similar feature.

Eddies with Loop Current water mass properties also have been observed on the MAFLA Shelf. Gaul (1967) and SUSIO (1975) report on these features, which are similar to the eddies found on the west Florida Shelf. The eddies observed by Gaul have a horizontal scale of 100 km and appear to be in geostrophic balance.

Winter conditions on the shelf are characterized by isothermal water columns, with winter extremes observed in February. The summer conditions, as on most shelves, are characterized by a quasi-two-layer system with a strong thermocline. Gaul (1967) noted that extreme summer conditions occur in August. Transitions from summer to winter conditions and vice versa appear to be dependent respectively on the first and last occurance of cold fronts over the shelf. To repeat, these climatological conditions are modulated by intrusions of Loop water or river run-off. In particular, the Loop waters possess temperature characteristics different than those normally found on the shelf.

Gaul (1967) also found evidence for a quasi-permanent anticyclonic circulation feature at the head of the De Soto Canyon, 87.5°W, 28.5°N (Figure 1). This feature has a horizontal scale of 100 km, and a vertical scale of 500 m. The climatological geostrophic velocities given in Figure 2 also show an anticyclonic circulation feature centered at approximately 87.5°W and 28.5°N.

6) Central Gulf Basin

As one procedes west in the Gulf the amount of data available is less. Most data collected in the coastal Gulf from 89°W to 92°W were obtained as investigators were in transit to the eastern Gulf. Thus the distribution of data during most cruises is insufficient to define circulation features.

The climatological charts of Whitaker (1971) show a trough of higher temperature water with a southwesterly trend extending from the eastern to the western Gulf. In April a low temperature ridge begins to penetrate north into the trough from the Campeche Ridge. In August the trough no longer appears as a continuous circulation feature, as the ridge appears to separate the eastern and western Gulf. The trough reappears as a continuous feature in September.

If the flow along the trough were in geostrophic balance, the circulation along the northern side would be to the east, and along the southern side to the west. At 26°N, the annual circulation is to the east between 92.5°W and 90.5°W (Figure 2), but no corresponding westerly flow exists to the south of the trough. Grose (1966) and Nowlin (1972) find indirect evidence for westerly flow along and over the Campeche Bank. However, Rossov (1966) proposed an easterly flow along this Bank.

A 1966 eddy drifted to the west into the central Gulf after separating from the Loop Current. Leipper (1970) called this phenomenon "fall spreading" of the Loop. Nowlin and Hubertz (1972) found remnants of a detached eddy at 92°W during June 1967. The eddy still retained a volume transport of 10×10^6 m^3/sec. A 1969 eddy (Figure 8) moved rapidly to the west during July at 2 to 3 nautical miles per day (Cochrane, 1972). By early September the eddy had moved west of 90°W.

The 1966, 1967, and 1969 eddies were centered at approximately 26°N. However, in 1965 a detached eddy was found considerably farther to the north. Remnants of the anticyclonic eddy which separated in July 1965 were found off the Mississippi Delta as late as February 1966 (Figure 5).

Cochrane (1966, 1967, 1968) reported on the hydrographic conditions over the eastern Campeche Bank. The spring and early summer temperatures and salinities of the shelf are determined by the intensity of the upwelling which occurs during this season. Upwelling occurred during all of Cochrane's May cruises along two branches extending from the northeastern corner of the Yucatan Peninsula. The May and June bottom temperatures over the southeastern Campeche Bank are colder than the winter temperatures, this feature is a possible manifestation of the upwelling. Upwelling was not observed during three years of data collected in October and November. The temperature structure over the Bank in February is

isothermal, a condition similar to that observed on the northern Gulf shelves.

The water mass characteristics of the central basin are very similar to those of the eastern basin. However, the extremes in the T-S relation are reduced due to mixing. The salinity maximum of the SUW and the salinity minimum of the AIW are both eroded as distance from the Loop Current increases. (Nowlin and McLellan, 1967)

The water mass characteristics of the north central Gulf, particularly at the surface, are complicated by the introduction of Mississippi River run-off. River run-off is found to the west as well as to the east of the Delta (Drennan, 1968).

7) Western Gulf of Mexico and Bay of Campeche

Nowlin and McLellan (1967) and Nowlin (1972) proposed a winter circulation pattern for the central western Gulf of Mexico. An anticyclonic gyre is centered at 23.5°N, and 95.5°W (Figure 2). South of the Texas shelf, at approximately 24°N and 25°N, eastward flow existed in February 1962 and February 1964. The maximum velocities measured were 70 cm/sec. The current decelerates and broadens from 95°W to 91°W (also seen in the climatological data of Figure 2).

A broader and weaker flow is found on the southern side of the gyre. This portion of the gyre may be a segment of the Yucatan Current which separates from the main

flow and flows around the Campeche Bank (Nowlin, 1972). There is no indication of a connection between the two systems in Figure 2. Nowlin (1971) further hypothesized that a northward flowing boundary current may exist along the east coast of Mexico.

The climatological temperature distributions of Whitaker (1971) indicate that the western Gulf gyre is strongest in winter, and weakest in the spring. According to Sturges and Blaha (1976) the western Gulf gyre is driven by the wind stress field over the western Gulf, exactly analagous to the forcing of the western Atlantic gyre by the overlying wind field. Furthermore, a western boundary current along the coast of Mexico is necessary to close the circulation, similar to the function of the Gulf Stream. The wind stress data considered by Sturges and Blaha would produce the strongest boundary currents in December, January, and February, with a secondary maximum in June, July, and August. The gyre should have transports of some $6 \times 10^6 m^3/sec$ during these periods. The wind stress forcing function essentially vanishes during the spring and fall.

Rossov (1966) and Nowlin (1972) found evidence for the existence of a cyclonic gyre in the Bay of Campeche. There are indications of such an eddy in the climatological surface velocities given in Figure 2.

The water mass properties for the western Gulf, given by Grose (1966), Nowlin and McLellan (1967), and

Caruthers (1972), show further erosion of the extreme in the T-S relation noted in the central Gulf. Furthermore, the oxygen data collected in winter 1962, suggest a longer residence time in the Gulf for these waters than indicated for the eastern Gulf waters (Nowlin, 1972).

8) Texas Shelf

The circulation and water mass distribution along the south and east Texas shelves appear to be strongly dependent on river run-off from the Mississippi River and on meteorological disturbances. Low salinity waters from the Mississippi and Atchafalaya Rivers can be traced as far south as 26°N in the winter (Nowlin, 1972). The low salinity waters existed in a band some 75-110 km wide in February-March 1962, and January 1966, but were not found in January-February 1964.

A westward flowing counter-current located between the northern arm of the western Gulf gyre and the Texas Shelf has been observed. However, this current is not a permanent winter circulation feature, and its occurence may depend on the existence of low-salinity water on the Texas Shelf (Nowlin, 1972). The countercurrent is not found in the annual circulation pattern shown in Figure 2.

Ichiye and Sudo (1971a) and Nowlin and Parker (1974) reported on the winter water mass characteristics of the Shelf. During cold-air outbreaks water mass formation may

occur on the shelf as the waters located below the core of SUW (see Figure 4) in offshore areas have the same T-S characteristics as waters found on the shelf after an outbreak (Nowlin and Parker, 1974).

9) Abyssal circulation

Pequegnat (1972) presented the only current meter records obtained and analyzed from the deep basin. However, his records are too short to establish meaningful average velocities.

The majority of the information regarding deep currents has been obtained from indirect current measurements. For instance, the deep waters of the Gulf are neutrally stable with no significant horizontal variations in temperature or salinity below 2000 m (McLellan and Nowlin, 1963). However, oxygen and phosphorous data in the western Gulf suggest the west Gulf gyre to be a feature of the deep circulation. Ichiye and Sudo (1971) traced saline deep water located at 1500-1750 m clockwise around the Campeche Slope suggesting advection at these depths. Finally, Betzer and Pilson (1971), studying the nepheloid layer in the Gulf, hypothesized that the distribution of particulate iron indicates stronger bottom currents in the eastern than the western Gulf.

10) Model Studies And Summary

The few studies which consider the Gulf as one system have been either analytical or numerical studies

of the circulation. But, the results of these efforts have been analyzed primarily in relation to the eastern Gulf circulation. The driving mechanism for the circulation in most of these studies has been the mass transport through the Yucatan Straits. Paskausky and Reid (1972), in a barotropic numerical model, and Wert and Reid (1972), in a two-layer model, both varied the cross-stream velocity structure at the Yucatan Straits while keeping the total transport into the Gulf fixed. The effect of the boundary condition is to vary with time the relative vorticity distribution at the input boundary. Similarly Ichiye (1962) and Reid (1972) indicate in analytical studies that the intrusion of the Loop is a function of the earth's rotation, and the relative vorticity at an initial point.

Both numerical studies are able to reproduce an annual cycle of Loop penetration which approximates the cycle suggested by Leipper (1970). As part of the present study, an attempt was made to use the Wert and Reid model to test the effect of various boundary conditions. However, a balance in the conservation of energy equation could not be obtained in the model runs. The validity of Wert and Reid's (1972) results are therefore open to question, as it appears that spurious energy is entering the system. Because of time constraints, work on the two-layer model was stopped before the inconsistency in the energy balance was resolved.

To summarize, although the Gulf in the past has been studied as a series of isolated regions, new data suggest that such a regional approach can not be successful. The penetration of the Loop Current has an effect on the MAFLA and Florida Shelf circulations. Eddies detached from the Loop Current migrate towards the western Gulf bringing water mass and momentum distributions not typically found in this area. Shelf circulations established and maintained by river run-off advect shelf water out into the deep basin. Loop Current water drifts onto one area of the shelf displacing shelf water in another. These phenomena and others have been observed, and their importance stressed. However, to describe fully and to understand eventually these processes, a one-system approach to the Gulf circulation problem must be adopted.

Finally,the importance of the wind distribution to the circulation in the Gulf has not been fully explored. Sturges and Blaha (1976) proposed one of the first hypothesis which attributes movement of waters in the deep basin of the Gulf to the wind field. However, he considers only the circulation in the western Gulf. Most studies of the eastern Gulf have assumed that the circulation here is not significantly affected by the wind. This assumption should be more closely inspected in view of the work of Sturges and Blaha.

III. DESCRIPTION OF THE MODELS

1) Geostrophic Model

The geostrophic approximation is used in physical oceanography to permit computation of ocean currents from measurements of the density field. This "indirect" method of determining currents has provided much of the information presently available on ocean circulation.

The approximation states that the horizontal equations of motion are replaced by the geostrophic balance between the pressure gradient term, and the Coriolis acceleration term. As other accelerations, retarding forces, and driving forces are neglected, the approximation can introduce errors in areas of accelerating flow such as the Straits of Florida or Yucatan Straits, or in areas where bottom friction is important such as on the continental shelves. The errors are a function of the magnitude of the accelerations or the magnitude of the bottom friction.

The geostrophic equations of motion are:

$$-fv + \frac{1}{\rho}\frac{\partial p}{\partial x} = 0, \qquad (1)$$

$$fu + \frac{1}{\rho}\frac{\partial p}{\partial y} = 0, \qquad (2)$$

where (u,v) are the component (x,y) speeds, ρ is the density; $f=2\ \Omega \sin \phi$ is the Coriolis parameter for the earth's angular velocity, Ω, and latitude, ϕ; and p is the pressure.

Following Fomin (1964), it is necessary to assume that the hydrostatic equation is valid in the vertical, and that a level of either zero horizontal velocity or known velocity exists. Equations (1) and (2) now become:

$$-fv + \frac{\partial D}{\partial x} = 0, \qquad (3)$$

$$+fu + \frac{\partial D}{\partial y} = 0. \qquad (4)$$

where the dynamic height, D, of surface p_1 relative to surface p_2 is:

$$D = \int_{P_1}^{P_2} \frac{dp}{\rho} \qquad (5)$$

The dynamic height values are computed by a numerical integration of (5) after the density profile is determined from observed temperature and salinity values. As these currents are derived from the density distribution, they are inadequate for computing flow in homogeneous or weakly stratified flow such as often found on continental shelves (Neumann and Pierson, 1966).

Equations (3), (4), and (5) imply that only relative currents, the current at level p_1 relative to p_2, can be computed using the geostrophic approximation. This limitation has caused the evolution of many techniques to determine

a true level of no-motion (see Neumann and Pierson (1966), for instance); however, no satisfactory method has been developed. Frequently, the choice of the reference level is based on the depth to which data are available. Therefore, it is necessary to remain cognizant of the fact that geostrophic currents are only relative currents. To convert them to absolute currents requires knowledge of the absolute velocity at some level.

Another difficulty associated with geostrophic computations occurs when large depth changes occur. Various techniques exist for extrapolating deep water dynamic height data onto the shelf in order to compute realistic geostrophic currents (Schlitz, 1973). However, as with most geophysical extrapolation techniques, care must be taken in applying these methods as well as in interpreting the results from their application.

The limitations listed above are functions of the assumptions used in deriving the geostrophic equations. Other errors are introduced through inaccurate data collection procedures. Erroneous ship positions, and inaccurate temperature and salinity determinations can lead to unreliable geostrophic velocities. Fomin (1964) discussed the functional dependence of the geostrophic calculations on some of these factors to indicate the measurement accuracy required to obtain meaningful results.

Finally, data collection schemes which obtain information at discrete points are limited by the distance between data points in the features which can be resolved. Thus, density stations placed 40 km apart in the Yucatan Straits can not resolve the cross-stream velocity structure within this band,nor will stations placed 50 km apart on the west Florida Shelf provide data which can be used to realistically map the distribution of high salinity cells. When considering circulation maps produced from geostrophic computations,it is important to know the station spacing, since the details of the distributions presented are dependent on this spacing.

2) Numerical Model

The numerical model chosen to simulate the circulation of water in the Gulf of Mexico has been adapted from the model for the general oceanic circulation developed by Bryan (1969) and his co-workers at the Geophysical Fluid Dynamics Laboratory of NOAA. The model has been described in detail in the Guide. The development and limitations of the numerical model will be briefly repeated in this section for those readers not concerned with the details given in the Guide. Knowledge of the model limitations, in particular, is necessary for a meaningful evaluation of the model results.

The basis of the numerical model is the set of physical laws governing the motion of fluid on the rotating

spherical earth. For the ocean these laws represent the conservation of matter, the conservation of momentum (Newton's second law of motion), the conservation of heat energy (the second law of thermodynamics), the conservation of salinity, and an equation of state which relates the density to the pressure, temperature, and salinity. The mathematical expression of these laws is a set of partial differential equations which govern the temporal evolution of seven independent field variables: three components of velocity (eastward, northward, vertical), temperature, salinity, pressure, and density.

In order to construct the numerical version of these equations, the model region is first filled with a three-dimensional array of grid points. Then a set of finite difference equations is constructed which approximate the differential equations at the grid points. The finite difference equations are algebraic and can be solved by computer.

The equations which are used are not the most general form of the physical laws; they have been simplified by taking advantage of certain characteristics of the ocean. These simplifications are required to obtain solutions because of reasons discussed in the Users Guide. The most important approximations are the following.

1) The ocean is assumed to be a Boussinesq Fluid. That is, the density of the ocean differs only slightly from a

reference state in which entropy and salinity are constant, and there is no motion. A simple formal analysis, based on this assumption (Phillips 1969), shows that the ocean can be considered incompressible, and that variations of density are only important when they affect the buoyancy of the water.

2) The ocean is assumed to be in hydrostatic balance. This means that the vertical balance of forces differs only slightly from a reference state of no motion. Thus, the conservation equation for the vertical component of momentum is replaced by the hydrostatic balance between the vertical gradient of pressure and the buoyancy force per unit volume. Vertical accelerations of the water are neglected. Although dynamically driven upwelling and downwelling are not significantly affected by the assumption, rapid convective sinking is made impossible. This difficulty is corrected by the parameterization of convection (when dense water overlies less dense water it is instantaneously mixed downward until neutral static stability is achieved). Fofonoff (1962) gave an analysis of the hydrostatic approximation.

3) The surface of the ocean is not flat relative to the geoid even if the wind waves are neglected. Variations in the elevation of the surface are an important part of the dynamics of the circulation. However, the surface of the model ocean is fitted with a rigid lid. Under the rigid

lid approximation, the relative elevation of the surface is replaced by an equivalent surface pressure. The approximation filters out surface gravity waves and slightly distorts other time-dependent motions. The mean circulation is not significantly affected. Clearly, this assumption should not be used in studies in which surface gravity waves are important; these would include tidal studies (Hendershott and Munk 1970), storm surge problems (Reid and Bodine 1968), and estuarine studies (Leendertse 1970).

4) The equations which are used govern only the large scale motion. Formally these equations are derived by an averaging procedure from the more general equations representing all scales of motion (Phillips 1969; Monin and Yaglom 1971). If each of the field variables is expressed as the sum of a large scale part and small scale part, then the averaged equations are written entirely in terms of the large scale variables with the exception of a single term in each of the momentum, heat, and salinity equations which represents the effect of all the small scale variability. In a numerical model, the small scale variations are those with amplitudes less than the distance between grid points. For convenience, all of the unresolved small scale motions are called eddies. Because the eddy effects are not resolved, they must be parameterized where they appear in the averaged equations. In analogy with the theory of turbulence, it might be assumed that the net effect of all eddy processes was to enhance the diffusion of momentum, heat and salinity. Based on this assumption the model parameterizes the eddy fluxes by the

negative gradient of the appropriate large scale variable multiplied by a constant, positive eddy coefficient.

The spatial resolution of the numerical model is determined by the distance between grid points. For example, the Gulf of Mexico model with 37,26, and 7 grid points in the zonal, meridional, and vertical directions respectively, has a uniform horizontal resolution of about 50 kilometers and a variable vertical resolution of 70 to 930 meters. An increase in the number of grid points allows a finer resolution but also requires more computer memory and time to perform a calculation.

5) The model assumes that the frictional drag of the bottom is negligible in all areas except for those with the shallowest model depths. This is a reasonable assumption for deep water where the vigorous wind-driven circulation is confined to the surface layers. However, in regions where strong currents extend to the bottom, the assumption breaks down. There is some distortion of the simulated continental shelf circulation in regions with no bottom friction. Also, a certain amount of dissipation is missing from the model. However, because the missing dissipation represents a very small fraction of the total dissipation in the model due to eddy viscosity, the effect on the energetics of the model as a whole is negligible.

All of these approximations are included in the basic Bryan model; no additional approximations have been made in the Gulf version of the model. However, the Gulf model does

include modifications to accommodate the open boundaries at the Straits of Yucatan and Florida. Separate experiments have been done using two distinct treatments of the boundary conditions at the Straits. In one case, the user supplies the model with information about the direction and vertical structure of the flow at the open boundaries; while in the other case, the model itself specifies the freer condition that the flow does not change direction at the boundaries. In addition, in both treatments the user must specify the total transport of water through the boundaries. A comparison of the results using these different treatments at the boundaries shows only slight differences in the interior of the Gulf.

The model has been run in a diagnostic mode. To make such a calculation, the initial value of temperature, salinity, and horizontal velocity at all grid points of the model must be specified. In addition, the values of wind stress, the flux of heat through the surface, and the apparent flux of salt through the surface as a result of evaporation and precipitation are required at each surface grid point. During the calculation the temperature, and salinity fields are held fixed while the velocity field is allowed to evolve to a steady state. The validity of the velocity field determined in a diagnostic study depends strongly on the quality and quantity of the temperature and salinity data put into the calculation.

IV DATA PREPARATION

Figures 12, 13, and 14; 15; and 16 show the distribution by 1° squares of station, expendable bathythermograph (XBT), and mechanical bathythermograph (MBT) data collected in the Gulf of Mexico. Figures 12, 13, and 14 also list the distribution of station data by 10° square and month. The lack of adequate spatial or temporal coverage is apparent in these figures and tables for all areas except the eastern Gulf. Much of the subjectivity used in the processing of these data is necessary because of this sparse data-set.

More sophisticated methods have been developed to manipulate data-sets, in particular objective analysis, (Gandin, 1963), but time constraints precluded the adoption of these techniques into the present study. However, in view of the difficulties encountered with the methods implemented, and the need for more refined data handling methods for preparing data-sets for the prognostic models, the last section of this report will discuss the need to expand the second year work to include development of advanced techniques.

The numerical model when used in the diagnostic mode requires four types of data, in addition to the interior temperature and salinity fields, to define the boundary conditions. The lateral boundaries and bottom topography of the Gulf of Mexico, the surface wind stress field, and the total volume transport through the Florida and Yucatan Straits, must be specified. The geostrophic model requires

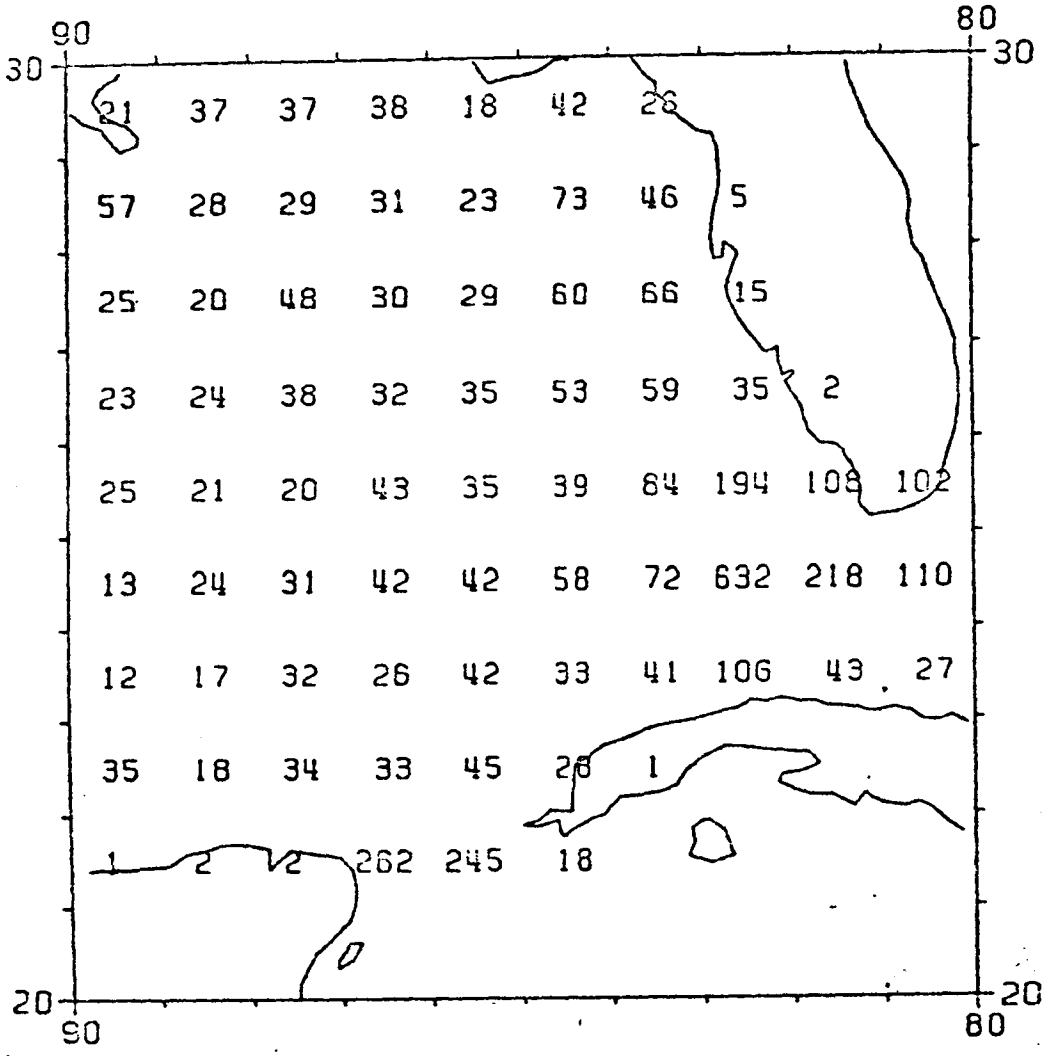

STATION DATA INVENT.
FOR TEN DEGREE SQUARES 1110

JAN	120	JUL	130	STATIONS	
FEB	440	AUG	638	JAN-MAR	851
MAR	291	SEP	219	APR-JUN	1754
APR	370	OCT	148	JUL-SEP	987
MAY	739	NOV	236	OCT-DEC	529
JUN	645	DEC	145	TOTAL	4121

Figure 12. The distribution of Nansen station data collected in Marsden Square 1110 in the Gulf of Mexico from 1900 to 1975. The distribution by months is also listed.

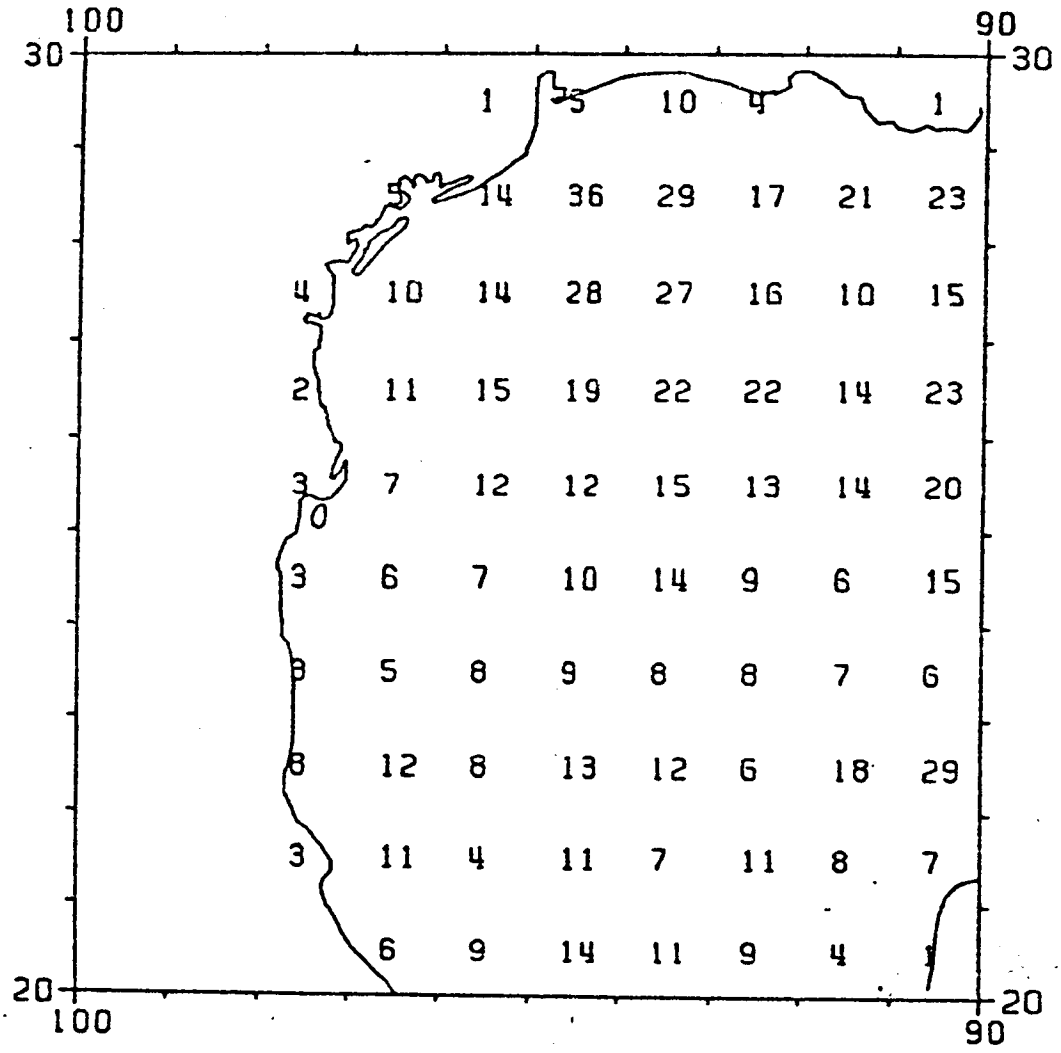

STATION DATA INVENTORY
FOR TEN DEGREE SQUARES 1111

JAN	97	JUL	37	STATIONS	
FEB	95	AUG	121	JAN-MAR	345
MAR	153	SEP	57	APR-JUN	159
APR	23	OCT	40	JUL-SEP	215
MAY	39	NOV	71	OCT-DEC	141
JUN	97	DEC	30	TOTAL	860

Figure 13. The distribution of Nansen station data collected in Marsden Square 1110 in the Gulf of Mexico from 1900 to 1975. The distribution by months is also listed.

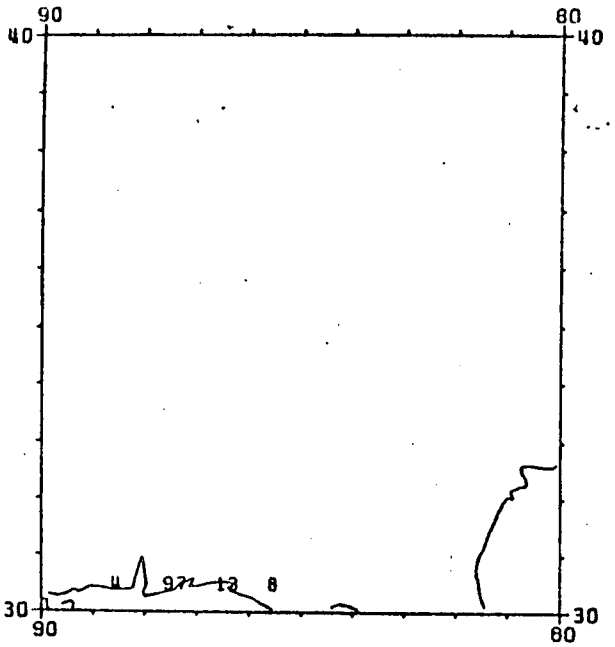

STATION DATA INVENTORY
FOR TEN DEGREE SQUARES 1210

JAN	6	JUL	0	STATIONS	
FEB	1	AUG	8	JAN-MAR	8
MAR	1	SEP	99	APR-JUN	7
APR	0	OCT	0	JUL-SEP	107
MAY	1	NOV	0	OCT-DEC	0
JUN	6	DEC	0	TOTAL	122

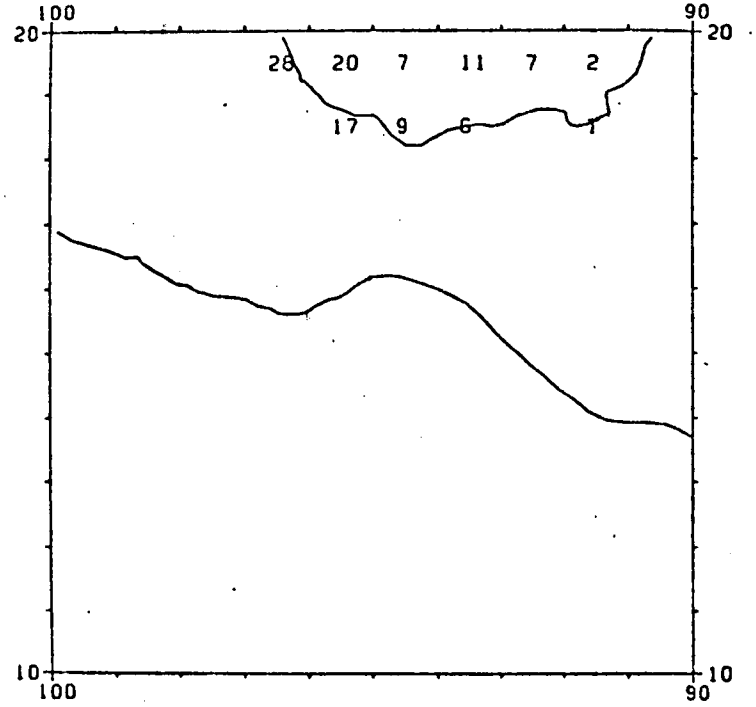

STATION DATA INVENTORY
FOR TEN DEGREE SQUARES 1011

JAN	4	JUL	0	STATIONS	
FEB	2	AUG	15	JAN-MAR	14
MAR	8	SEP	3	APR-JUN	59
APR	0	OCT	6	JUL-SEP	18
MAY	52	NOV	11	OCT-DEC	17
JUN	7	DEC	0	TOTAL	108

Figure 14. The distribution of Nansen station data collected in Marsden Squares 1011 and 1210 in the Gulf of Mexico from 1900 to 1975. The distribution by months is also listed.

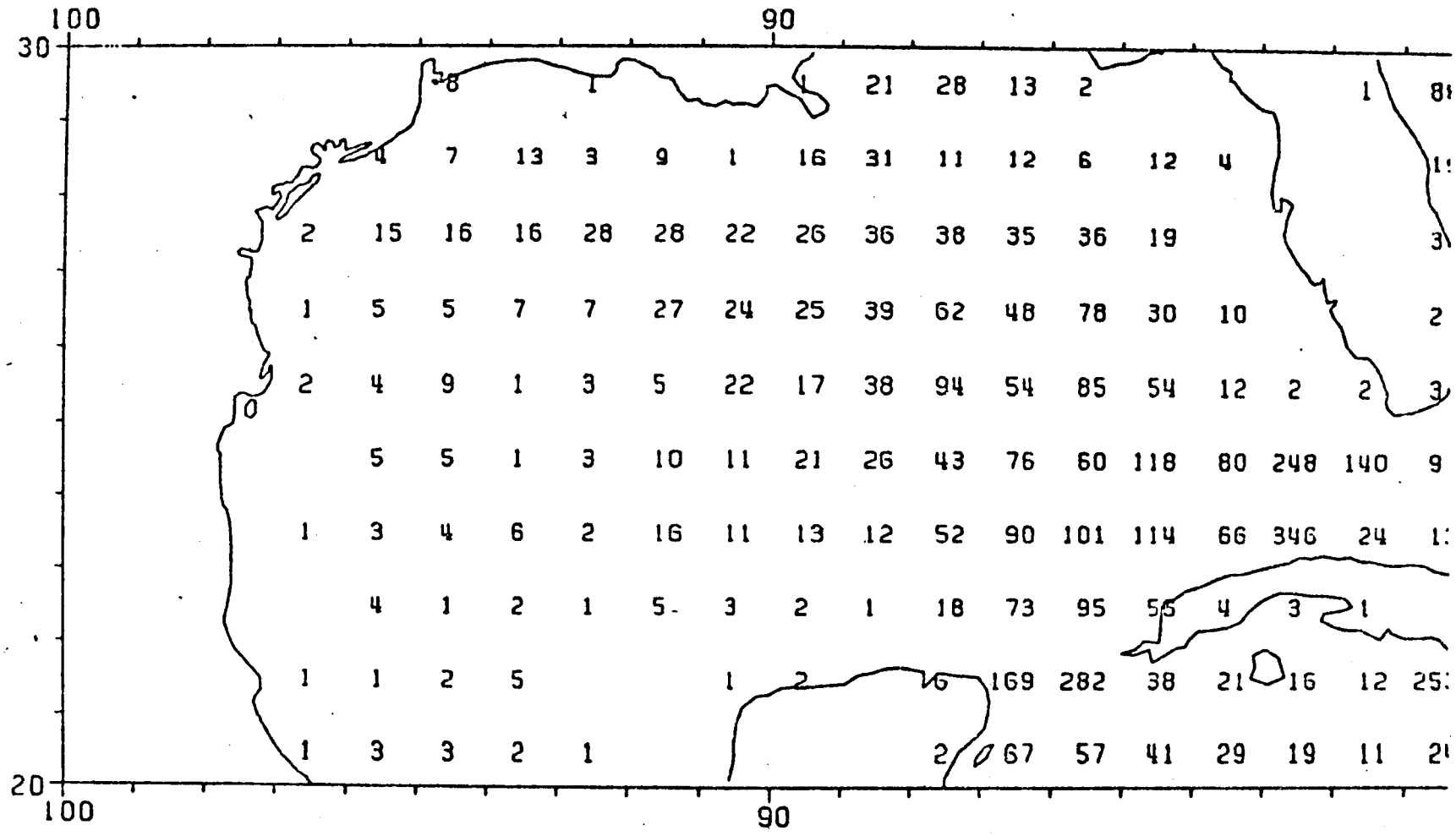

Figure 15. The distribution of expendable bathythermograph(XBT) data collected in the Gulf of Mexico from 1962 to 1975.

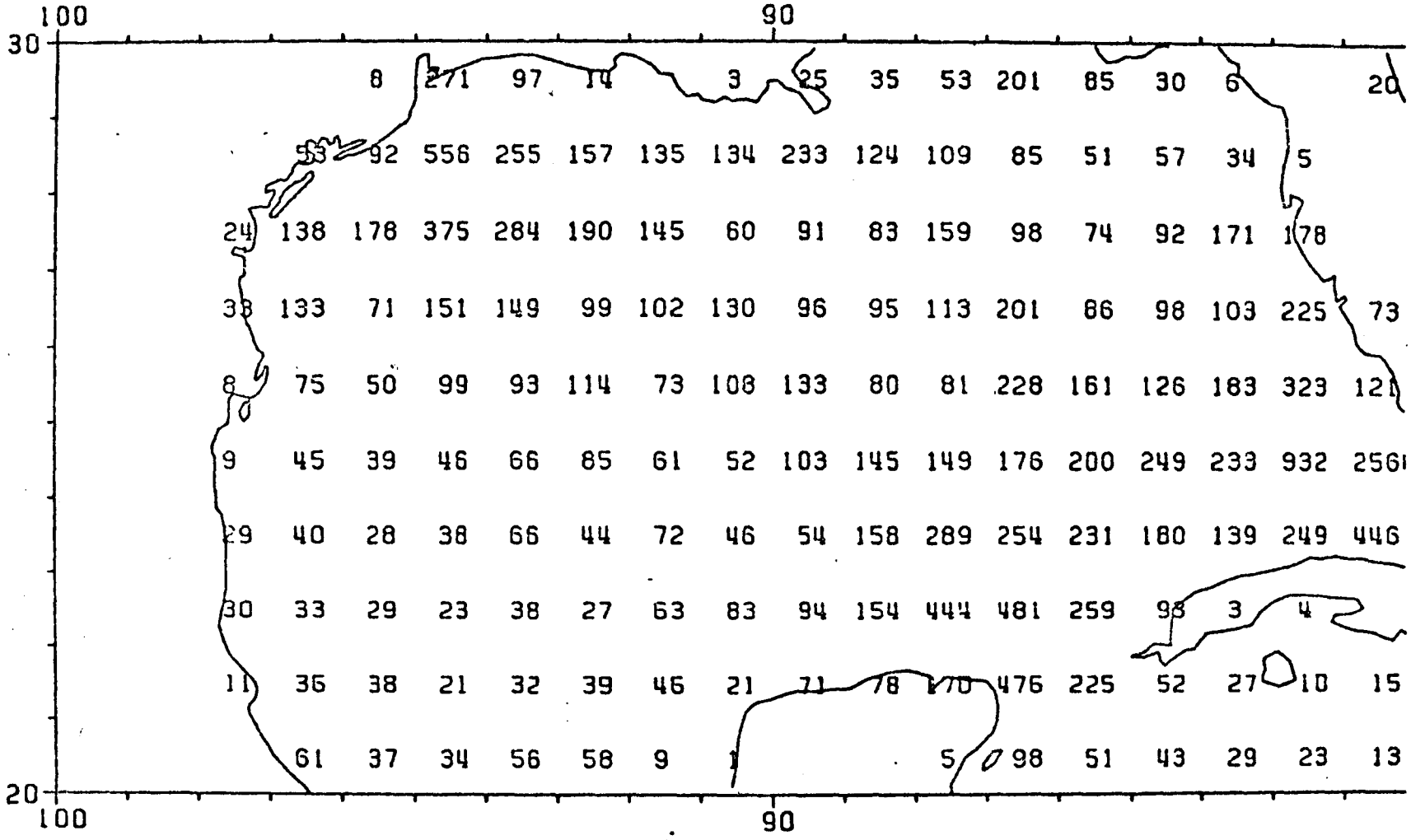

Figure 16. The distribution of mechanical bathythermograph data collected in the Gulf of Mexico from 1941 to 1975.

temperature and salinity values at each grid-point to determine velocities. The data-handling techniques used to obtain this information will be described next.

1) Bottom Topography and Lateral Boundaries

A digitized bottom topography of the Gulf of Mexico, including lateral boundaries, was supplied by Drs. Yin-Shang Soong and Ya Hsueh of the Department of Oceanography, Florida State University. The bottom is digitized at a one-quarter degree grid interval, using three maps prepared by the Geological Survey: Uchupi (1971), and USGS I-457, and I-521. The digitized topography, contoured at 500 m intervals, is presented in Figure 17.

2) Surface Wind Stress

The surface wind stress over the Gulf of Mexico was supplied by Mr. Andrew Bakum of the Pacific Environmental Group of the National Marine Fisheries Service, NOAA. Surface wind stress components are generated from monthly mean atmospheric pressure data obtained from January 1946 to June 1974. The geostrophic wind speed is computed from the surface pressure distribution. A wind speed squared stress law and a drag coefficient of .0013 are used. The zonal and meridional wind stress components are determined for each month at 3^{o} intervals.

The 28 monthly values for each 3^{o} square and month are averaged to obtain monthly mean stress values for January through December. A spline interpolation routine obtained

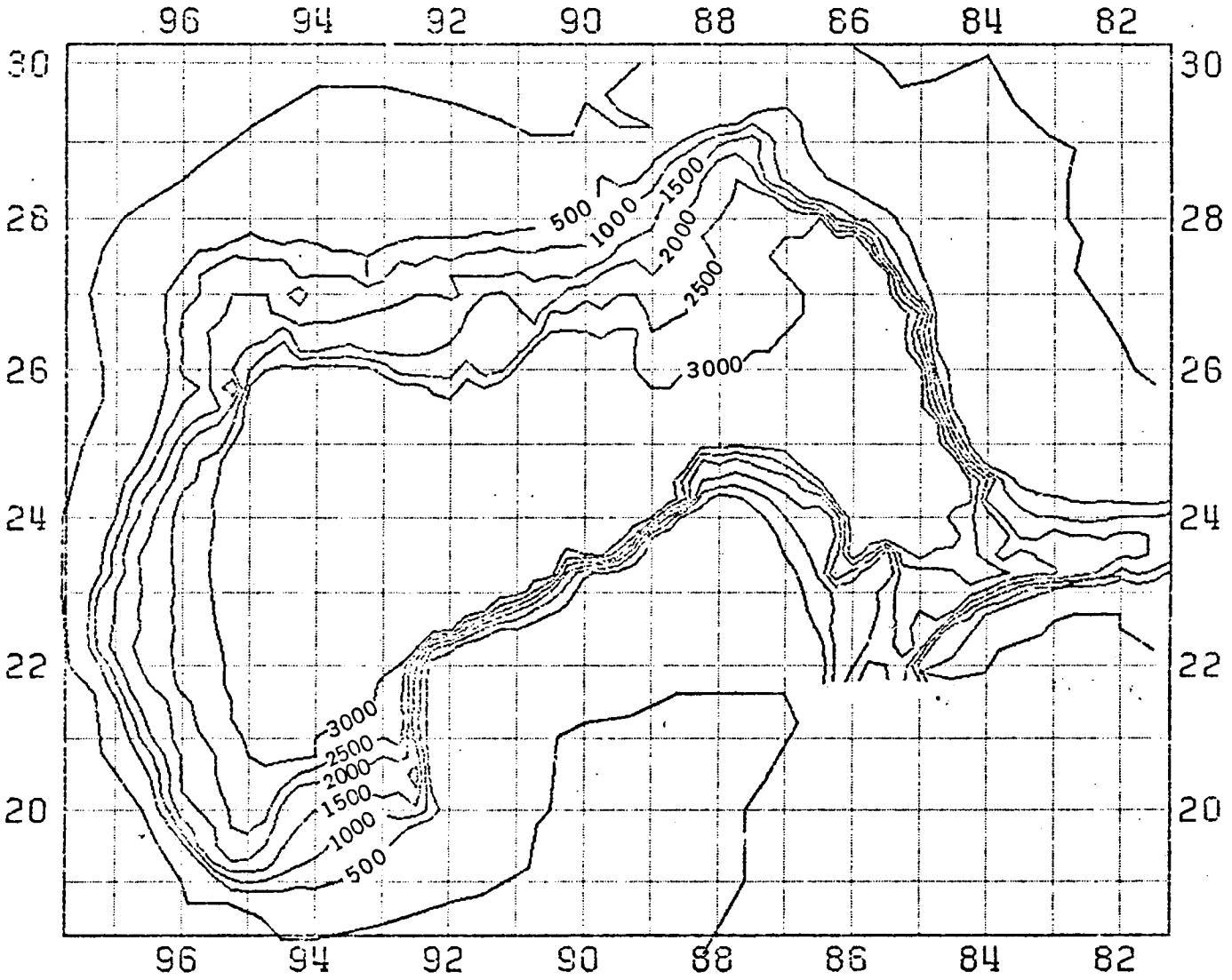

Figure 17. Bathymetry of the Gulf of Mexico. The contour interval is 500 meters. The maximum depth is 3400 meters. The resolution is 1/4 degree.

from the NCAR Library of Subroutines (NCAR, 1971) is used to interpolate the stress values to the model's $1/2^{\circ}$ increment. Figures 18 to 23 give the distributions of monthly mean wind stress vectors at this interval.

3) Yucatan Straits Transport

The Yucatan Straits is divided into eight subregions. Each subregion is an area 12' of longitude by 18' of latitude, except for the eastern most region which extends over 18' of longitude. Figure 24 shows the eight subregions overlaid on a bathymetric chart of the Yucatan Straits.

For each subregion, the National Oceanographic Data Center (NODC) produced bi-monthly vertical array summaries of temperature, salinity, and dynamic heights at the standard NODC levels. The dynamic height data were integrated to form a transport function (McLellan, 1965), and volume transports were computed from this function.

Considerable noise existed in the computed transport values even though the data were averaged spatially and temporally. The sparsity of data during certain months and in some subregions probably causes much of the noise.

The raw dynamic height data were subjectively smoothed, using as a criterion the assumption that the average dynamic height distribution should vary smoothly in time and space. A similar criterion was employed by Whitaker (1971)

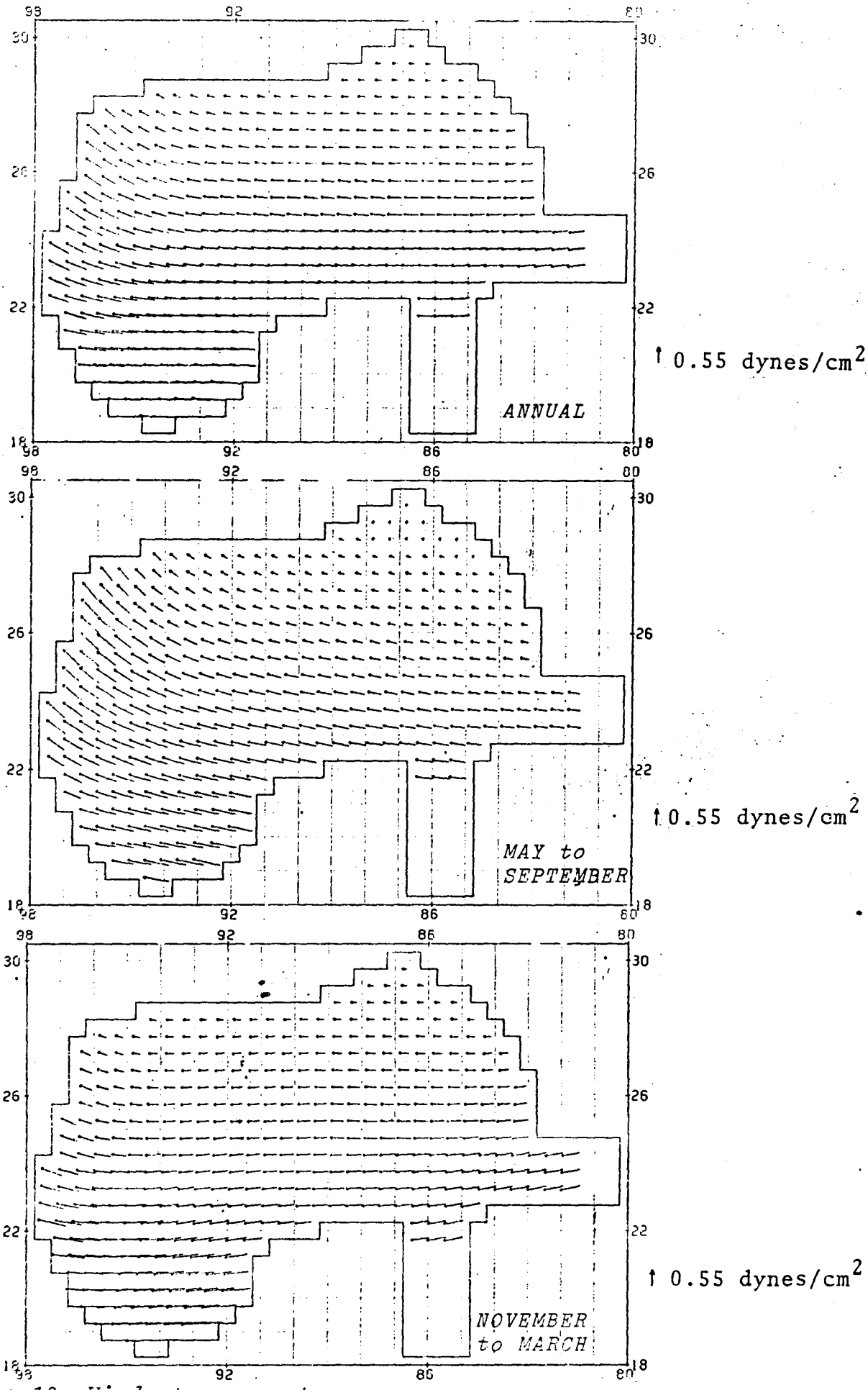

Figure 18. Wind stress vectors.

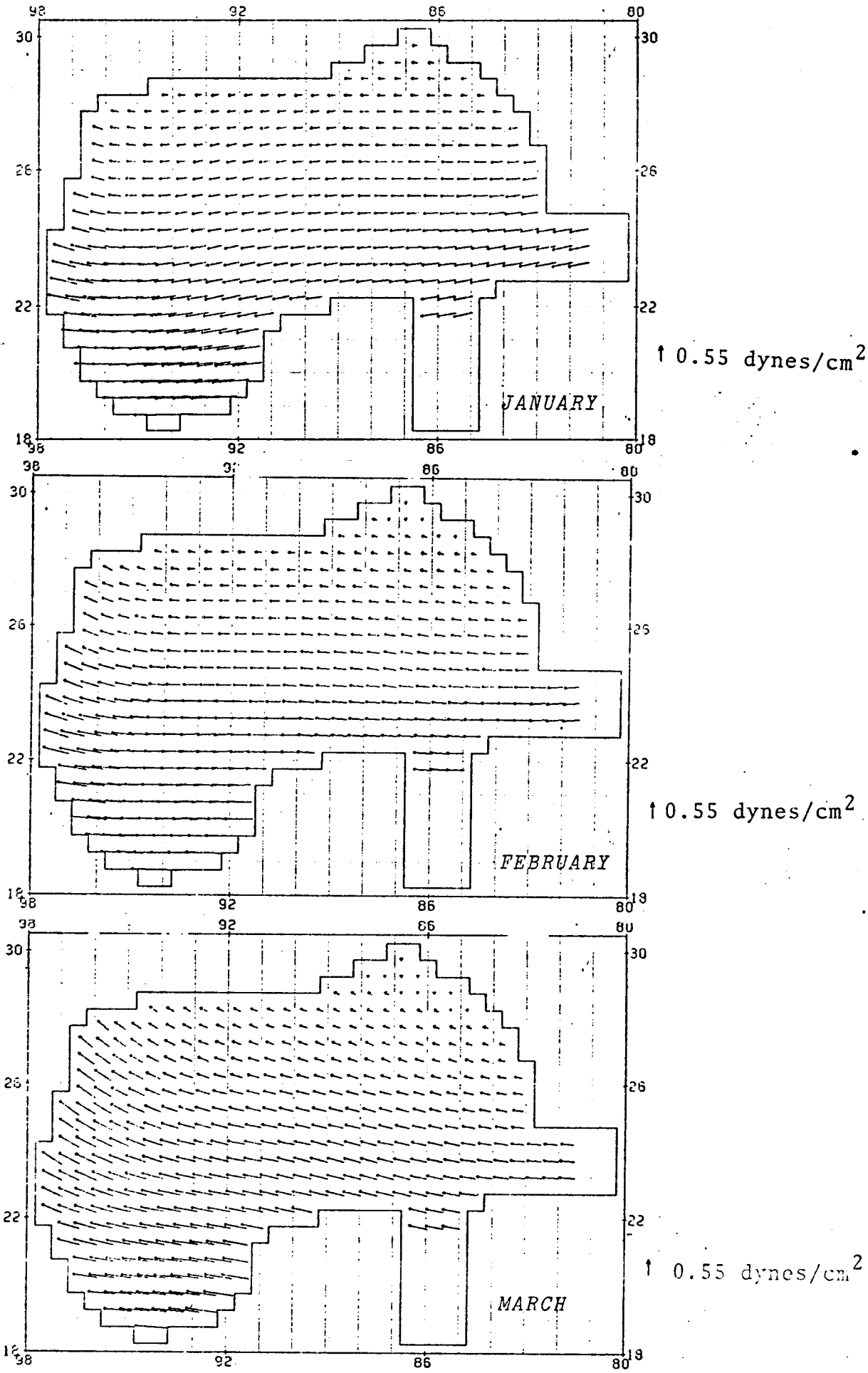

Figure 19. Wind stress vectors.

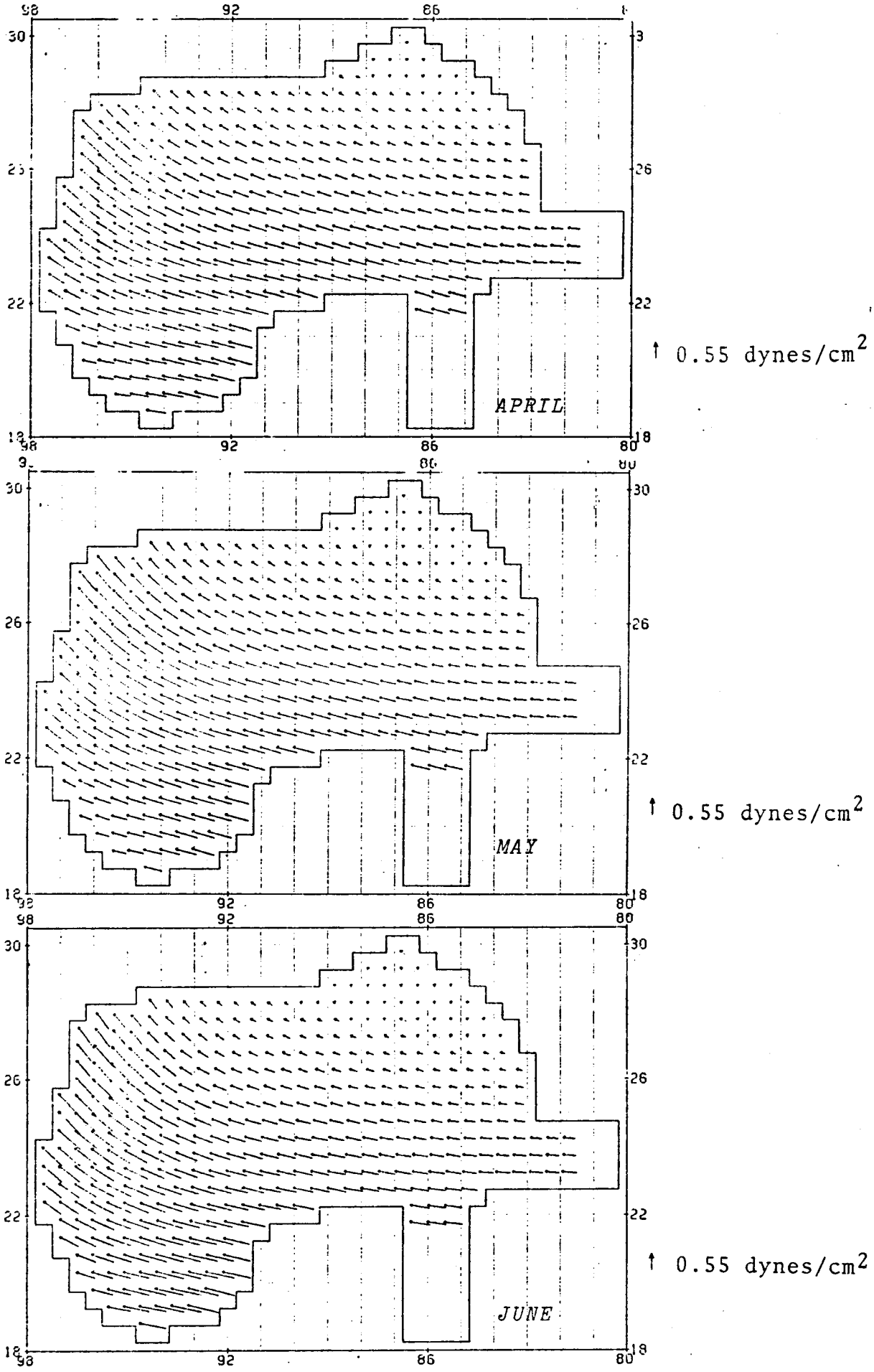

Figure 20. Wind stress vectors.

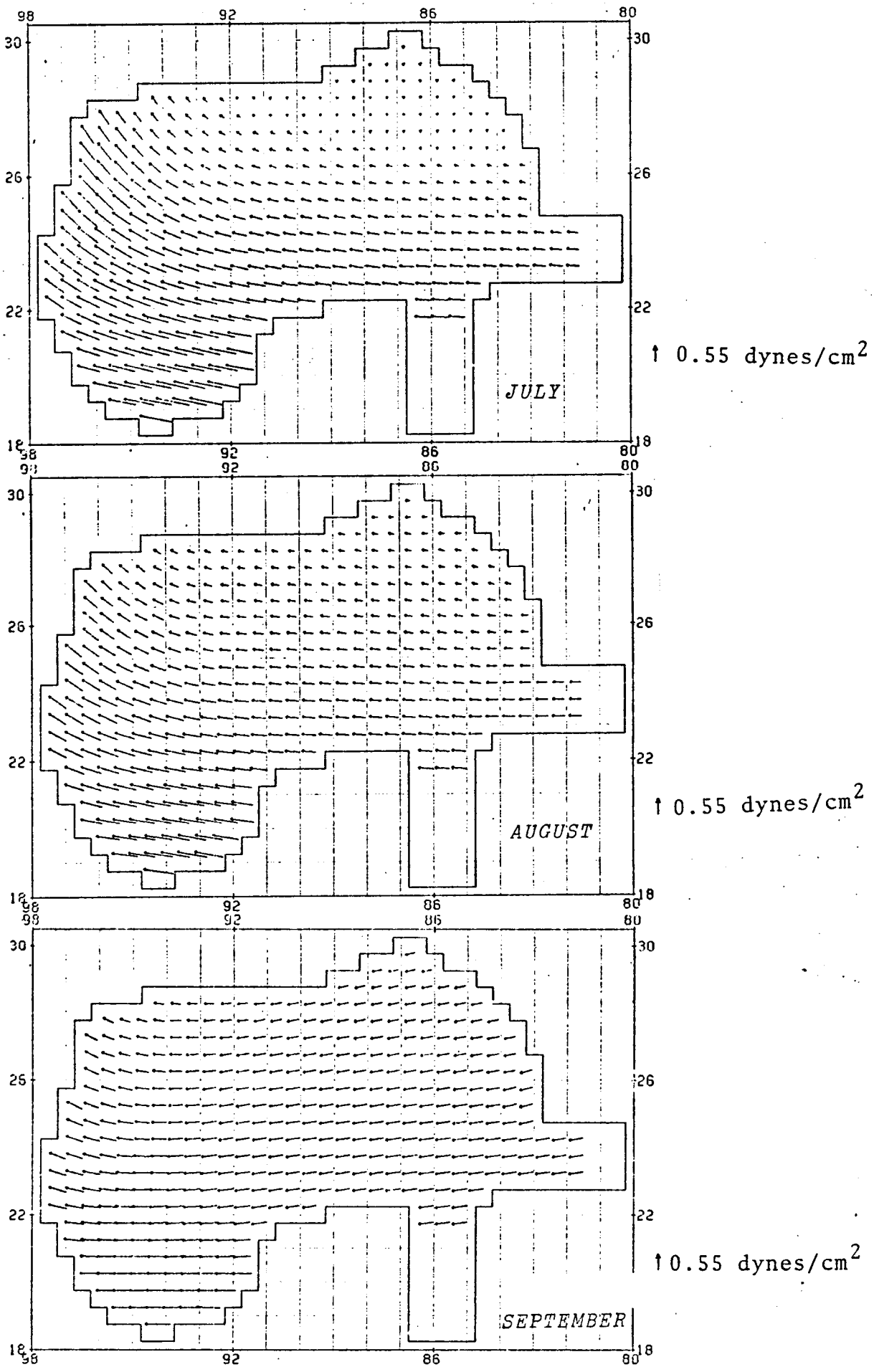

Figure 21. Wind stress vectors.

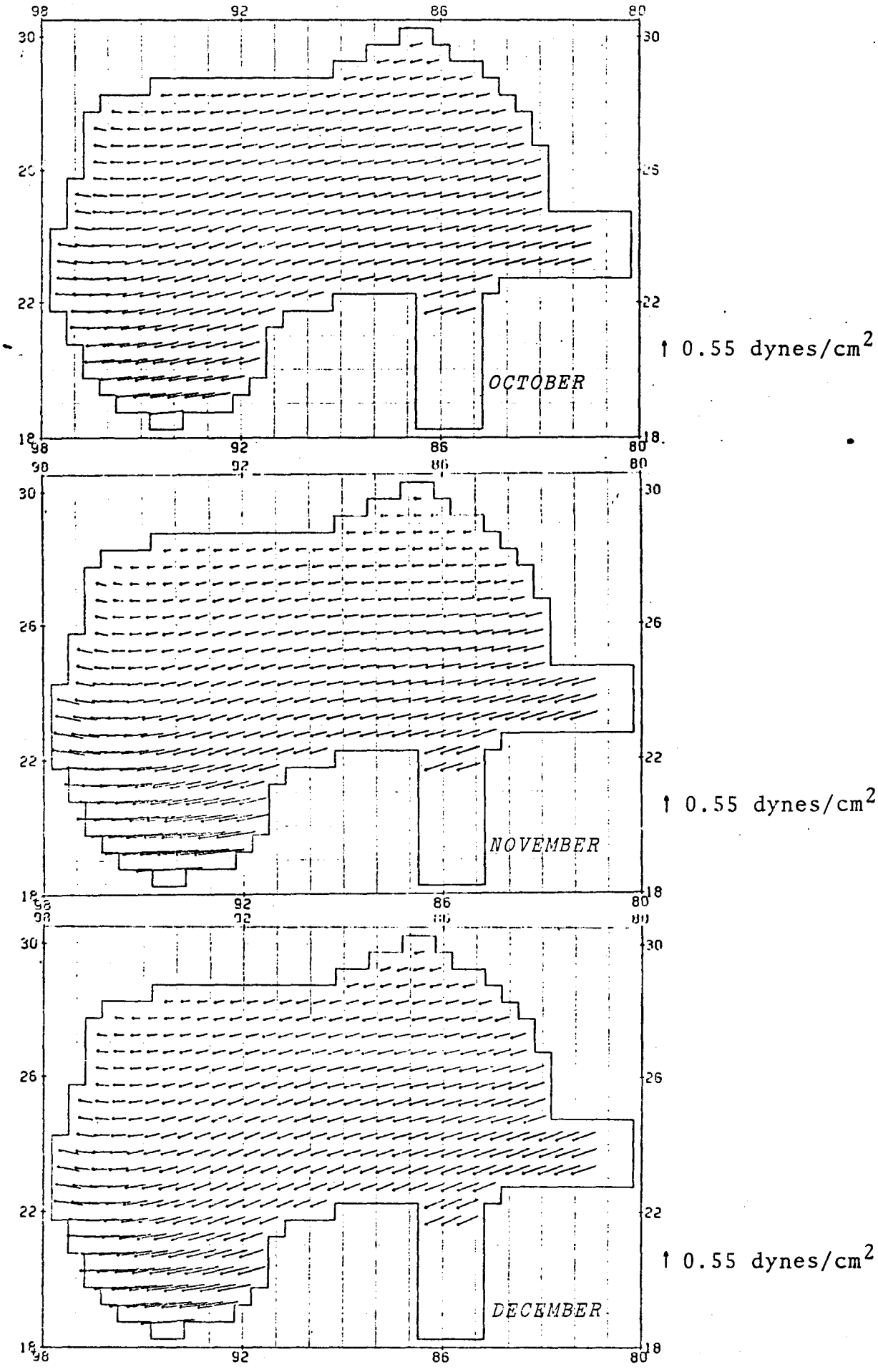

Figure 22. Wind stress vectors.

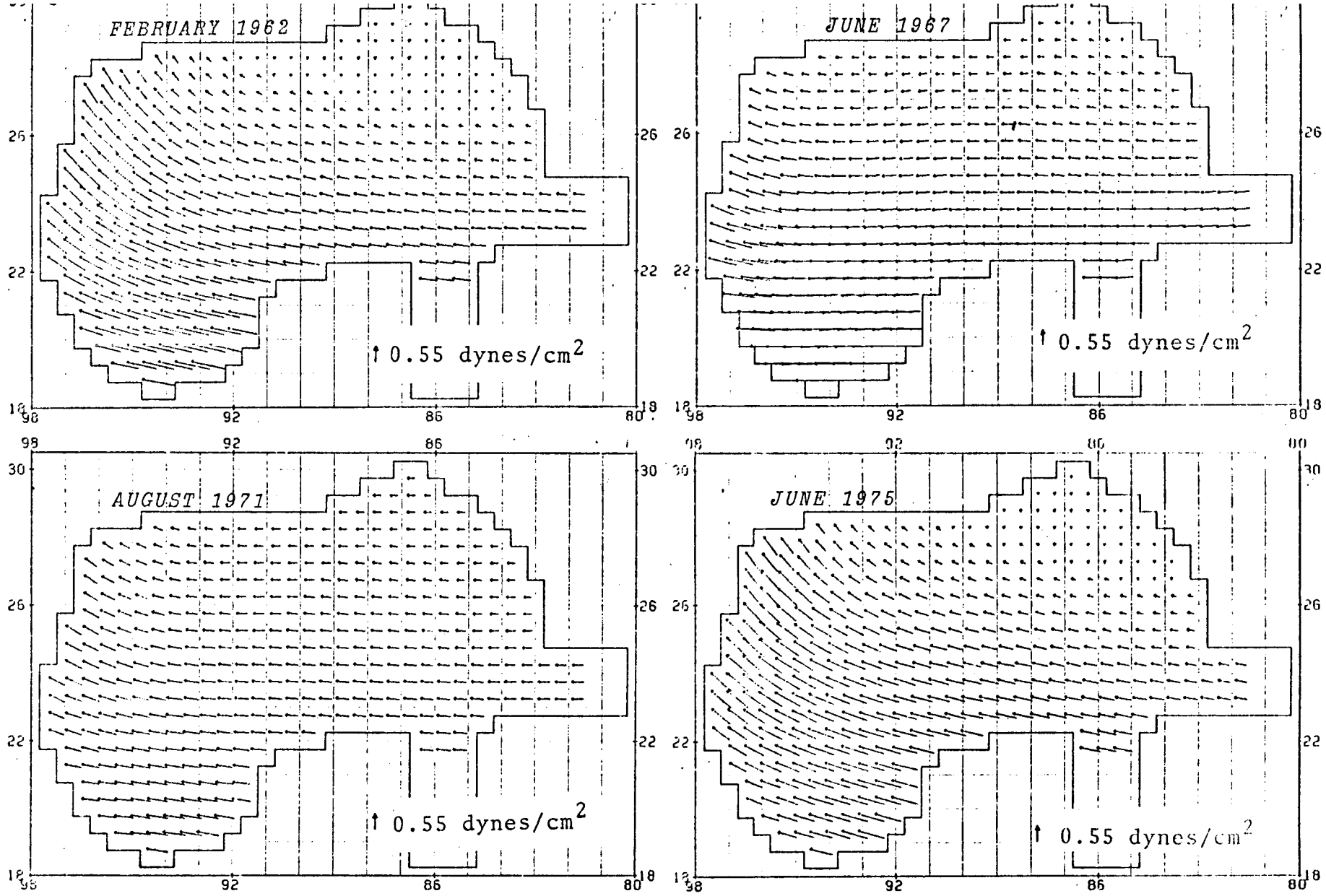

Figure 23. Wind stress vectors.

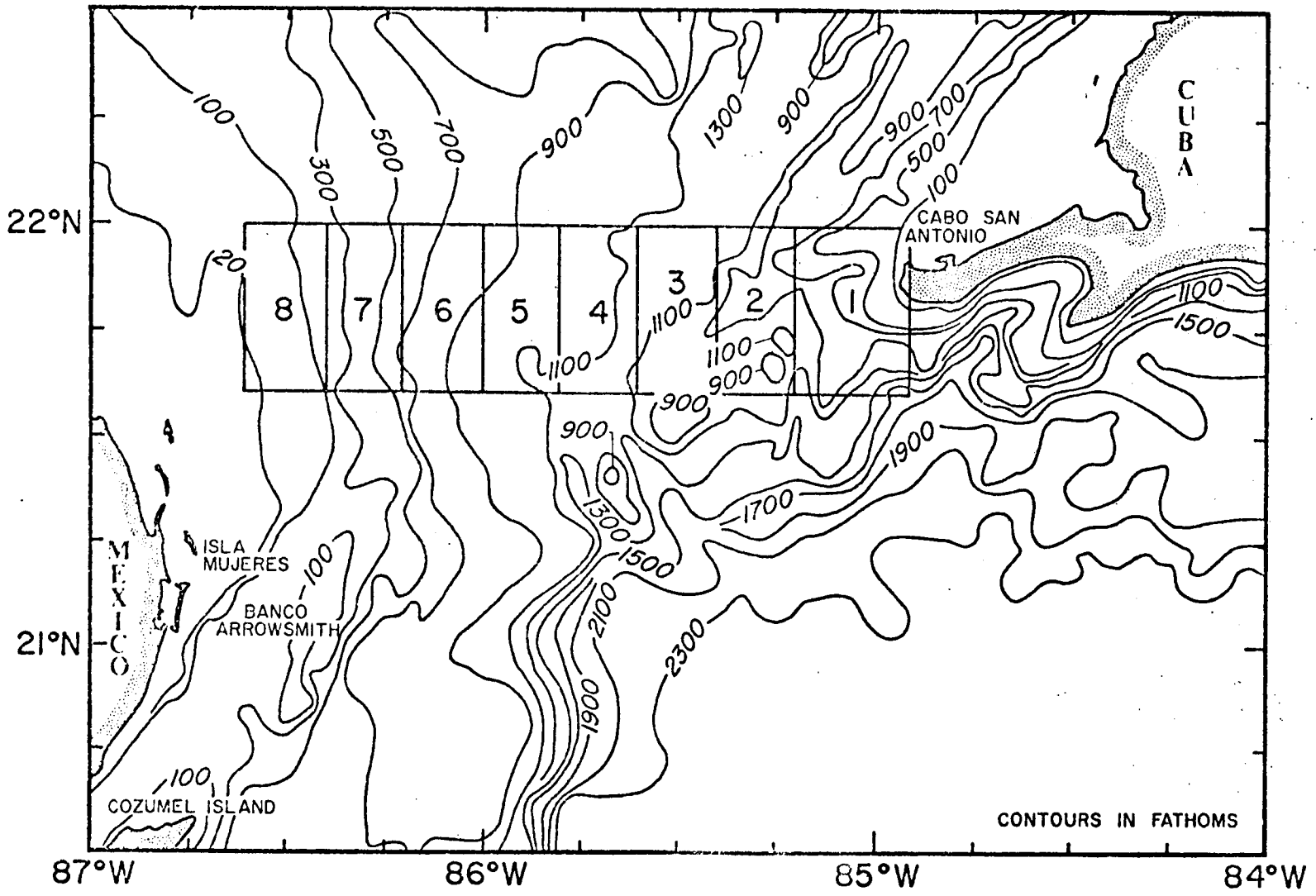

Figure 24. The eight subregions of the Yucatan Straits for which average dynamic height profiles are computed.

and Robinson (1973) in their studies of the climatological temperature distributions.

The transports determined after smoothing the dynamic height values were further smoothed by applying a triangle weighting filter to three successive transport values. The annual harmonic is fitted to these six transport values, and the resulting curve represents a mean transport of $30.1 \times 10^6 m^3/sec$, an amplitude of $3.3 \times 10^6 m^3/sec$, and a phase shift from January 1 of plus four months (i.e. the maximum transport occurs on May 1). Figure 25 presents the observed transports and the annual harmonic curve. These values compare favorably to the average values obtained at the Straits of Florida by Niiler and Richardson (1973); mean transport, $29.5 \times 10^6 m^3/sec$; amplitude $4.1 \times 10^6 m^3/sec$, and a phase shift of maximum transport to early June.

4) Climatological Temperature and Salinity Data

The temporal and spatial distribution of Nansen station data (Figures 12,13 and 14) indicate poor spatial coverage on time increments less than bi-annual. Therefore, an approach was devised whereby temperature data from XBT and MBT stations could be used to supplement the Nansen station data. This larger data-set is used as input to both the numerical and geostrophic models.

The basis of this approach is to match observed temperature values with salinity values obtained from an average T-S relation. Emery (1975) reviews this procedure and finds it adequate in regions of small scatter about an average T-S

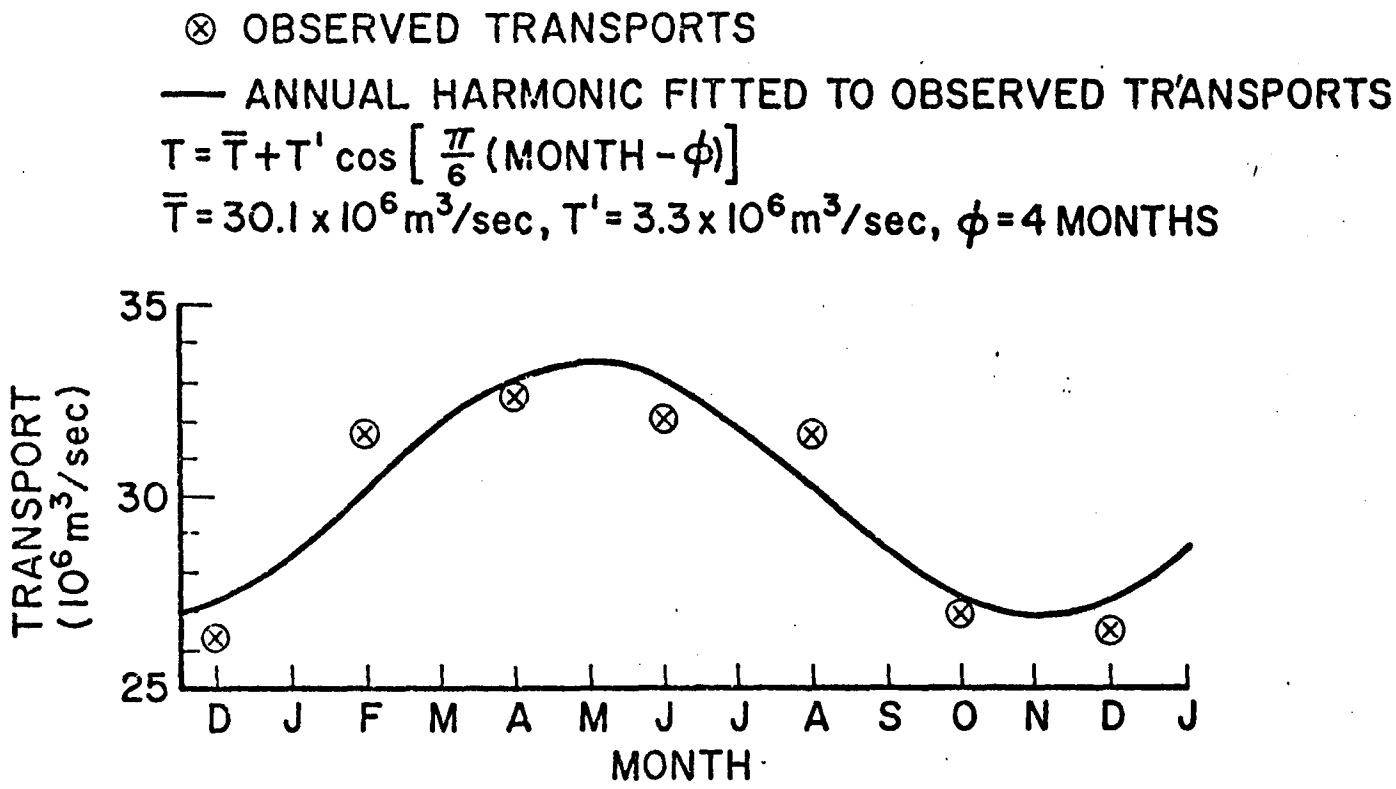

Figure 25. The bimonthly values of total geostrophic transport through the Yucatan Straits computed relative to 1000 db. The annual harmonic fitted to these data in a least squares sense is also shown.

relation. As a first step, the Gulf was divided into the nine regions shown on Figure 26. These regions were chosen on the basis of the results of past investigations which suggested common circulation and water mass characteristics for each region. The year was divided into four seasons, December-February, March-May, June-August, and September-November; the season's based on the annual cycle of the Loop penetration given first by Leipper (1970).

For each region, NODC provided a list of average salinities for 1/2°C temperature intervals. To reduce the raggedness in the T-S relations, particularly in areas of little data, the salinities at consecutive intervals were averaged to obtain salinities at 1°C intervals. The resulting four T-S relations for each region were plotted and edited. In regions 1 through 6 there was little variability with season in the T-S relations below 17°C (as previously reported on by Caruthers (1972), for instance). Areas 7,8, and 9 which encompass shelf regions exhibited considerable temporal variability in the T-S relations.

The T-S relations above 17°C for areas 1 through 6 were examined for systematic variations in the T-S relations. The examination was cursory, and no clear-cut seasonal variability was found. Therefore, an annual mean T-S relation was produced for these areas. Although areas 7,8 and 9 exhibit seasonal changes in the T-S characteristics,

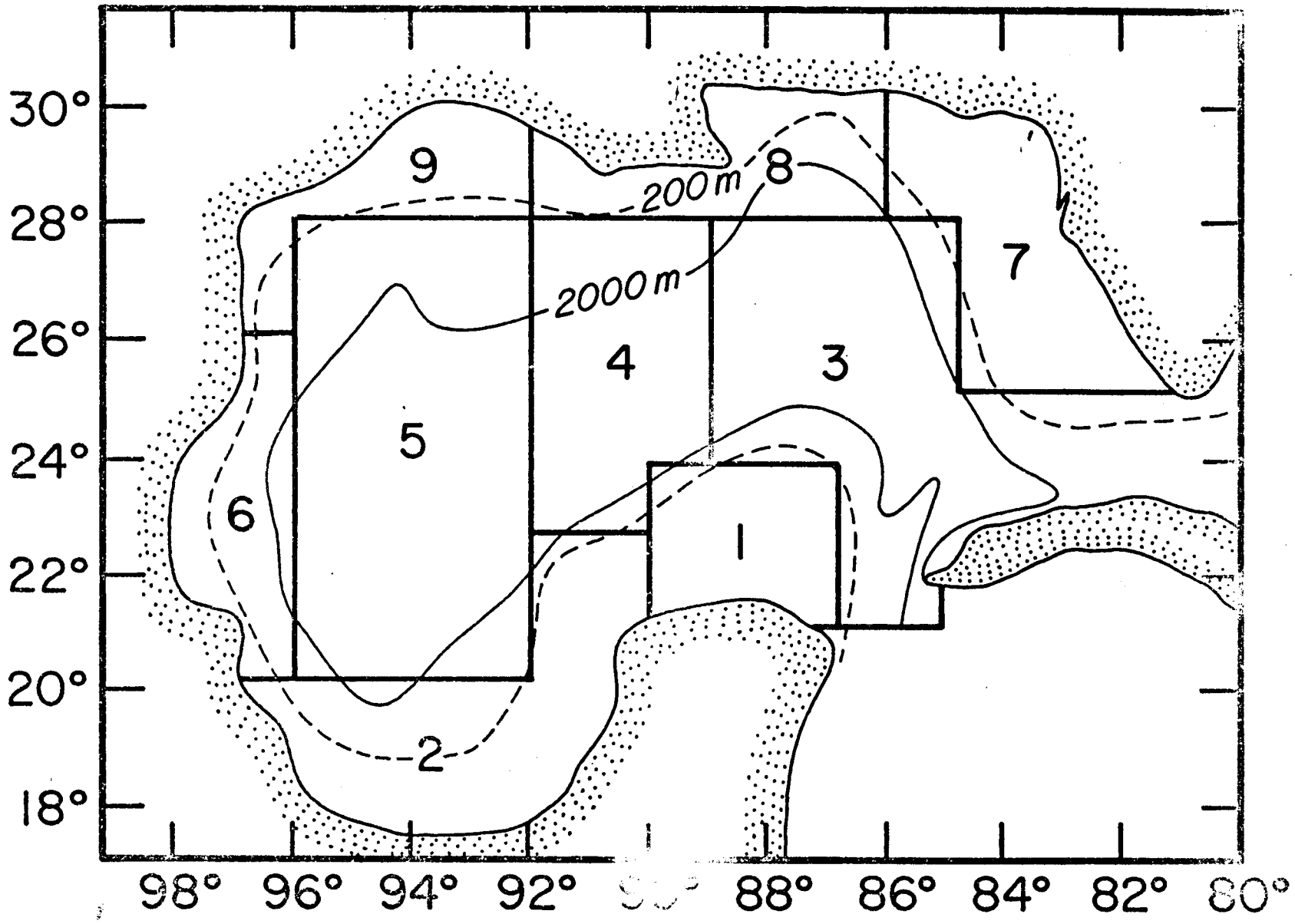

Figure 26. The nine subregions of the Gulf of Mexico for which average T-S relations are computed.

annual averages were also produced for these regions, for consistency. Unfortunately, area 8 includes both shelf and deep waters. In order to avoid complications in dynamic height and model computations, the T-S relation for this area was subjectively smoothed with a bias toward deep water conditions (i.e., higher salinities). The accepted T-S relations produced from these manipulations are given in Figure 27.

NODC also provided listings of mean monthly temperature at NODC standard depths, and by 1^{o} square. These monthly data were further averaged to form an annual mean temperature profile, and two seasonal profiles (summer, May to September, and winter, November to March) at each 1^{o} square.

The distribution of the mean monthly temperature data, particularly in the western and central Gulf, is sparse. Therefore, a three-month average centered at the desired month was computed to compensate for the lack of adequate spatial coverage. These average conditions will serve to represent the monthly temperature distributions. Seasonal representations of the circulation based on three month averages were also to be produced. In view of the averaging required to generate monthly data, no separate seasonal patterns are presented.

Temperature data and salinity data are mated to obtain vertical profiles of both parameters at each 1^{o} square. First, the subregion (Figure 26) in which a particular 1^{o} square temperature value lies is determined. The T-S relation for that region gives salinity values for each

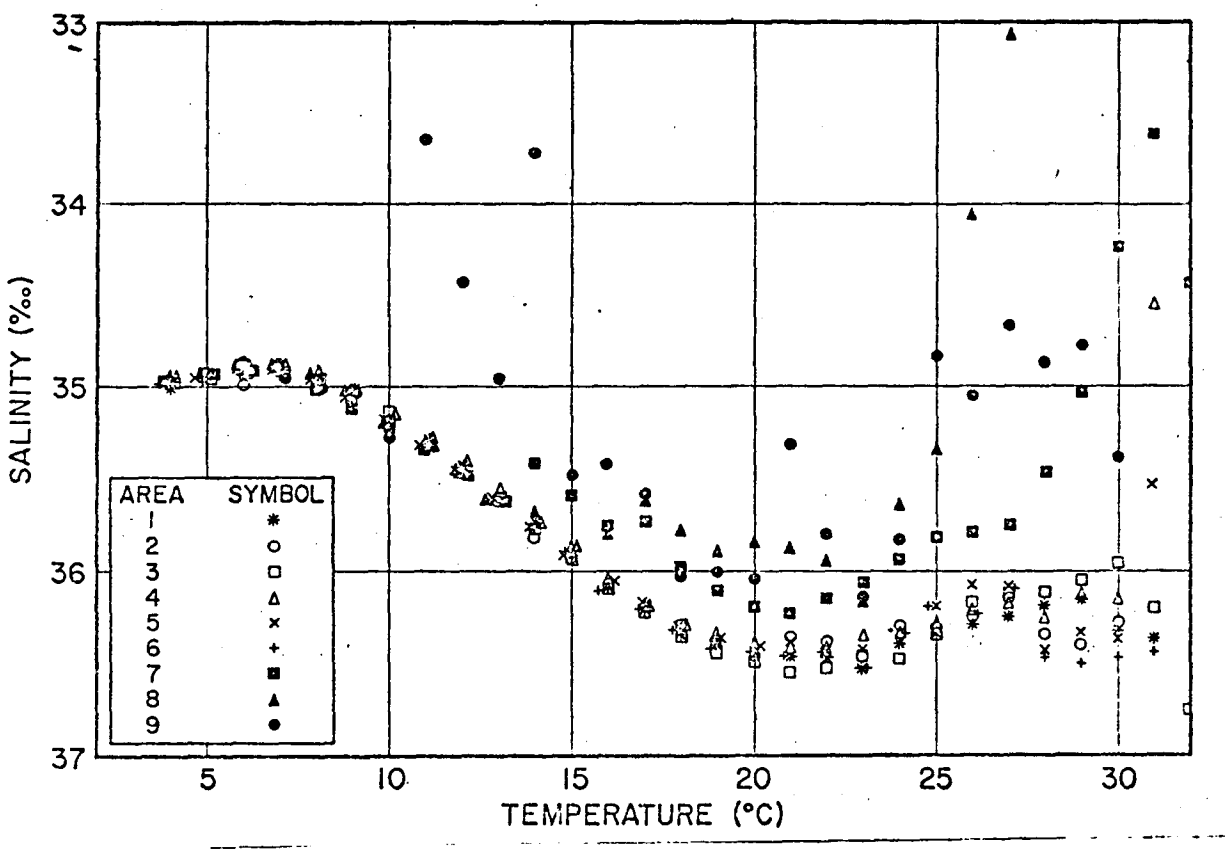

Figure 27. The average T-S relations for the nine subregions defined in Figure 26.

1^{o}C of temperature, therefore a linear interpolation is used to compute the salinity at the desired temperature.

Temperature and salinity values at the model depths are computed from the resulting vertical profiles by using a spline interpolation routine (NCAR, 1971). A horizontal interpolation scheme given by Haltiner (1971) is used to obtain temperature and salinity values on the $1/2^{o}$ square grid required by the numerical model. The climatological data are then subjectively edited, and obviously bad points are replaced by the average of the surrounding data. Finally, before input to the model, the data are averaged by taking a weighted average at each grid point with the surrounding four points.

5) Climatological Dynamic Height Data

The annual, semi-annual, and monthly temperature and salinity data available at the NODC standard depths, and on a 1^{o} square grid are used to compute dynamic heights. The same horizontal interpolation scheme discussed above (Haltiner, 1971) is used to obtain dynamic height values on a $1/2^{o}$ square grid. These data then are used to compute geostrophic velocities and to produce dynamic height maps relative to various levels. The geostrophic velocities are computed at each interior grid point using a centered difference analogue. At the boundaries, velocities are computed using a forward or backward interpolation analogue.

The dynamic height fields are also subjectively edited to remove bad data points. Some extrapolation is per-

formed in the Yucatan Straits and Straits of Florida to increase the spatial coverage. The extrapolation is performed by subjectively filling in missing data points with dynamic height values that are consistent with upstream and/or downstream data.

6) Synoptic Cruise Data

Data from four synoptic cruises are prepared for input to the numerical and geostrophic models. The station data from synoptic cruises normally do not occur at the model grid points; therefore, it is necessary to interpolate the observed data to the required positions.

Another technique described by Haltiner (1971) has been adapted to accomplish this task. If an observed point is located within one grid interval of a model point, the observed value is multiplied by a weighting function which is proportional to the distance from the point to the grid point. The weighted observation values are stored at the appropriate grid points; and after the entire field has been scanned, weighted averages are taken at the grid points. The result of the averaging is the accepted value of the scalar property at the grid point. It should be emphasized that the influence of any observed point is only propagated one grid interval.

Three of the four synoptic cruises did not provide spatial coverage of the entire Gulf of Mexico. Therefore, those grid points without observed values were filled with data taken from the appropriate monthly distributions.

The combined 1° square temperature and salinity distributions at the model levels are subjectively edited to remove obviously bad points. The data are then interpolated onto a 1/2 ° square grid, using the method of Haltiner, (1971); subjectively edited again ; smoothed ; and finally input to the primitive equation model.

The dynamic height data from the synoptic cruises are interpolated onto a 1/2° square grid using the above technique. However, these data are not smoothed. Geostrophic velocities are computed from the data using the same techniques as applied to the climatological dynamic height data.

Finally, when available, sea surface current vectors computed from surface drifter data are decomposed into component speeds. These scalar speeds are then interpolated to a 1/2° square grid by the Haltiner (1971) approach.

V. GULF OF MEXICO CIRCULATION

The results of the geostrophic and primitive equation experiments are presented in the form of a set of horizontal charts and vertical sections. To repeat a previous caution, the assumptions used in the formulation of both models must be considered when interpreting these results. In particular, both models have limited ability to simulate realistically the circulation on the continental shelf. Therefore, the existence of a shelf feature must be suspect unless additional corroborating data exist.

The ability of either technique to reproduce the deep basin circulation is limited more by the quantity and quality of the data than by the assumptions used in formulating the models. Therefore, in regions where data are sparse, such as in the western Gulf, circulation features may be artifacts of the limited data distribution rather than real. One measure of the validity of the model results is a month-to-month persistence in the circulation features.

The geostrophic and primitive equation simulations of the large-scale (order of 100 km and greater) circulation features appear qualitatively similar. That is, the month-to-month variability of the intensity, position, etc. of the major current regimes of the Gulf exhibit similar properties in the solutions of both models. The quantitative aspects of the circulation (i.e. current directions and speeds at a particular point) simulated by either model

can not be evaluated without further analysis.

Therefore, the description of the Gulf circulation will focus on the results of the primitive equation model. The assumptions used in the development of this model are less restrictive than those of the geostrophic model. For instance, the numerical model simulates absolute velocities rather than relative velocities, the numerical model does not use extrapolation techniques when large depth changes occur as does the geostrophic model, and the numerical model includes some effects of friction on the continental shelf.

The horizontal spatial resolution of the numerical model is $1/2^{o}$. Seven layers, with varying thicknesses, are modelled in the vertical. The mid-points of each level are taken as the model depths; 35.0 m, 145.5 m, 369.5 m, 768.0 m 1369.5 m, 2145.5 m, and 3035.0 m. The coefficients of friction, are specified as; lateral coefficient of friction, 4×10^{7} cm^{2}/sec; vertical coefficient of friction, 1 cm^{2}/sec; and bottom coefficient of friction (applied only where the shallowest layer exists), $7 \times 10^{-8} sec^{-1}$.

The total transport through the Yucatan Straits for the time increment modelled is obtained from Figure 25. The condition that the flow does not change direction at the open boundaries is applied. The wind stress distributions used to specify the surface boundary conditions are given in Figures 18 to 23. Finally, a steady-state solution is attained

in a particular experiment when the time rate of change of the total energy is less than a prescribed constant.

Geostrophic velocities are computed relative to the 1000 db and 250 db pressure surfaces. Below 1000 db, the observed speeds are small (Nowlin, 1972), and few data have been collected. Geostrophic currents can be computed on portions of the continental shelf if the reference level is 250 db.

The annual circulation patterns simulated by both models are presented first to establish the framework for the following discussions. An experiment in which the form of the average annual temperature and salinity profiles is changed is described next. Finally, the results of the bi-annual, monthly, and synoptic circulation studies are reviewed.

1) Annual Circulation

Surface velocities and total volume transport stream functions determined by the primitive equation model for the annual increment are given in Figure 28. The circulation patterns computed for the 145.5 m, 369.5 m, 768.0 m, and 1369.5 m levels are similar to the surface patterns, except that the velocities are lower at each subsequent level. The flow in the bottom two layers, centered at 2145.5 m and 3035.0 m, are much weaker, and it is difficult to discern consistent circulation patterns. The results of the bi-annual, monthly and synoptic experiments exhibit similar velocity profiles. Therefore, the circulation fields

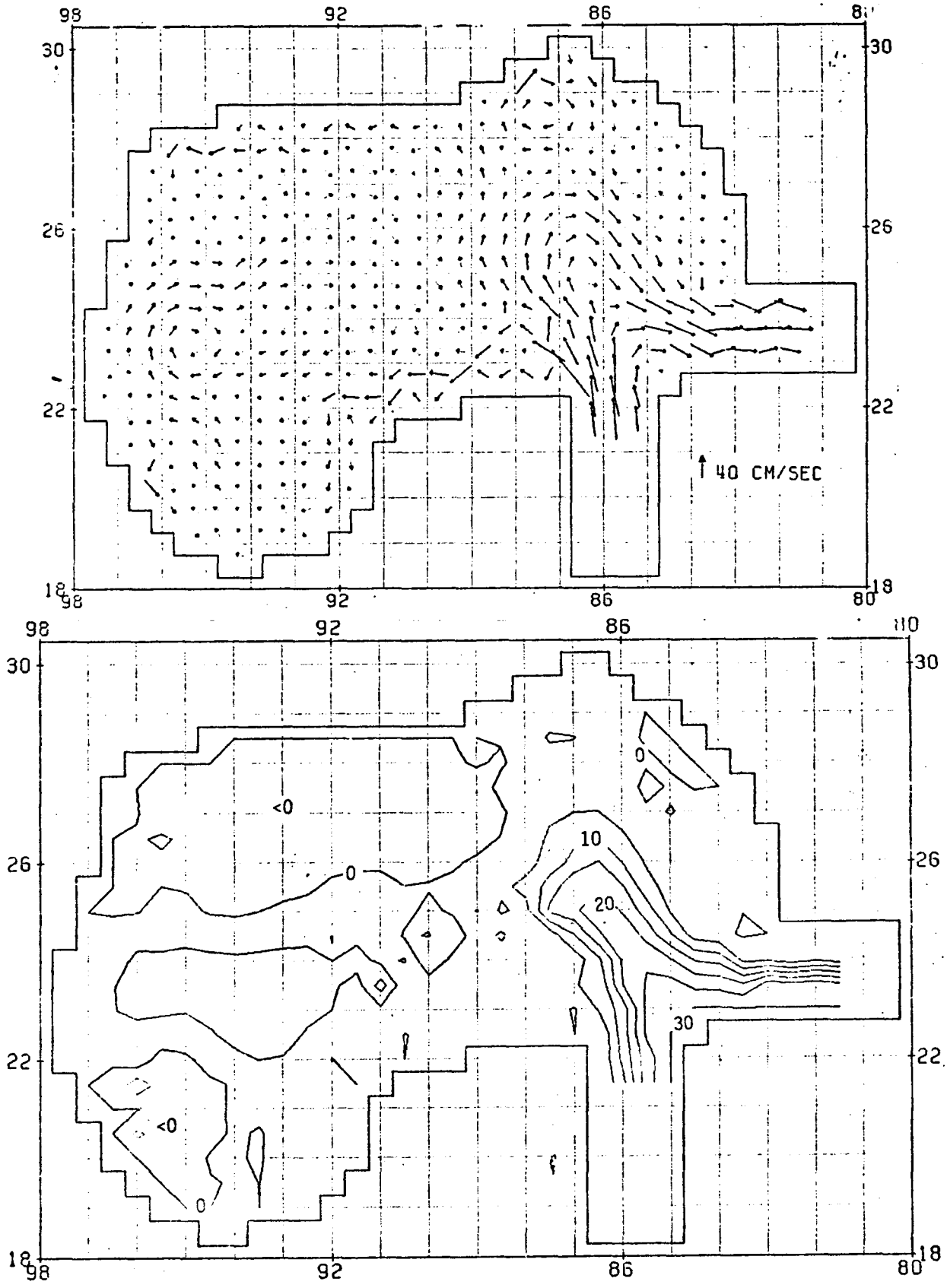

Figure 28. Upper panel. The steady state surface velocity vectors computed by the primitive equation model for the annual increment. Arrows with lighter shafts indicate speeds of less than 5 cm/sec. Lower panel. Streamfunctions of total volume transport for the annual increment. Contour interval is 5X10^6 m^3/sec.

for all levels except the surface are given in Appendix I.

Geostrophic current distributions computed relative to 250 db and 1000 db are given for the annual increment in Figure 29. The dynamic height maps from which these currents are computed and the distribution of data points are given in Appendix II. Vertical sections of geostrophic velocity computed relative to the 1000 db surface were constructed. These sections indicate that the majority of the geostrophic flow is above 700 m, with the speeds normally decreasing monotonically with depth. Therefore, only four representative sections for each geostrophic computation are given in Appendix II.

The circulation will be described in terms of the six large-scale gyres which are evident in Figures 28 and 29. The abbreviations to be used for each gyre are given on Figure 28. The anticyclonic (clockwise circulation) Loop Current, (LC in following discussions) is the largest and most intense circulation feature in the Gulf of Mexico.

The West Central Gulf of Mexico Gyre (WCG), an anti-cyclonic feature, is centered at approximately 23.5°N and 95.5°W. A cyclonic gyre (counterclockwise circulation) in the Bay of Campeche (BCG), 20.5°N, and 95°W, is a feature of the annual circulation. To the north of the WCG,a cyclonic current pattern is found along the Texas-Louisiana Shelf, heretofore referred to as the Texas-Louisiana Gyre (TLG).

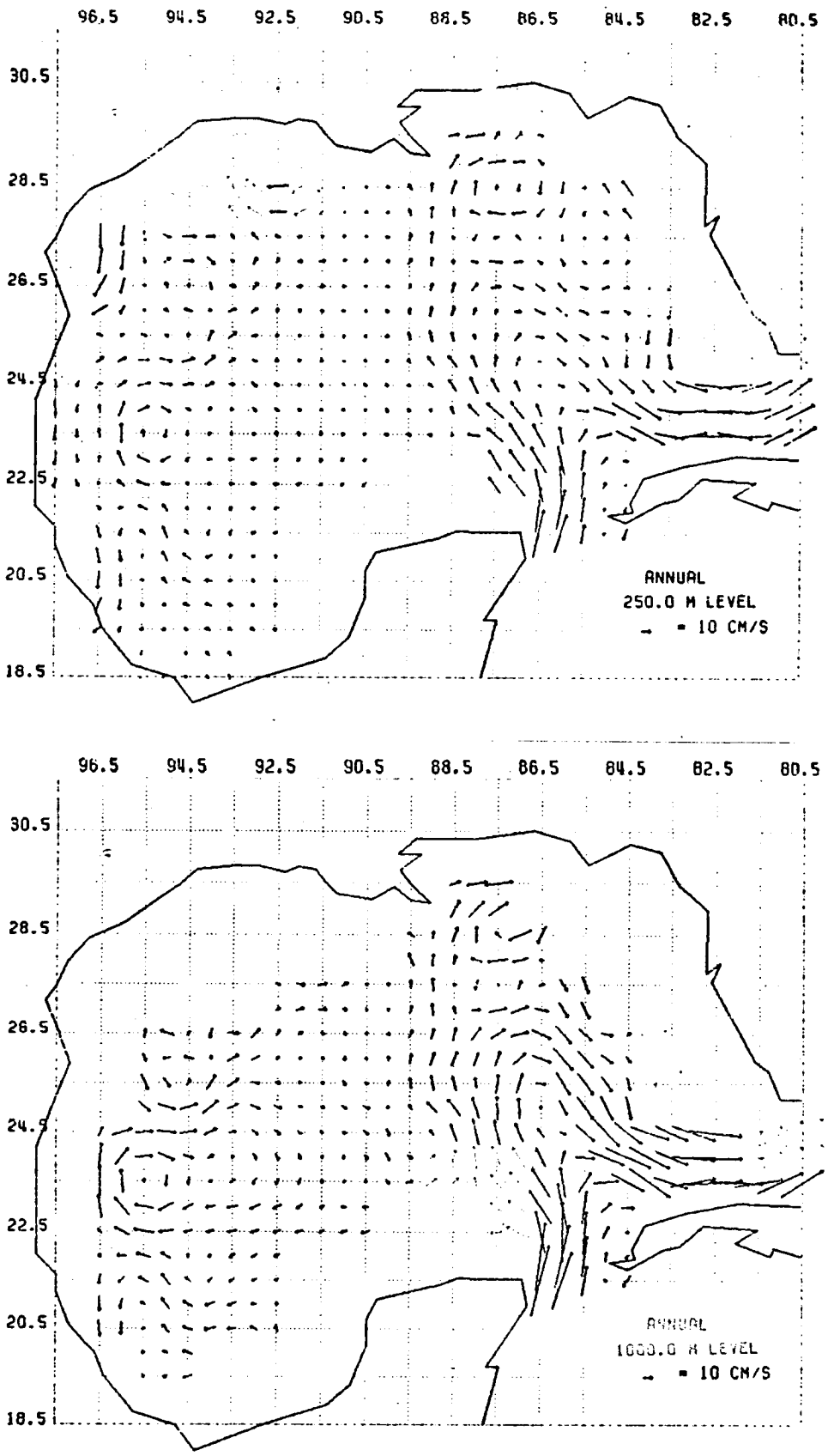

Figure 29. Upper panel. Geostrophic surface velocity vectors computed relative to the 250 db pressure surface for the annual increment. Lower panel. Geostrophic surface velocity vectors computed relative to the 1000 db pressure surface for the annual increment. Arrows with lighter shafts indicate vectors determined from extrapolated data.

This elongated and narrow feature has a wave-like southern boundary and extends from the Mississippi Delta to the Texas Shelf.

The De Soto Canyon Gyre (DCG) is centered at 28.5° and 87°W, approximately at the head of the De Soto Canyon (Figures 28 and 29). Finally, the west Florida Shelf Gyre (WFSG) is a weak cyclonic current feature centered at 27.5°N, and 85.5°W.

Five of the six gyres have been identified previously For instance, Leipper (1970) discussed the LC; Nowlin (1972), the WCG and BCG; Gaul (1967), the DCG; and Ichiye, Kuo, and Carnes (1973), the WFSG. The TLG has been observed in the form of an intermittent westerly current flowing along the Texas continental shelf (Nowlin, 1972).

2) Varying Input Data

Mean annual temperature and salinity profiles averaged by 1° square were computed by NODC. Dynamic height topographies and geostrophic velocity maps were computed from these data. These maps are compared to charts prepared using the T-S mating technique described earlier. The comparison is made to evaluate qualitatively the reliability of the data obtained from the mating scheme.

Figure 30 presents geostrophic velocities computed relative to 1000 db from the 1°square temperature,and salinity data. The large scale circulation features discussed previously in relation to Figure 29 are found in Figure 30, with only minor differences in the velocity distributions.

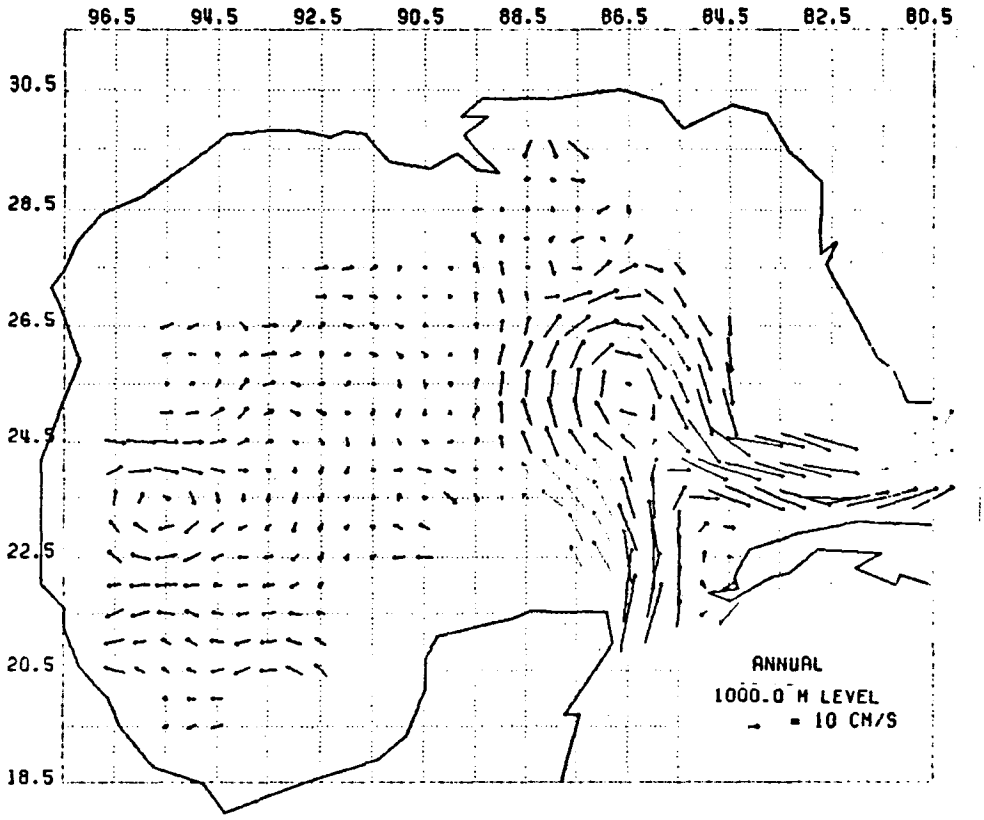

Figure 30. Geostrophic surface velocity vectors computed relative to the 1000 db pressure surface for annual increment dynamic height data. The latter determined from 1° square average temperature and salinity profiles.

3) Bi-annual circulation

The 1^{o} square temperature data are averaged over two five-month periods; the resulting temperature distributions are presented as the average summer (May to September) and winter (November to March) conditions. These average temperature profiles are mated to salinity values by the method described previously.

The surface circulation and volume transport distributions determined from the primitive equation model for the summer and winter seasons are given in Figures 31 and 32. Summer and winter geostrophic velocities computed relative to the 250 db and 1000 db surfaces are given in Figures 33 and 34.

The summer Loop Current is found farther to the north and west than the winter Loop Current in all data presentations (Figures 31 to 34). The apex of the Loop is at 26.5^{o}N in the summer, and 25.0^{o}N in the winter. The western limb of the Loop extends to 88.5^{o}W in the summer, and to 87^{o}W in the winter.

A portion of the Yucatan Current separates from the main stream to flow along the Campeche Bank in both seasons (Figures 31 and 32). However, the volume transport is not great because of the shallow depths found on the shelf. The current maps for the lower levels, Appendix I, show no consistent flow to the west along the continental slope of the Campeche Bank.

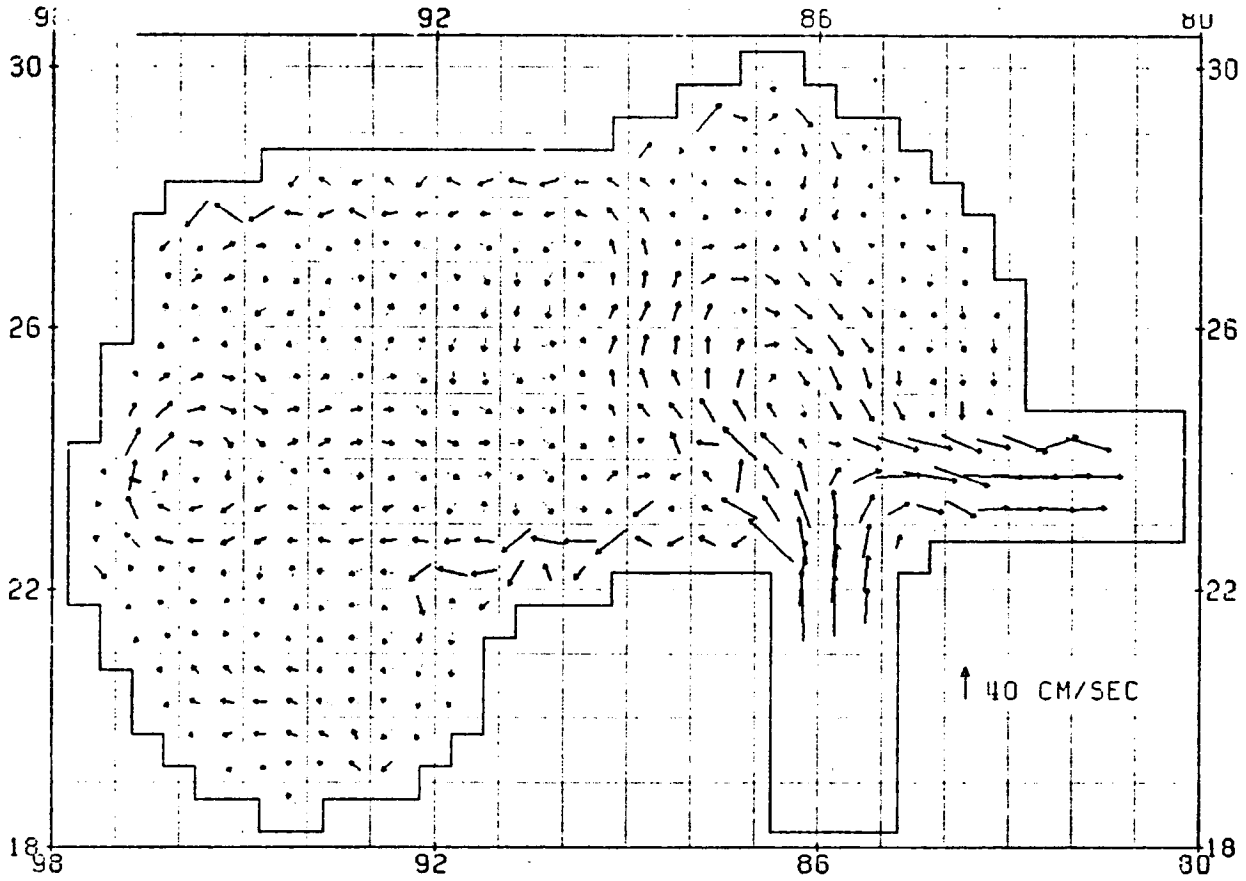

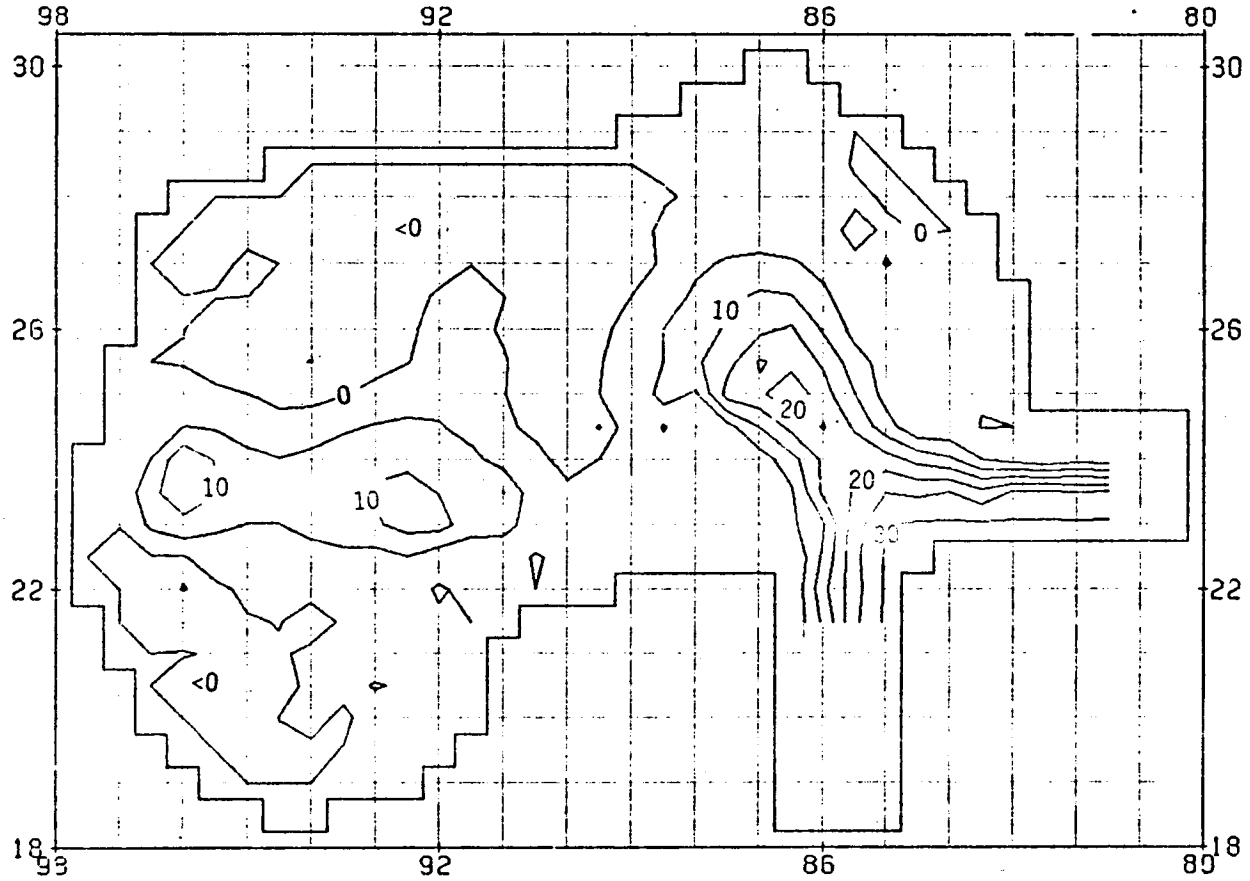

Figure 31. Same as Figure 28 except for the summer season.

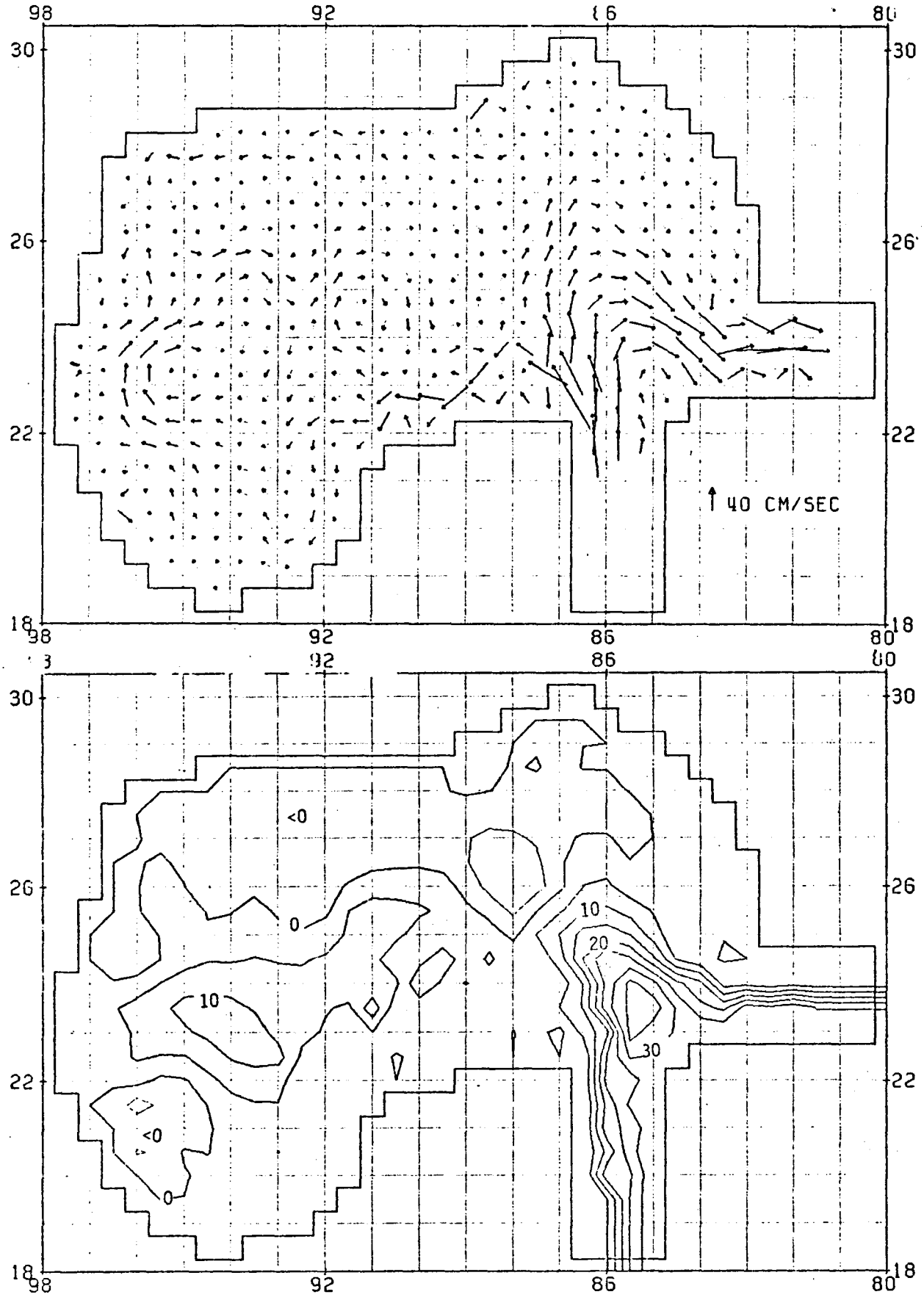

Figure 32. Same as Figure 28 except for the winter season.

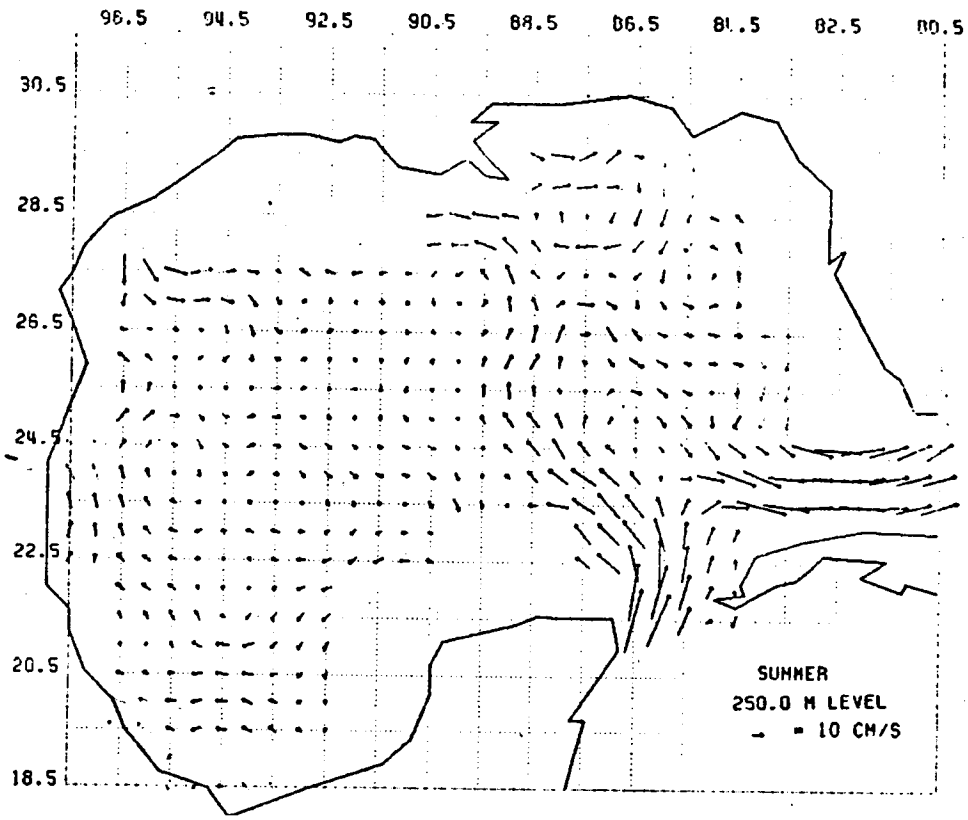

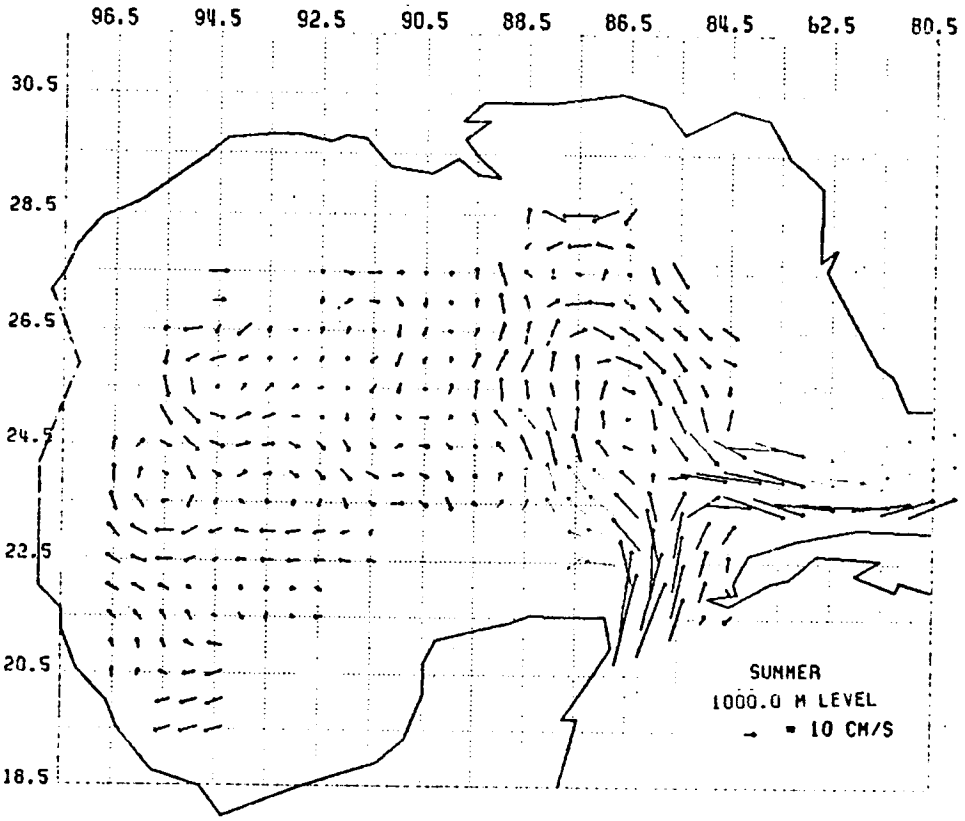

Figure 33. Same as Figure 29 except for the summer season.

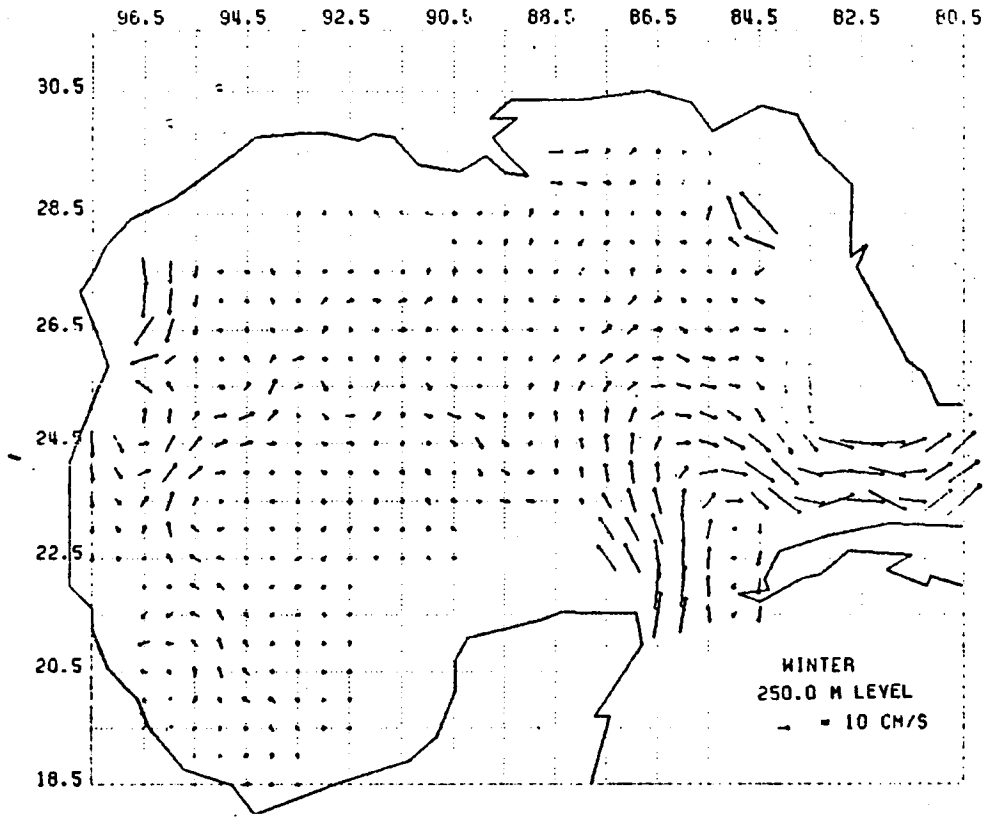

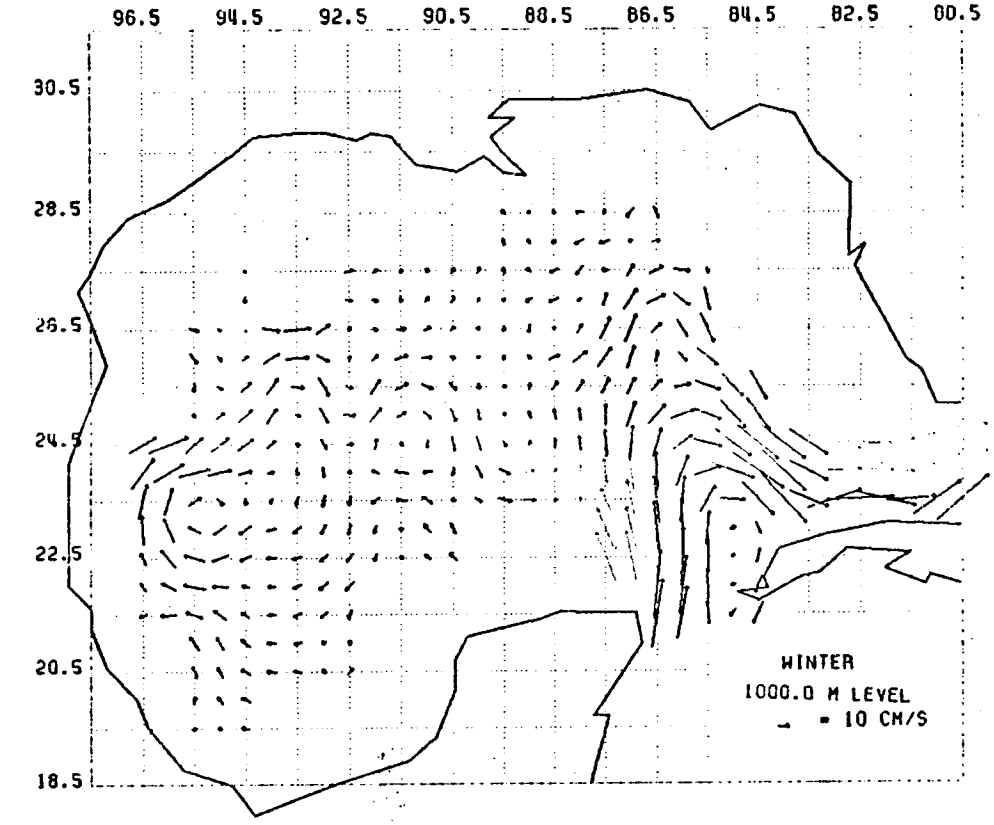

Figure 34. Same as Figure 22 except for the winter season.

The center of the WCG is located farther to the northwest in the summer than in the winter (Figures 31 to 34). The velocities of the northern limb of the gyre appear higher in the winter, but the total volume transport of the eddy is the same in both cases.

The CBG is evident in both volume transport streamfunction maps (Figures 31 and 32) and is discernable at 20.5°N and 96.5°W in the surface velocity maps for the winter (Figure 32).

The TLG extends east to the northeastern Gulf in the winter (Figure 32), but only to the Mississippi Delta in the summer (Figure 31). The northern limb of this gyre is more intense in the summer, and the scuthern limb in the winter.

The DCG and WFSG appear on the surface velocity maps but not on the transport streamfunction maps (Figures 31 and 32). Both gyres appear more developed in the summertime with higher velocities around the DCG (Figure 33).

4) Monthly Circulation

The monthly surface circulation and total volume transport streamfunction maps produced by the primitive equation model are given in Figures 35 to 46. The monthly geostrophic surface velocities compare favorably to the surface current vectors simulated by the numerical model. Therefore, only the January, April, July, and October geostrophic velocities computed relative to the 250 db and

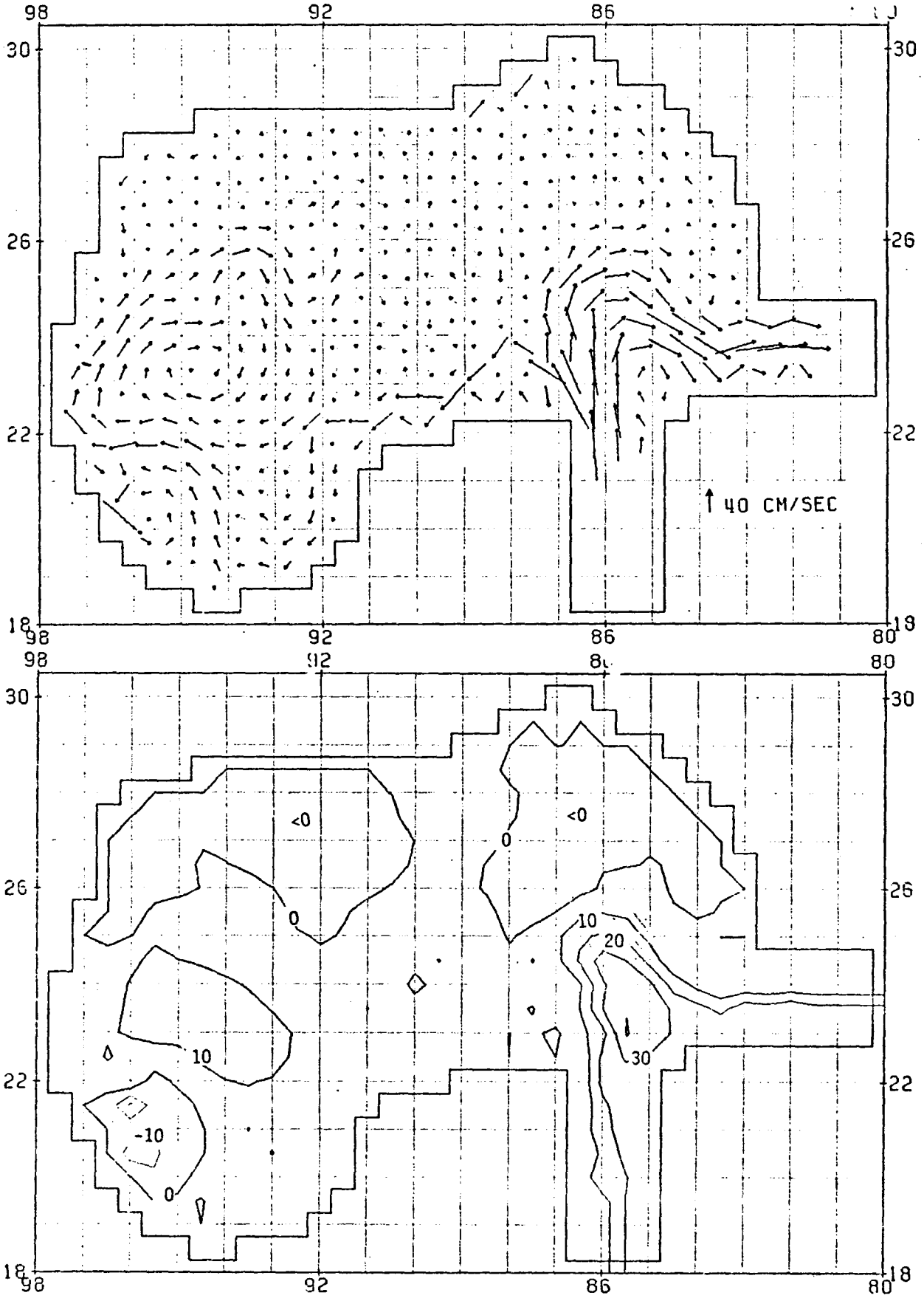

Figure 35. Same as Figure 28, except for the month of January.

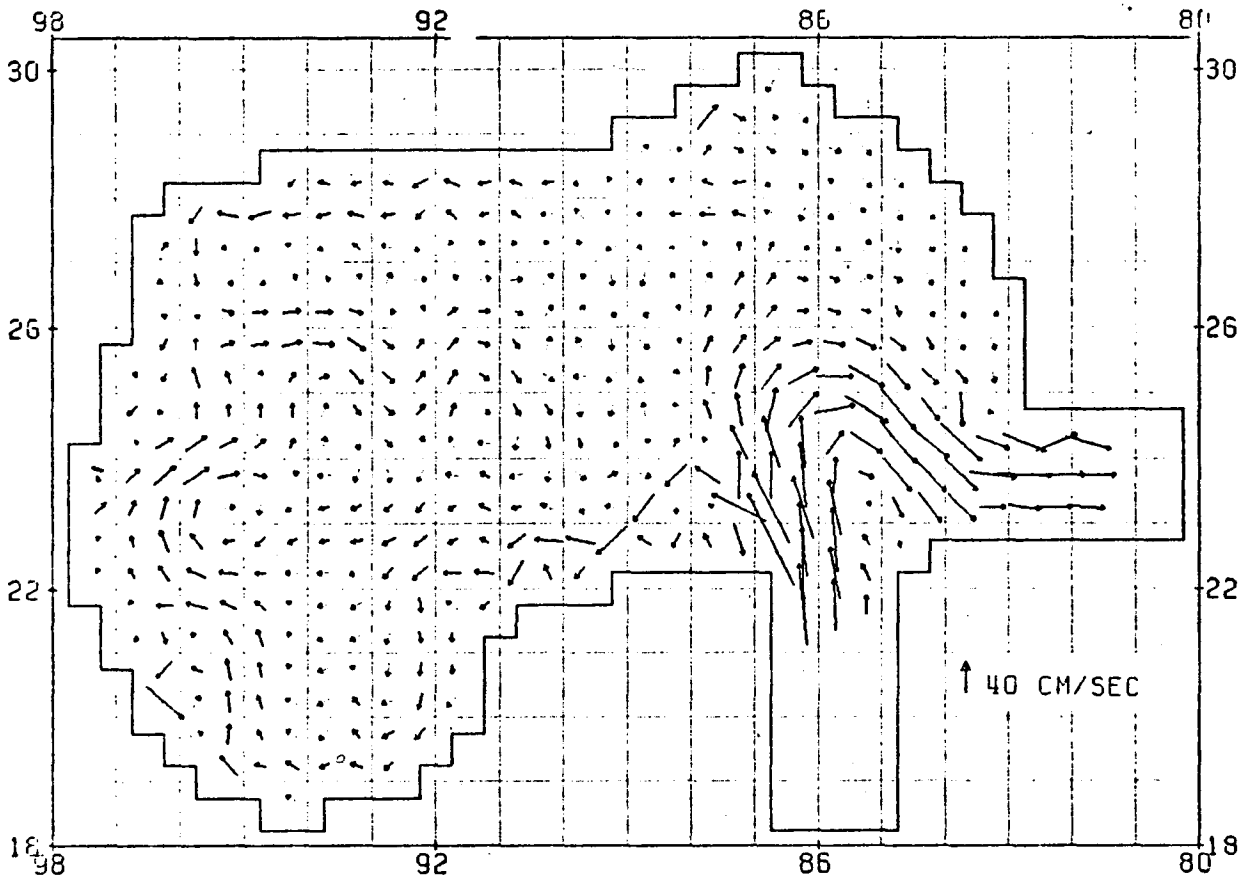

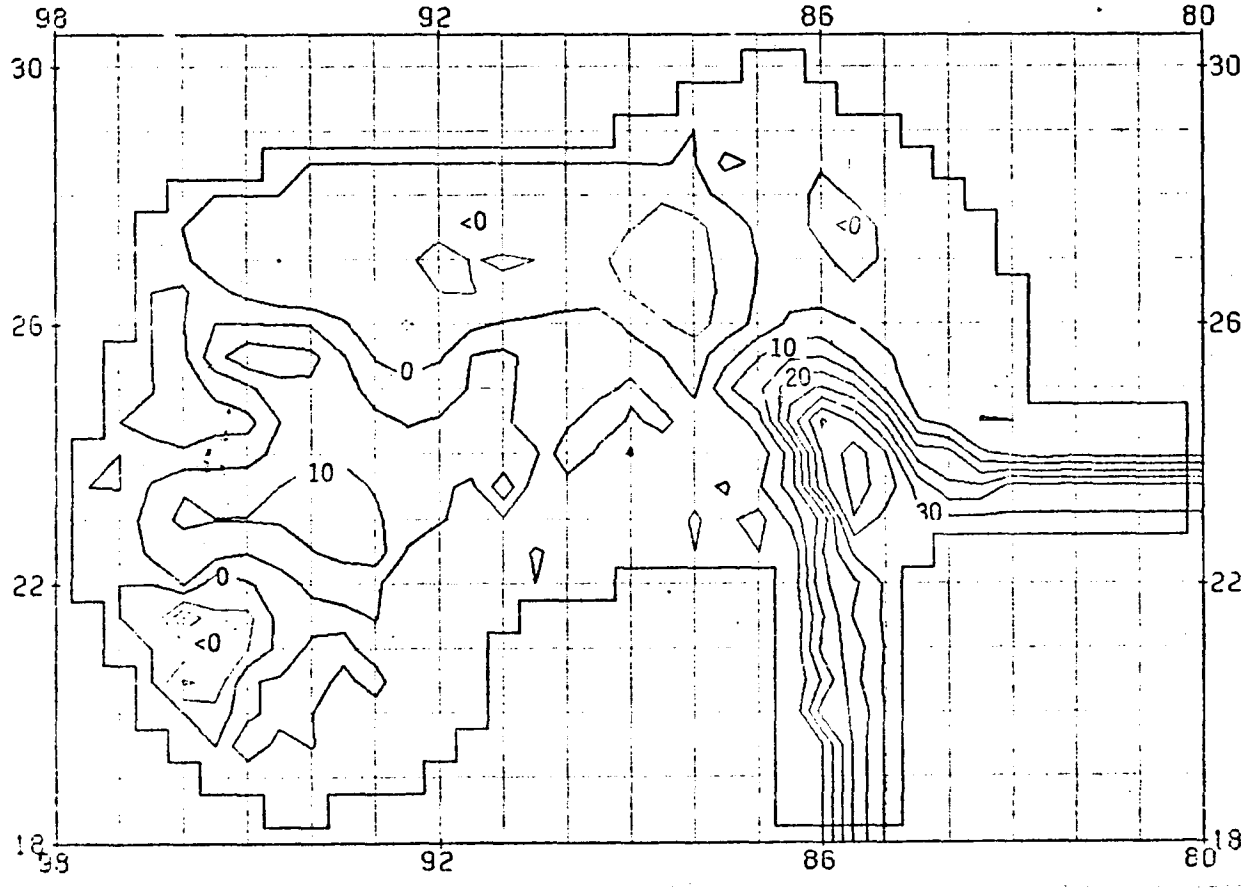

Figure 36. Same as Figure 28, except for the month of February.

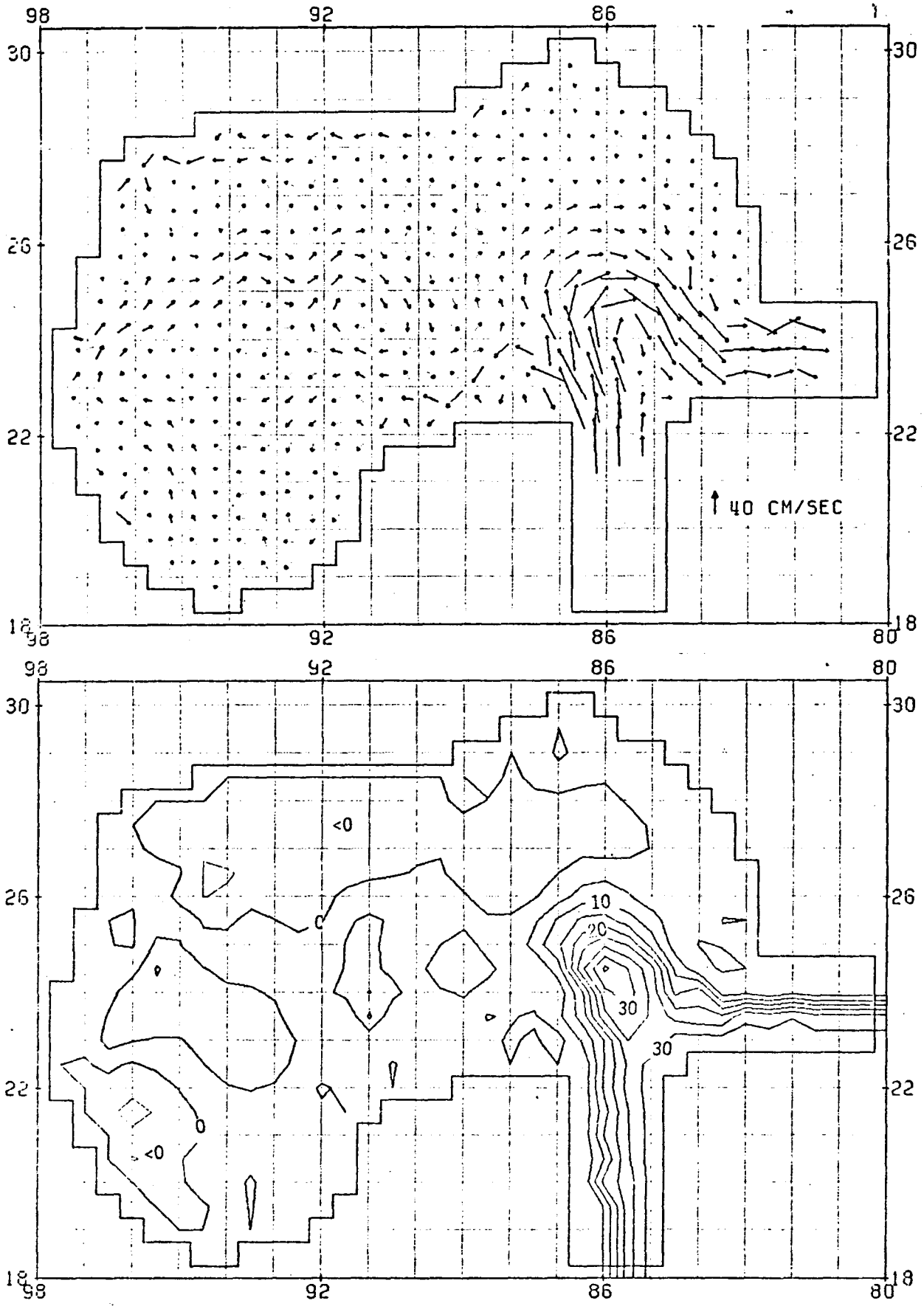

Figure 37. Same as Figure 28, except for the month of March.

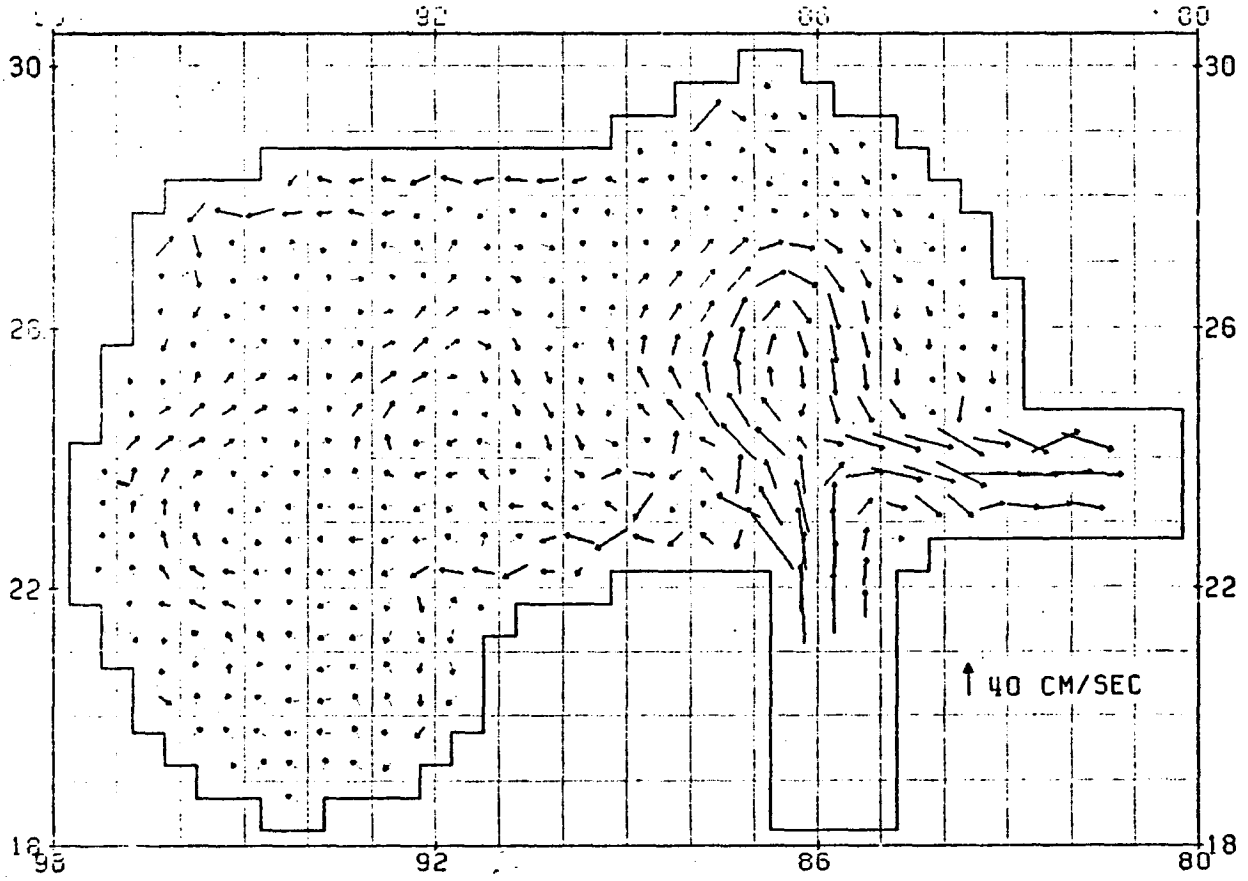

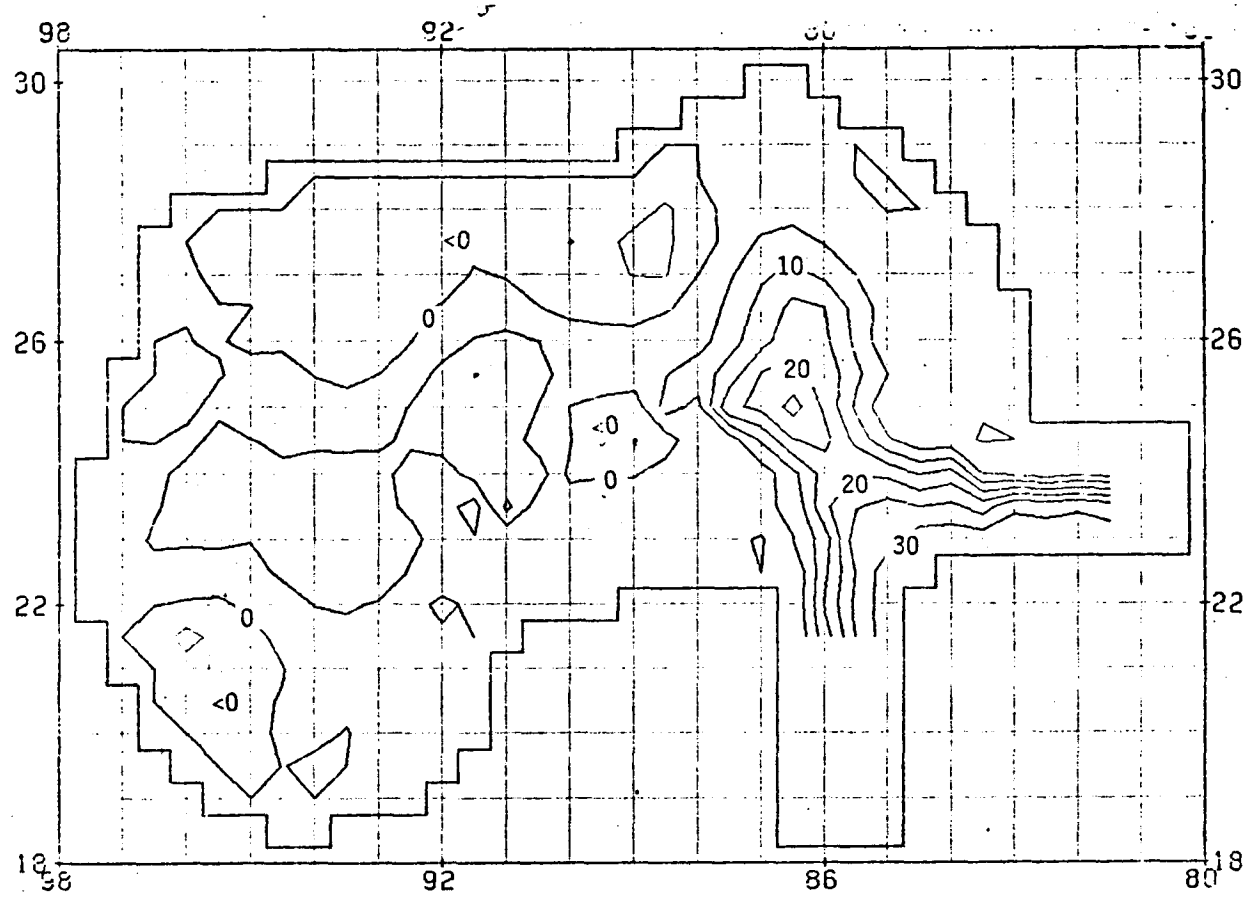

Figure 38. Same as Figure 28, except for the month of April.

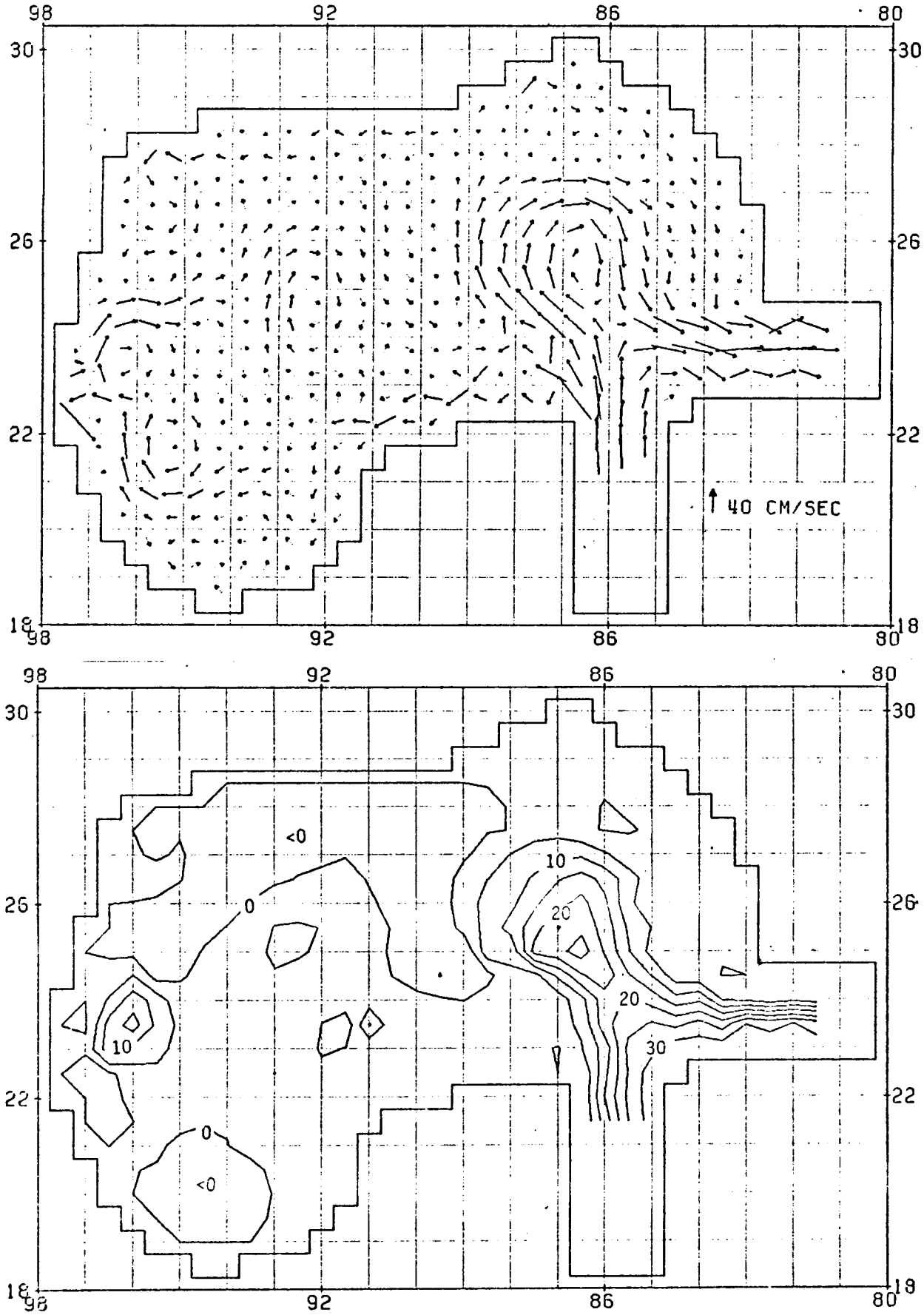

Figure 39. Same as Figure 28, except for the month of May.

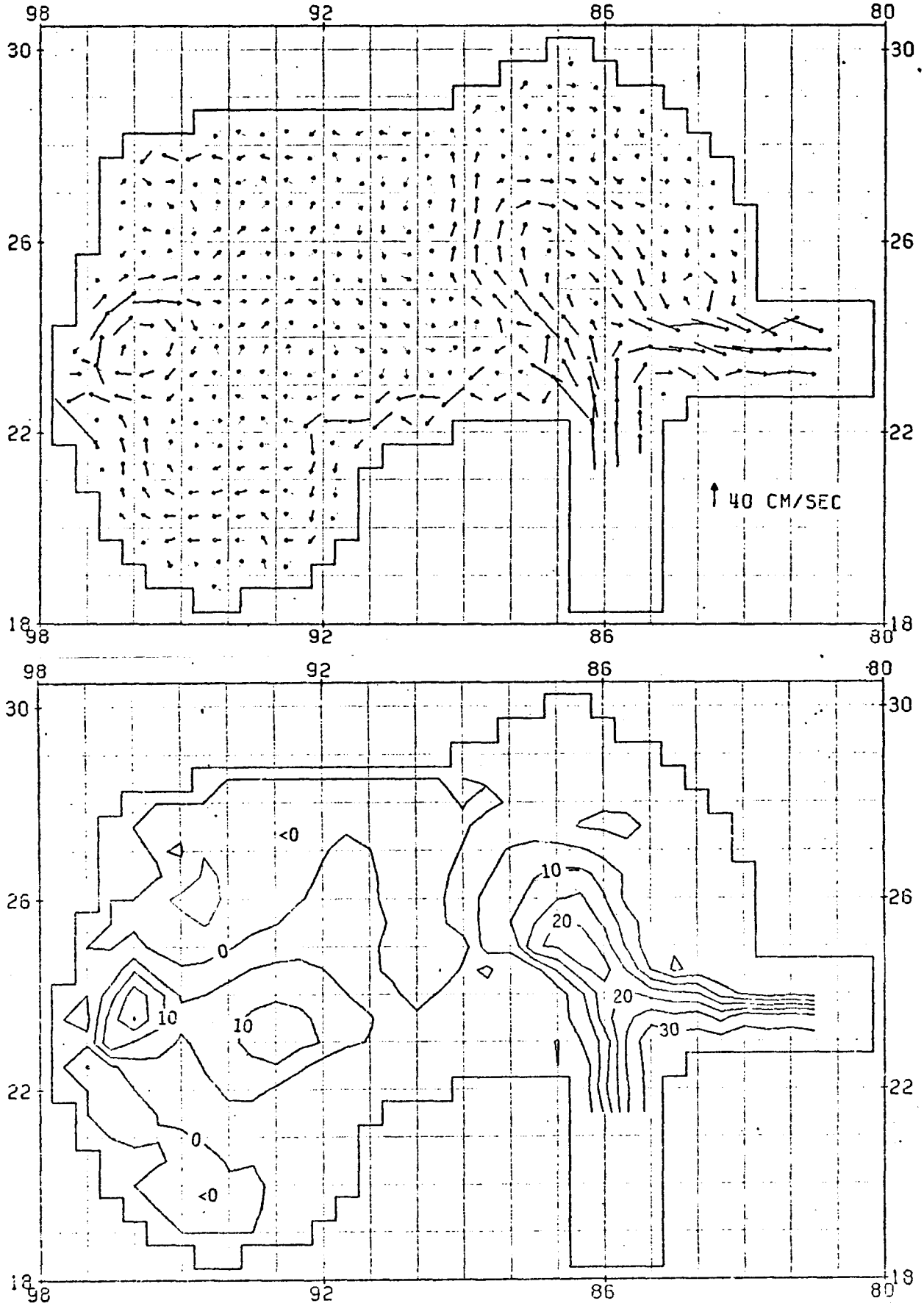

Figure 40. Same as Figure 28, except for the month of June.

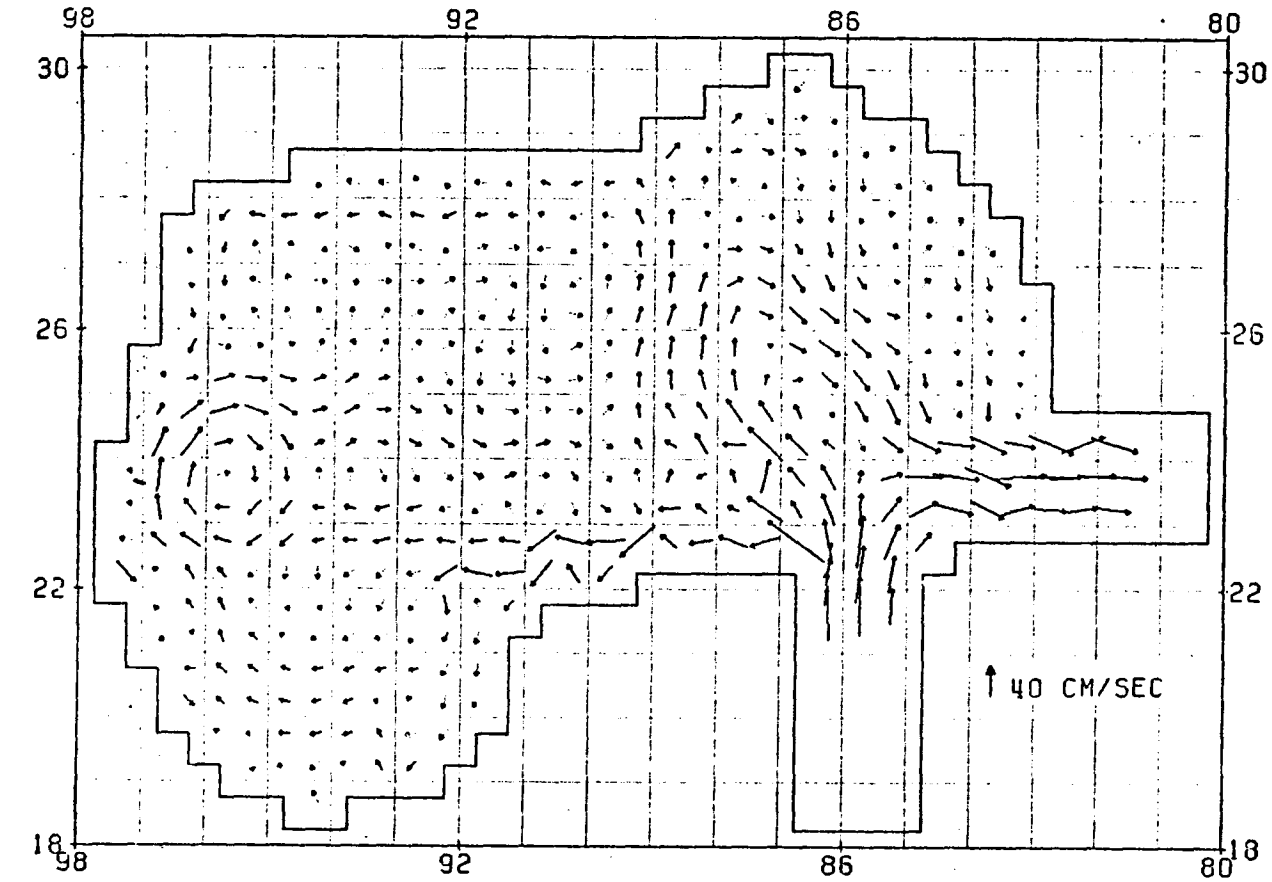

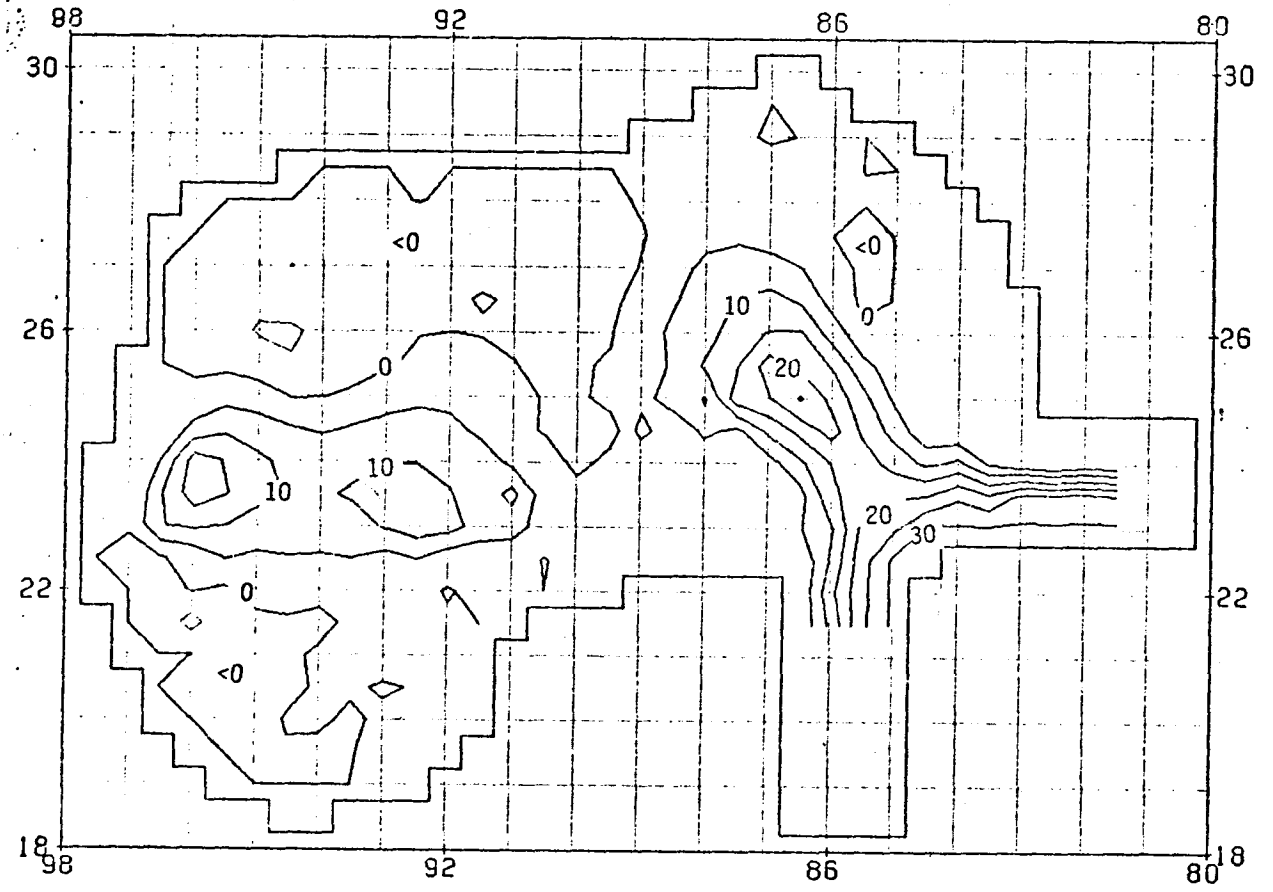

Figure 41. Same as Figure 28, except for the month of July.

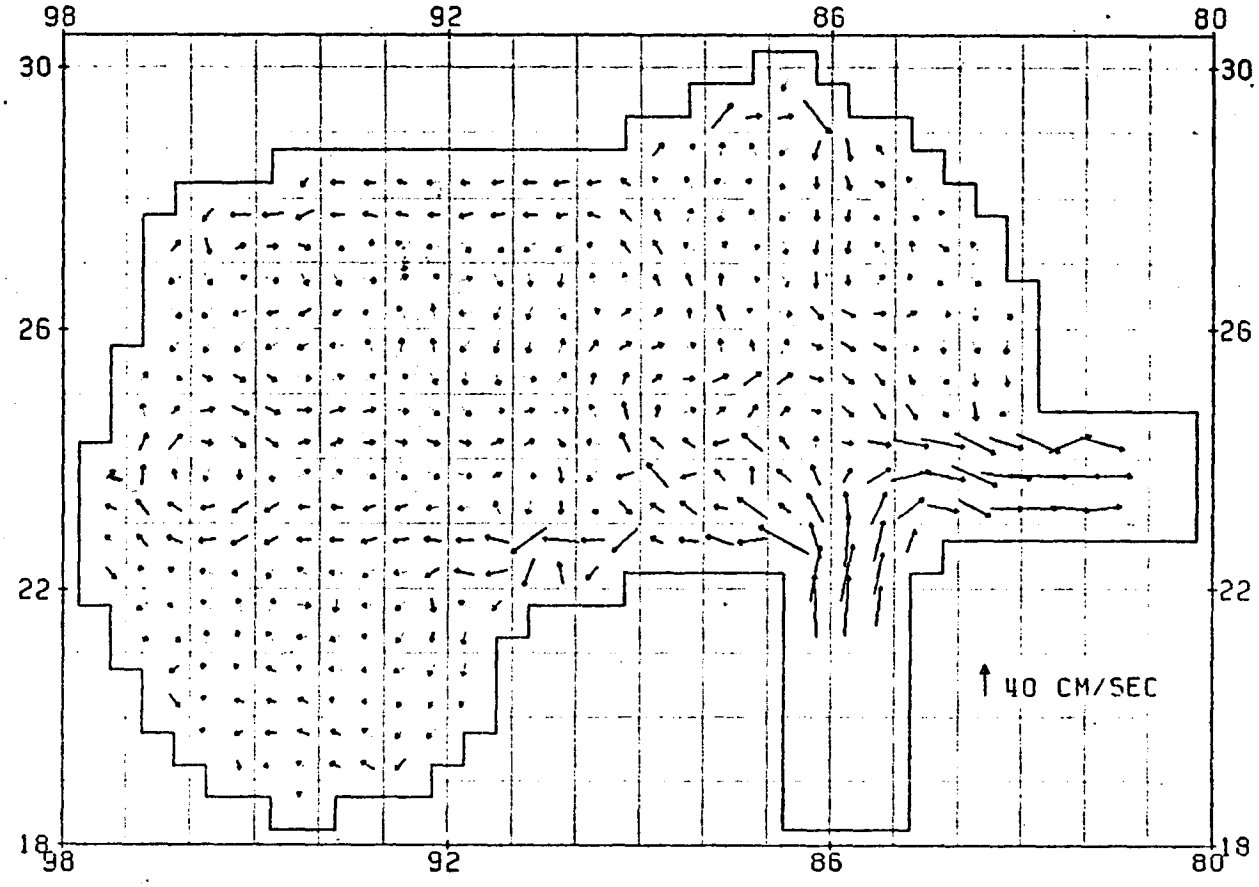

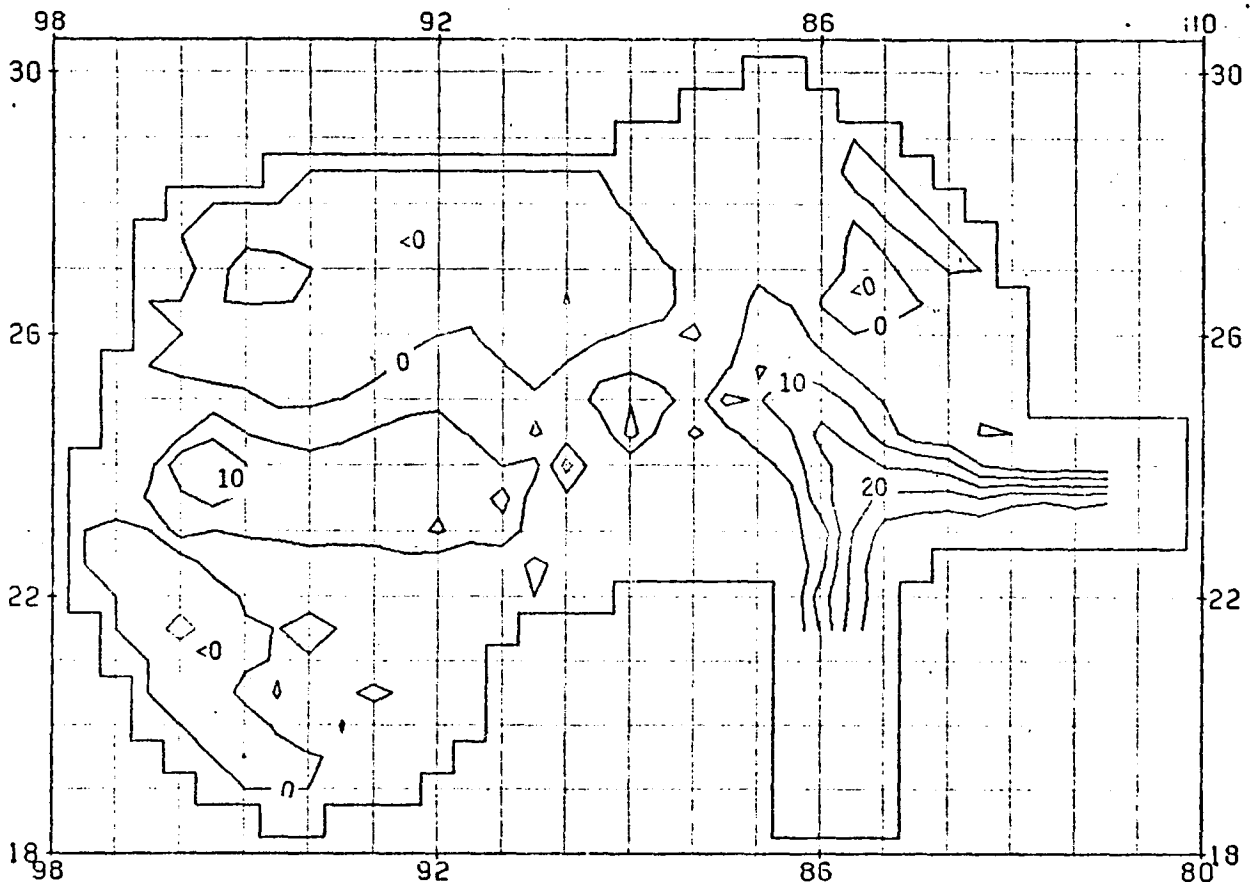

Figure 42. Same as Figure 28, except for the month of August.

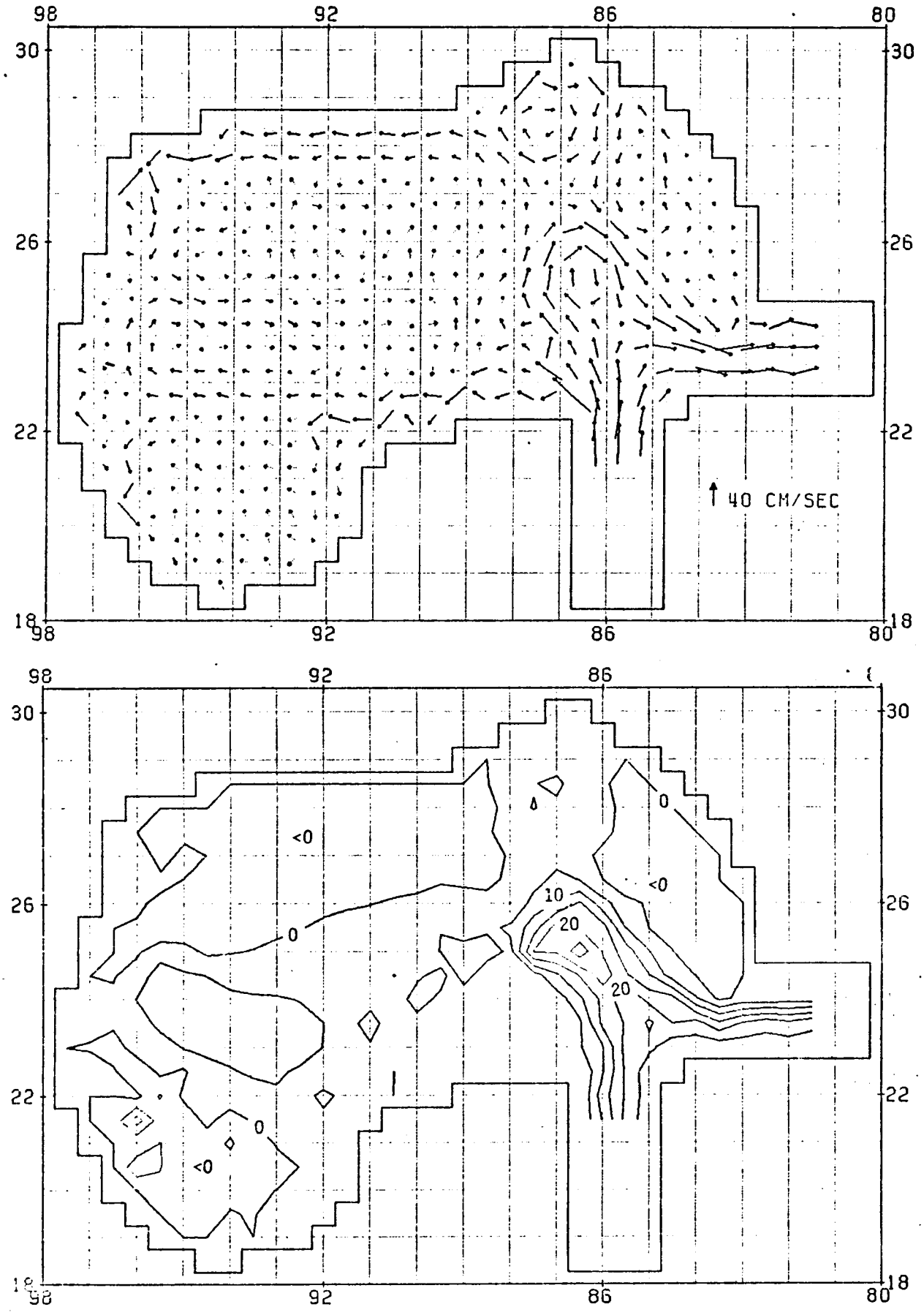

Figure 43. Same as Figure 28, except for the month of September.

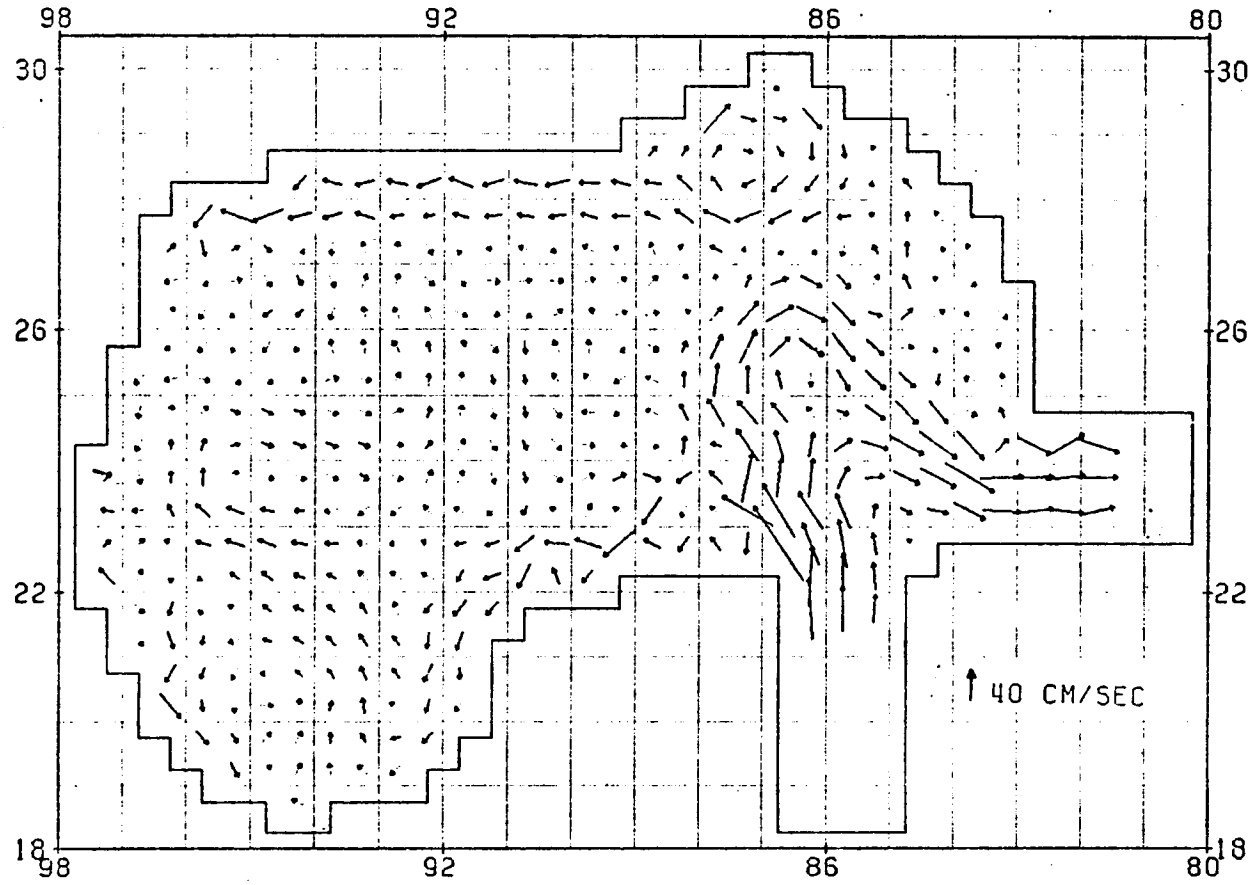

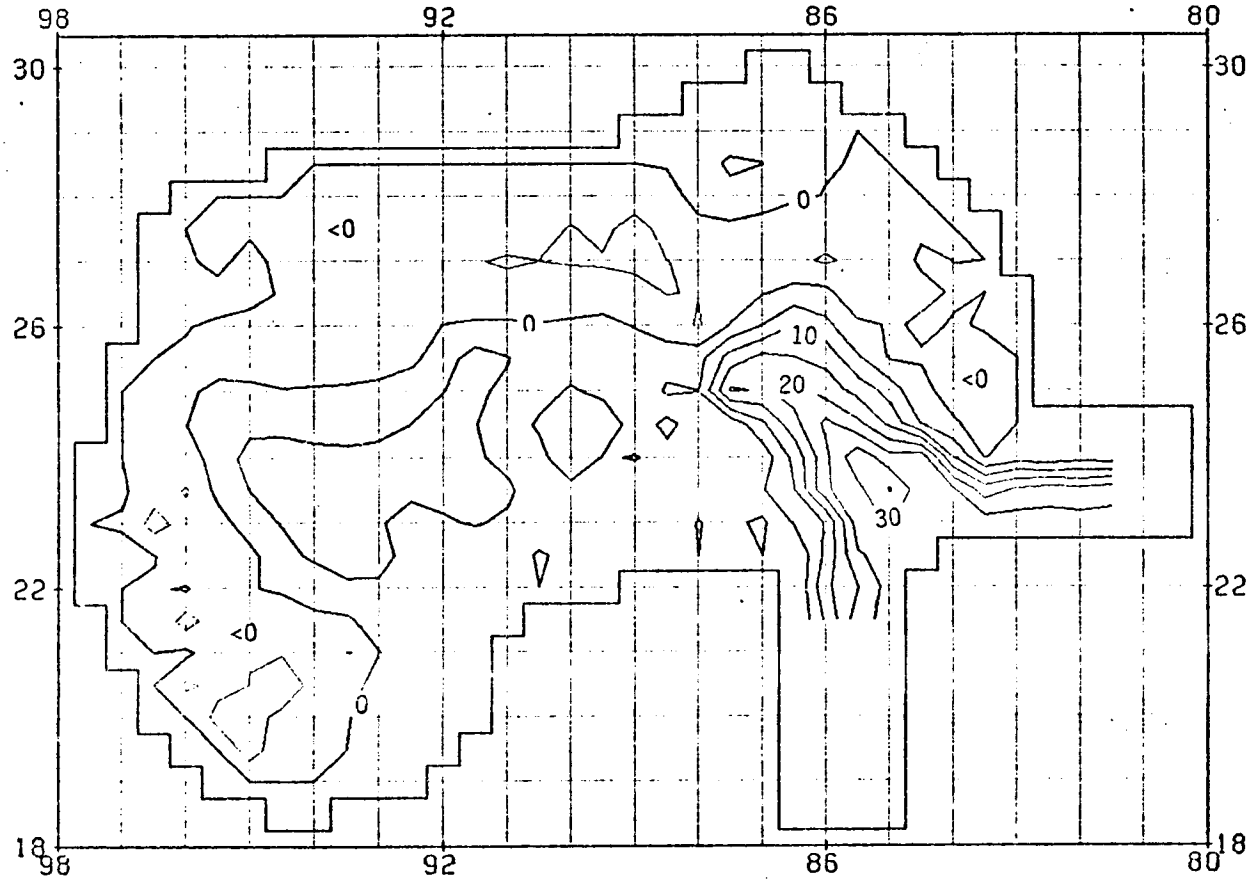

Figure 44. Same as Figure 28, except for the month of October.

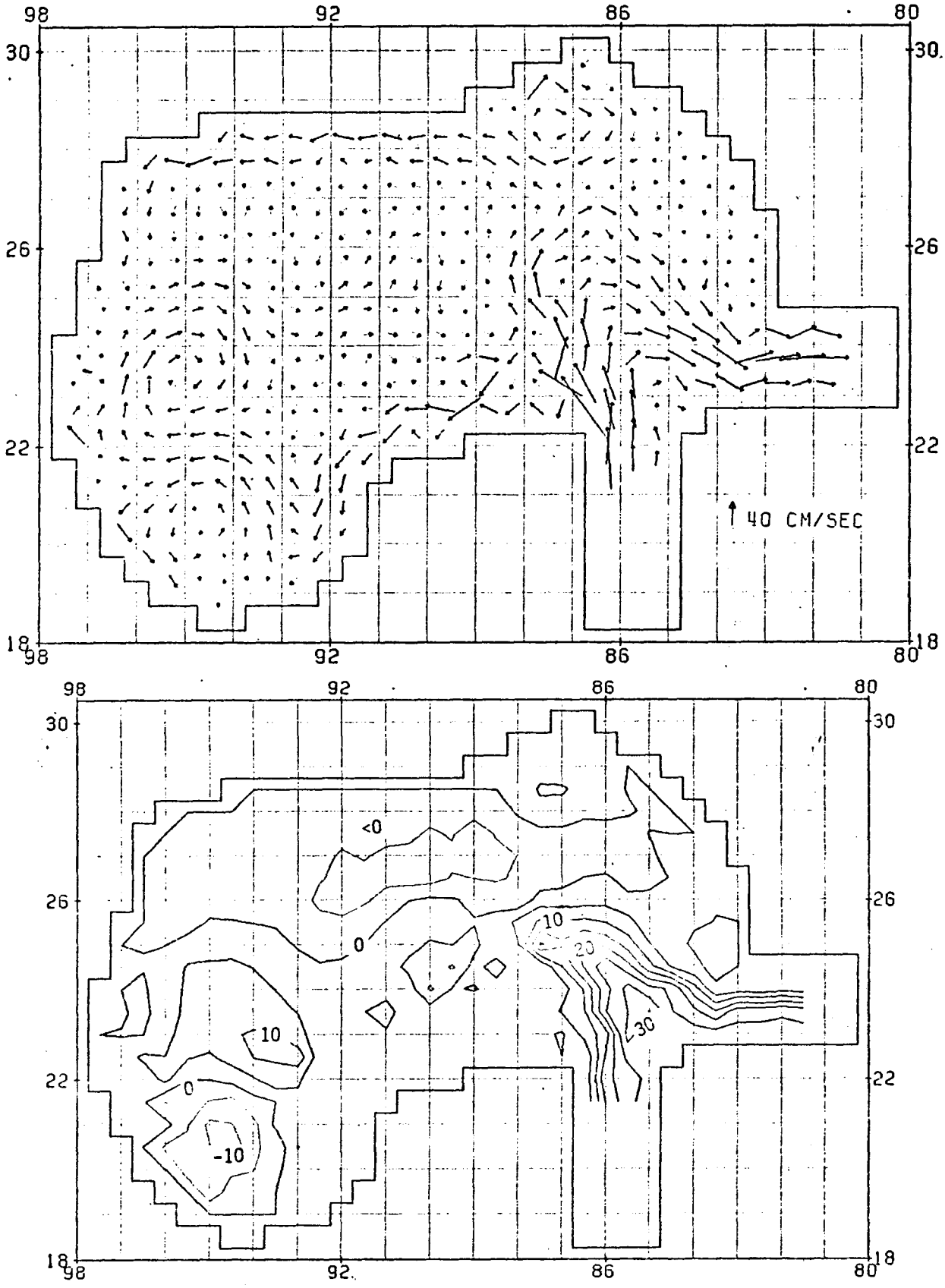

Figure 45. Same as Figure 28, except for the month of November.

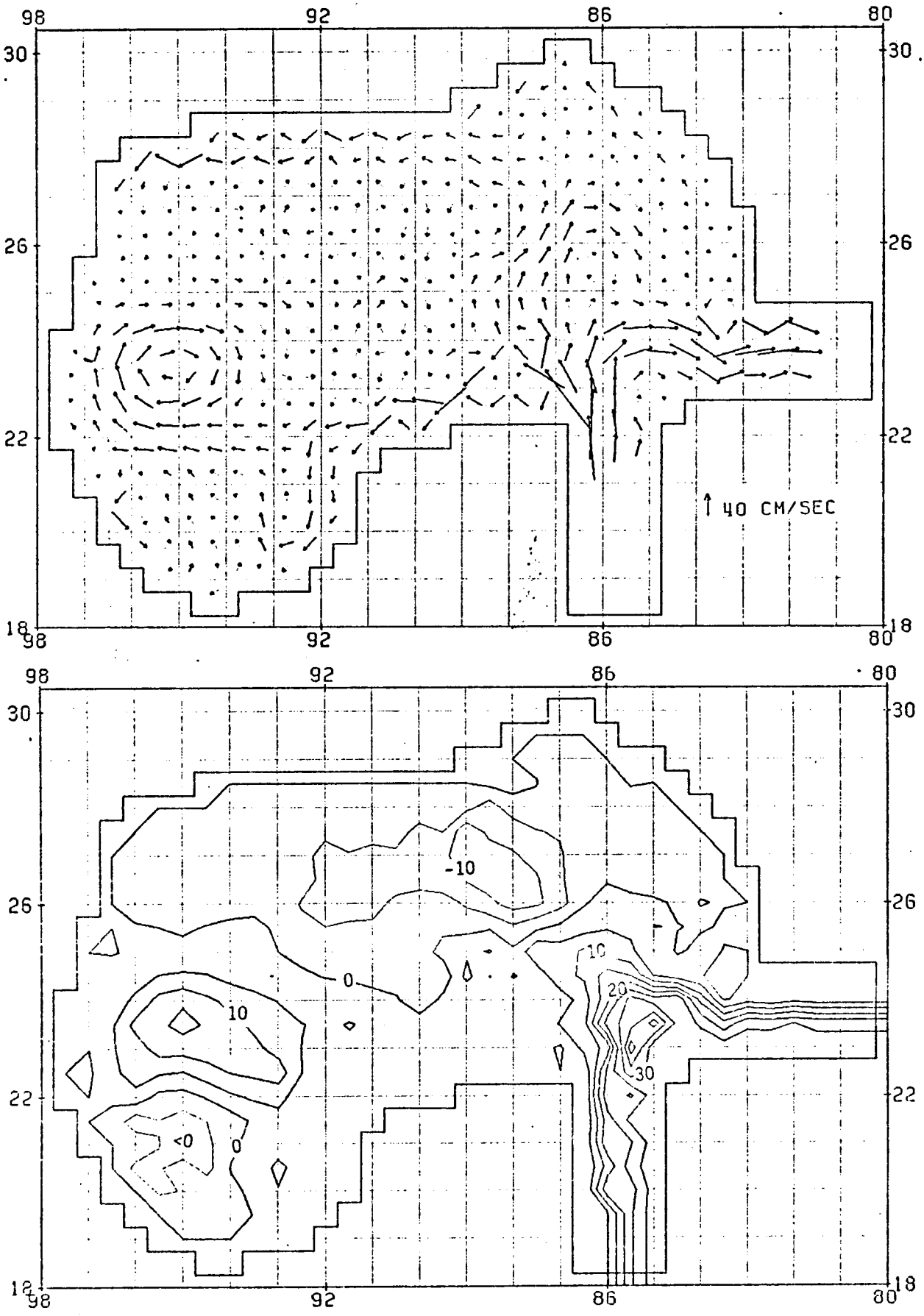

Figure 46. Same as Figure 28, except for the month of December.

1000 db pressure surfaces are given in this section (Figures 47 to 50). The complete set of geostrophic maps and related data is presented in Appendix II.

The Loop Current penetrates farther north and west into the Gulf from January to July. (Figures 35 to 40). In August, the surface manifestation of the Loop axis recedes dramatically to the south (Figure 42). However, in September the Loop appears to reform in the north, and from October to December the Loop recedes to the south (Figures 43 to 46). The apex of the Loop is farthest to the south in December.

In the spring and summer months, April to July, the Yucatan Current appears to split at 24°N and 86°W, with one limb transporting water to the east, and the other to the north. The results of both models exhibit this bifurcation (Figures 38 to 41, and 48 and 49). The interpretation of this feature, assuming the models simulate correctly the circulation fields associated with the input data, raises the fundamental question of what the monthly maps represent.

For instance, do Figures 38 to 41 indicate that during the majority of the April to July cruises a split in the Yucatan Current was observed? Or does the Yucatan Current have two modes, one in which the flow is predominantly to the north and another in which the flow is to the east? Similarly, do the July to September Loop Currents represent a rapid recession and then intrusion of the monthly mean Loop, or is the variability of the Loop Current's position in August responsible for the observed circulation?

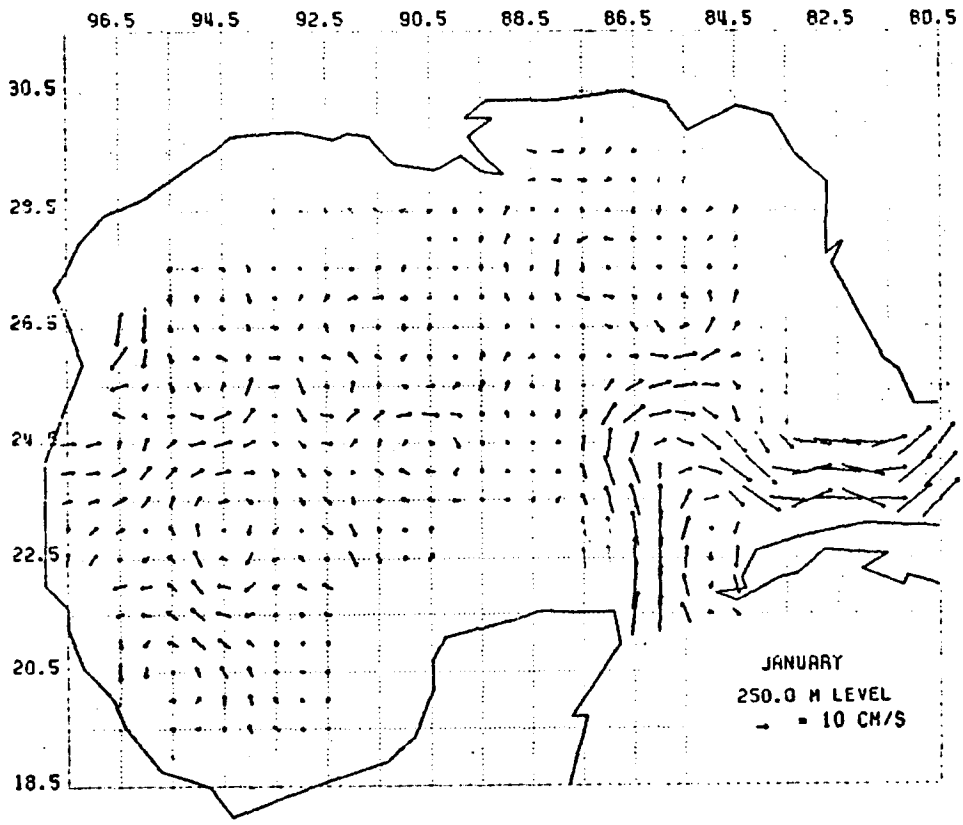

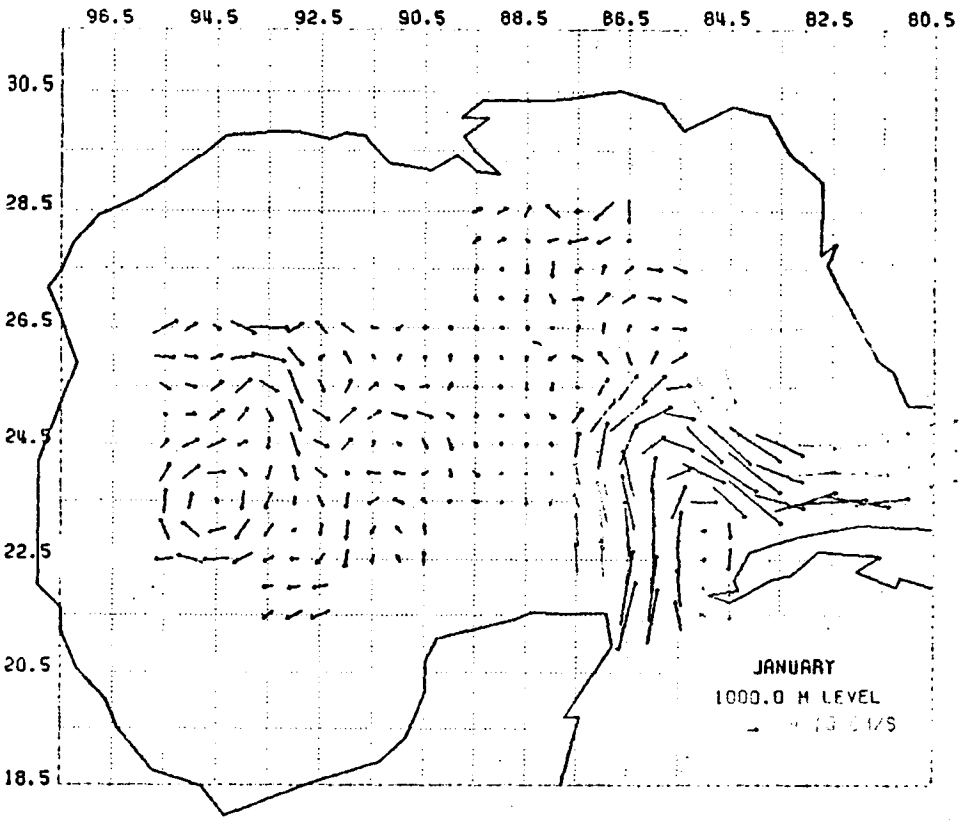

Figure 47. Same as Figure 29, except for the month of January.

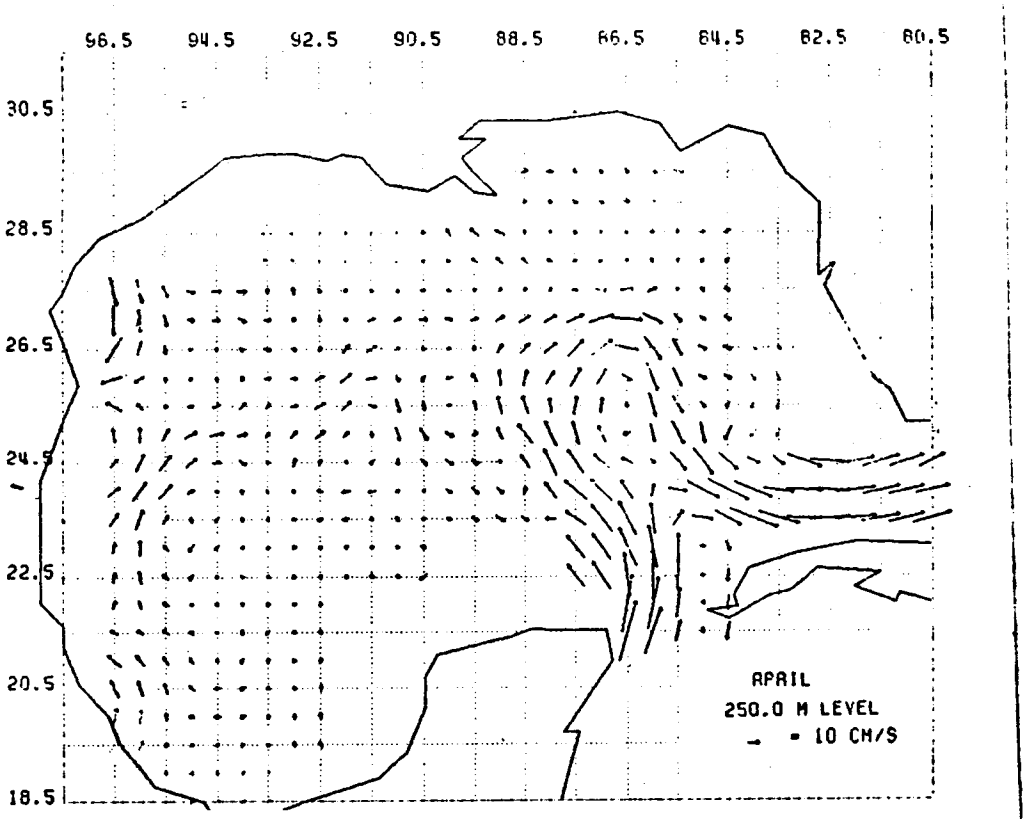

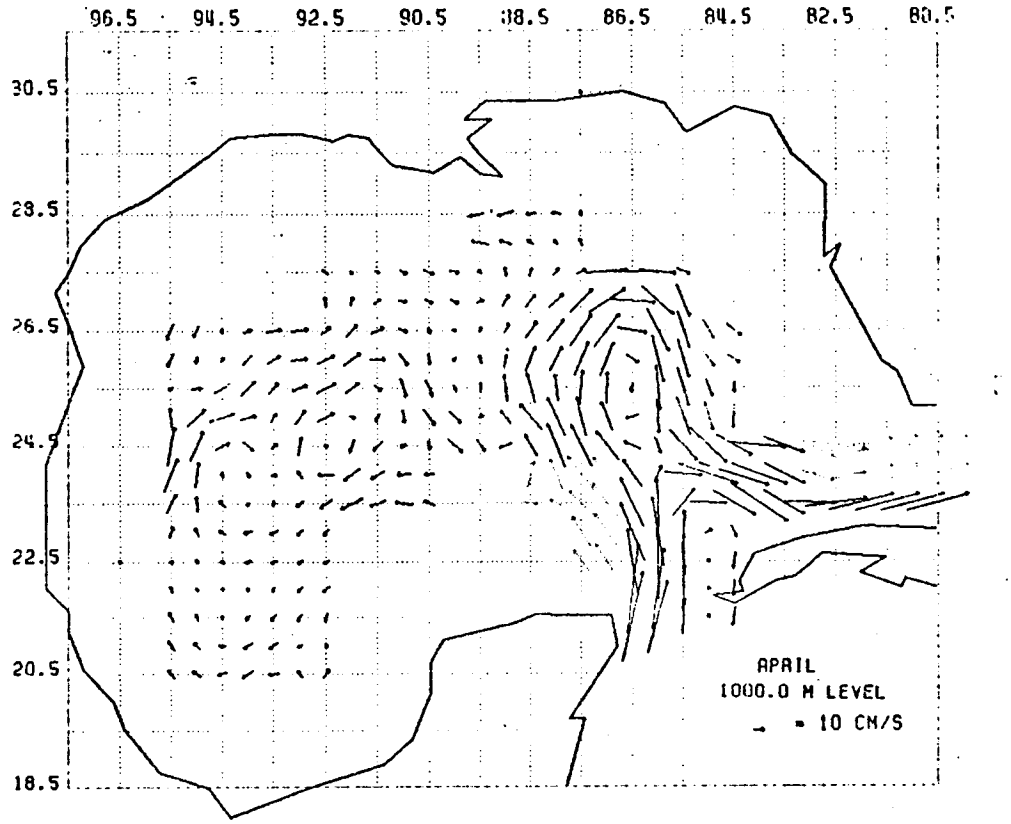

Figure 48. Same as Figure 29, except for the month of April

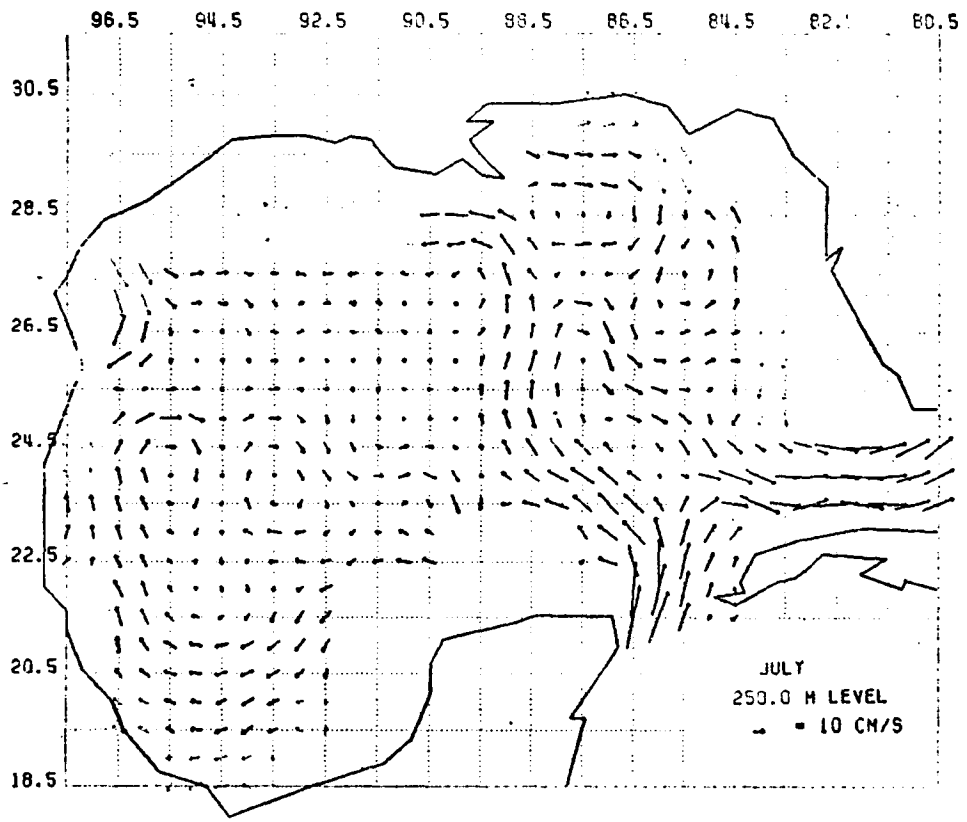

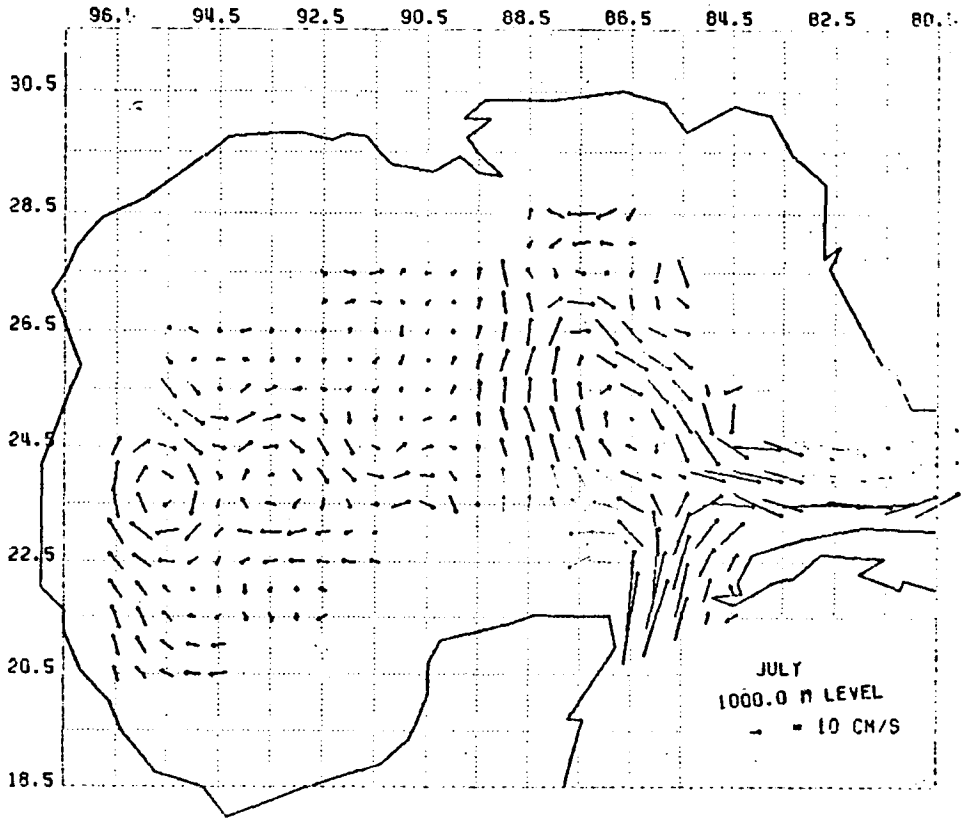

Figure 49. Same as Figure 29, except for the month of July.

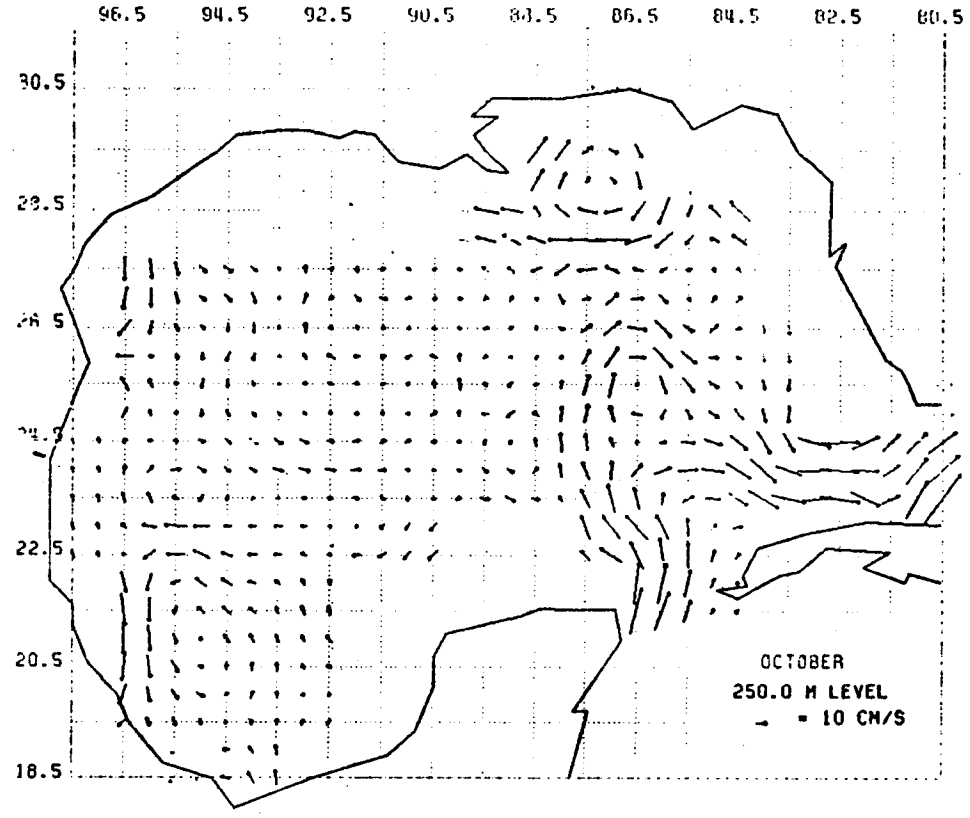

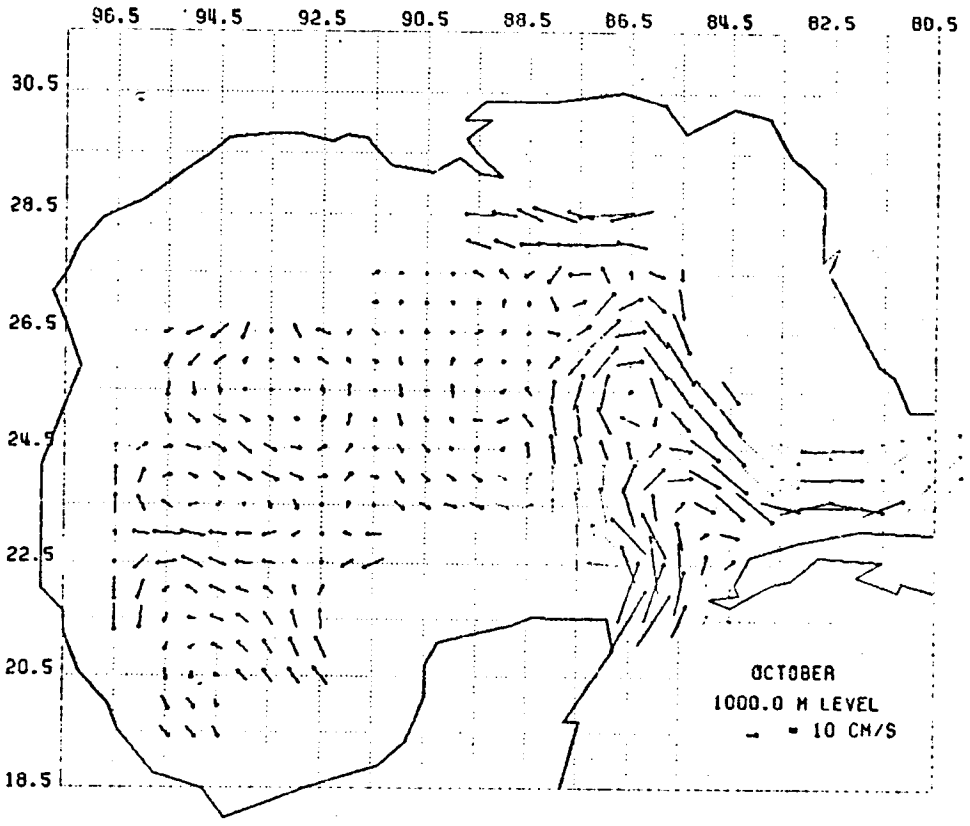

Figure 50. Same as Figure 29, except for the month of October.

A measure of the variability of the flow during the monthly increments is required to address these questions. The problem of the variability of the flow has not been considered in a quantitative study, but some qualitative statements can be made about the variability of the Loop Current during the monthly increments.

The variability of the current regimes in other portions of the Gulf within each month can not be discussed at this time because of the lack of appropriate data.

Figure 51, taken from SUSIO (1975), gives 150 m isopleths of the 20°C surface obtained from both bi-monthly climatological topographies, and topographies observed during synoptic cruises. Again, the 150 m isopleth is considered an indicator of the current core (SUSIO, 1975). The data represented on Figure 51 are only a portion of the information used in obtaining the monthly temperature profiles, used as input to the primitive equation and geostrophic models.

The few January to April isopleths presented in Figure 51 suggest little variability in the position of the Loop Current core. Therefore, the January to April Loop Current patterns simulated by both models (Figures 35 to 38) should represent the mean conditions during these months.

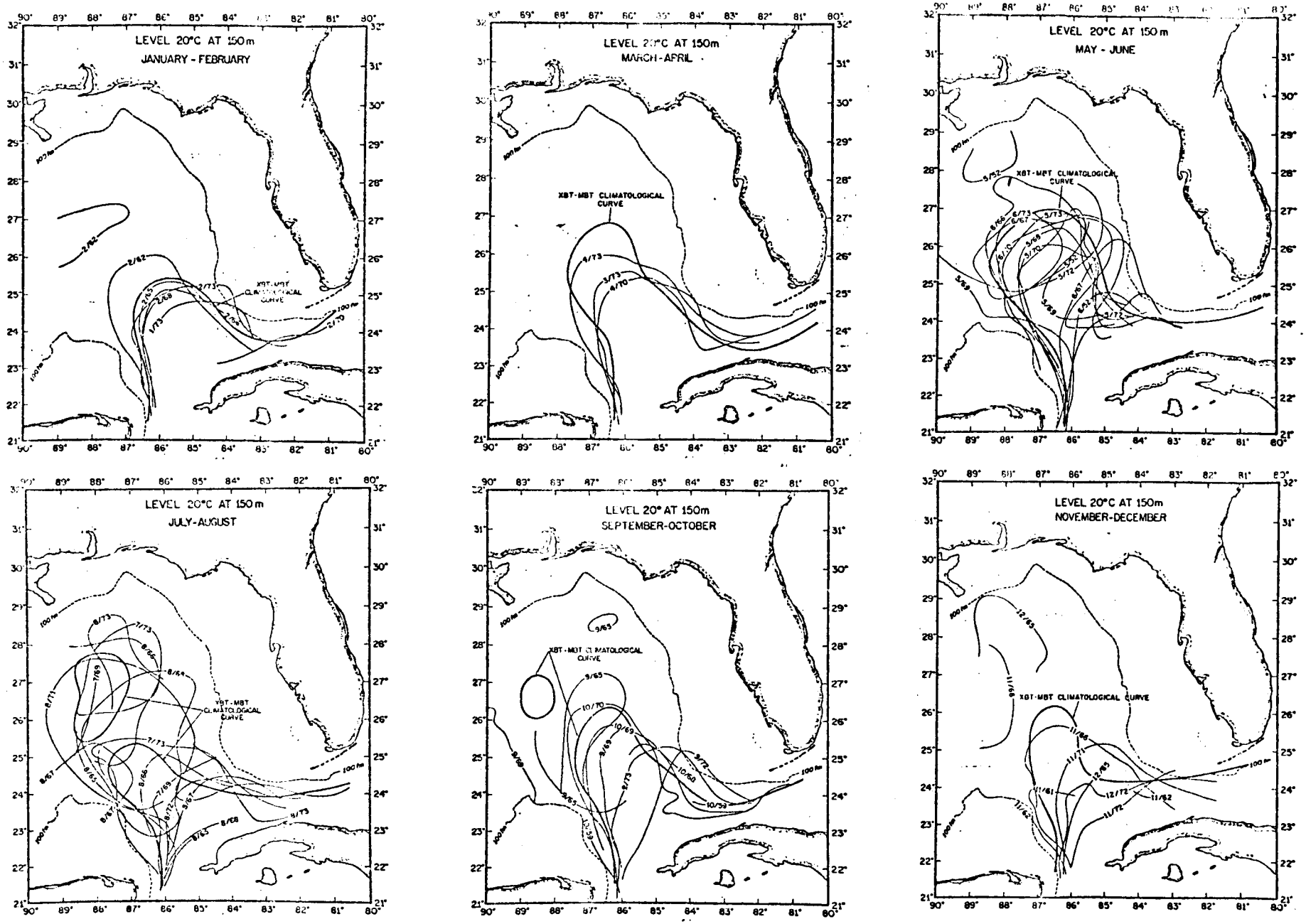

Figure 51. The 150 m isopleths of the 20°C surface observed during the month/year indicated taken from SUSIO (1975). The XBT-MBT climatological curves are obtained from bi-monthly averages of 1° square temperature profiles (SUSIO, 1975).

The core of the Loop Current migrates considerably from May to July. However, there do appear to be two distinct modes for the position of the main current. When the Loop is well developed, the Yucatan Current procedes north into the Gulf (e.g.,6/66, 5/70,8/71). When an eddy has detached, the Yucatan Current has a shorter pathlength in the Gulf (e.g.,6/52, 6/67, 8/68, 7/73).

The disappearance of a well developed Loop during August is a function of the large variability in the position of the Current's core during this month. Figure 52 gives the 20°C topography observed during four separate August cruises. Averaging of such variable data tends to smooth the intense gradients found during any one cruise.

Finally, the September to December isopleths show a reduction in the variability of the core of the Loop Current from that observed during the summer. However, the variability is still greater than that indicated by the January to April data.

The monthly circulation pictures do not show any deep currents branching off from the Yucatan Current and flowing west along the Campeche Bank (Appendix I). The only transfer of water from the Yucatan Straits during all months (Figures 35 to 46) occurs along the northern boundary of the Yucatan Peninsula. The shallow depths of Campeche Bank preclude the possibility of large transports of water occuring (Figures 35 to 46).

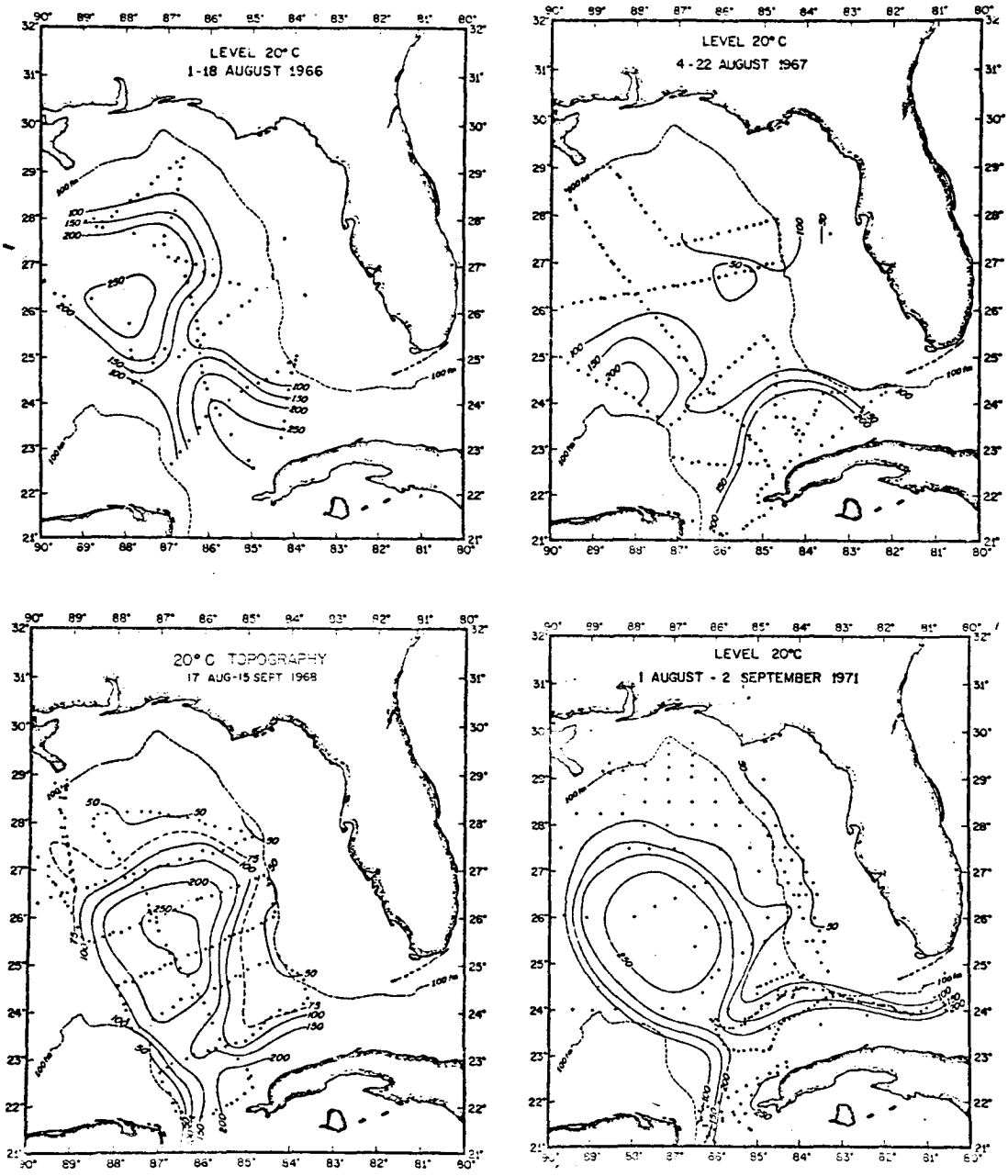

Figure 52. The 20°C surface observed during four August cruises.

A deep westerly flow centered between 22.5°N and 23.5°N is observed in all months, from the Campeche Bank to the east coast of Mexico. At the Mexican coast, the flow splits into two limbs, one flowing south and the other north.

The south-flowing current becomes the western side of the BCG. This gyre is most evident in the fall and winter months. The most intense southerly flow occurs along its western edge from September to February. The common boundary it shares with the WCG, a westerly current centered at approximately 23°N, also exhibits large velocities during this period.

The anticyclonic WCG is located to the north of the BCG. The currents of the former gyre are strongest in December (Figure 46),with a secondary maximum in the intensity of this gyre occuring in June-July (Figures 40 and 41). The seasonality of the WCG simulated by the two models is consistent with the seasonality predicted by Sturges and Blaha (1976). Their hypothesis was based on the wind stress field over the western Gulf, which has a maximum current inducing distribution in December and a secondary one in July. The center of the gyre migrates towards the Mexican coast from February to June; and away, from July to January. Thus, the western arm of the gyre with its northerly currents is widest in December-January.

The northern limb of the WCG is continuous from the coast of Mexico to the western limb of the Loop Current only during the summer. The transport of west Gulf waters to the eastern Gulf occurs along 24.5°N during the months June through September (Figures 40 to 43). At other times of the year, the majority of the WCG water recirculates in this gyre, with return southerly flow observed between 93°W and 90°W.

A concise distinction between the northern limb of the WCG, and the southern limb of the TLG is difficult to make without further data. For instance, during the winter months, November through February, the two limbs appear to coincide (Figures 35,36,45, and 46) but in the summer months, July and August, they appear as two distinct flows (Figures 41 and 42).

The northern limb of the TLG is a westerly current which is observed in all months on the Texas Shelf at 28°N (Figures 35 to 46). The feature is evident in the results of the geostrophic model only in the summer, Figure 49, and Appendix II. When the current is intense, February to April (Figures 36 to 38) and August to November (Figures 42 to 45), a continuous westerly flow can be traced from 86°W to 96°W. When the current is weak, the westerly flow occurs only from the Mississippi Delta to 96°W.

The anticyclonic DCG centered at 28.5°N and 87.5°W, is most evident in the results of the primitive equation model during the months September to November (Figures 43 to 45). It appears in the results of the geostrophic model in October also at 28.5°N and 87.5°W (Figure 50).

The WFSG begins to form in July at 27.5°N and 85.5°W (Figure 41). The cyclonic gyre begins to intensify and expand to the south over the west Florida Shelf from August through October (Figures 42 to 44). The gyre weakens and decreases in areal extent through the spring and summer months.

Corroborating evidence for some of the model features observed on the MAFLA Shelf is found in the analysis of drift bottle data. Tolbert and Salsman (1964) released two drift bottles each day at 30°N and 85° 54' W from September 1960 to October 1961. Drennan (1963) released some 32,000 drift bottles off the Mississippi Delta from September 1960 through October 1962. Finally, Gaul (1964,1965,1966). launched drift bottles during 1963 to 1965 along the MAFLA shelf.

These data have been reanalyzed and the results are presented in Figures 53 to 57. The contours represent the percentage of returns from the areas indicated. For instance, a dashed 50% contour line indicates that for those stations within this contour 50% of those bottles returned (not deployed) were found on the MAFLA Shelf.

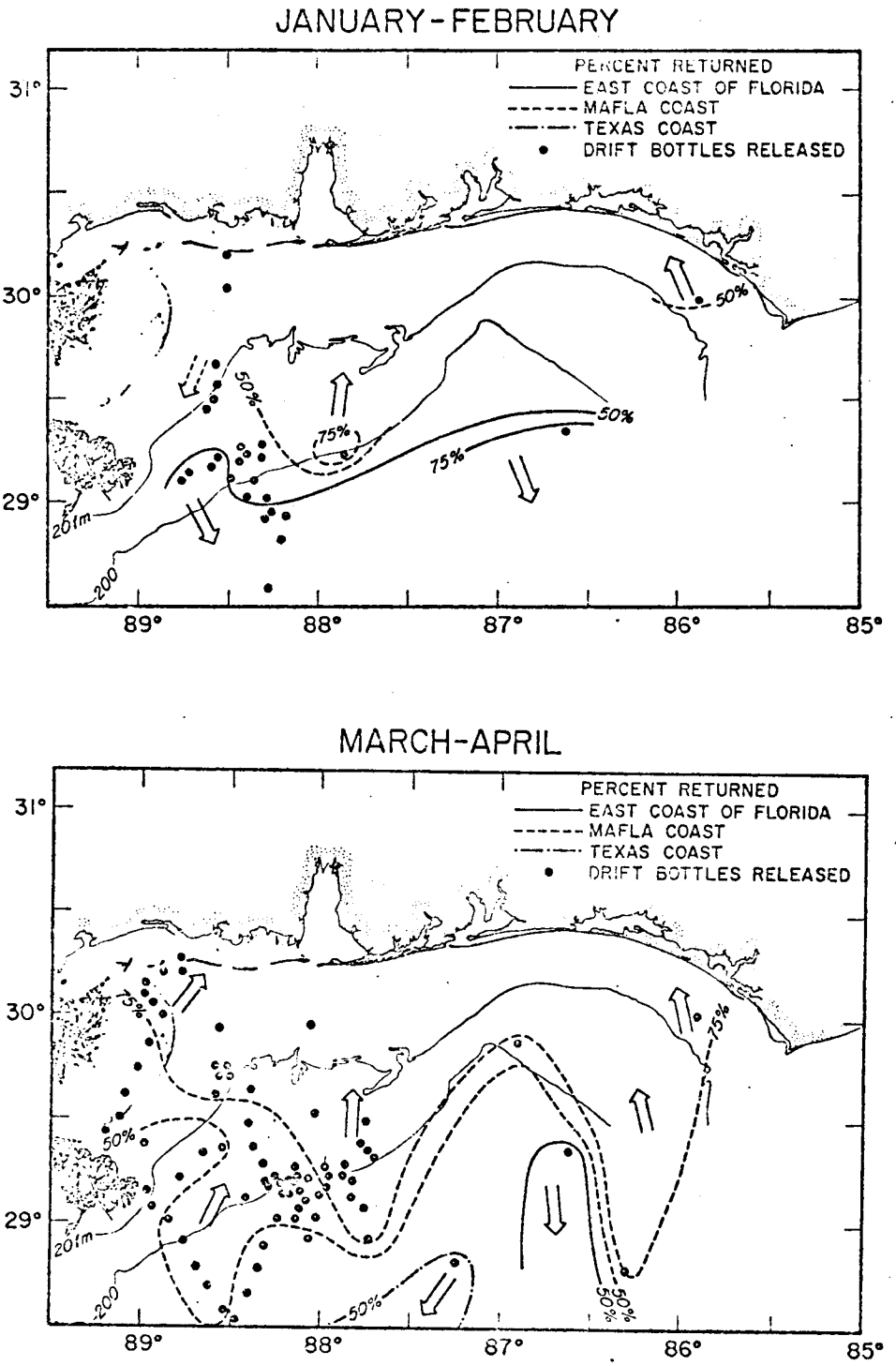

Figure 55. January - February and March - April drift bottle release stations. The contours represent the ratio of bottle returns to the total returned (expressed as a percentage) for the three regions indicated. Arrows pointed to the northeast, the MAFLA coast; to the southeast, the east coast of Florida; and to the southwest, the coasts of Mexico and Texas.

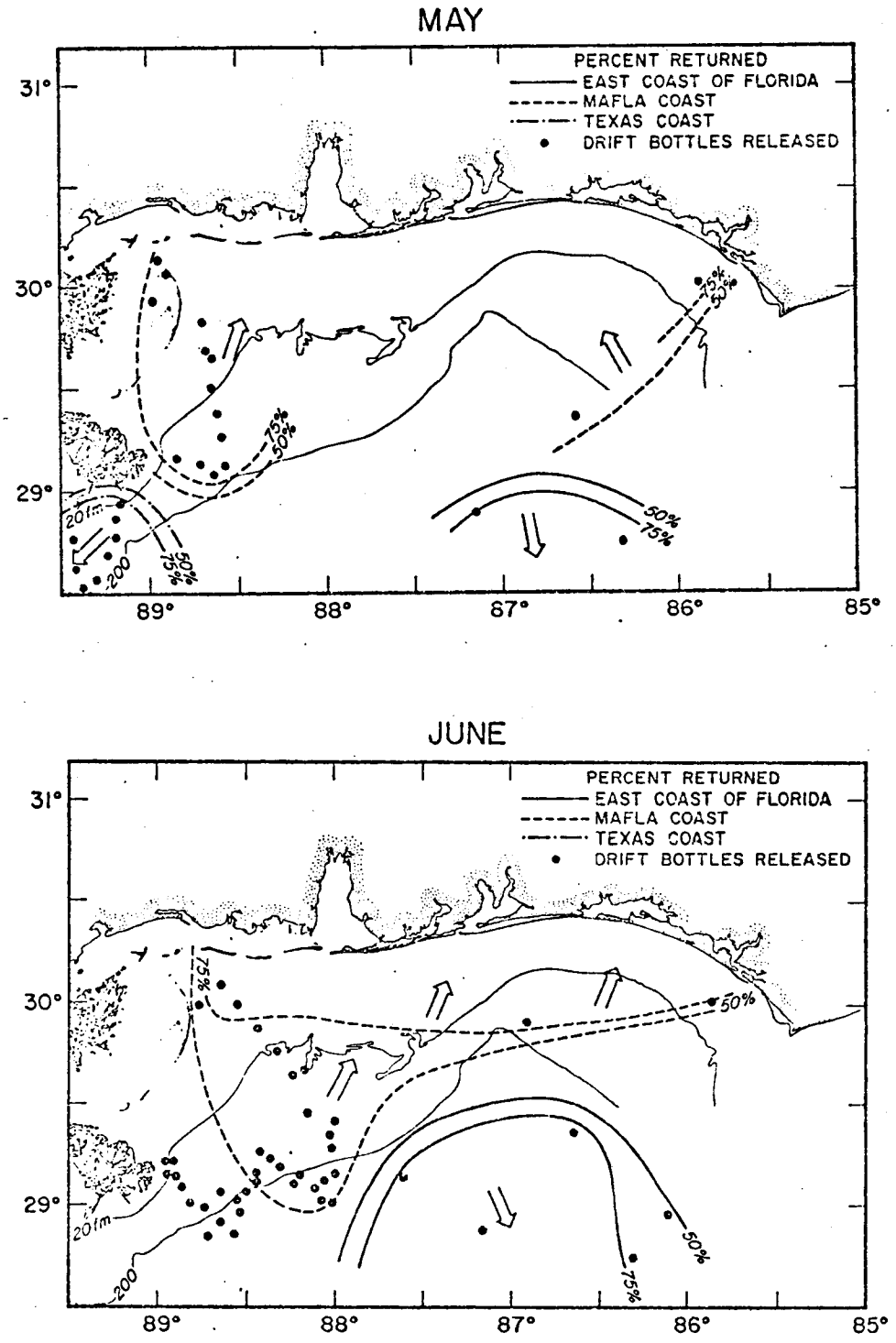

Figure 54. Same as Figure 53, except for May and June.

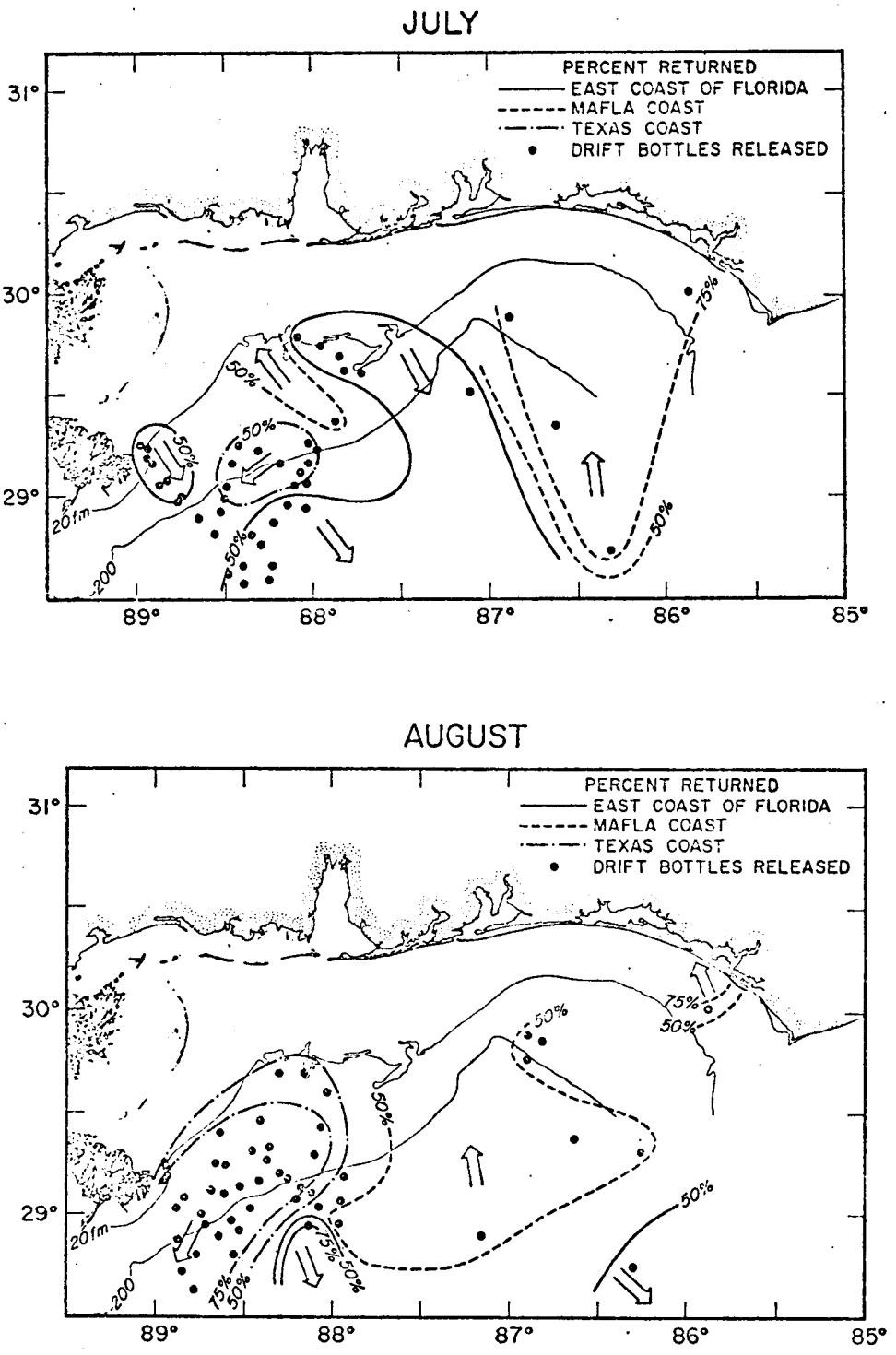

Figure 55. Same as Figure 53, except for July and August.

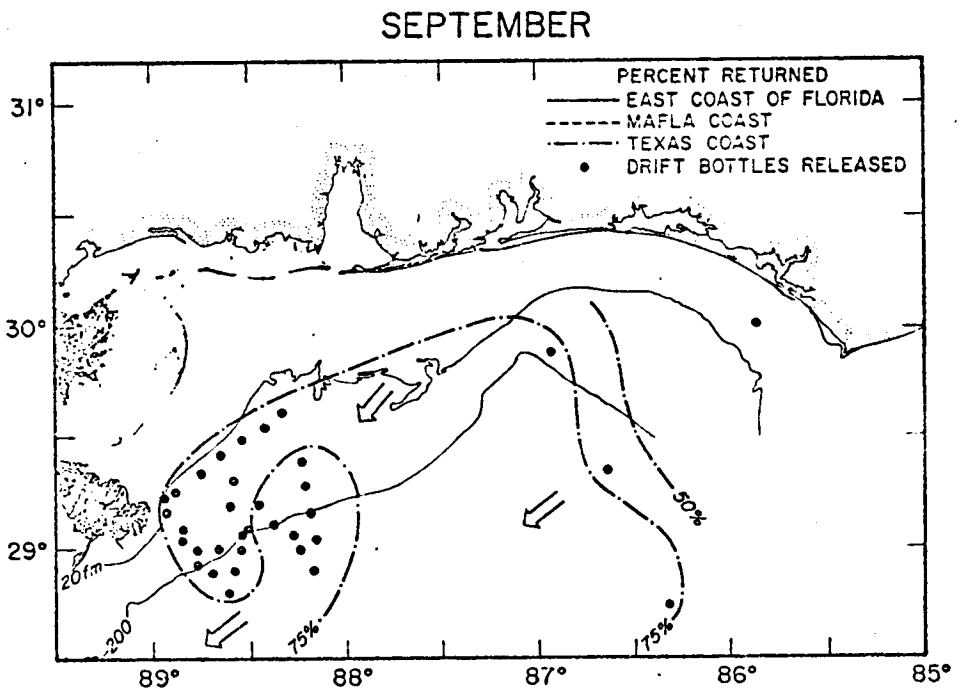

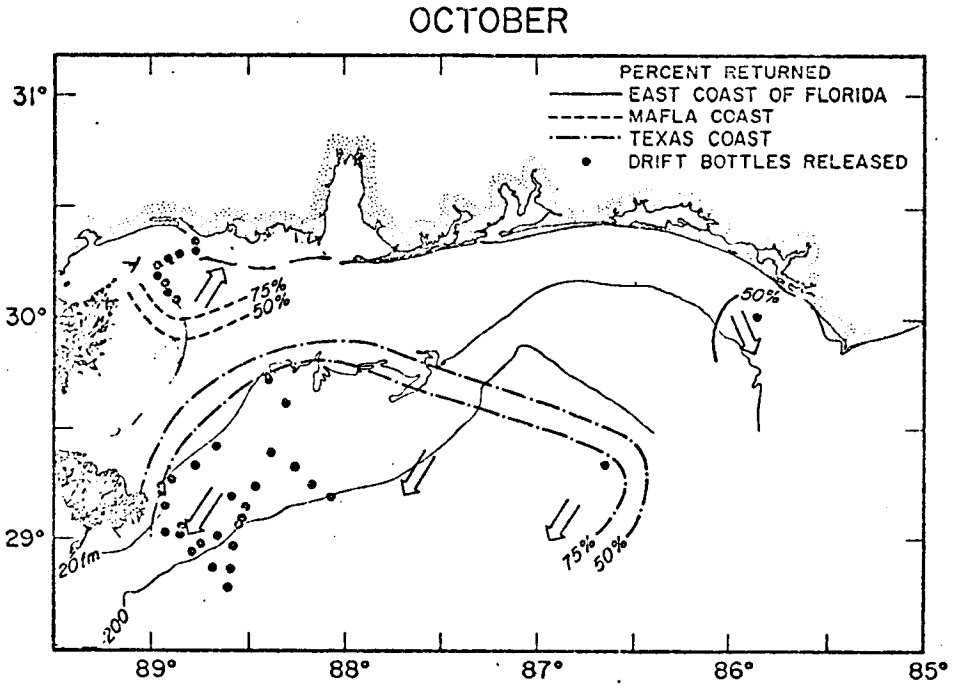

Figure 56. Same as Figure 53, except for September and October.

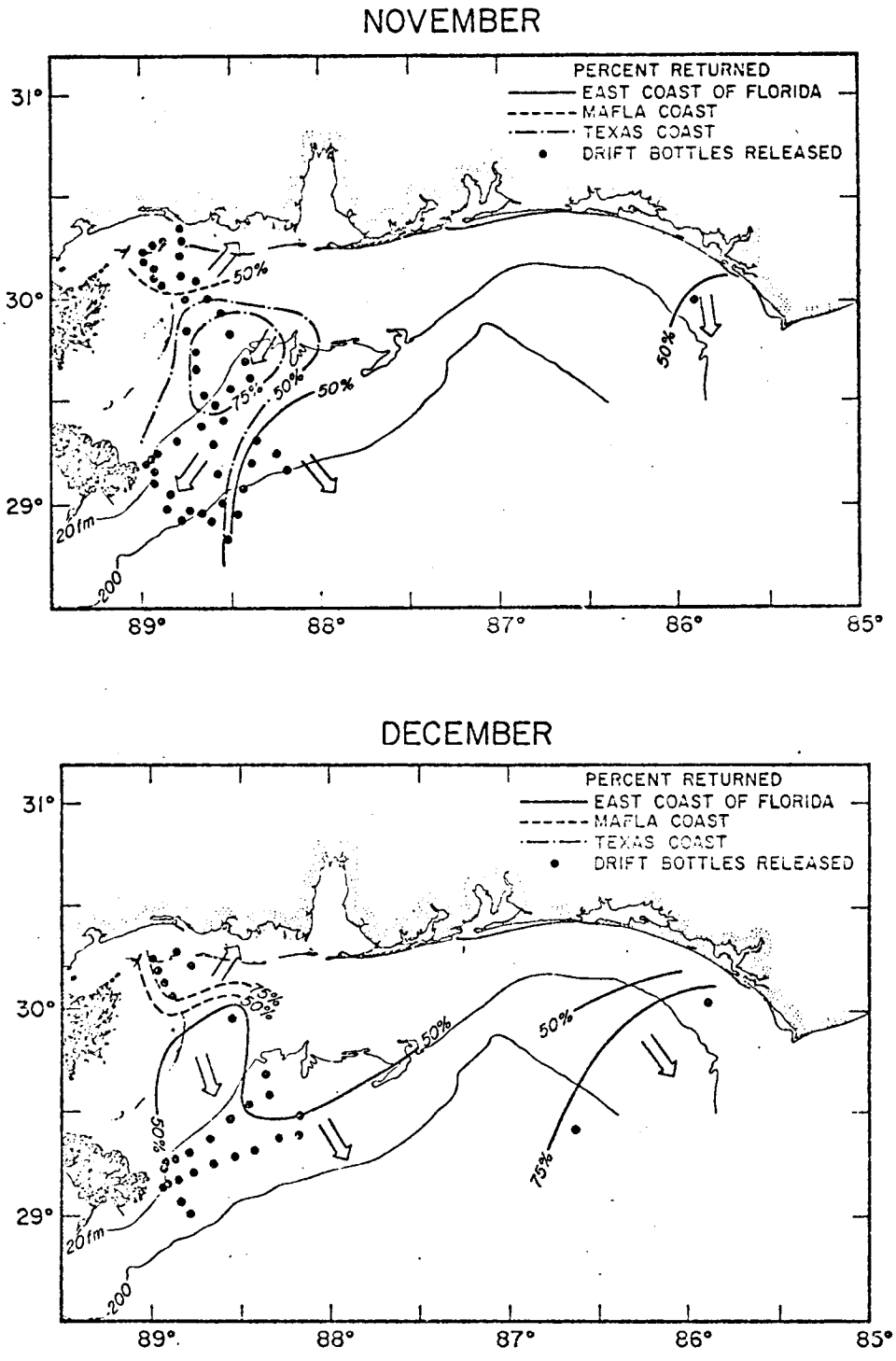

Figure 57. Same as Figure 56, except for November and December.

Bottle trajectories can not be determined from these data, but the returns are consistent with the results of the numerical model. For instance, returns from the Texas-Mexican coastlines are greatest during the months July to November (Figures 55 to 57). As discussed, a strong continuous westerly flow exists along 28°N, from 86°W to 96°W, from August to November (Figures 42 to 45). This current could be the mechanism for transporting bottles from the MAFLA shelf to the Texas-Mexico coastline. It should be noted that a hurricane passed over the area in September 1961. Chew, Drennan, and Demoran (1962) reported that passage times for the bottles to reach the Texas-Mexico coast were considerably reduced after the passage of the hurricane.

The drift bottle data suggest that from January to June the returns from releases north of approximately 29°N are primarily along the MAFLA coasts; and from releases south of 29°N, along the Texas and east Florida coasts (Figures 53 and 54). The model results do not indicate a plausible cause for these results.

5) Synoptic circulation

The data from four synoptic cruises are input to the primitive equation model. The type and/or distribution of the data obtained are different for each cruise. For instance; Nansen bottle data were obtained throughout the Gulf in February - March 1962 only in the eastern

Gulf during June - July 1967 and June 1975 and in portions of the western and eastern Gulf during August - September 1971. In addition, XBT data were collected during August-September 1971.

Temperature and salinity values at the model grid-points are obtained through interpolation of the observed Nansen cast profiles (as described previously). XBT temperature profiles are mated with the appropriate salinity values, and then the resulting data are treated as a Nansen cast to obtain the input to the model.

The numerical model requires information at each grid-point, therefore it is necessary to specify temperature and salinity values at those grid-points lacking data. These values are obtained from the appropriate mean monthly data-sets (i.e.,the June-July 1967 model fields are filled with data from the climatological June data-set, etc.).

Dynamic height distributions computed relative to 700 db from data obtained in the 1962, 1967, and 1975 experiments are presented both to show the distribution of observations, and to illustrate the circulation pattern. The 700 db surface is chosen as a reference level because the spatial coverage available at deeper levels is insufficient to define the current field.

XBT profiles available in the eastern Gulf during August 1971 are used to supplement the Nansen cast data, as most Nansen casts during this period on file at NODC

are on the shelf. Two figures are presented for 1971 to illustrate the distribution of both the deeper stations and XBT's, and the shallower shelf stations.

Surface drifter data, interpolated to a $1/2^{o}$ square grid, are presented for the August 1971 and June 1975 experiments for comparison with the model results. Geostrophic surface currents are computed for the June 1967 data set, and also used for comparison with the model results. A surface current map is not presented for the 1962 data. Because of the large spacing between stations the interpolation routine when applied to the dynamic height field results in unrealistic current fields. The smoothing of the interpolated temperature and salinity fields reduces this problem for the data input to the model.

i) February - March 1962

Nowlin and McLellan (1967) and Nowlin (1972) have analyzed the 1962 data (Figure 58) and described the circulation. Their results suggest the currents observed in 1962 are typical of winter conditions in the Gulf.

The primitive equation model is able to simulate the major circulation features observed during this period. The model streamfunctions (Figure 59), and the observed geostrophic transport (Figure 1-35, Nowlin, 1972) are very similar. Both show a Loop penetrating to $26^{o}N$, a detached eddy at approximately $25^{o}N$ and $90^{o}W$ and an intense WCG.

The magnitude of the velocities simulated by the primitive equation model are considerably less than those directly

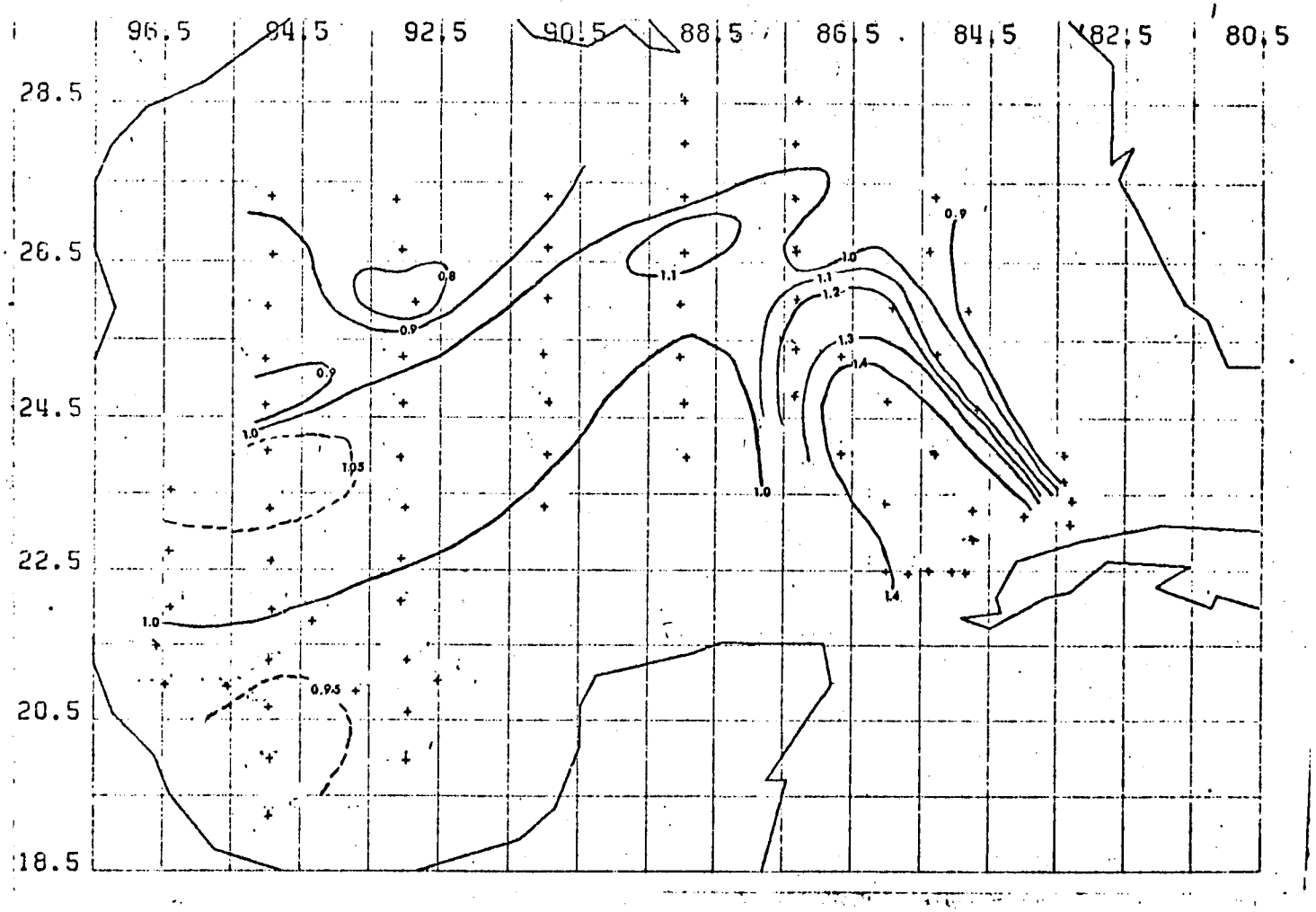

Figure 58. The positions of Nansen stations occupied during February, March 1962. The dynamic height distribution computed relative to 700 db is also shown. The contour interval is 0.1 dynamic meters.

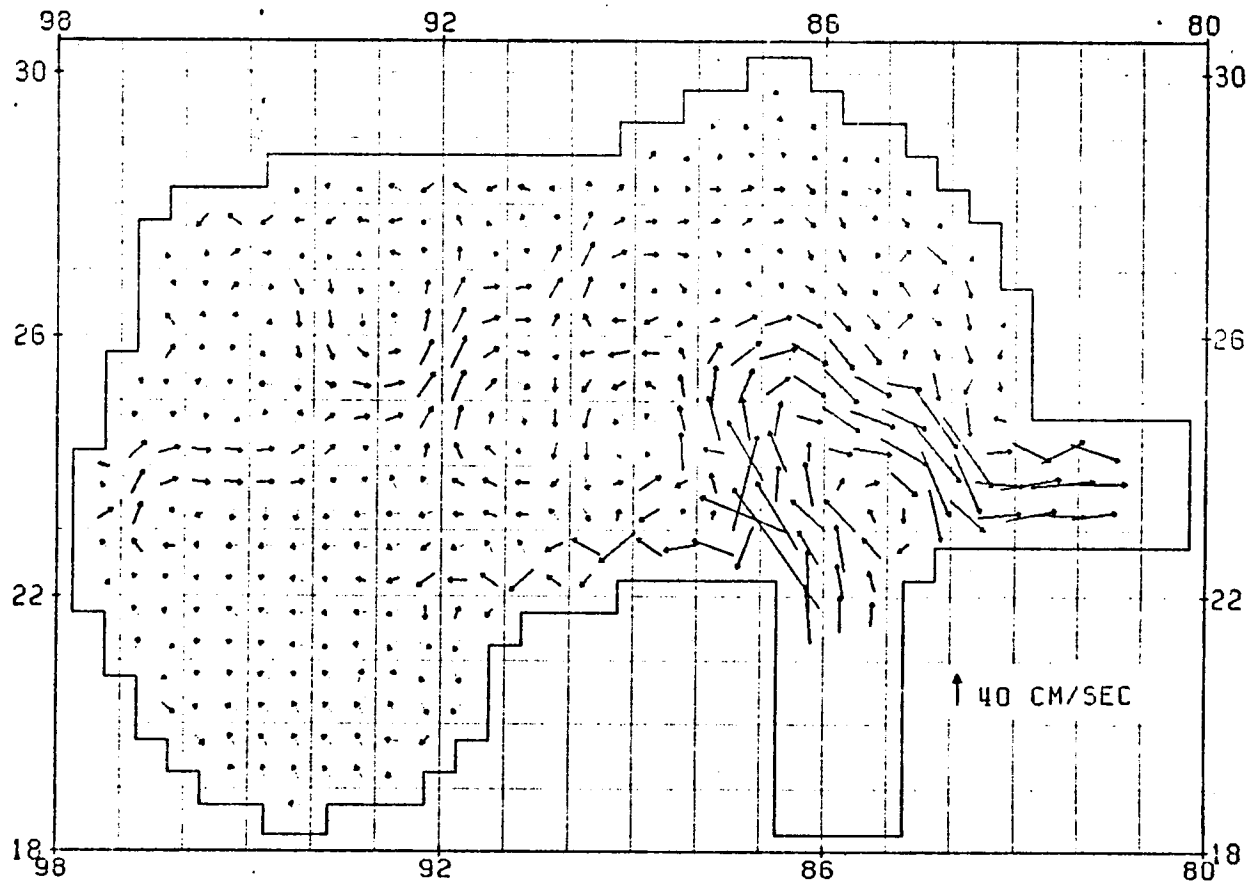

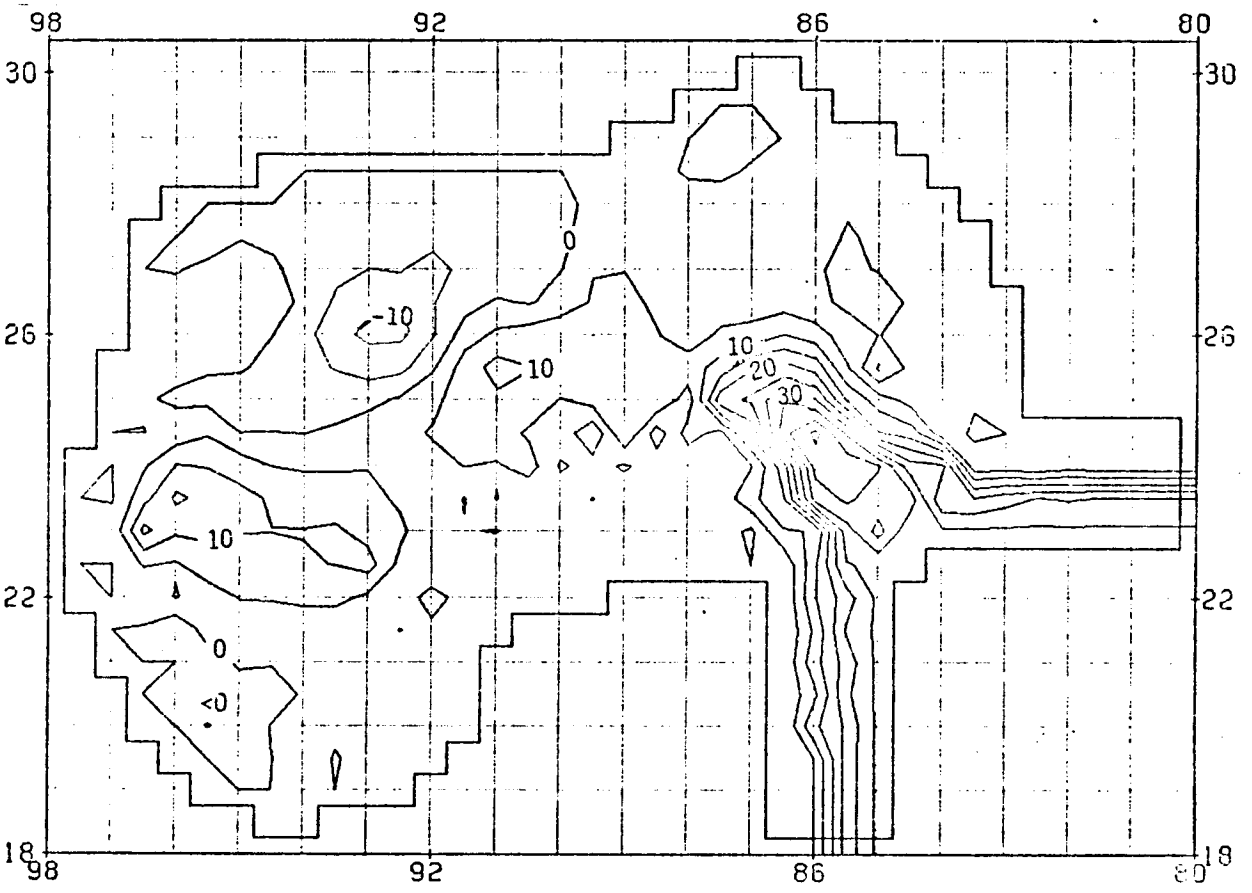

Figure 59. Same as Figure 28 except for February - March 1962.

observed (Nowlin, 1972). The observations are made at discrete points. However, in the numerical model only the average velocity in the interval between grid points can be determined. Since the high velocities normally occur in bands less than $1/2^{o}$ wide, the model computation of speeds tends to smooth extrema in these fields. The geostrophic model with large station spacing experiences the same difficulty.

ii) June - July 1967

The positions of the Nansen stations occupied during the June - July 1967 experiment are given in Figure 60. The contoured dynamic height distribution relative to 700 db is also shown on this figure. In addition, geostrophic surface speeds have been computed on a $1/2^{o}$ square grid, after interpolation of the station data to those points (Figure 60).

Nowlin and Hubertz (1972) have described the characteristics of the detached eddy and main flow. The primitive equation model is able to resolve the eddy as a feature separate from the main flow (Figure 61). Again the surface speeds of the simulations (geostrophic and primitive equation) are less than those observed (Nowlin and Hubertz, 1972).

iii. August - September 1971

The positions of the shallow Nansen stations and XBT's occupied during 1971 is given on Figure 62, and of the deep stations and XBT's on Figure 63. During August - September

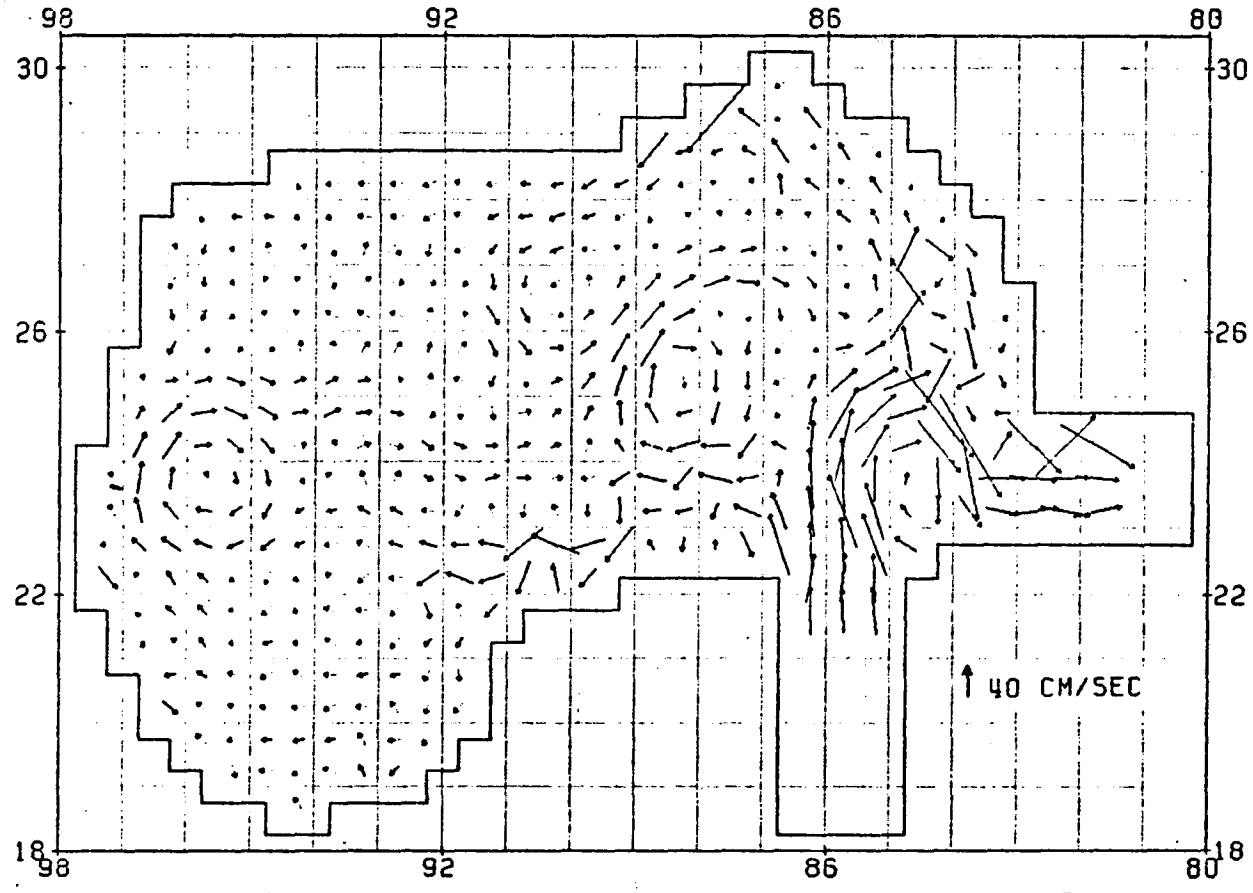

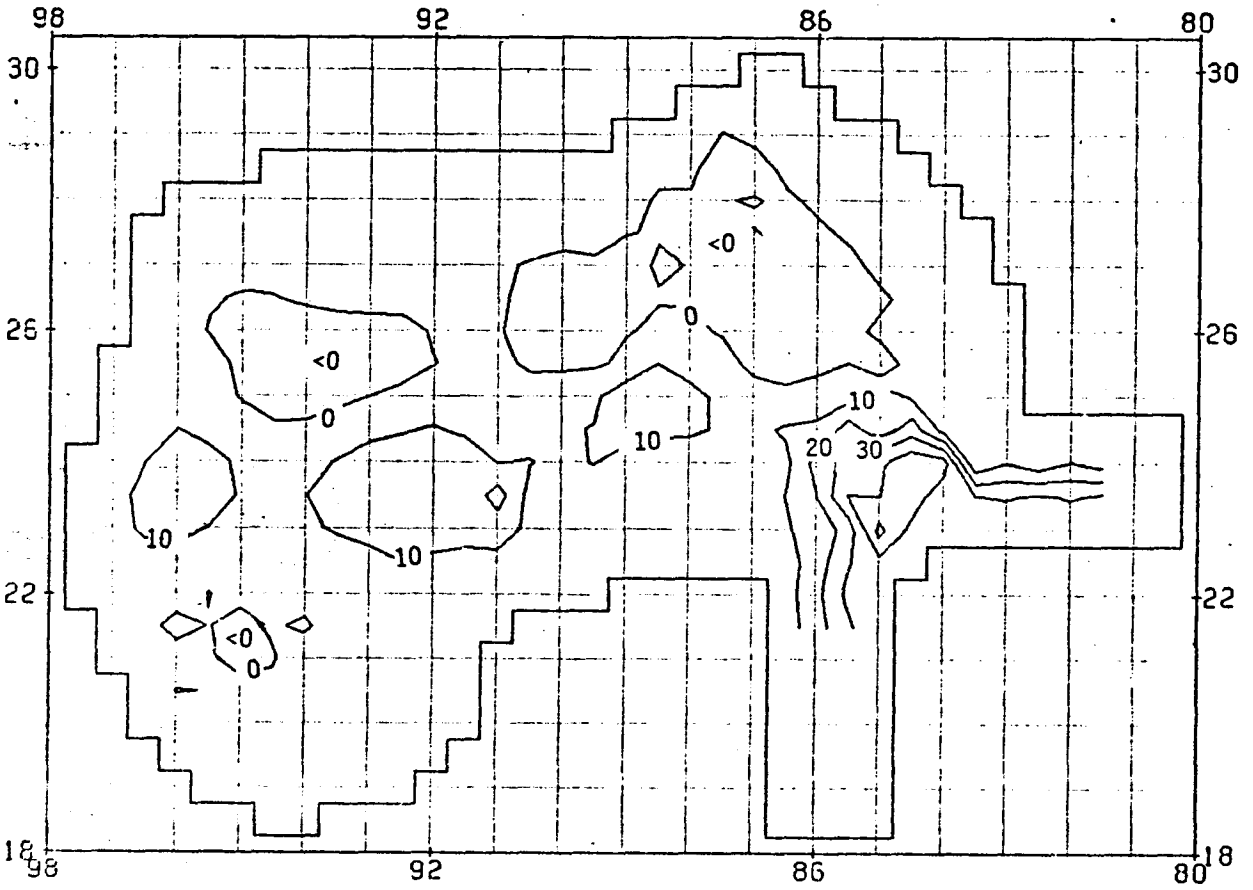

Figure 61. Same as Figure 28, except for June 1967.

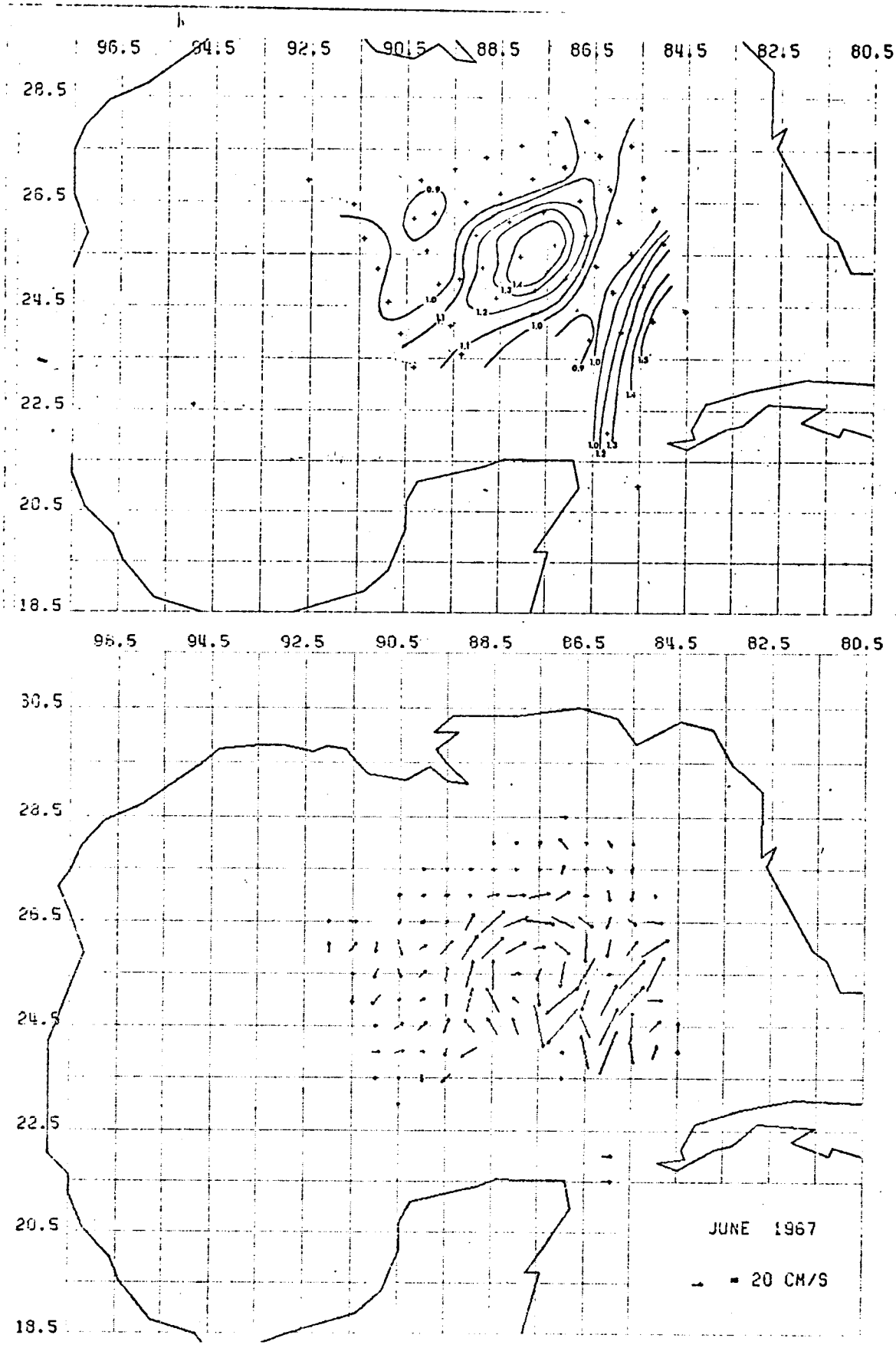

Figure 60. Upper panel. Same as Figure 58, except for June 1967. Lower panel. Geostrophic surface vectors computed from these dynamic height data after interpolation onto a 1/2° square grid.

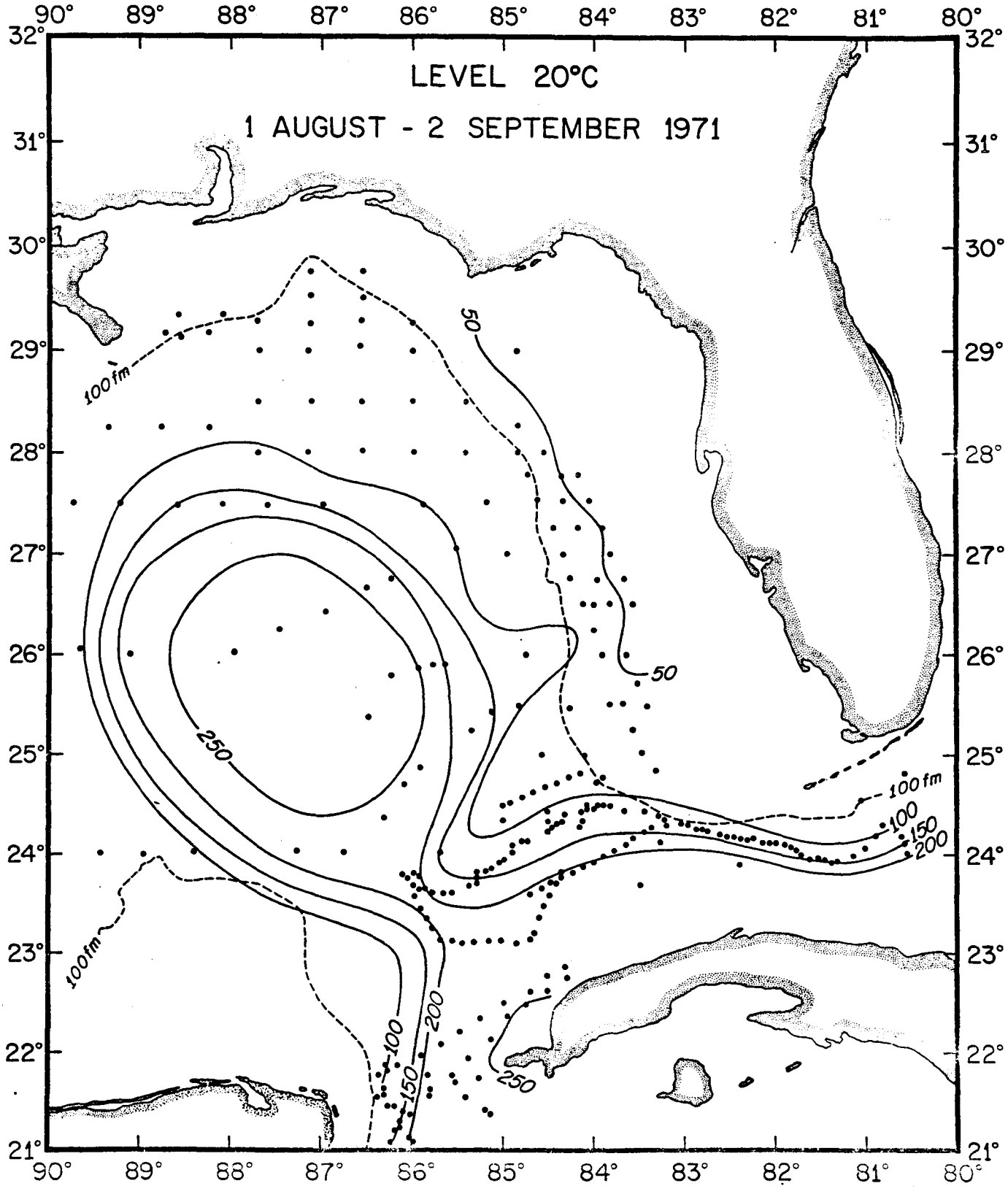

Figure 62. The 20° topography, and the distribution of station positions in the eastern Gulf from an August - September 1971 experiment.

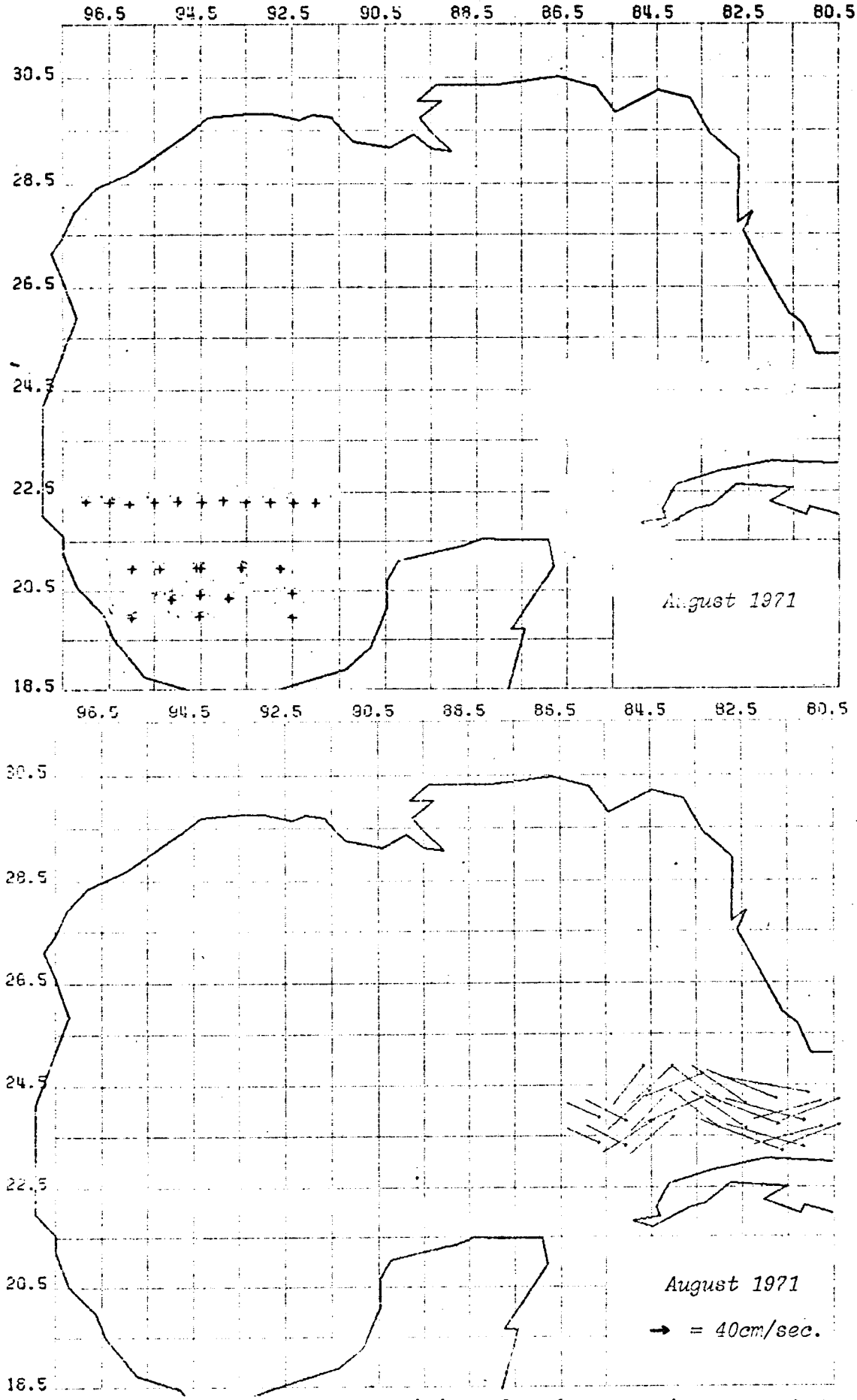

Figure 63. Upper panel. Nansen cast positions for those stations occupied in the western Gulf. Lower panel. Surface current vectors obtained from drogue data which are interpolated onto a 1/2° grid.

1971, the Loop intruded deep into the Gulf. The 20°C topography (Figure 62) suggests that an eddy separation event has not yet occurred but could be imminent. A large meander is found at 24°N off the west Florida Shelf.

The primitive equation model is able to simulate the observed features. The model Loop penetrates to 27°N (Figure 64), an eddy is not indicated, and the stream-function contours show a meander at 24°N extending from the Florida Shelf. In addition, the model results show an intense WFSG. Further analysis of the observations is required to verify this portion of the simulation.

The surface speeds measured by the drifters (Figure 63) are considerably higher than those predicted by the model. These measurements are made at discrete points; and as explained previously, the model computes average velocities for a 1/2° increment.

iv) June 1975

The positions of Nansen cast stations occupied during June 1975 are shown in Figure 65. The contoured dynamic height field and surface drifter trajectories indicate a winter-like penetration of the Loop Current to only 24.5°-25°N. Above the Loop a large cyclonic gyre is found.

The model results closely resemble the observational results (Figure 66). The Loop penetrates to 24.5°-25°N, and a large but weak cyclonic gyre is located to the north of the Loop.

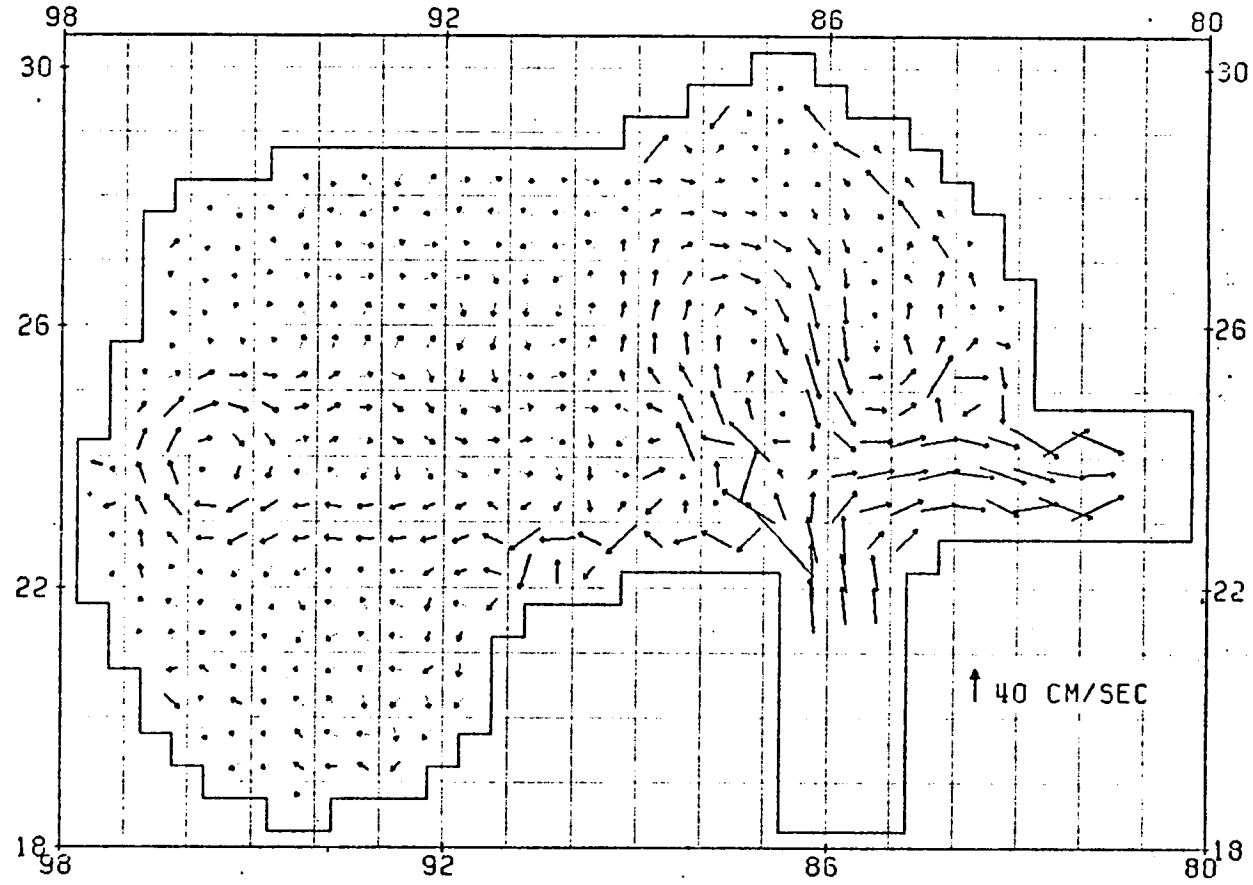

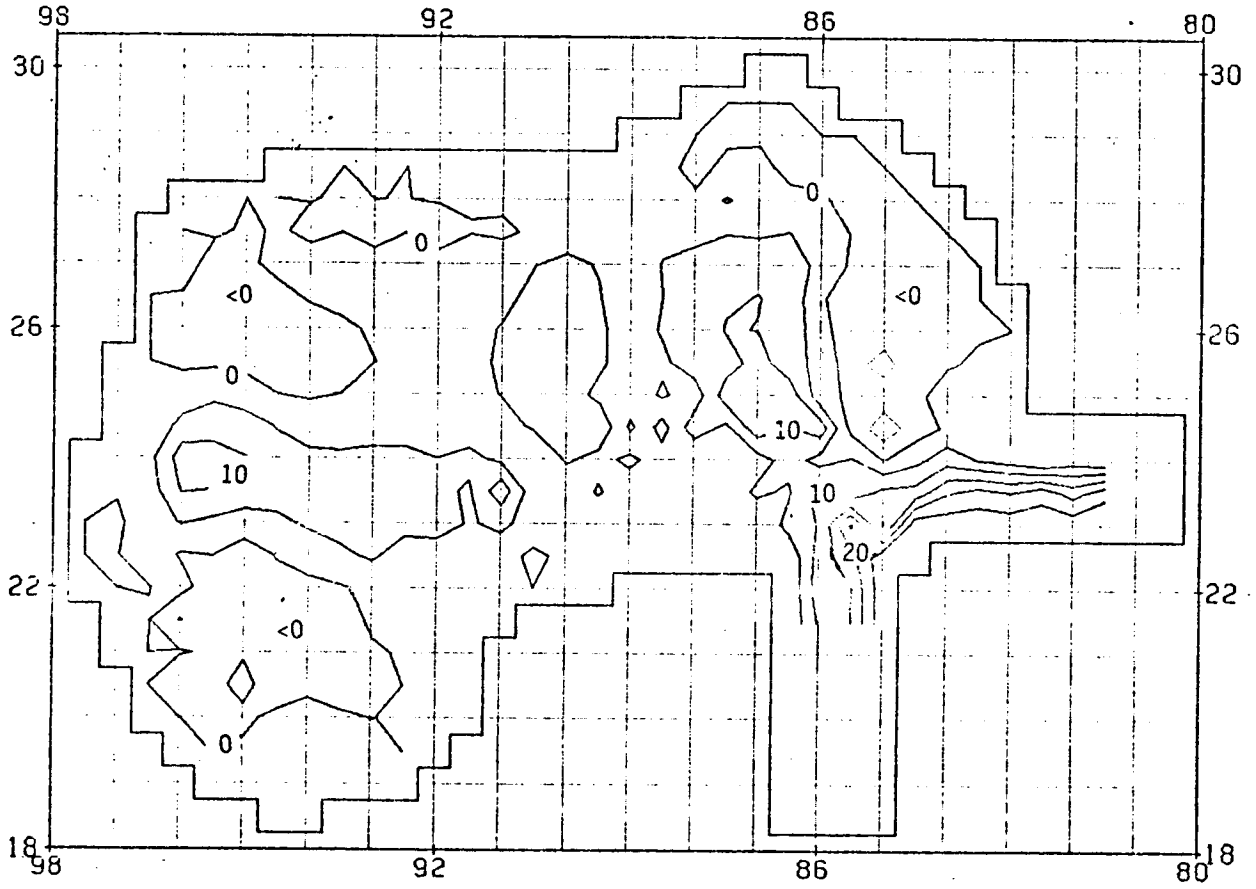

Figure 64. Same as Figure 28, except for August - September 1971.

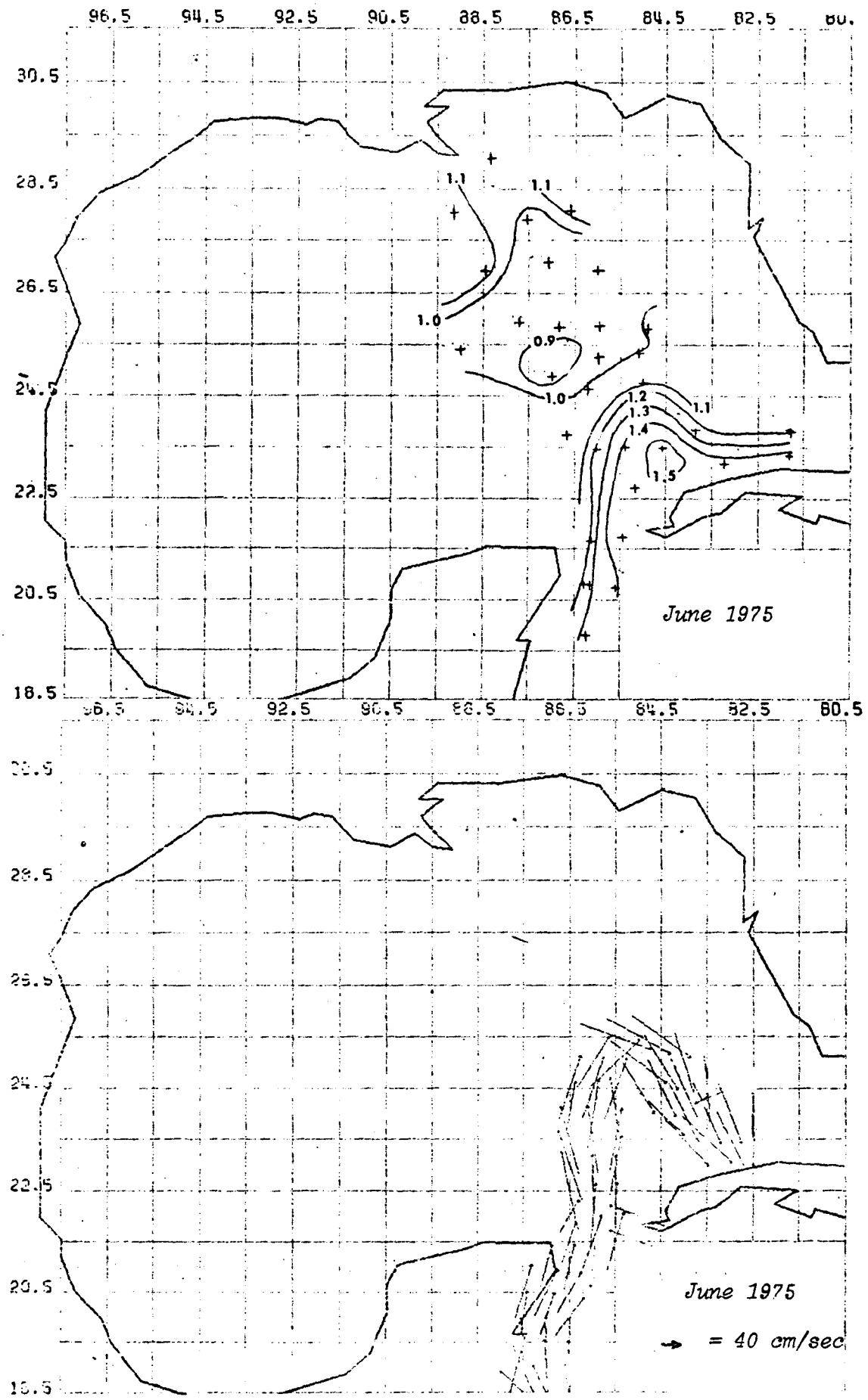

Figure 65. Upper panel. The positions of Nansen stations occupied during June 1975. Also, dynamic height distribution computed relative to 700 db. Lower panel. Surface current vectors obtained from drogue measurements after interpolation onto a 1/2° square grid.

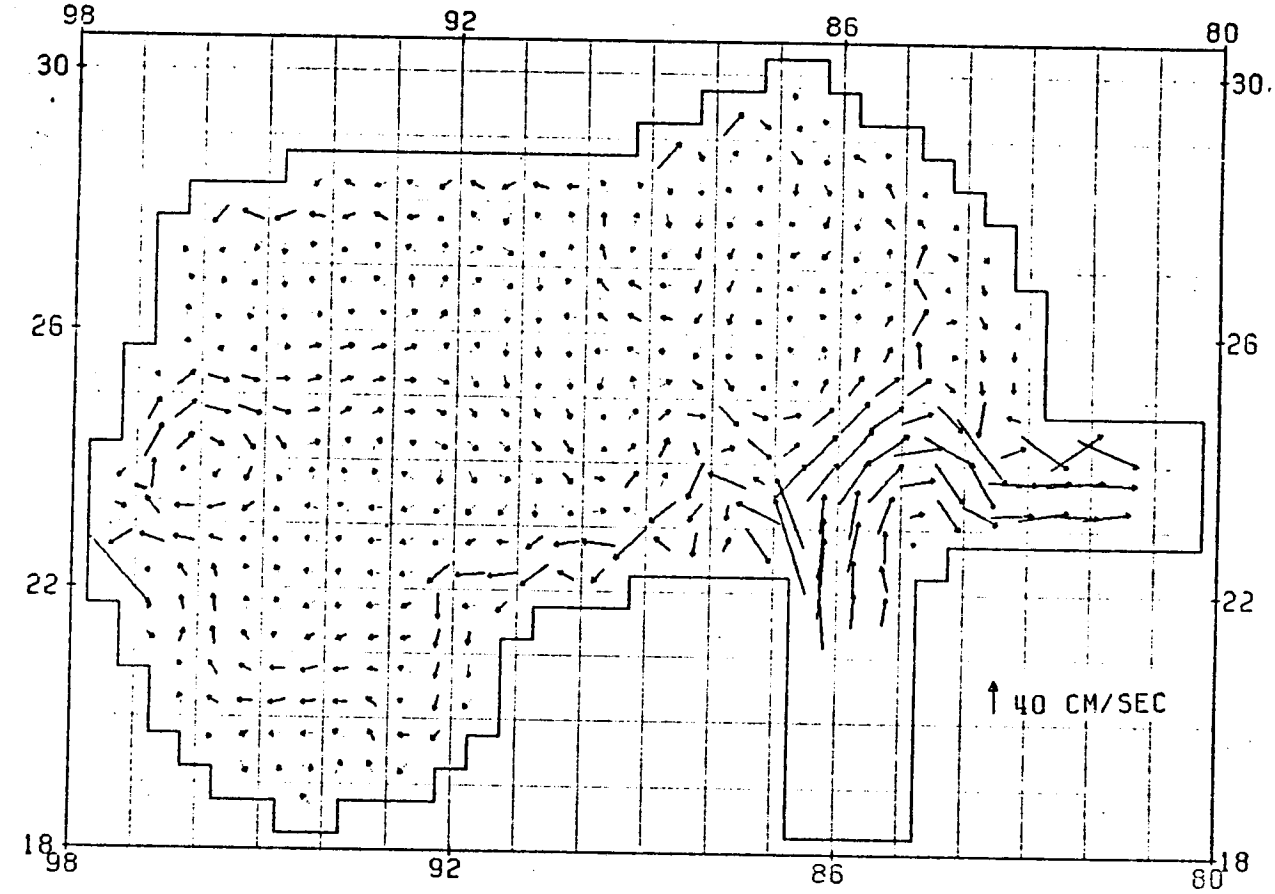

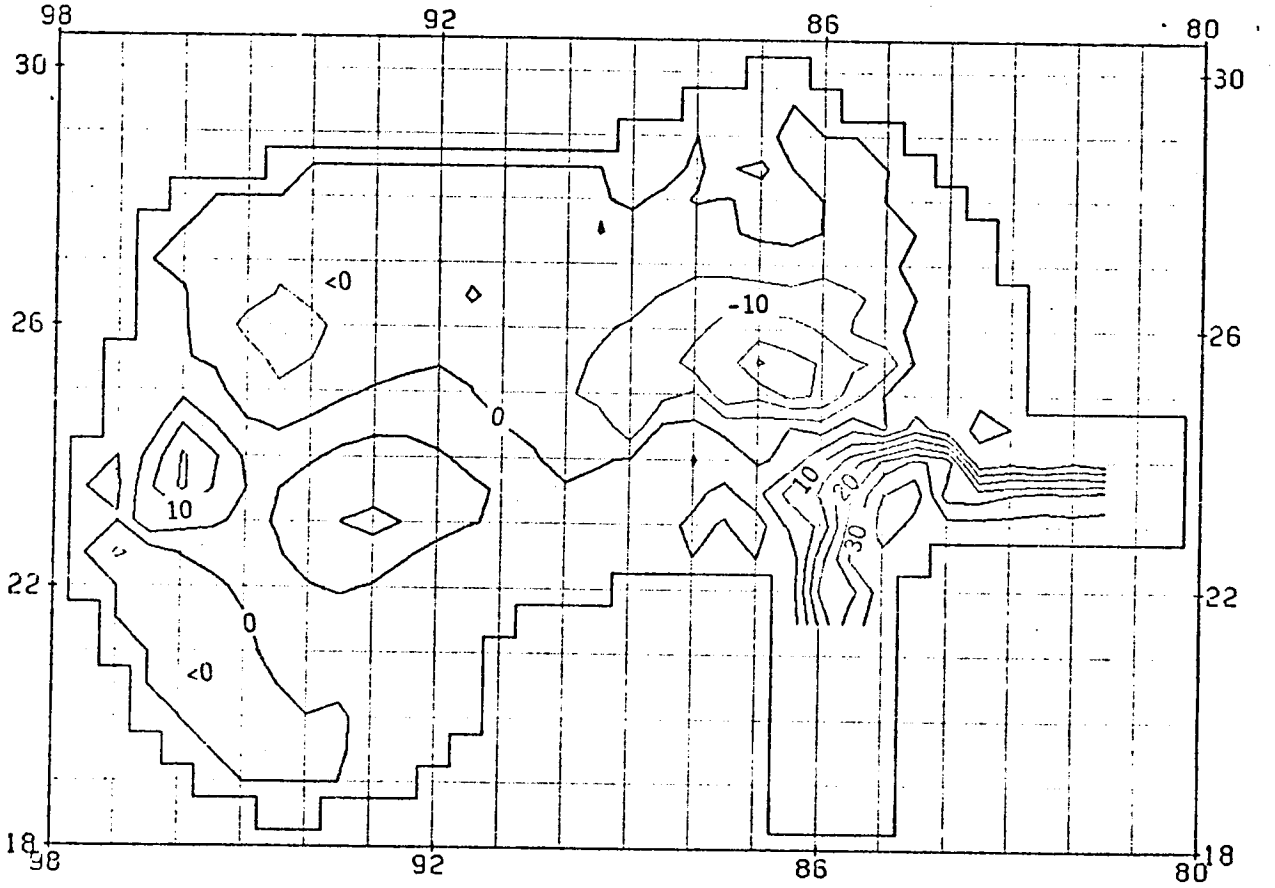

Figure 66. Same as Figure 28, except for June 1975.

6) Summary

The results of the primitive equation model are consistent with the findings of previous investigations. In particular, the cycle of the Loop Current intrusion simulated by the model is similar to the cycle presented by Leipper (1970) and Whitaker (1971). In addition, the temporal variability of the WCG predicted by the model agrees with the hypothesis of Sturges and Blaha (1976) that the gyre should be most intense in winter and summer.

Although the CBG, DCG, WFSG, and TLG have been observed previously, the model results present the first description of the temporal variability of these gyres. In addition, the model solutions identify certain currents which can transport water across the Gulf of Mexico. For instance, the northern limb of the TLG appears to be continuous from the eastern to the western Gulf during the fall; while the northern limb of the WCG can be tracked across the central Gulf in the summer.

The primitive equation model also has demonstrated the ability to accept data from synoptic cruises, and to simulate realistically the current fields. The model could resolve the detached eddy observed in June 1967

even though the grid spacing is 1/2°. In addition, the success of the August 1971 simulation verified the technique of inputting to the model XBT temperature profile data mated with climatological salinity data.

Only the large-scale intense current gyres simulated by the model have been discussed. The model results in regions outside these gyres, where the flows are weaker and probably less persistent, must be considered suspect until additional analysis is performed. In addition, the vertical structure of the circulation cannot be verified.

The vertical sections of geostrophic velocity presented in Appendix I I are computed relative to the 1000 db level. Although these figures suggest that the majority of the flow is above 700 db, direct measurements are required to substantiate this fact.

The model could not reproduce the magnitude of the observed current speeds of the synoptic experiments because of the 1/2° grid spacing,as discussed. A grid with a smaller grid-point separation is not warranted, because during most cruises the interpolation of data to a finer grid would not produce the intense gradients observed (i.e., most station spacing during Gulf cruises is between 30 and 60 nautical miles). Furthermore,

the NODC data are supplied on a 1^{o} square grid, and an interpolation to less than $1/2^{o}$ is not justified for a similar reason.

Finally, the presentation of mean monthly current charts without an indication of the variability around these means can lead to erroneous conclusions about the circulation. The example pertaining to the August Loop Current demonstrates this problem. However, the analysis to date allows only qualitative statements about the year-to-year Loop Current variability, and no statements about the variability outside the Loop.

VI. SECOND YEAR PROGRAM

The primary objective of the second year of this study is to evaluate the ability of the numerical model when run in the prognostic mode "to estimate the density and current patterns in the Gulf of Mexico, ... , using real-time environmental information". As a spin-off from this evaluation, many of the questions remaining after the first year of the study will be addressed. The variability of the currents in the Gulf, the forces which cause the circulation, and the interactions between the major gyres will be considered in the second year as the prognostic model tests are run. The following outline is proposed as the framework for performing the evaluation.

1) Data Preparation

The climatological data received from NODC were obtained by averaging all the temperature data, at the desired standard depth, and within a particular 1^{o} square and month. In regions of little data, such as the western Gulf, the temperature distributions produced by the simple averaging process were very irregular. The irregularities typically were manifested as waves in the contoured distributions. The wavelengths of these disturbances are

typically two grid-lengths. Such features are primarily artifacts of the data distributions. The temperature and salinity fields are averaged temporally and spatially in order to remove these features.

As discussed, the data input to the model were subjectively edited through a visual edit of the data fields. The resulting fields were then filled and averaged by a Laplacian operation, which performs a weighted average on each point with the surrounding four points.

The only step in the data preparation process in which the actual properties of the scalar distributions are considered is the subjective analysis performed by visual inspection of the fields. For instance, the flow in the Yucatan Straits is primarily north-south, or in the Straits of Florida east-west. These properties of the flow are used to eliminate points in the Straits which could introduce considerable east-west flow in the Yucatan area or north-south flow in the Florida area. This type of analysis is not possible in areas where the circulation is poorly defined such as in the western Gulf.

Objective analysis is a statistical approach used primarily in meteorology both to edit data and to interpolate data to regions where little or no data exist. Gandin (1963) presents the mathematical development of this analytical tool. Recently, oceanographers (Bretherton, Davis, and Fandry,

1976) have applied this technique to the problem of analyzing oceanographic data.

It is proposed that an attempt be made to develop a suitable objective analysis package for use on the Gulf of Mexico data-set. In particular, correspondence with Dr. Warren White at Scripps Institute of Oceanography indicates that such a package may already exist. White feels their approach is particularly appropriate in regions of little data.

In addition, the data editing package used at the Fleet Numerical Weather Central may be appropriate for adoption in the present study. Haltiner (1971) describes the salient properties of this method. Although it is used primarily to edit meteorological data, the generality of the technique argues for its applicability to oceanographic data-sets.

If the Scripps objective analysis package is evaluated as appropriate for use in the Gulf, two approaches are possible for the implementation of the method. The package could be used at NODC on their computer, or at AOML after receipt from NODC of the Gulf data-set. Discussions with NODC personnel are necessary to determine the most efficient approach.

If the Scripps approach is not suitable, it is proposed that NODC generate two-week, and $1/2^{\circ}$ square average temperature listings. These averages should produce better

temporal and spatial resolution of the data fields in the eastern Gulf. In addition, the T-S relations should be further reviewed to ascertain if a different averaging approach,i.e.,smaller averaging area and/or longer averaging time-step, for instance, might produce more detailed information for input to the model.

These steps are considered essential to produce data-sets suitable for use as input to the prognostic model runs. The more refined description of the circulation in the Gulf of Mexico which will result from these data analysis techniques is an equally important result. For instance, with objective analysis the important time-scales of the currents are obtained providing information on the variability of the flow.

2) Prognostic Modelling Tests

The prognostic modelling portion of the study will be conducted in three stages. In the first stage, the model will be run in a purely predictive mode. That is, only the surface boundary conditions and the total transports at the Yucatan Straits and Straits of Florida will be specified. The model will be allowed to predict the interior temperature, salinity and velocity fields.

At least two sets of boundary conditions will be used in these tests. The climatological annual cycle of both the volume transport through the Straits and the surface

wind stress will be input to the model. In addition, the data collected during 1975-1976 will be used to provide boundary conditions.

During the second stage, the model fields throughout the Gulf will be initiated with synoptic data-sets when available, or combinations of synoptic and climatological data-sets. The model will then be run in the predictive mode, with the boundary conditions to be specified by climatological and/or observed data. The predictive run will continue until a time-step at which additional synoptic data exist. A comparison of the model and observed current fields will be made to ascertain the validity of the prediction. Various historical and recent data-sets, with different time increments between observations, will be used in an attempt to determine over what intervals the circulation is predictable.

The final step of the second year's program will be an attempt to update the model fields with randomly spaced data-sets, such as is accomplished in meteorological forecasts. An objective analysis method which can accurately map the influence of a data point, both in time and space is an essential tool needed to insure the success of this procedure.

3) Data Analysis and Final Cruise

The completion of the analyses of data collected in 1975-1976, and a final cruise is proposed for the second

year program. The final cruise was originally planned for May 1976 but it was requested that the cruise be rescheduled to the second year of study.

However, as part of another program, a Virginia Key cruise to the Gulf did occur in May, funded by AOML. The Key retrieved a buoy which had entered the Gulf and had lost its drogue unit. The Key occupied two XBT transects while retrieving the buoy. In addition, the Researcher will occupy two additional XBT transects in late May and early June while enroute to a geological survey off the Mississippi Delta. This coverage, plus a trajectory obtained from a buoy still reporting in the Gulf, should serve to define the May circulation pattern. Therefore, it is proposed that the final BLM Key cruise be conducted in August to increase the temporal coverage of the Gulf current fields.

VII. ACKNOWLEDGMENTS

The excellent cooperation extended by NODC personnel, in particular Mr. Darrell Knoll, is gratefully acknowledged. The digitized bottom topography supplied by Dr. Ya Hsueh of Florida State University and the wind stress data provided by Mr. Andrew Bakum of the National Marine Fisheries Service resulted in a considerable savings of time and effort. Portions of this program were funded by the National Science Foundation, International Decade of Ocean Exploration Office, and the National Oceanic and Atmospheric Administration.

References

Betzer, R. R., and M. E. Q. Pilson (1971). Particulate iron and the nepheloid in the western North Atlantic, Caribbean and Gulf of Mexico. Deep-Sea Res., 18, pp. 753-761.

Bretherton, F. P., R. E. Davis, and C. B. Landry (1976). A technique for objective analyses and design of oceanographic experiments. Submitted to Deep-Sea Research.

Bryan, K. (1969). A numerical method for the study of the circulation of the world ocean. J. Comp. Phys., 4, pp. 347-376.

Brooks, I. H., and P. P. Niiler (1975). The Florida Current at Key West: Summer 1972. J. Mar. Res., 33, pp. 83-92.

Caruthers, J. W. (1972). Water masses at intermediate depths. In: Contributions on the Physical Oceanography of the Gulf of Mexico, Capurro and Reid Editors, Gulf Publ. Co., Houston, pp. 53-64.

Chew, F. (1974). The turning process in meandering currents: A case study. Jour. Phys. Ocn. 4, pp. 21-57.

Chew, F., K. L. Drennan, and W. J. Demoran (1962). Some results of drift bottle studies off the Mississippi Delta. Limnology and Oceanography, 1, pp. 252-257.

Cochrane, J. D. (1963). Yucatan Current. In Unpubl. Rept. of Dept. of Oceanogr. & Meteorol., The A.&M. College of Texas. Ref. 63-18A: pp. 6-11.

Cochrane, J. D. (1966). The Yucatan Current. In Unpubl. Rept. of Dept. of Oceanogr., Texas A.&M. University, Ref. 66-23T: pp. 14-25.

Cochrane, J. D. (1967). Upwelling off northeast Yucatan. In Unpubl. Rept. of Dept. of Oceanogr., Texas A.&M. University, Ref. 57-11T: pp. 16-17.

Cochrane, J. D. (1968). The currents and waters of the eastern Gulf of Mexico and the western Caribbean Sea. In Unpubl. Rept. of Dept. of Oceanogr., Texas A.&M. University, Ref. 68-8T: pp. 19-28.

Cochrane, J. D. (1969). The currents and waters of the eastern Gulf of Mexico and western Caribbean. In Unpubl. Rept. of Dept. of Oceanogr., Texas A.&M. University, Ref. 69-9-T: pp. 29-31.

Cochrane, J. D. (1972). Separation of an anticyclone and subsequent developments in the Loop Current (1969). In: Contributions on the Physical Oceanography of the Gulf of Mexico, Capurro and Reid Editors, Gulf Publ. Co., Houston, pp 91-106.

Defant, A. (1961). Physical Oceanography, Volume I. Pergamon Press, Oxford, London, 729 pp.

Drennan, K. L. (1963). Surface circulation in the northeastern Gulf of Mexico. Gulf Coast Res. Lab. Ocn. Sec. Tech. Rept. 1, 110 pp.

Drennan, K. L. (1968). Hydrographic studies in the northeast Gulf of Mexico. Gulf South Res. Lab, Ref. 68-0-1, 111 pp.

Duing, W. (1975). Synoptic studies of transients in the Florida Current. J. Mar. Res., 33, pp. 53-73.

Emery, W. J. (1975). Dynamic height from temperature profiles. Jour. Phys. Ocn., 5, pp. 369-375.

Florida Department of Natural Resources (1969). Memoirs of the Hourglass Cruises, Volumes 1 and 2. Marine Research Laboratory St. Petersburg, Florida.

Fofonoff, N. P. (1962). Dynamics of ocean currents. In: The Sea, Ideas and Observations, Volume 1. Pergamon Press, New York and London, pp. 323-396.

Fomin, L. M. (1964). The Dynamic Method in Oceanography. Elsevier Publishing Company, Amsterdam, 212 pp.

Gandin, L. S. (1963). Objective Analysis of Meteorological Fields. National Technical Information Service, TT 65-50007, Springfield, Va., 242 pp.

Gaul, R. D., and R. E. Boykin (1964). Northeast Gulf of Mexico hydrographic data collected in 1963. Texas A.&M. Univ. Dept. of Ocn. and Met. Ref., 64-26T, 81 pp.

Gaul, R. D., and R. E. Boykin (1965). Northeast Gulf of Mexico hydrographic survey data collected in 1964. Texas A.&M. Univ. Dept. of Ocn. and Met., Ref. 65-8T.

Gaul, R. D., R. E. Boykin, and D. E. Letzring (1966). Northeast Gulf of Mexico hydrographic survey data collected in 1965. Texas A.&M. Univ. Dept. of Ocn. and Met., Ref. 66-8T, 202 pp

Gaul, R. D. (1967). Circulation over the continental margin of the northeastern Gulf of Mexico. Doctoral dissertation, Texas A.&M. Univ., 172 pp.

Grose, P. L. (1966). The stratification and circulation of the subsurface waters of the Gulf of Mexico. Florida State Univ., Dept. of Oceanography Reference 1, 84 pp.

Haltiner, G. J. (1971). Numerical Weather Prediction. Wiley Publ. Co., New York, 317 pp.

Hansen, D. V. (1972). Deep currents in the Yucatan Strait. Abstract in EOS, Transactions, A. G. U., 53, p. 392.

Hendershott, M. and W. Munk (1970) Tides. Ann. Rev. Fl. Mech., 2, pp 205-224.

Ichiye, T. (1962). Circulation and water mass distribution in the Gulf of Mexico. Geofis. Inter., (Mexico City), 2, pp. 47-76.

Ichiye, T., H. H. Kuo, and M. R. Carnes (1973). Assessment of currents and hydrography of the eastern Gulf of Mexico. Texas A.&M. Univ., Dept. of Oceanogr. Contribution No. 601.

Ichiye, T., and H. Sudo (1971). Saline deep water in the Caribbean Sea and in the Gulf of Mexico. Unpubl. Rept., Dept. of Oceanogr. Texas A.&M. Univ., Ref. 71-16-T, 27 pp.

Ichiye, T., and H. Sudo, (1971a). Mixing processes between shelf and deep sea waters off the Texas coast. Unpubl. Rept., Dept. of Oceanogr., Texas A.&M. Univ.,Ref. 71-19-T, 29 pp.

Jones, J. I. (1973). Physical oceanography of the northeast Gulf of Mexico and Florida continental shelf area. In: A summary of knowledge of the eastern Gulf of Mexico, Coordinated by the State University System of Florida Institute of Oceanography.

Kirwan, A. D., Jr., G. Mc Nally, M. S. Chang, and R. Molinari (1975). The effect of wind and surface currents on drifters. Jour. Phys. Ocn., 5, pp. 361-368.

Leendertse, J. J. (1970). A water-quality simulation model for well-mixed estuaries and coastal seas. I. Principles of compilation. Memo RM-6230-RC. The Rand Corp., Santa Monica, Calif.

Leipper, D. F. (1970). A sequence of current patterns in the Gulf of Mexico. J. Geophys. Res., 75, pp. 637-657.

Leipper, D. F., J. D. Cochrane, and J. F. Hewitt (1972). A detached eddy and subsequent changes (1965). In: Contribution on the Physical Oceanography of the Gulf of Mexico, Capurro and Reid Editors, Gulf Publishing Company, pp. 107-117.

Maul, G. (1975). An evaluation of the use of the Earth Resources Technology Satellite for observing ocean current boundaries in the Gulf Stream System. NOAA Tech. Rept. ERL 335-AOML 18, 125 pp.

McLellan, H. J. (1965). Elements of Physical Oceanography. Pergamon Press, Oxford, 151 pp.

McLellan, H. J. and Nowlin, W. D., Jr. (1963). Some features of the deep water in the Gulf of Mexico. J. Mar. Res., 21, pp. 233-245

Molinari, R. L., and J. D. Cochrane (1972). The effect of topography on the Yucatan Current. In: Contributions on the Physical Oceanography of the Gulf of Mexico, Capurro and Reid Editors, Gulf Publ. Co., Houston, pp. 149-155.

Molinari, R. L., and R. Yager (1976). Upper layer hydrographic conditions at the Yucatan Strait during May 1972. Submitted to J. Mar. Res.

Monin, A. S., and A. M. Yaglom (1971). Statistical Fluid Mechanics. MIT Press, Cambridge, 769 pp.

Mooers, C. N. K., and J. F. Price (1975). General shelf circulation. In: Compilation and Summation of Historical and Existing Physical Oceanographic Data from the Eastern Gulf of Mexico. State University System Institute of Oceanography, Final Report Contract No. 08550-CT4-64, pp. 41-52.

NCAR (1971). Library Routines Manual. NCAR Technical Notes NCAR-TN/IA-67.

Neumann, G., and W. J. Pierson, Jr. (1966). Principles of Physical Oceanography. Prentice-Hall, Englewood Cliffs, N. J., 545 pp.

Niiler, P. P., and W. S. Richardson, Jr. (1973). Seasonal variability of the Florida Current. J. Mar. Res., 31, pp. 144-167.

Nowlin, W. D. (1971). Water masses and general circulation of the Gulf of Mexico. Oceanology, 6, pp. 28-33.

Nowlin, W. D. (1972). Winter circulation patterns and property distributions. In: Contributions on the Physical Oceanography of the Gulf of Mexico, Capurro and Reid Editors, Gulf Publ. Co., Houston, pp. 3-51.

Nowlin, W. D., and J. M. Hubertz (1972). Contrasting summer circulation patterns for the eastern Gulf Loop Current versus anticyclonic ring. In: Contributions on the Physical Oceanography of the Gulf of Mexico, Capurro and Reid Editors, Gulf Publ. Co., Houston, pp. 139-148.

Nowlin, W. D. and H. J. McLellan (1967). A characterization of the Gulf of Mexico waters. J. Mar. Res., 25, pp. 29-59.

Nowlin, W. D. and C. A. Parker (1974). Effects of a cold-air outbreak on shelf waters of the Gulf of Mexico. Jour. Phys. Ocn., 4, pp. 467-486.

Paskausky, D. F., and R. O. Reid (1972). A barotropic prognostic numerical circulation model. In: Contributions on the Physical Oceanography of the Gulf of Mexico, Capurro and Reid, Editors, Gulf Publ. Co. Houston, pp. 163-176.

Pequegnat, W. E. (1972). A deep bottom current on the Mississippi Cone. In: Contributions on the Physical Oceanography of the Gulf of Mexico, Capurro and Reid Editors, Gulf Publ. Co., Houston, pp. 65-87.

Phillips, O. M. (1969). The Dynamics of the Upper Ocean. Cambridge University Press, Cambridge, 261 pp.

Plaisted, R. O., K. M. Waters, and P. P. Niiler (1975). Current meter data report from the NSF continental shelf dynamics program 1973-1974. Nova University Scientific Data Report.

Price, J. F., and C. N. K. Mooers (1974a). Hydrographic data report from the winter 1973 experiment NSF Continental Shelf Dynamics Program. RSMAS University of Miami Scientific Report. UM-RSMAS-74006; 61 pp.

Price, J. F., and C. N. K. Mooers (1974b). Current meter data report from the winter 1973 experiment, NSF Continental Shelf Dynamics. RSMAS University of Miami Scientific Report. UM-RSMAS-74020, 78 pp.

Price, J. F., and C. N. K. Mooers (1974c). Current meter data report from the fall 1973 experiment, NSF Continental Shelf Dynamics Program. RSMAS University of Miami Scientific Report. UM-RSMAS-74035, 59 pp.

Price, J. F., and C. N. K. Mooers (1975). Hydrographic data report from the fall 1973 experiment, NSF continental Shelf Dynamics Program. RSMAS University of Miami Scientific Data Report. UM-RSMAS-75018, 52 pp.

Reid, R. O. (1972). A simple dynamical model of the Loop Current. In: Contributions on the Physical Oceanography of the Gulf of Mexico, Capurro and Reid, Editors, Gulf Publ. Co, Houston, pp. 157-159

Reid, R. O. and B. R. Bodine (1968). A numerical model for storm surges in Galveston Bay. J. Waterways and Harbors Div., ASCE, 94, Proc. Paper 5805, pp. 33-37.

Rinkel, M. O. (1974). Western Florida Continental Shelf Program. In: Proceedings of Marine Environmental Implications of Offshore Drilling , Eastern Gulf of Mexico, 1974. Edited by Robert E. Smith, SUSIO.

Robinson, M. K. (1973). Atlas of Monthly Mean Sea Surface and Sub-surface Temperature and Depth of the Top of the Thermocline Gulf of Mexico and Caribbean Sea. Scripps Institute of Oceanography. Ref. 73-8, 105 pp.

Rossov, V. V. (1966). Water circulation in the Gulf of Mexico and Caribbean Sea. Doklady Akad. Nauk SSSR, 166, pp. 202-204.

Schlitz, R. J. (1973). Net total transport and net transport by water mass categories for Yucatan Channel based on data for April 1970. Ph.D. Dissertation, Texas A.&M. University, Department of Oceanography. College Station, 107 pp.

Stommel, H. M. (1965). The Gulf Stream. A physical and dynamical description. Univ. of Calif. Press, Berkeley, 248 pp.

Sturges, W. and J. P. Blaha (1976). A western boundary current in the Gulf of Mexico. Science, 192, pp. 367-369.

SUSIO (1975). Compilation and summation of historical and existing physical oceanographic data from the eastern Gulf of Mexico. State University System Institute of Oceanography, Final Report Contract No. 08550-CT4-64.

Tolbert, W. H. and G. C. Salsman (1964). Surface circulation of the eastern Gulf of Mexico as determined by drift-bottle studies. Jour. of Geophys. Res, 69, p. 223-229.

Uchupi, E. (1971). Bathymetric Atlas of the Atlantic, Caribbean, and Gulf of Mexico. Woods Hole Ocn. Instit. Ref. No. 71-72.

Wennekens, M. P. (1959). Water mass properties of the Straits of Florida and related waters. Bull. Mar. Sci. Gulf Carib., 9, pp. 1-52.

Wert, R. J. and R. O. Reid (1972). A baroclinic prognostic numerical circulation model. In: Contributions on the Physical Oceanography of the Gulf of Mexico, Capurro and Reid, Editors, Gulf Publ. Co., Houston, pp. 177-209.

Whitaker, R. E. (1971). Seasonal variations of steric and recorded sea level of the Gulf of Mexico. Master's Thesis, Texas A.&M. University, Department of Oceanography, 109 pp.

Wunsch, C., D. V. Hansen, and B. D. Zetler (1969). Fluctuations of the Florida Current inferred from sea level records. Deep-Sea Res. Supplement to 16, pp. 447-470.

Wust, G. (1964). Stratification and circulation in the Antilles-Caribbean Basins. Columbia University Press, New York, 201 pp.

APPENDIX I

Numerical Model Solutions for Levels II to VII

Velocity vectors computed from the primitive equation model for levels II to VII are given in this Appendix. The arrows with lighter shafts indicate speeds of less than;

a) 4.0 cm/sec for level 2,

b) 2.0 cm/sec for level 3,

c) 1.0 cm/sec for level 4,

d) 0.7 cm/sec for level 5,

e) 0.5 cm/sec for level 6, and

f) 0.4 cm/sec for level 7.

The depth, DPT, indicated for each level represents the mid-point of the layer.

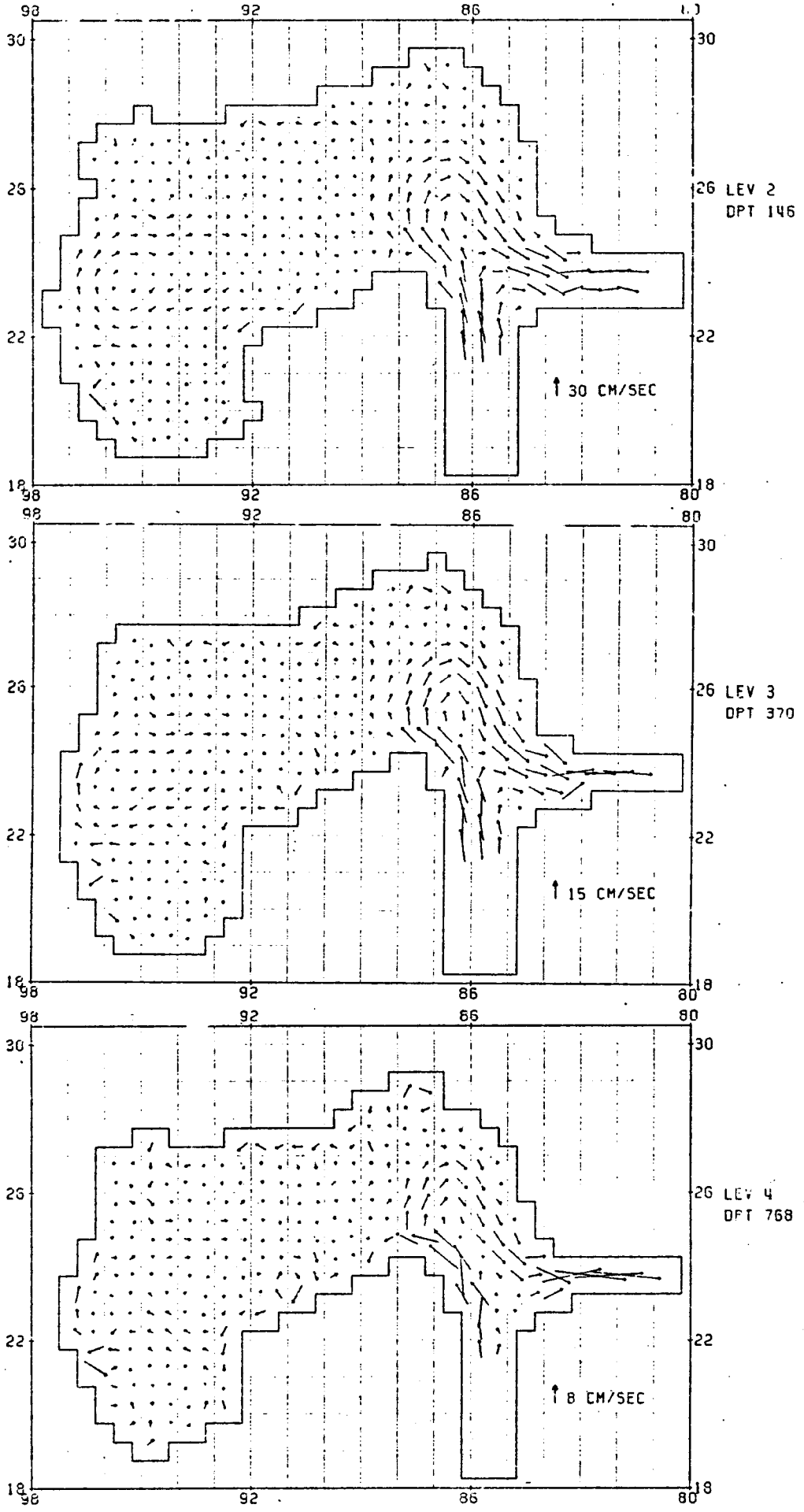

ANNUAL INCREMENT

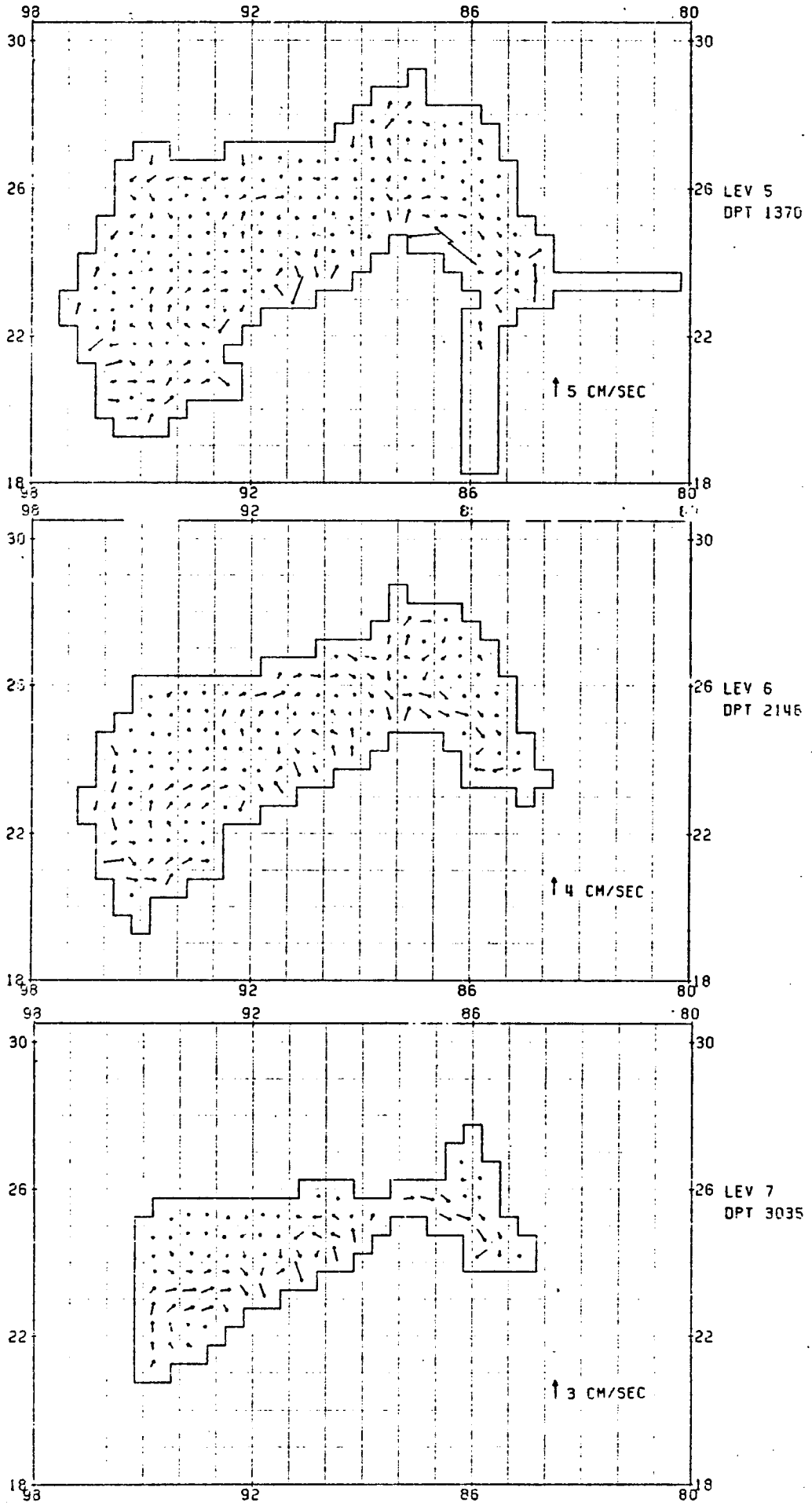

ANNUAL INCREMENT

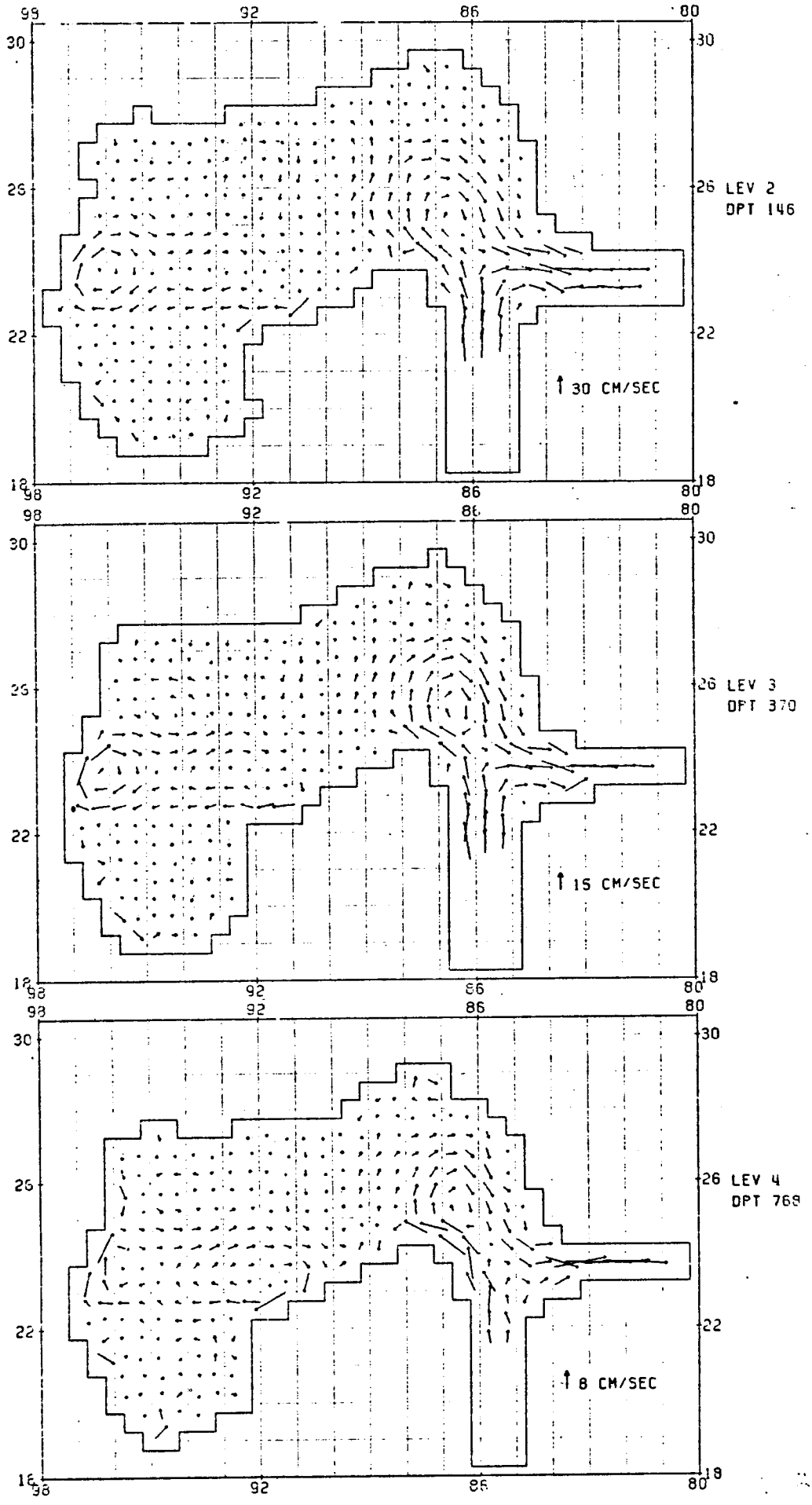

SEMI-ANNUAL INCREMENT
MAY-SEPTEMBER

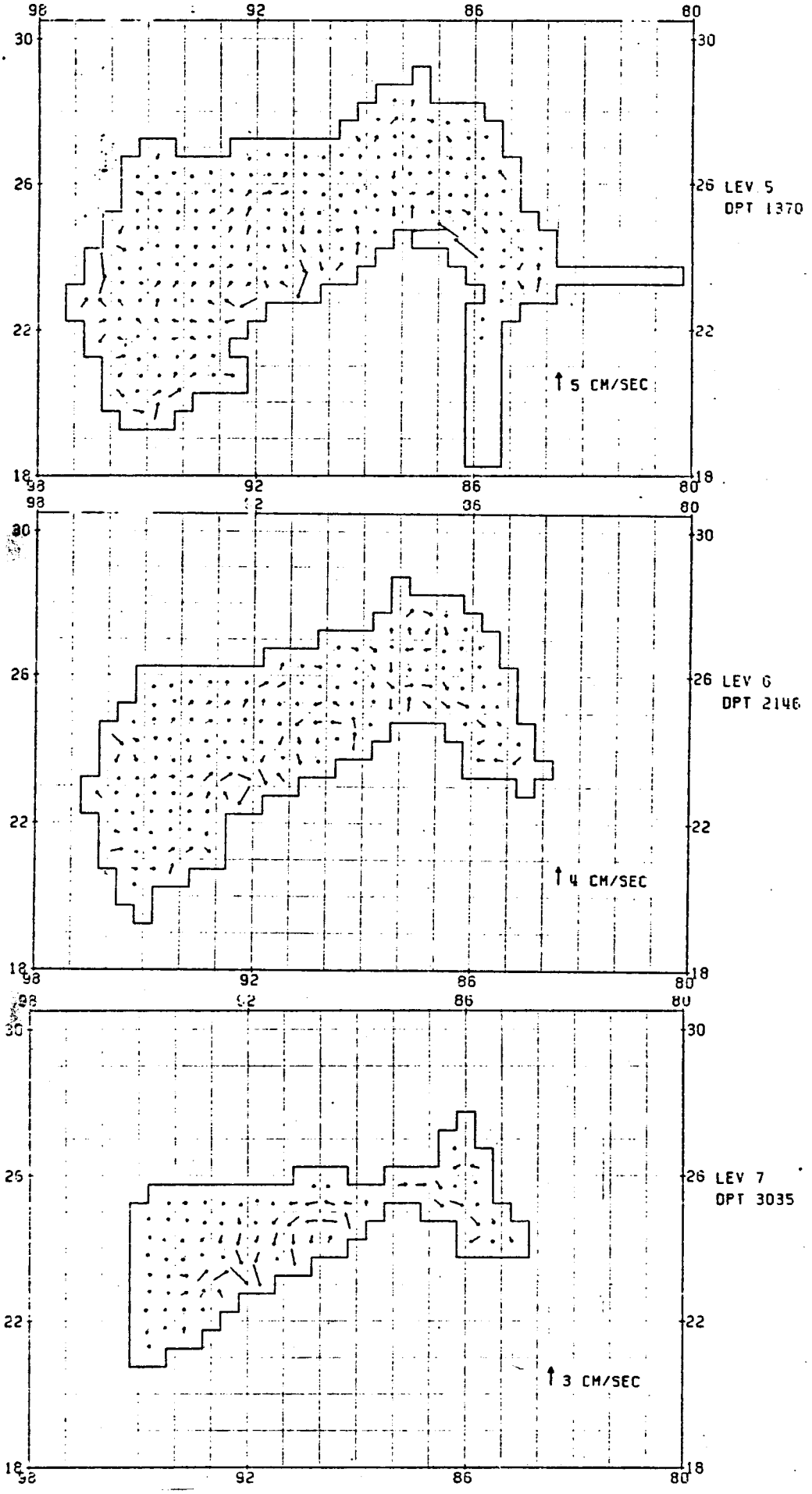

SEMI-ANNUAL INCREMENT
MAY-SEPTEMBER

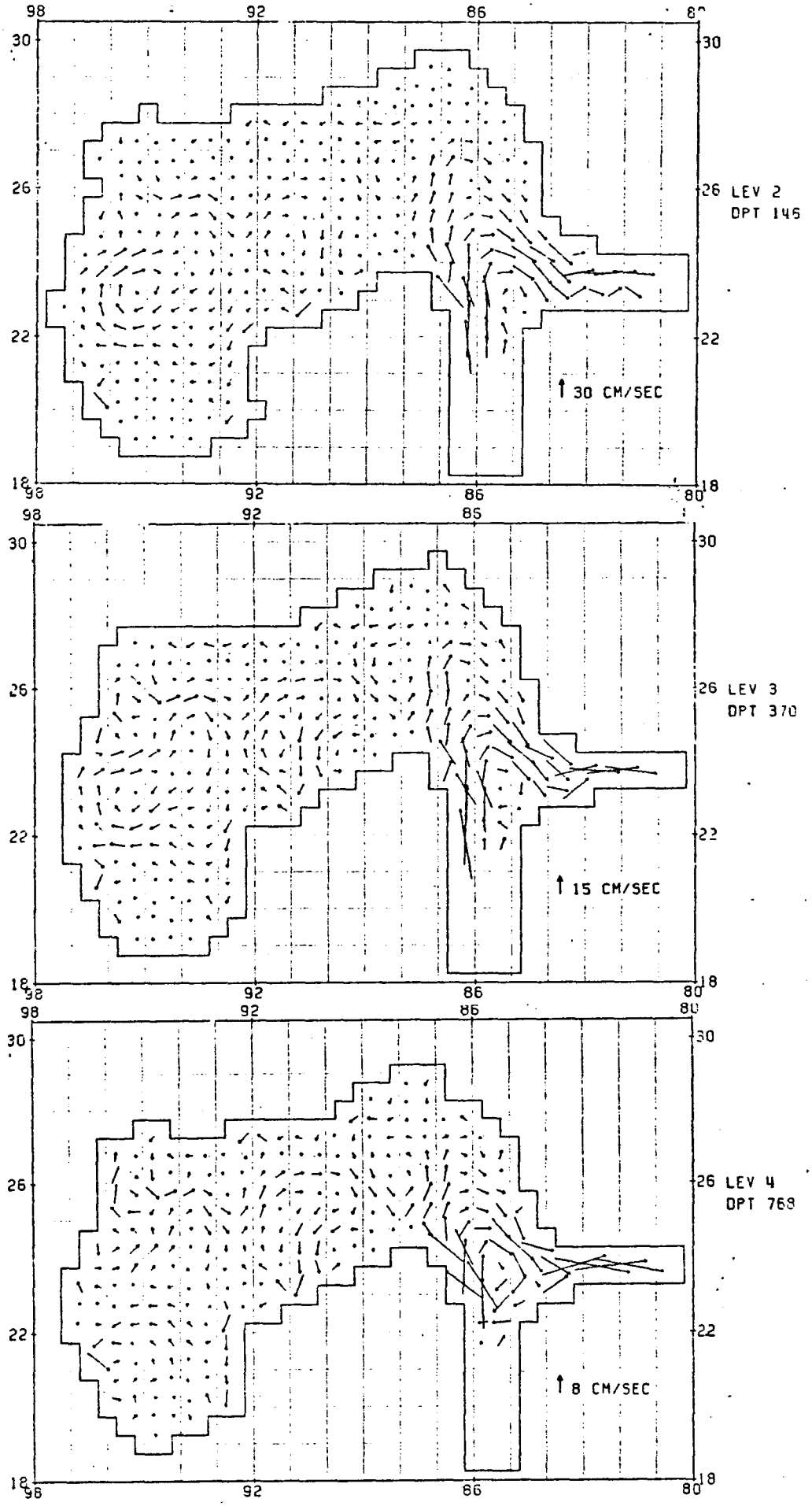

SEMI-ANNUAL INCREMENT
NOVEMBER-MARCH

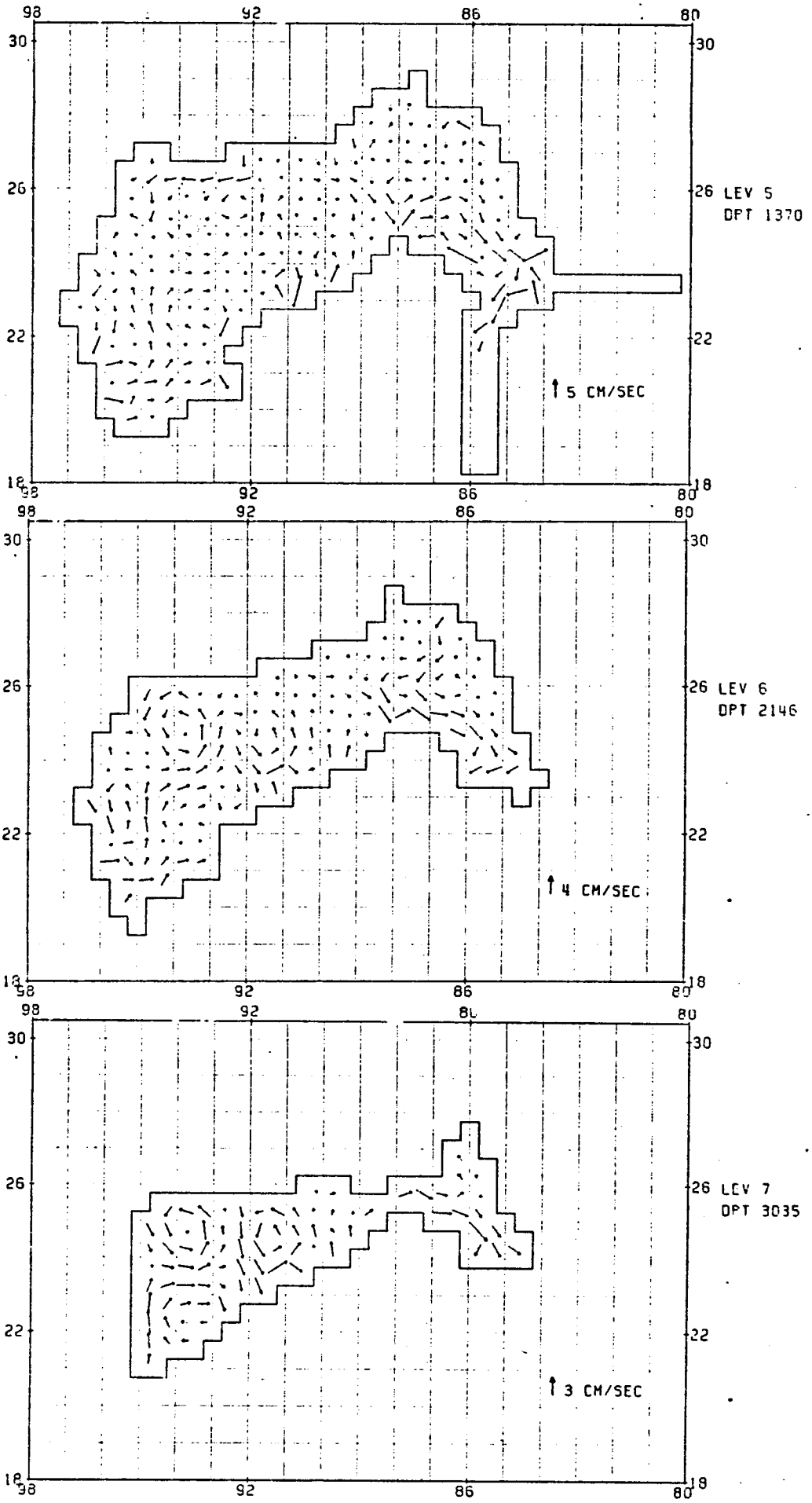

SEMI-ANNUAL INCREMENT

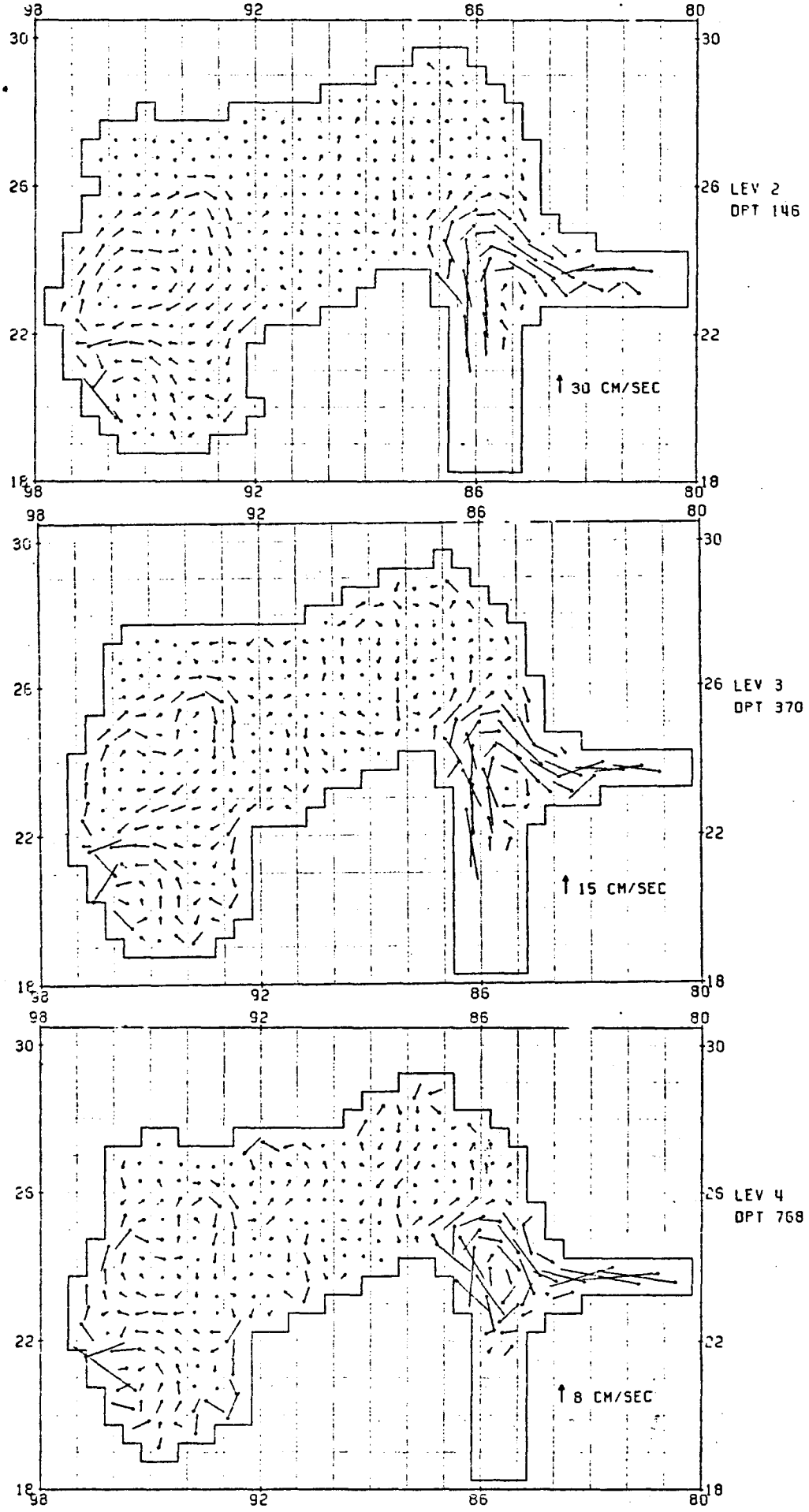

MONTHLY INCREMENT
JANUARY

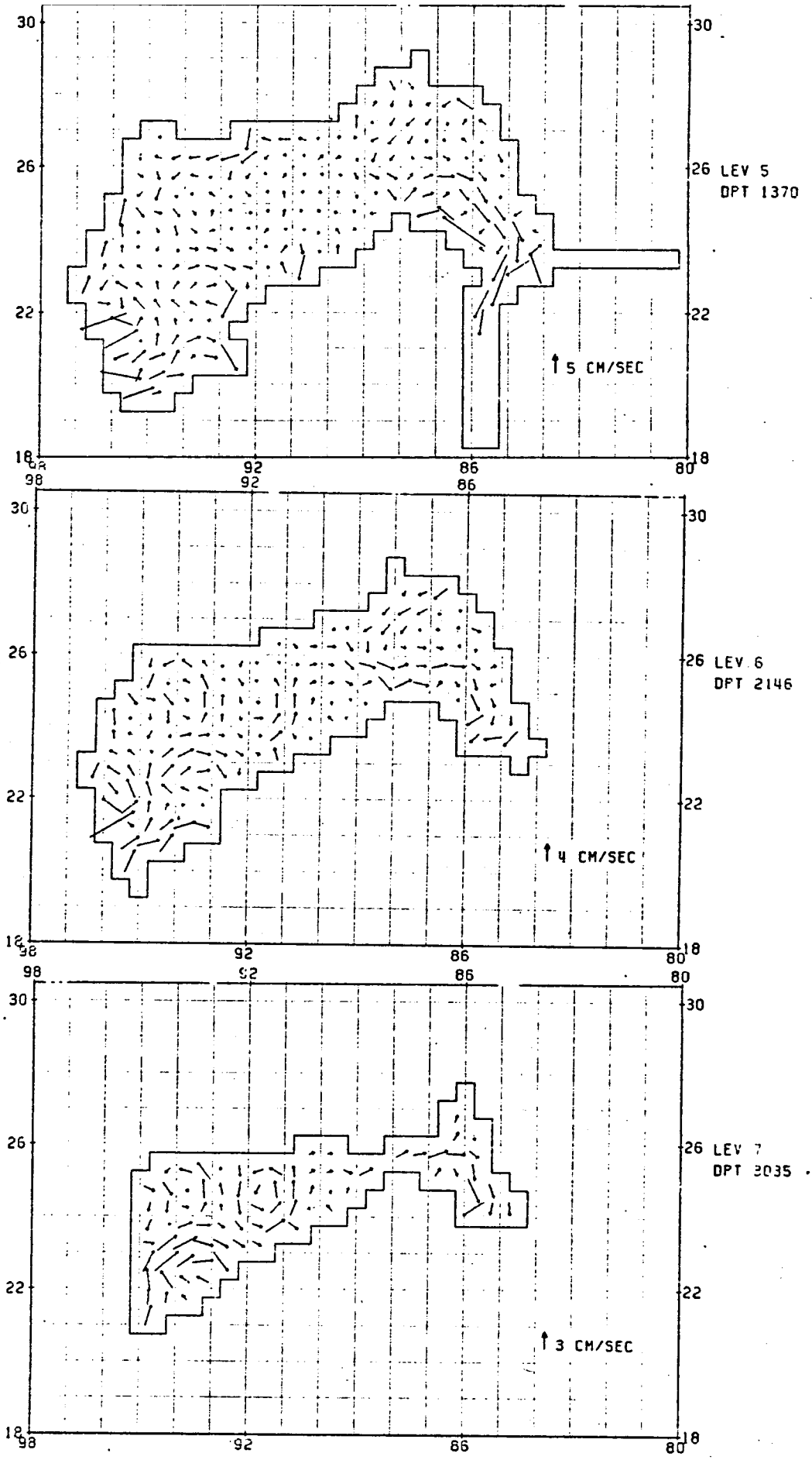

MONTHLY INCREMENT
JANUARY

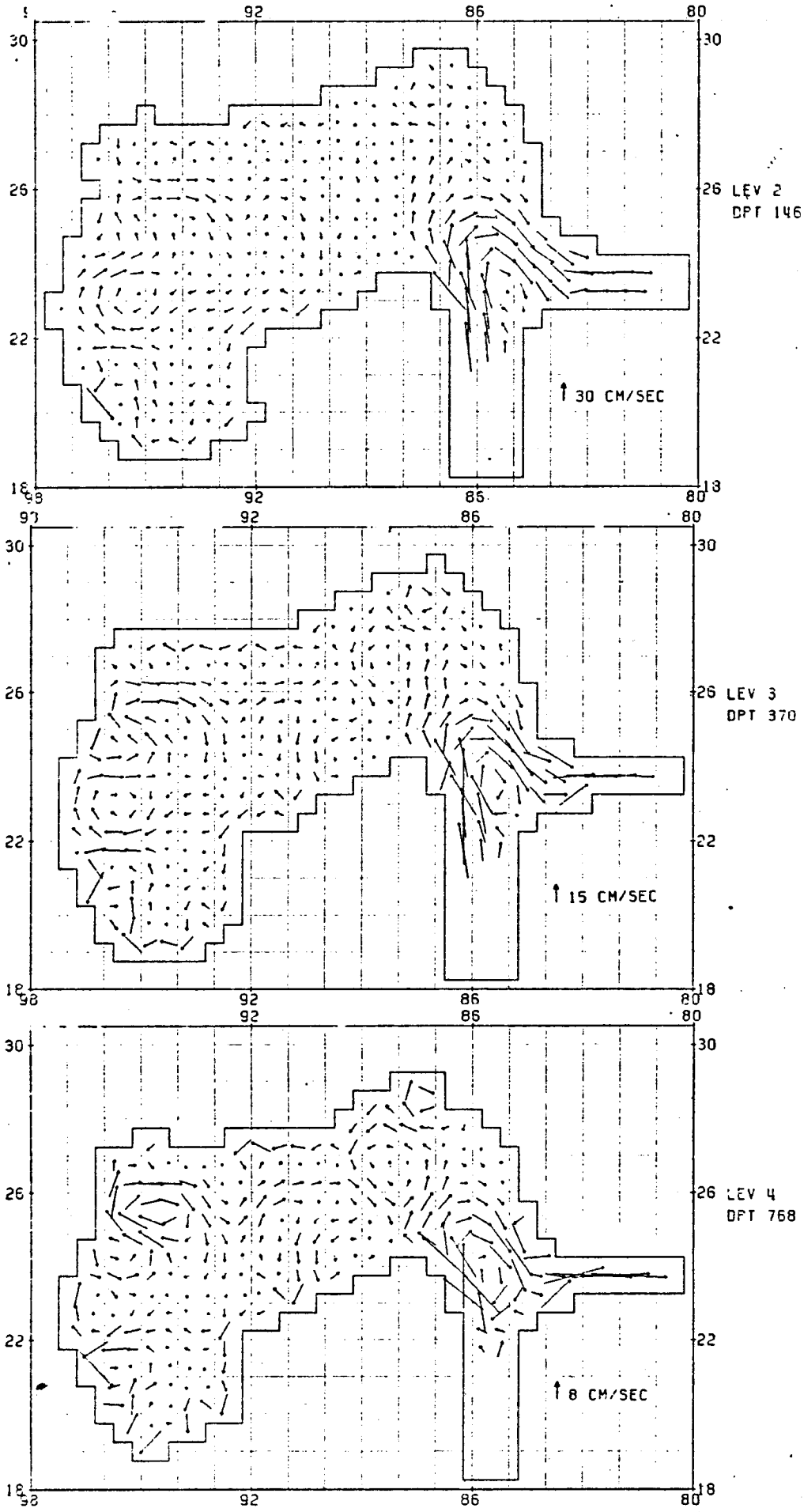

MONTHLY INCREMENT
FEBRUARY

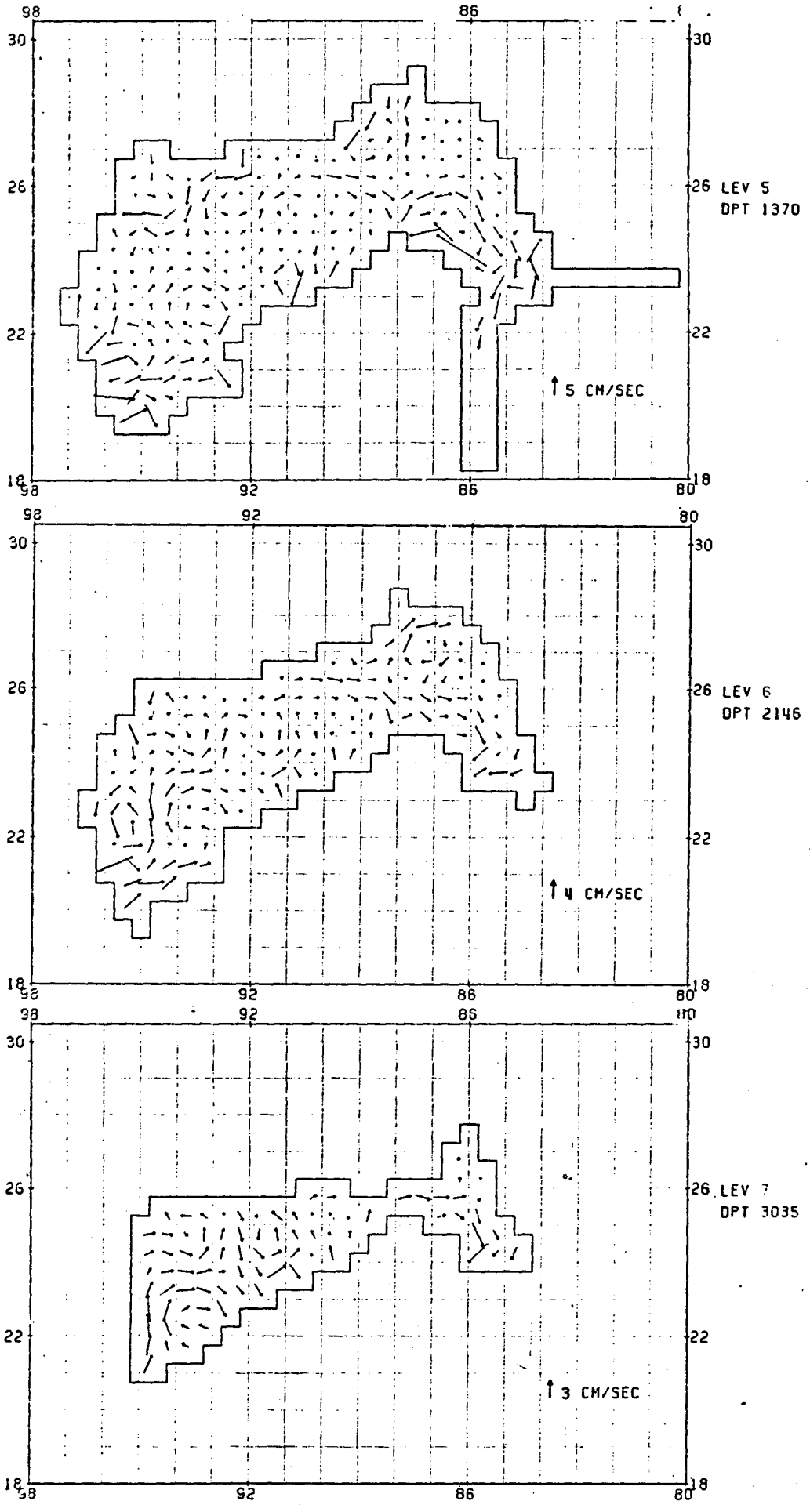

MONTHLY INCREMENT
FEBRUARY

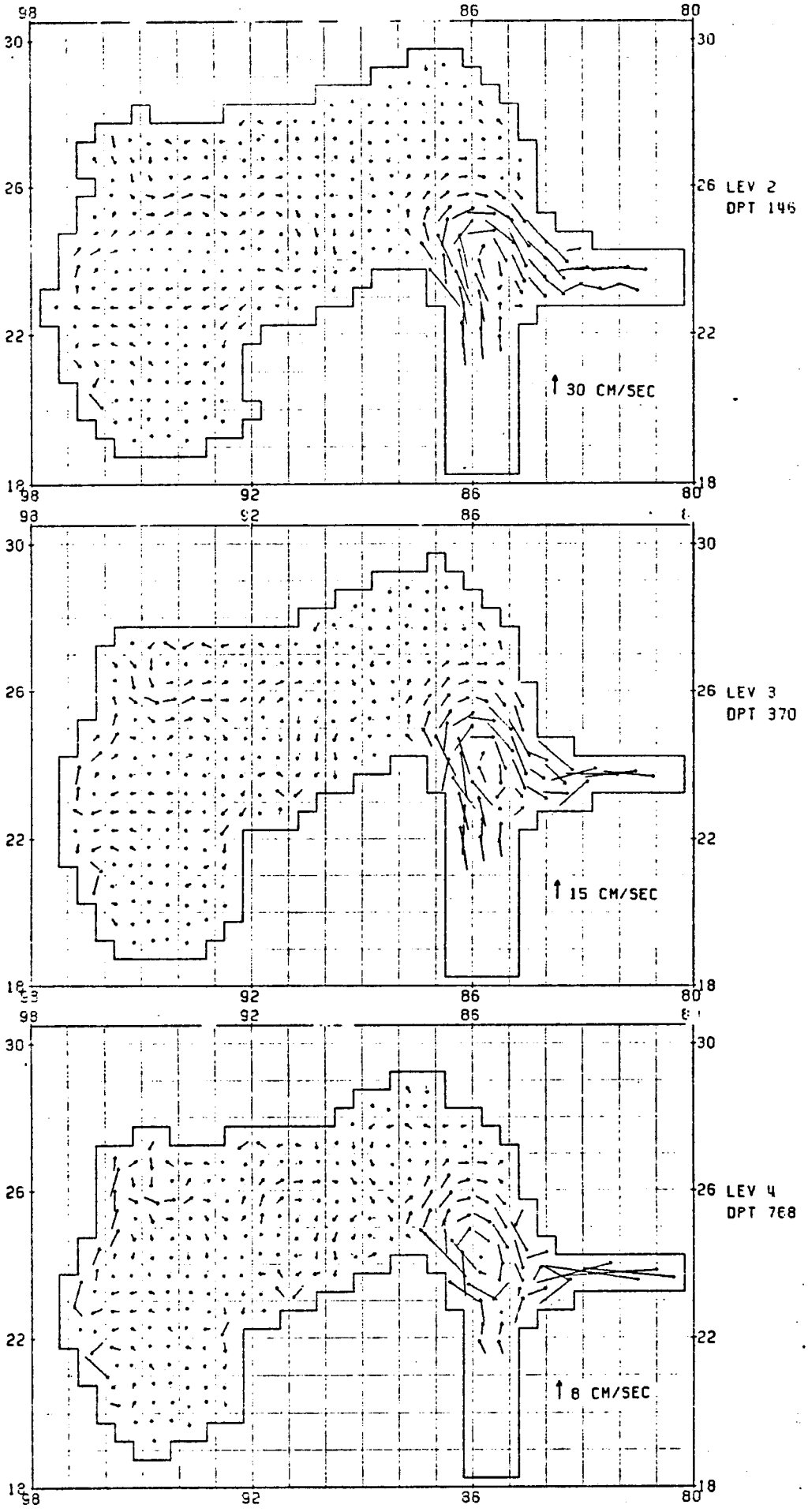

MONTHLY INCREMENT
MARCH

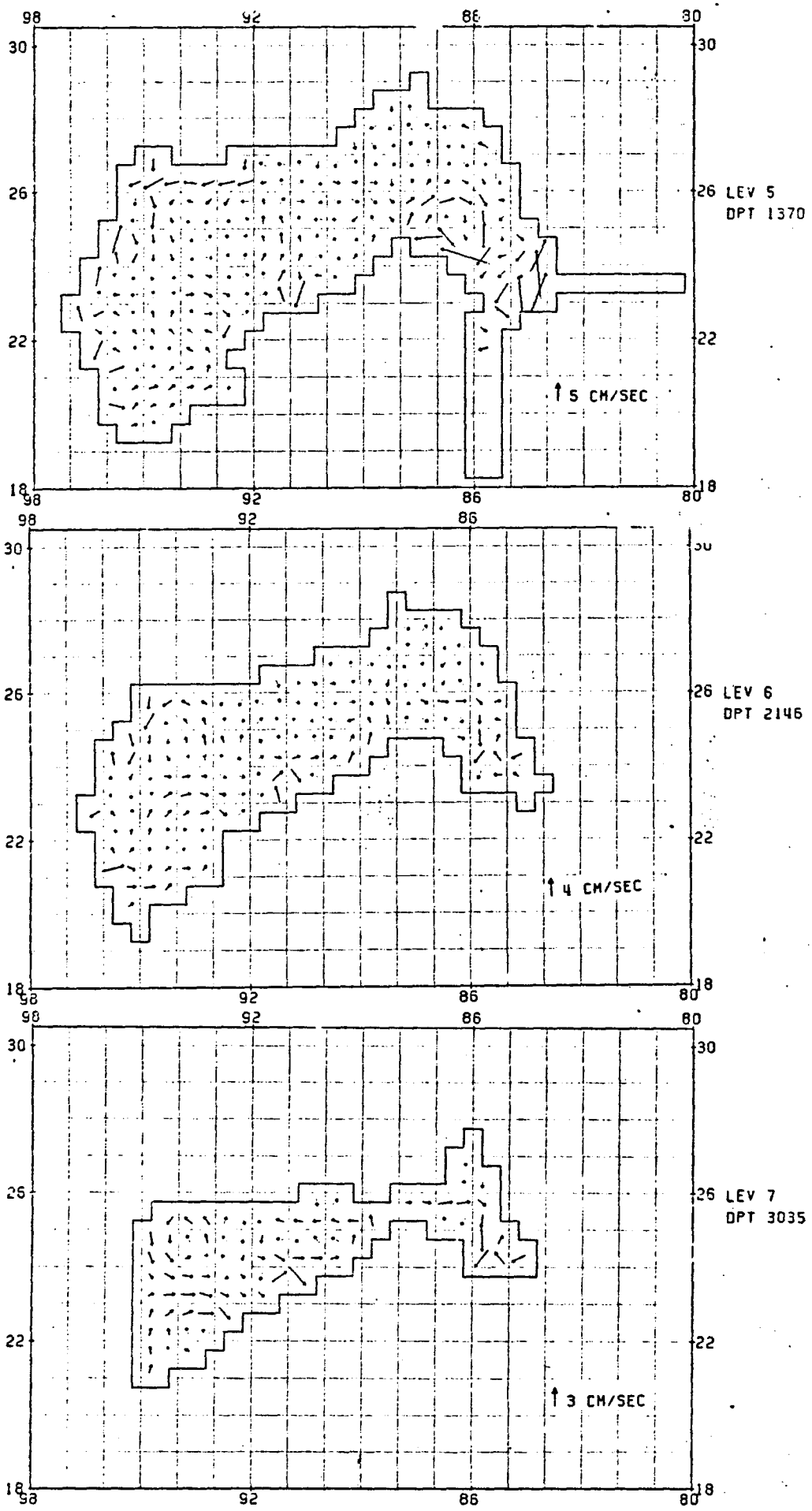

MONTHLY INCREMENT
MARCH

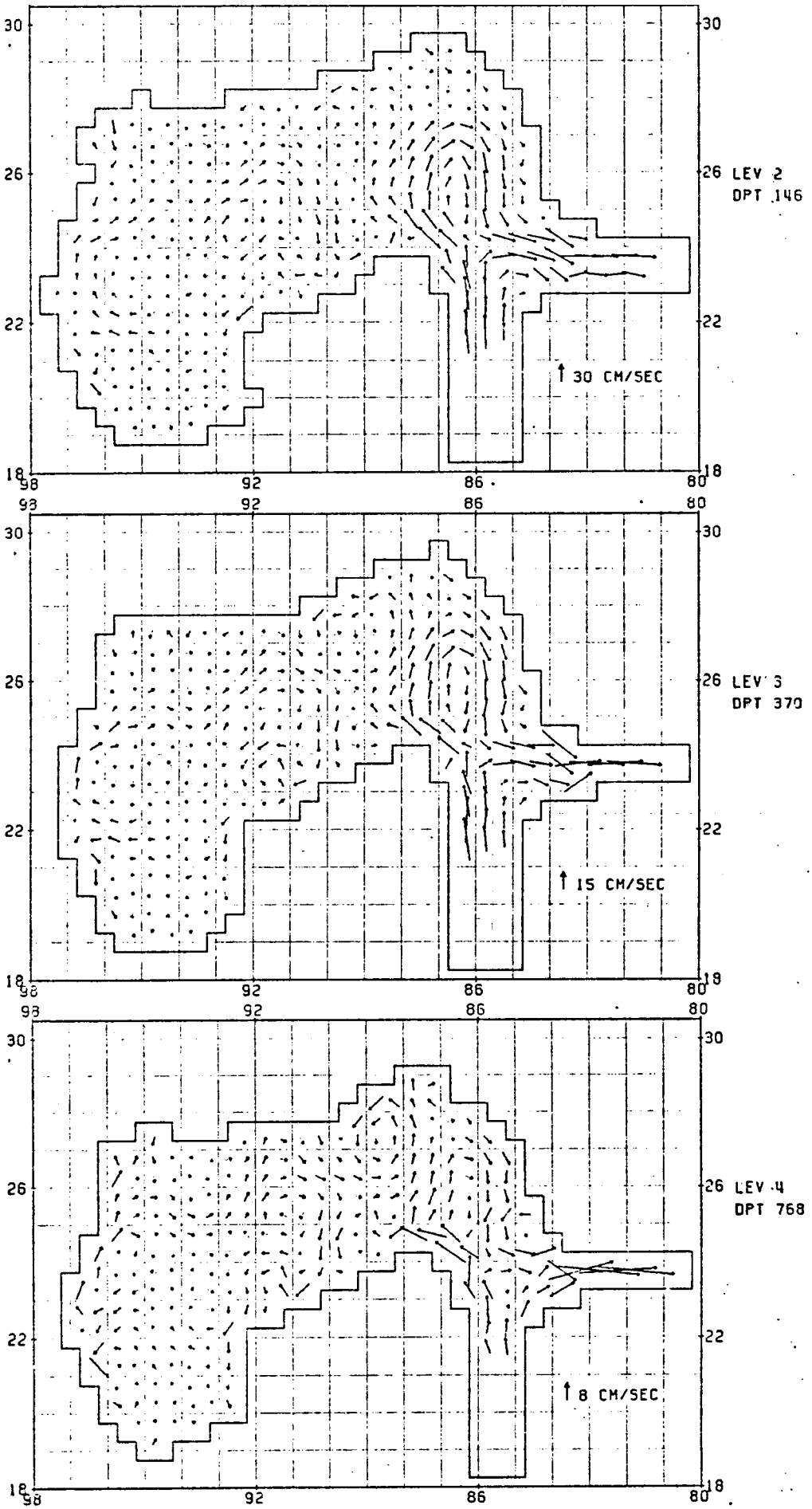

MONTHLY INCREMENT
APRIL

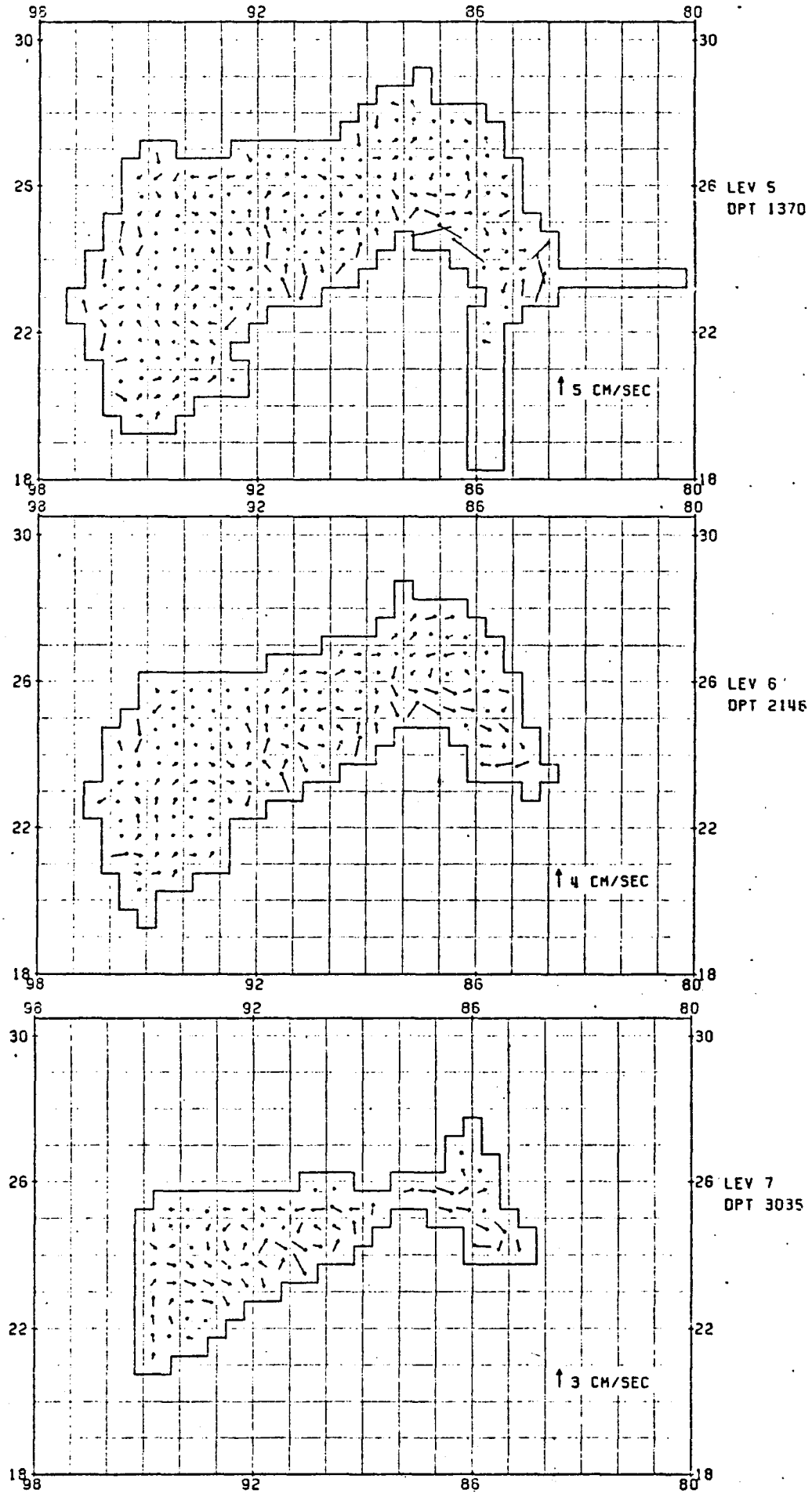

MONTHLY INCREMENT
APRIL

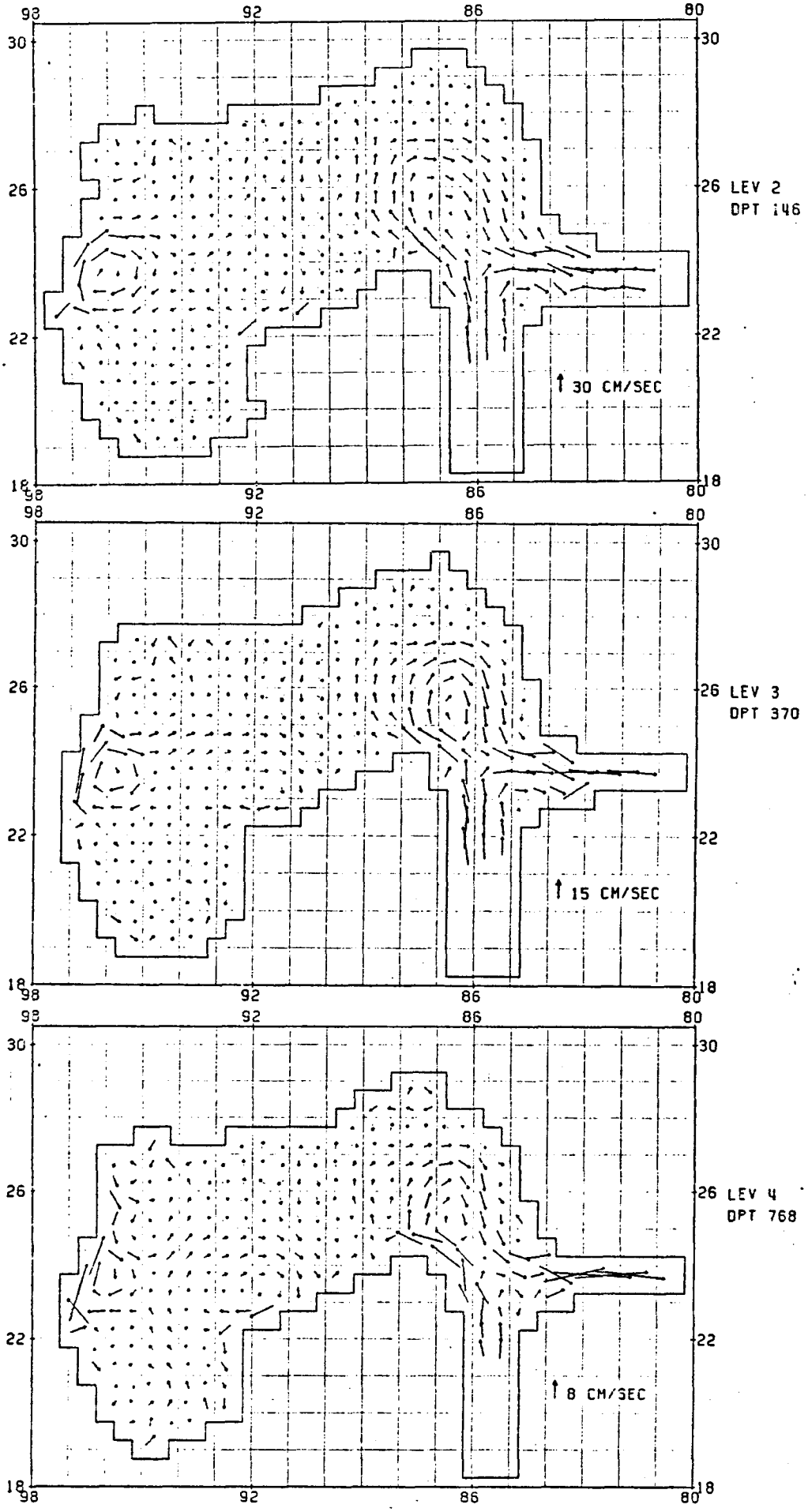

MONTHLY INCREMENT
JUNE

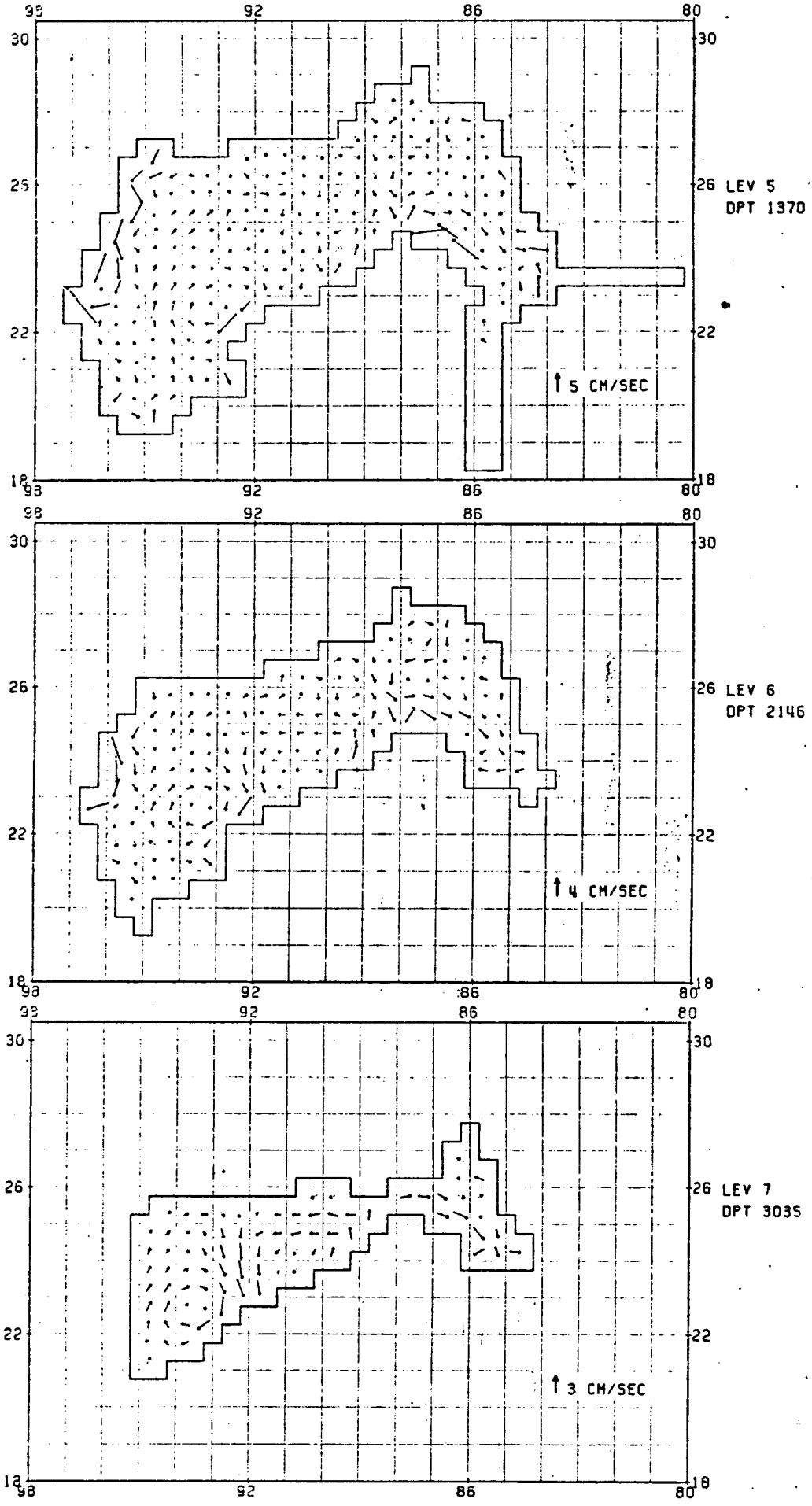

MONTHLY INCREMENT
JUNE

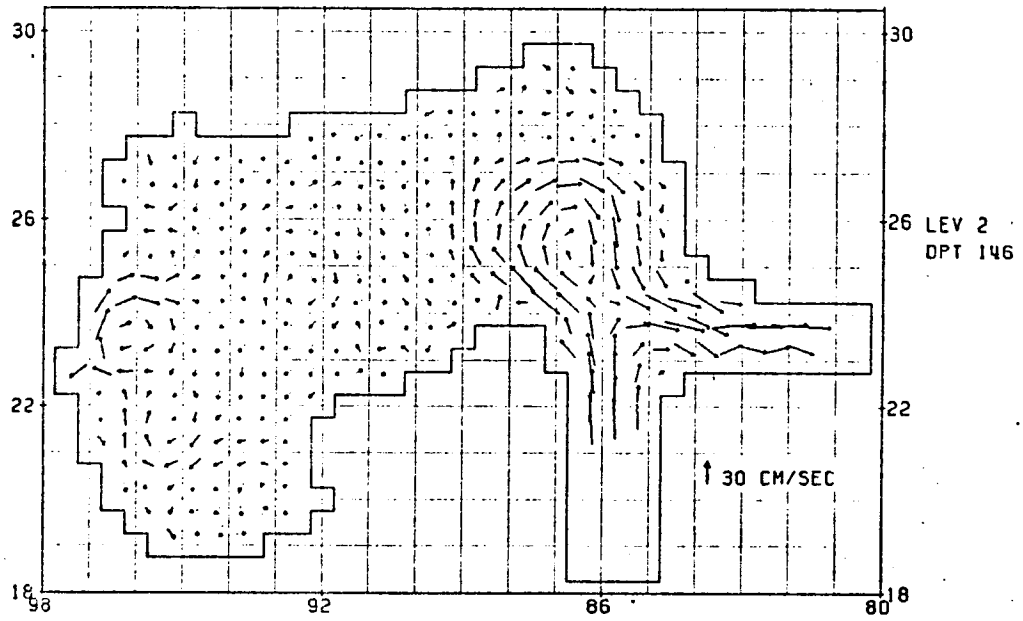

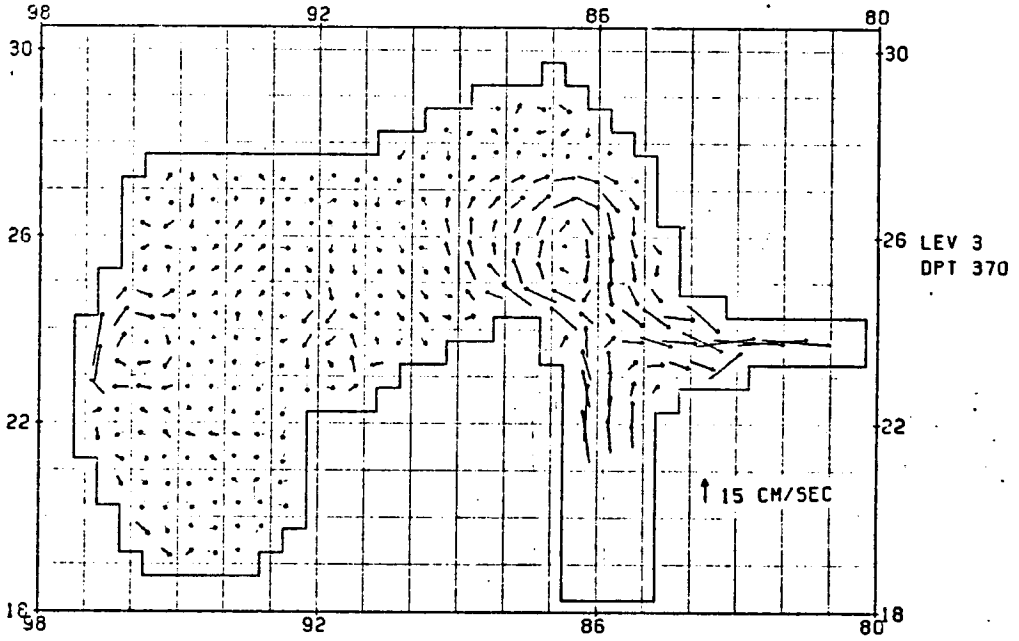

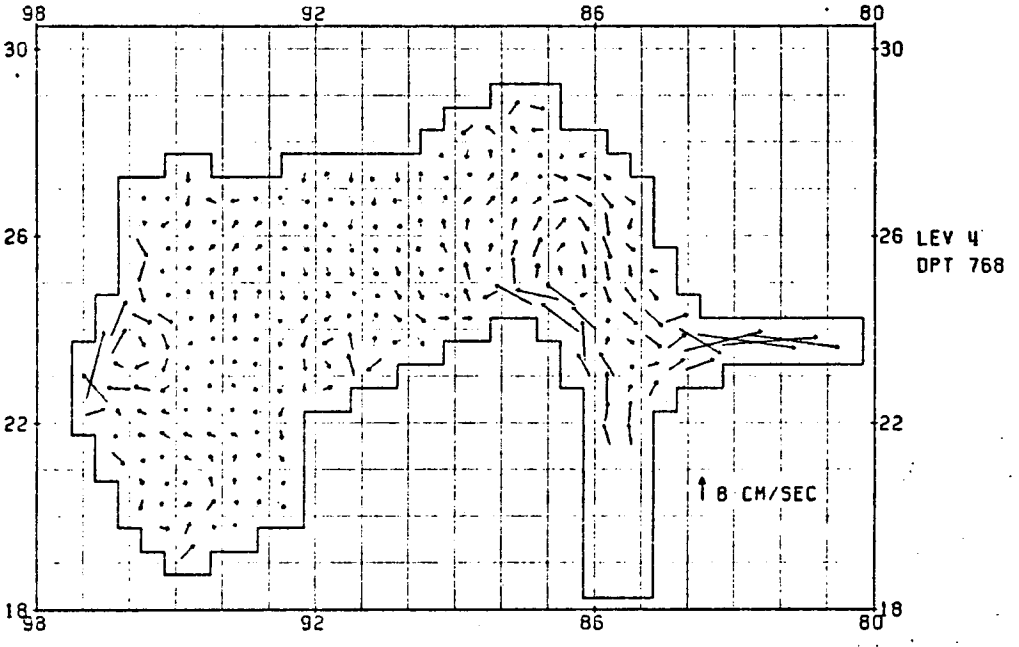

MONTHLY INCREMENT
MAY

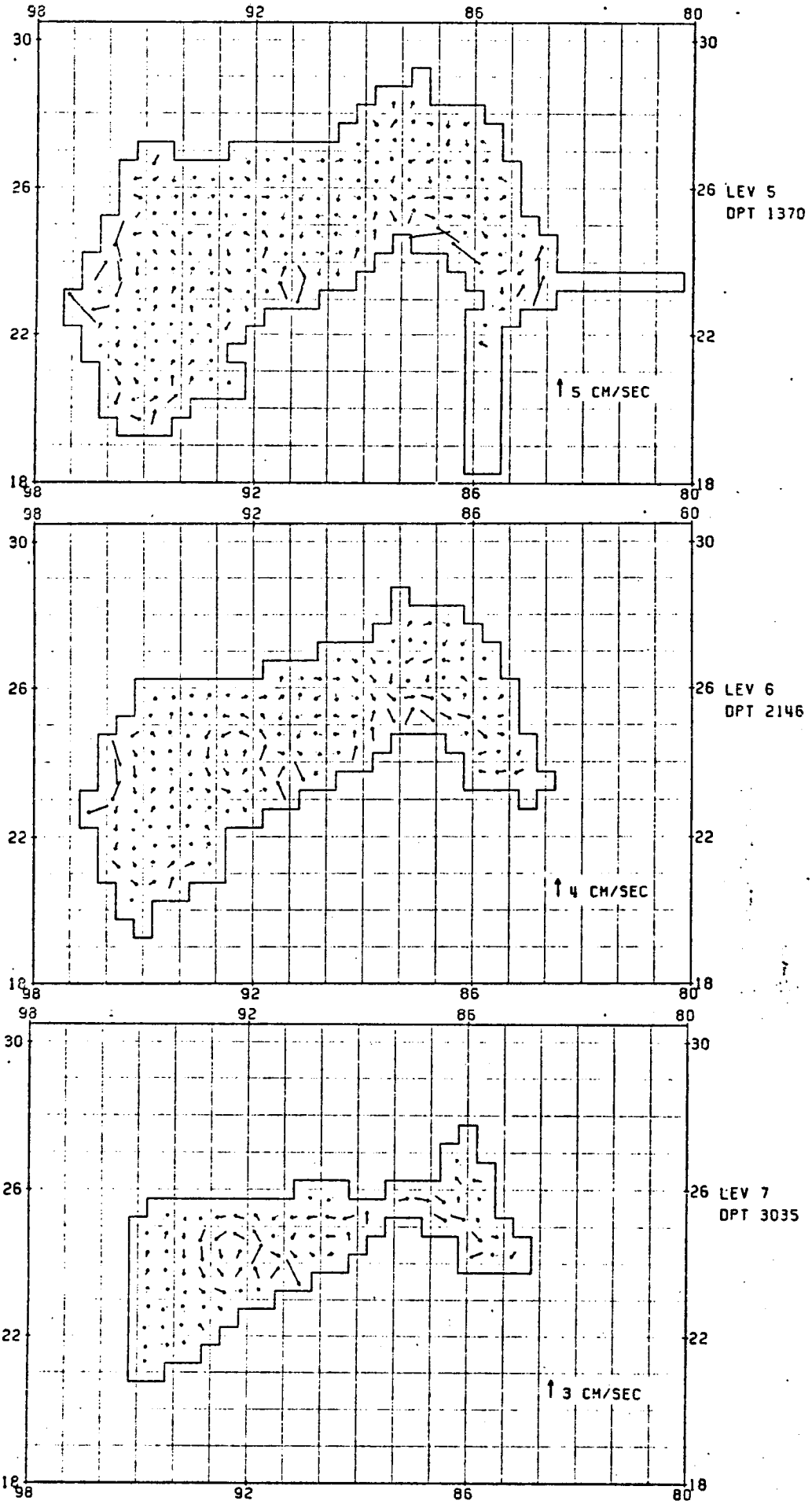

MONTHLY INCREMENT
MAY

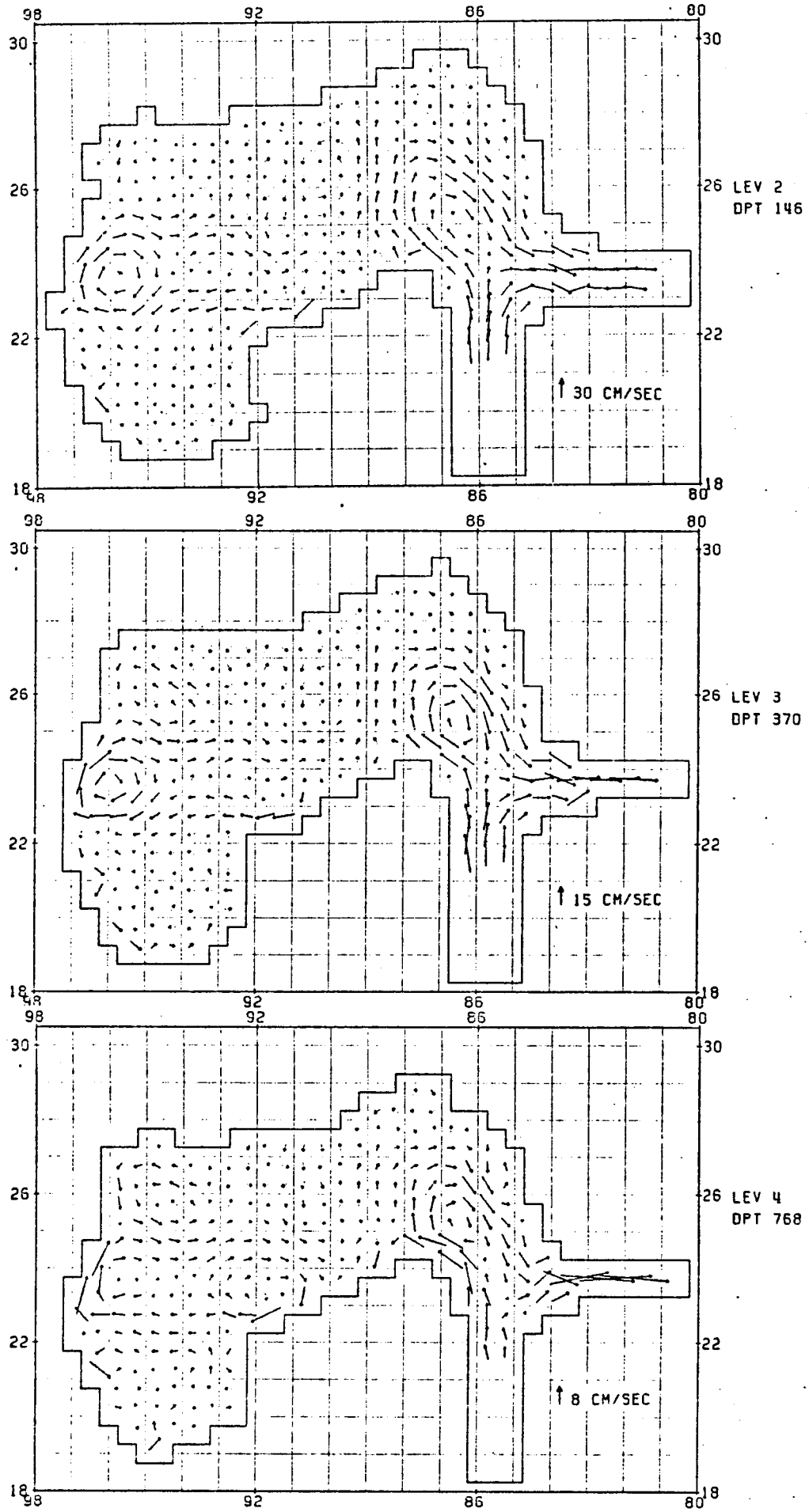

MONTHLY INCREMENT
JULY

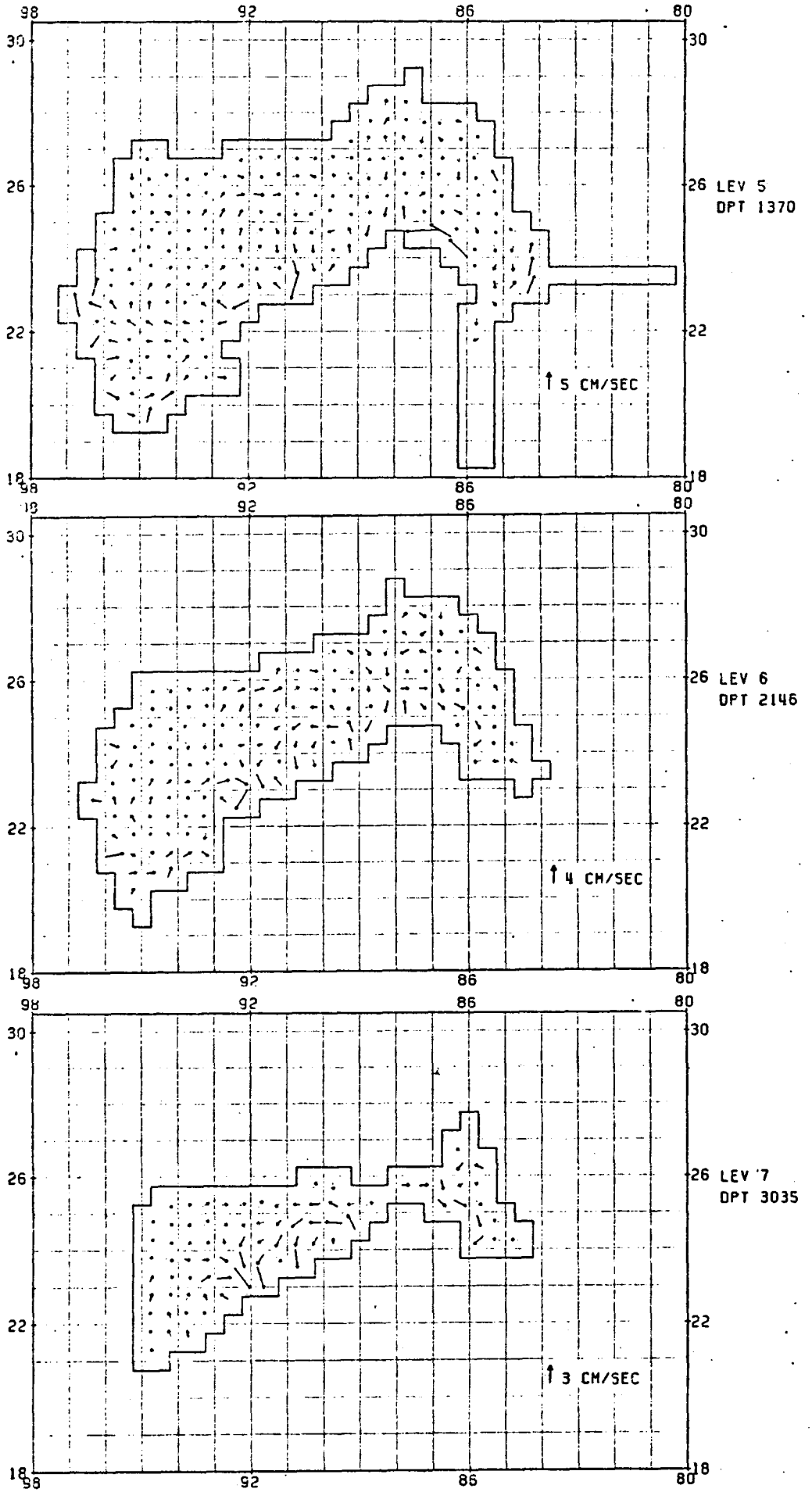

MONTHLY INCREMENT
JULY

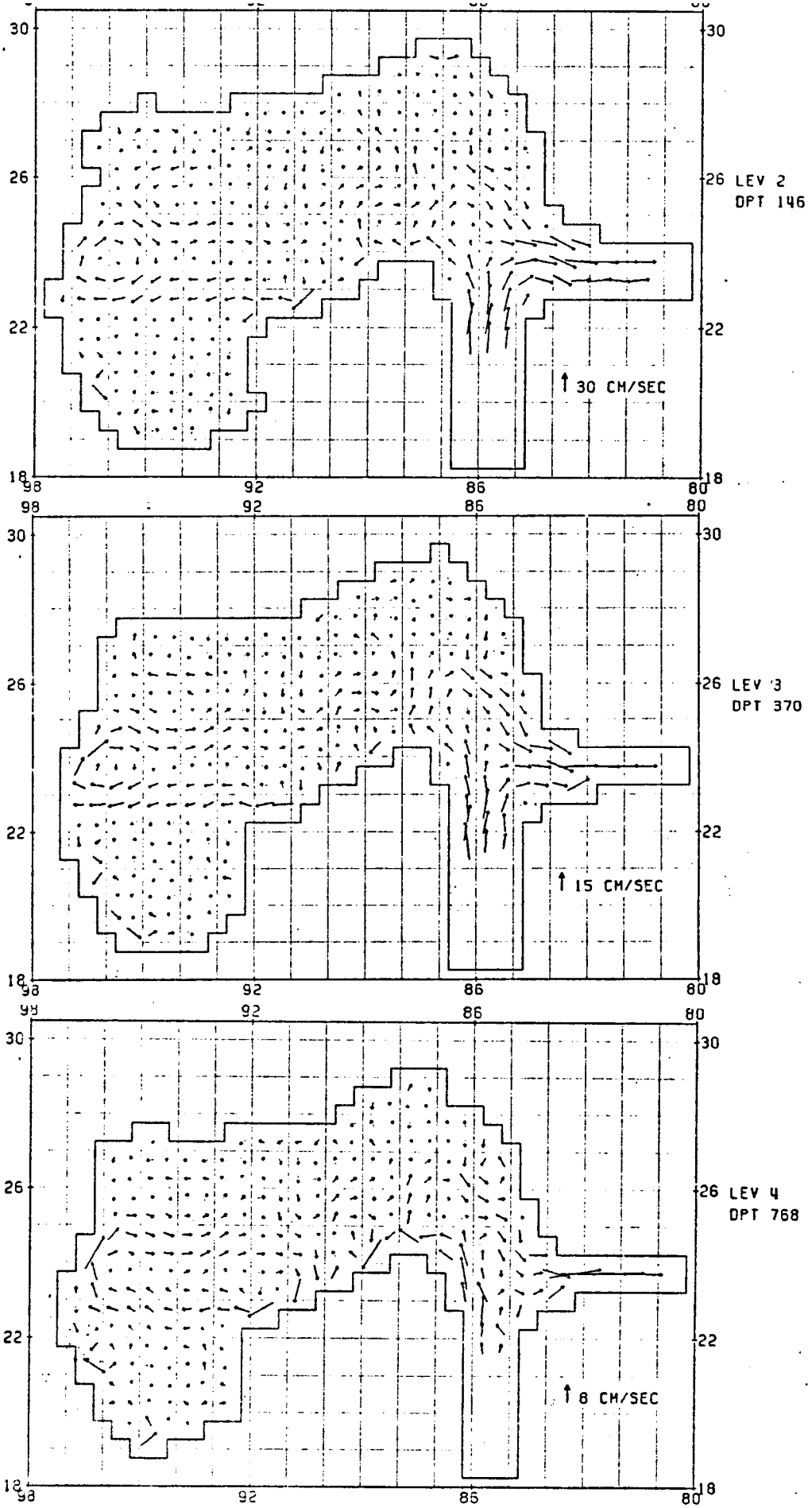

MONTHLY INCREMENT
AUGUST

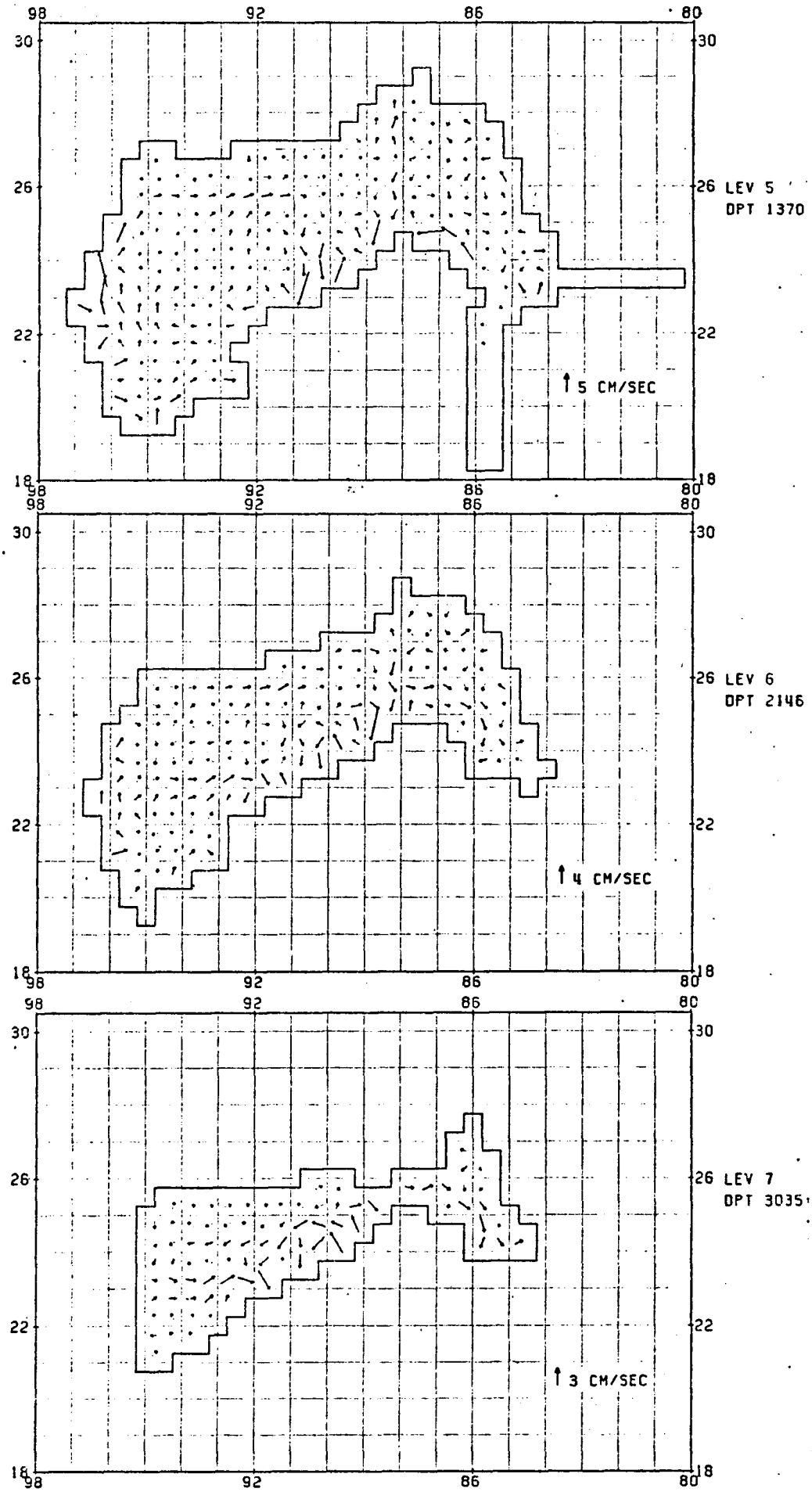

MONTHLY INCREMENT
AUGUST

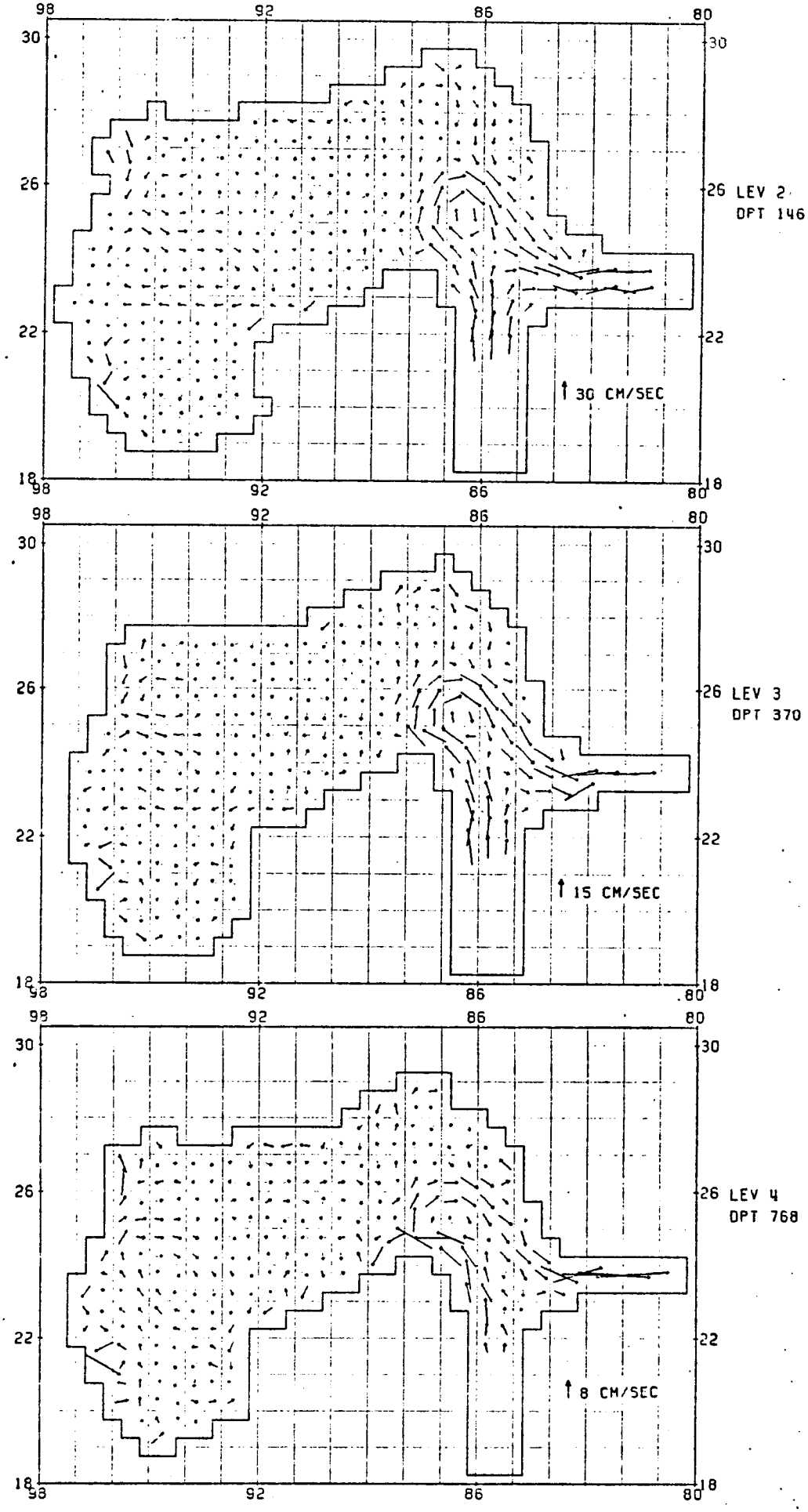

MONTHLY INCREMENT
SEPTEMBER

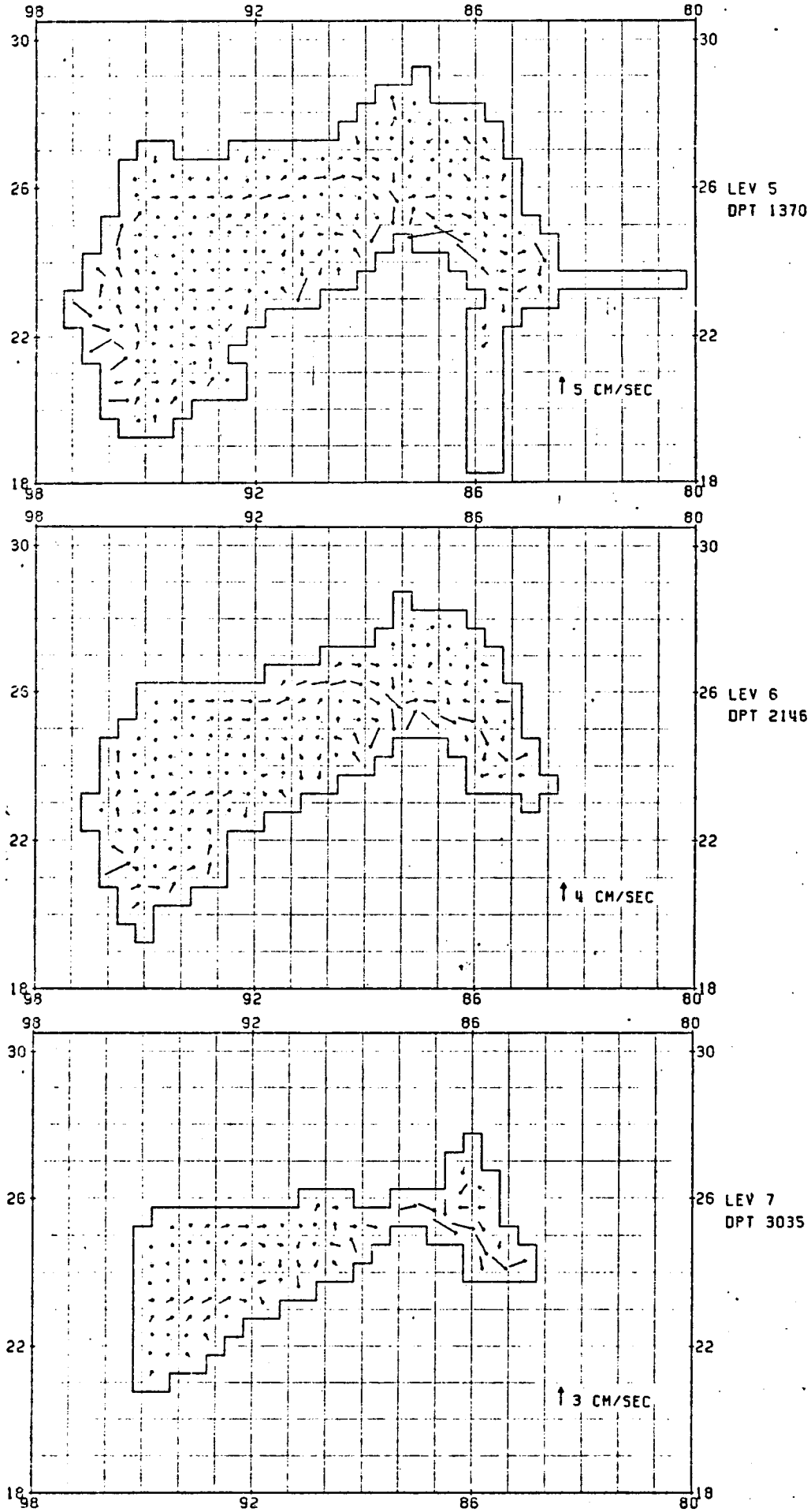

MONTHLY INCREMENT
SEPTEMBER

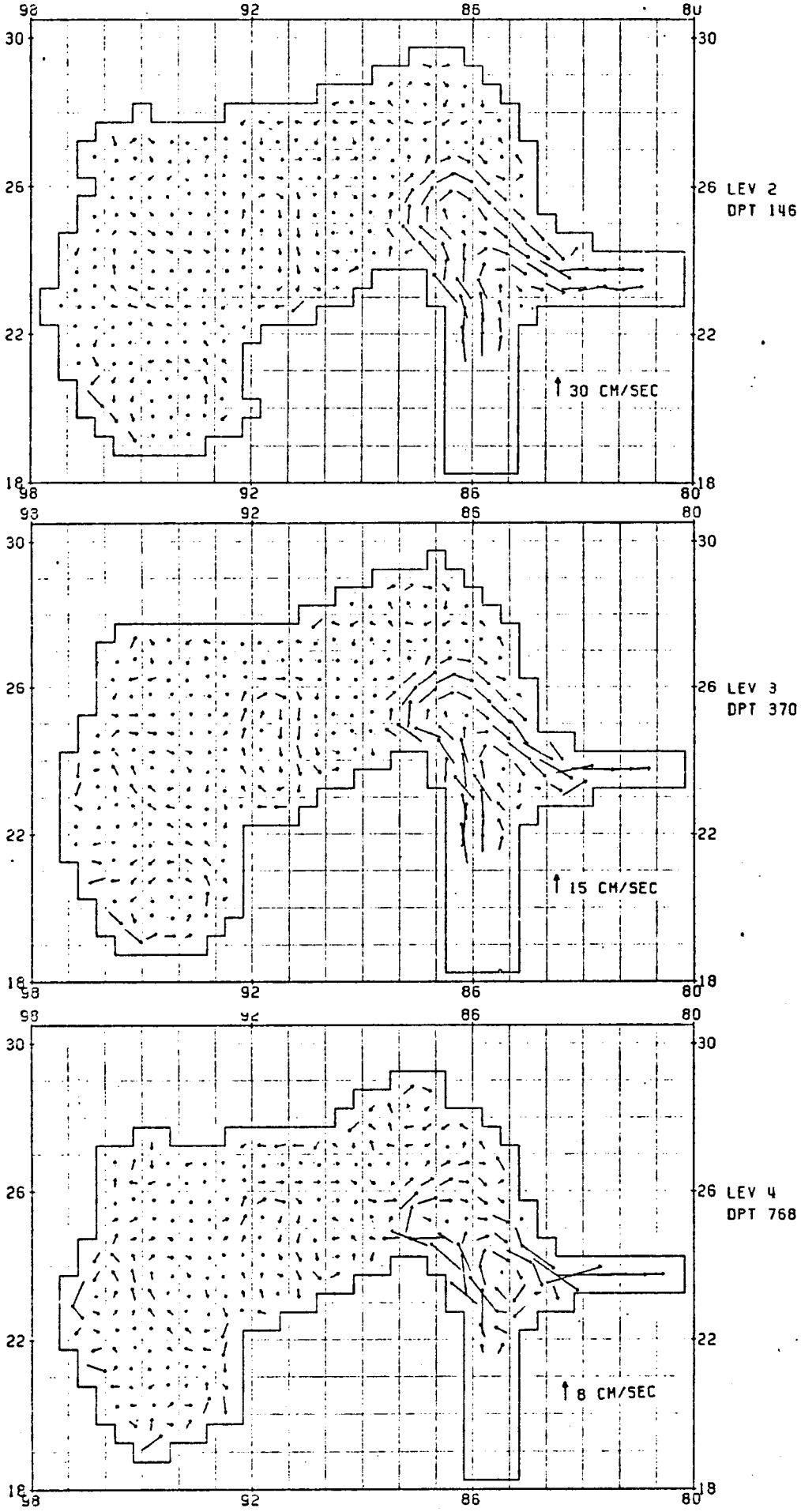

MONTHLY INCREMENT
OCTOBER

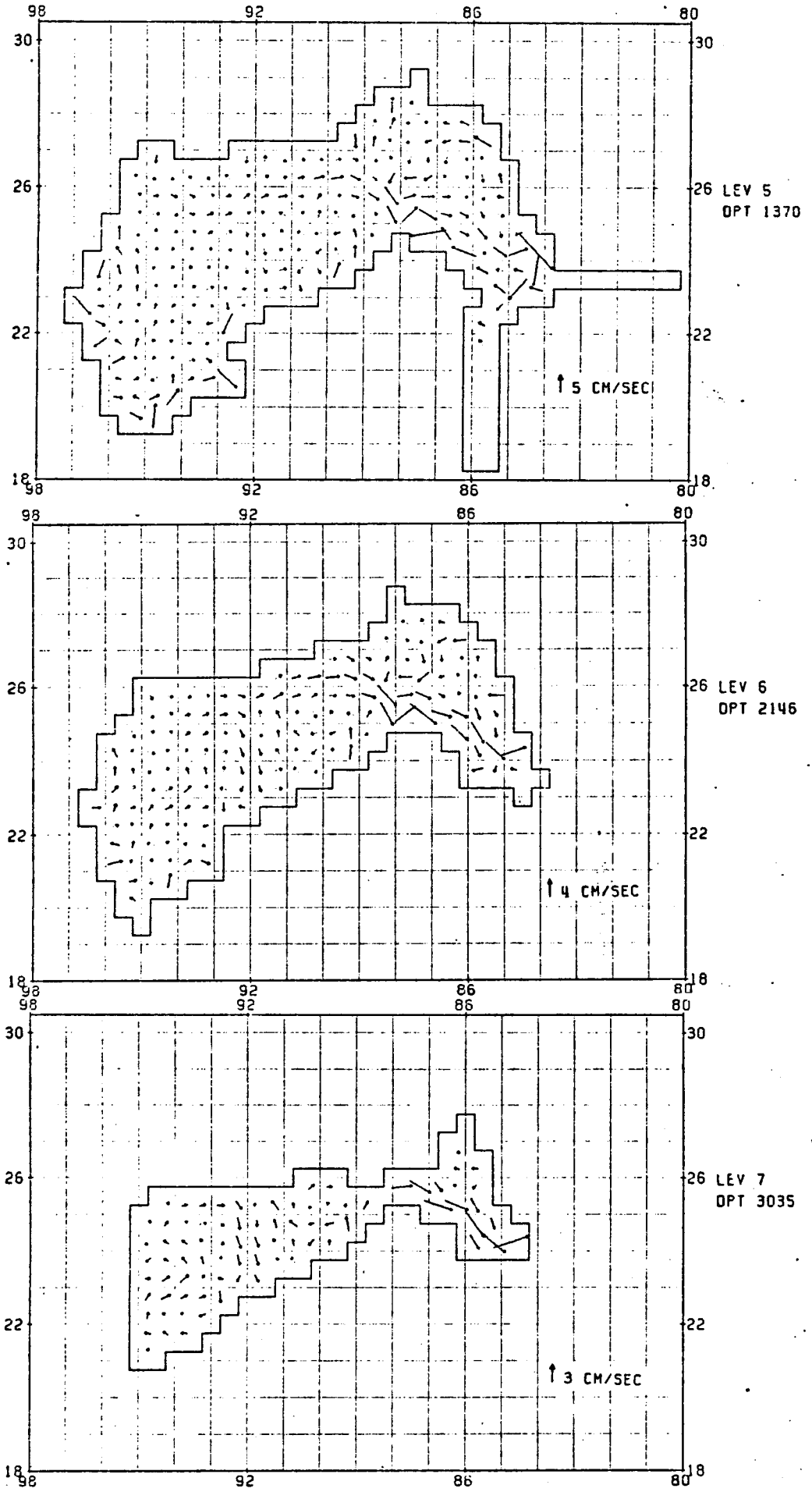

MONTHLY INCREMENT
OCTOBER

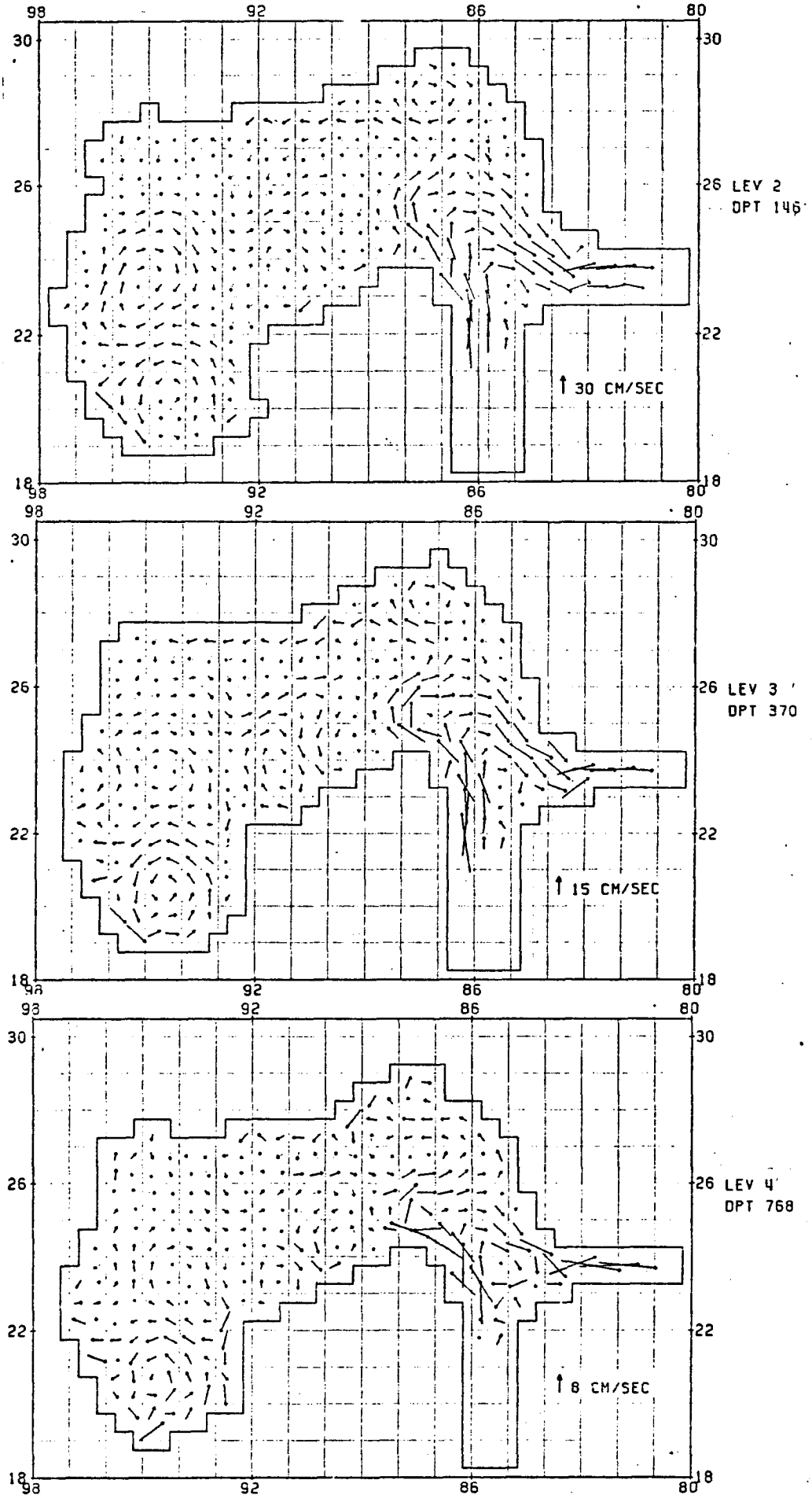

MONTHLY INCREMENT
NOVEMBER

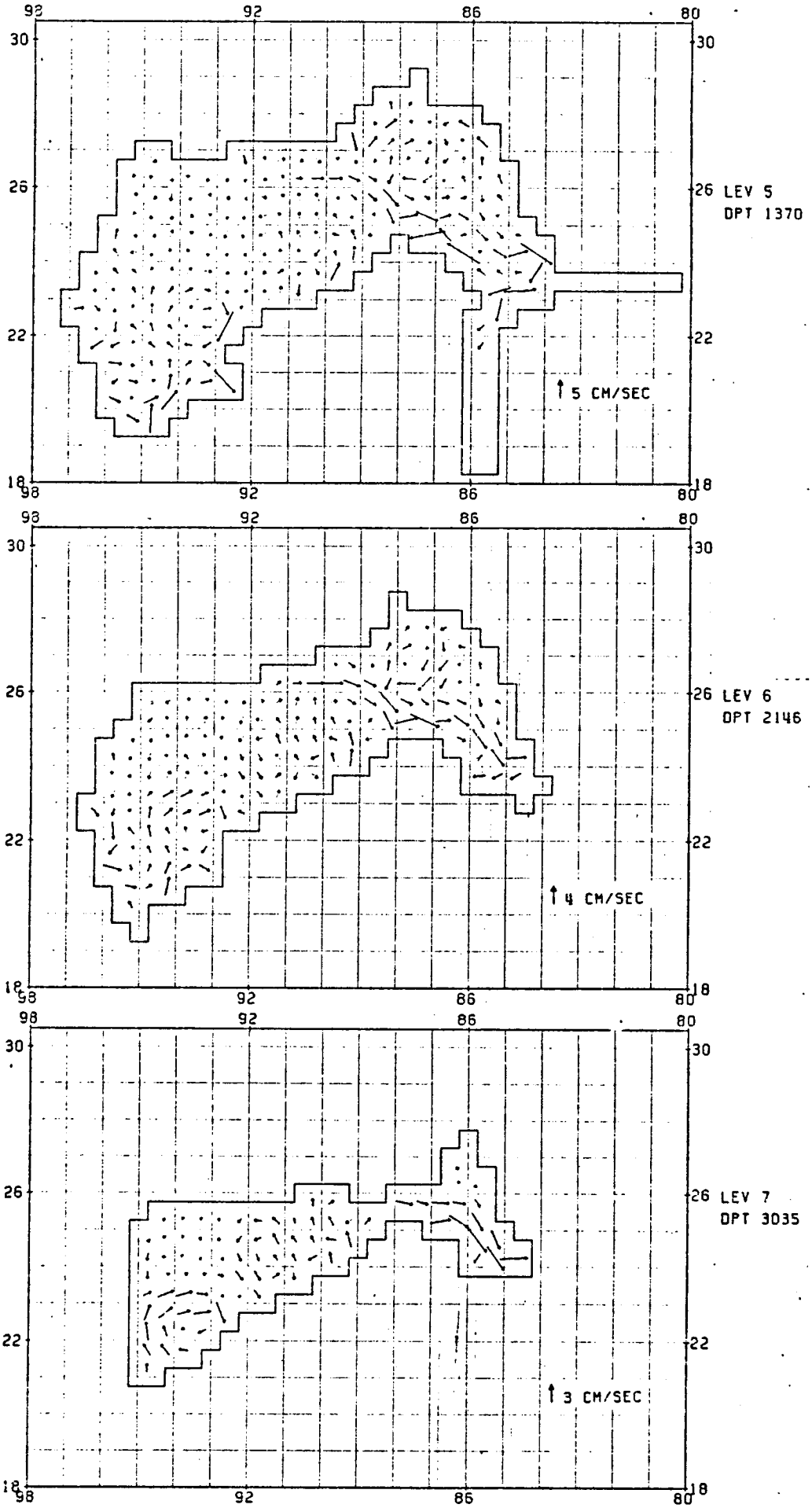

MONTHLY INCREMENT
NOVEMBER

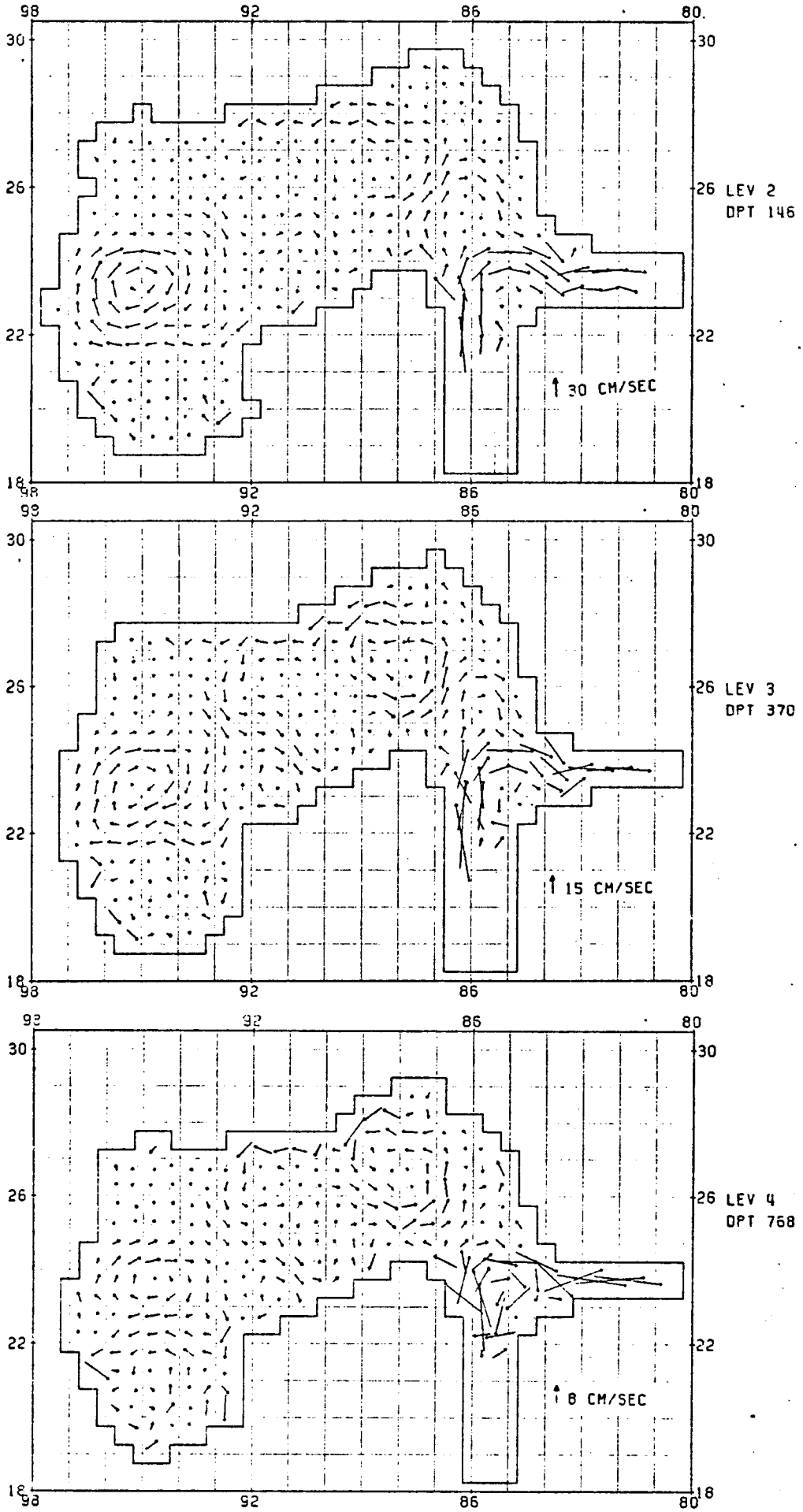

MONTHLY INCREMENT
DECEMBER

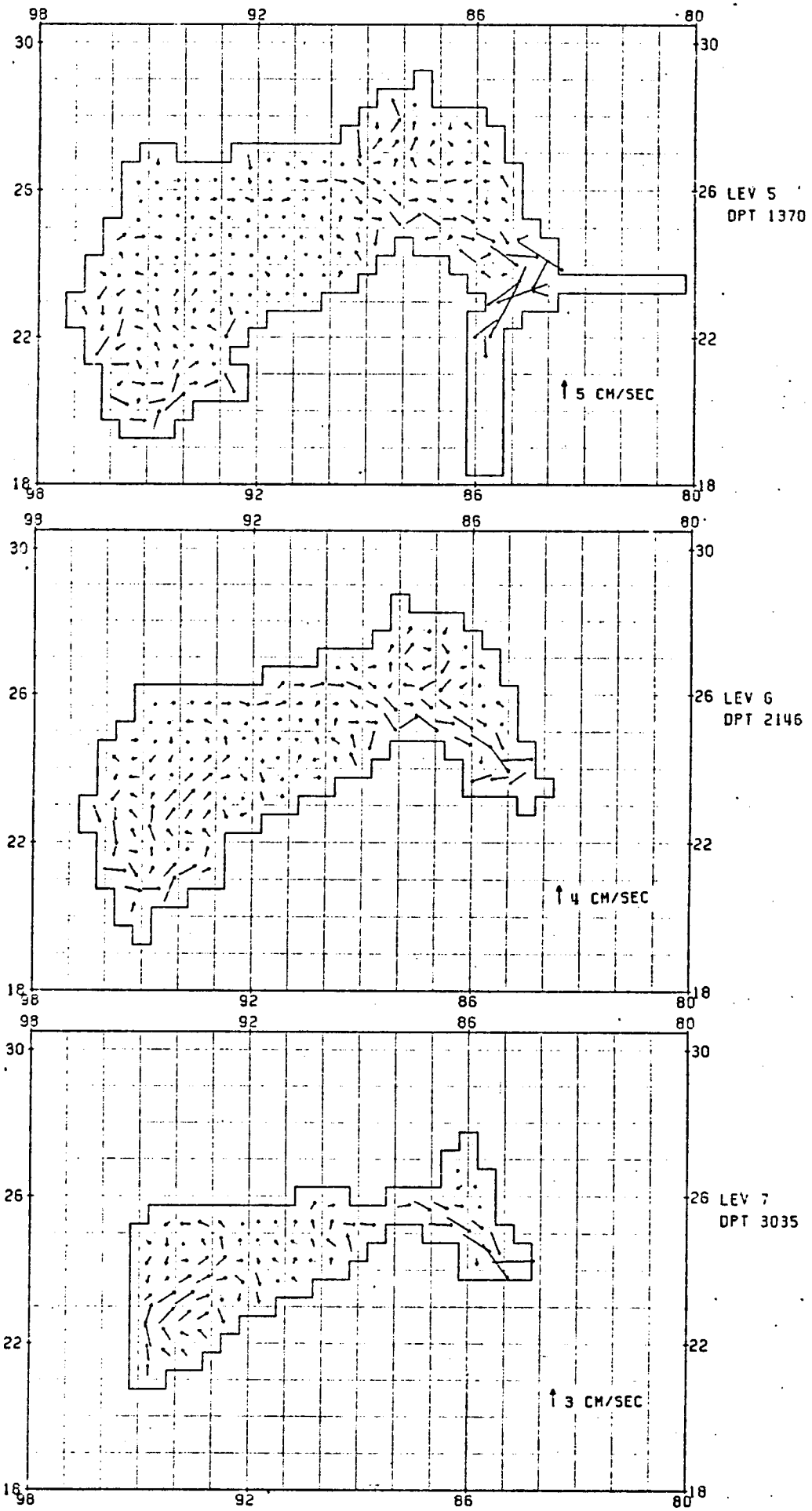

MONTHLY INCREMENT
DECEMBER

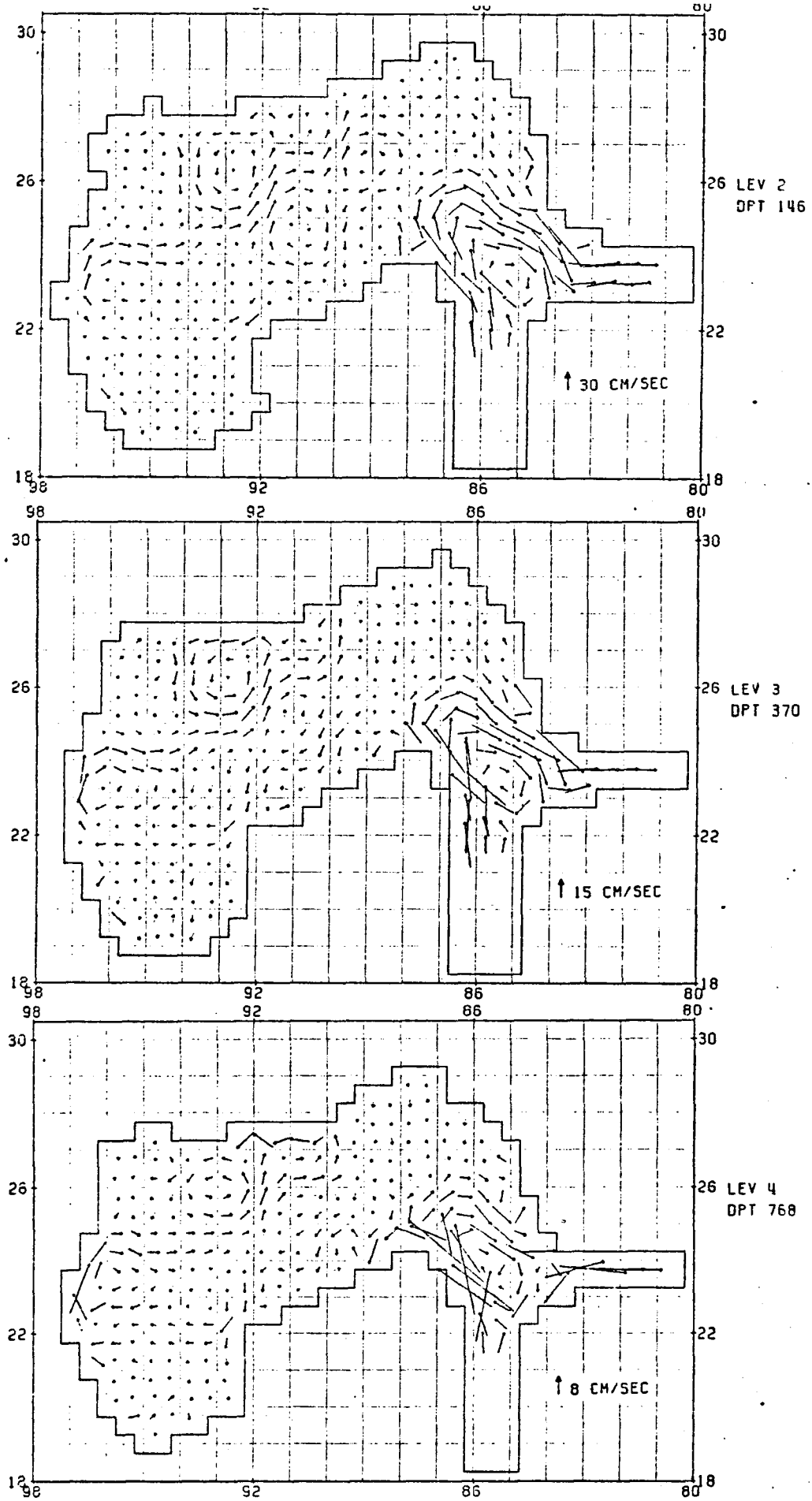

SYNOPTIC INCREMENT
FEBRUARY 1962

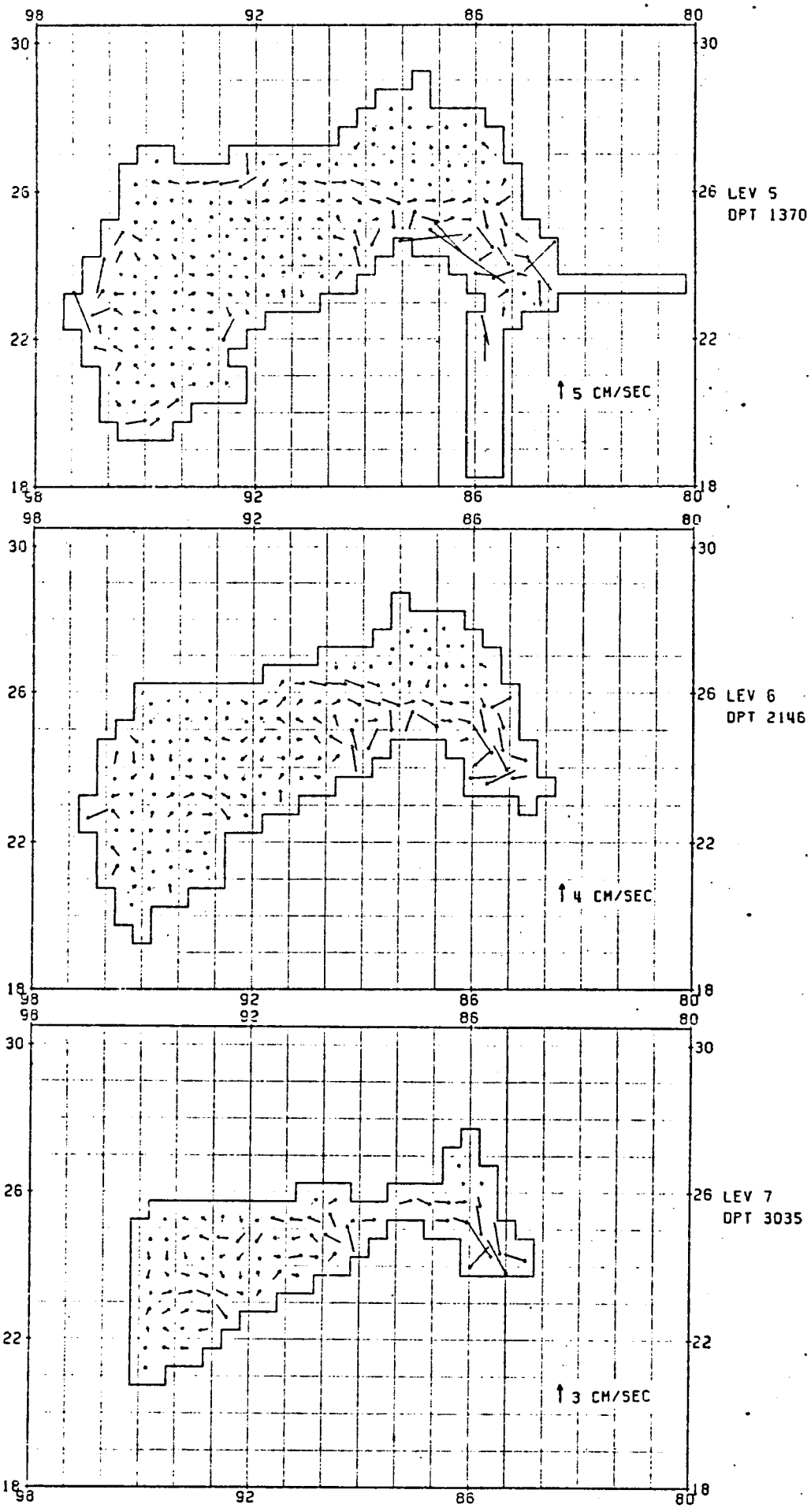

SYNOPTIC INCREMENT
FEBRUARY 1962

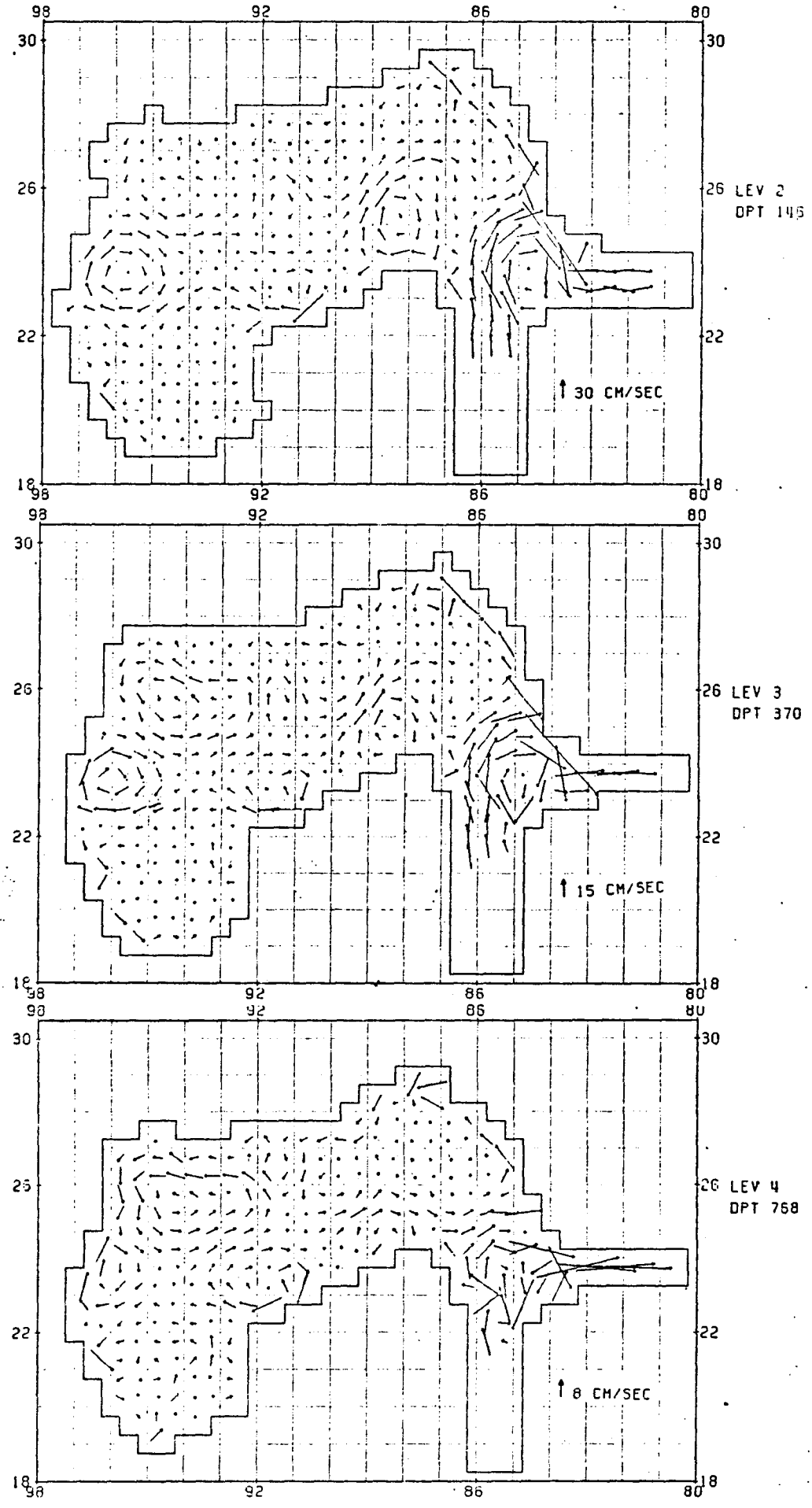

SYNOPTIC INCREMENT
JUNE 1967

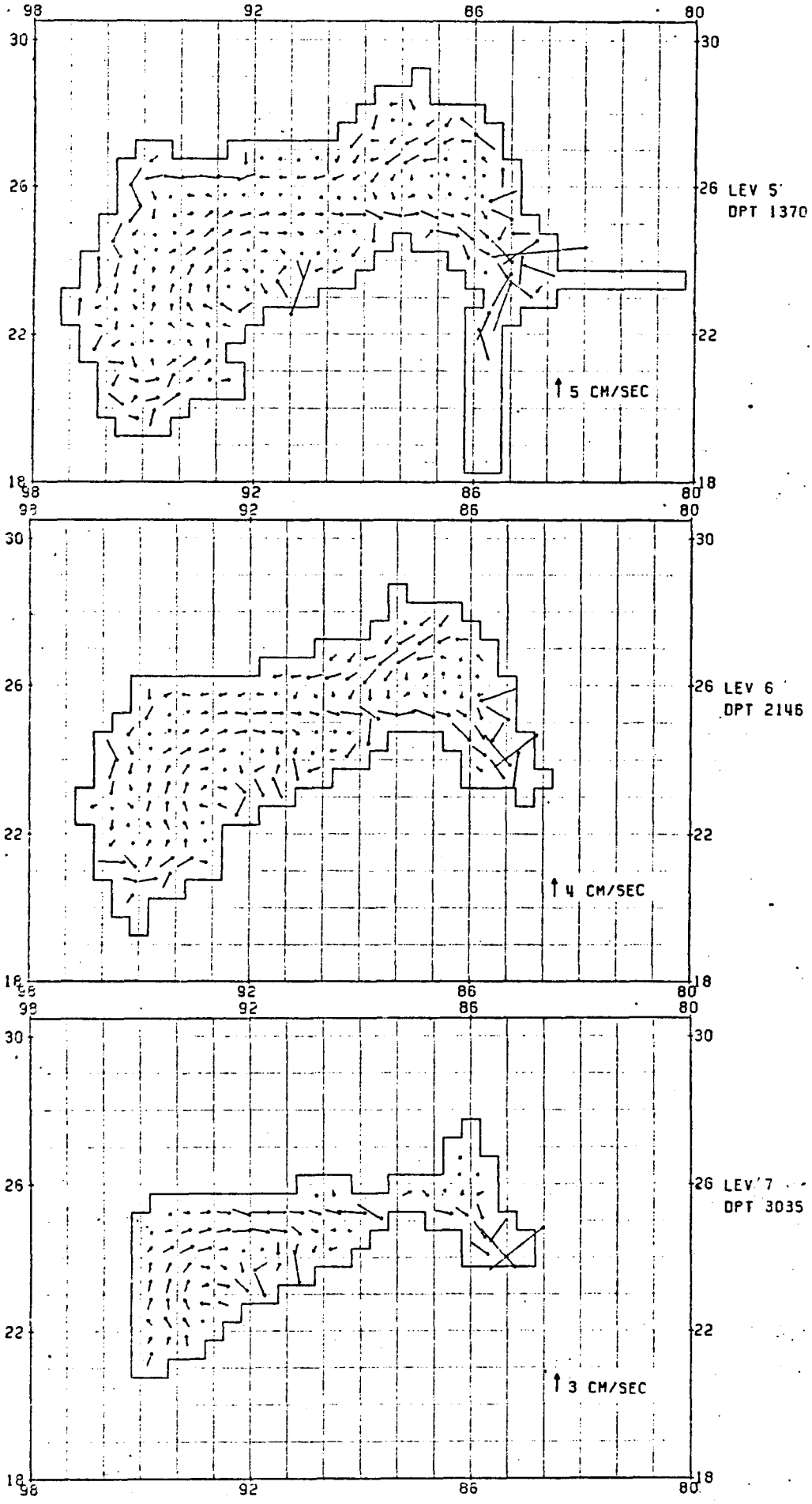

SYNOPTIC INCREMENT
JUNE 1967

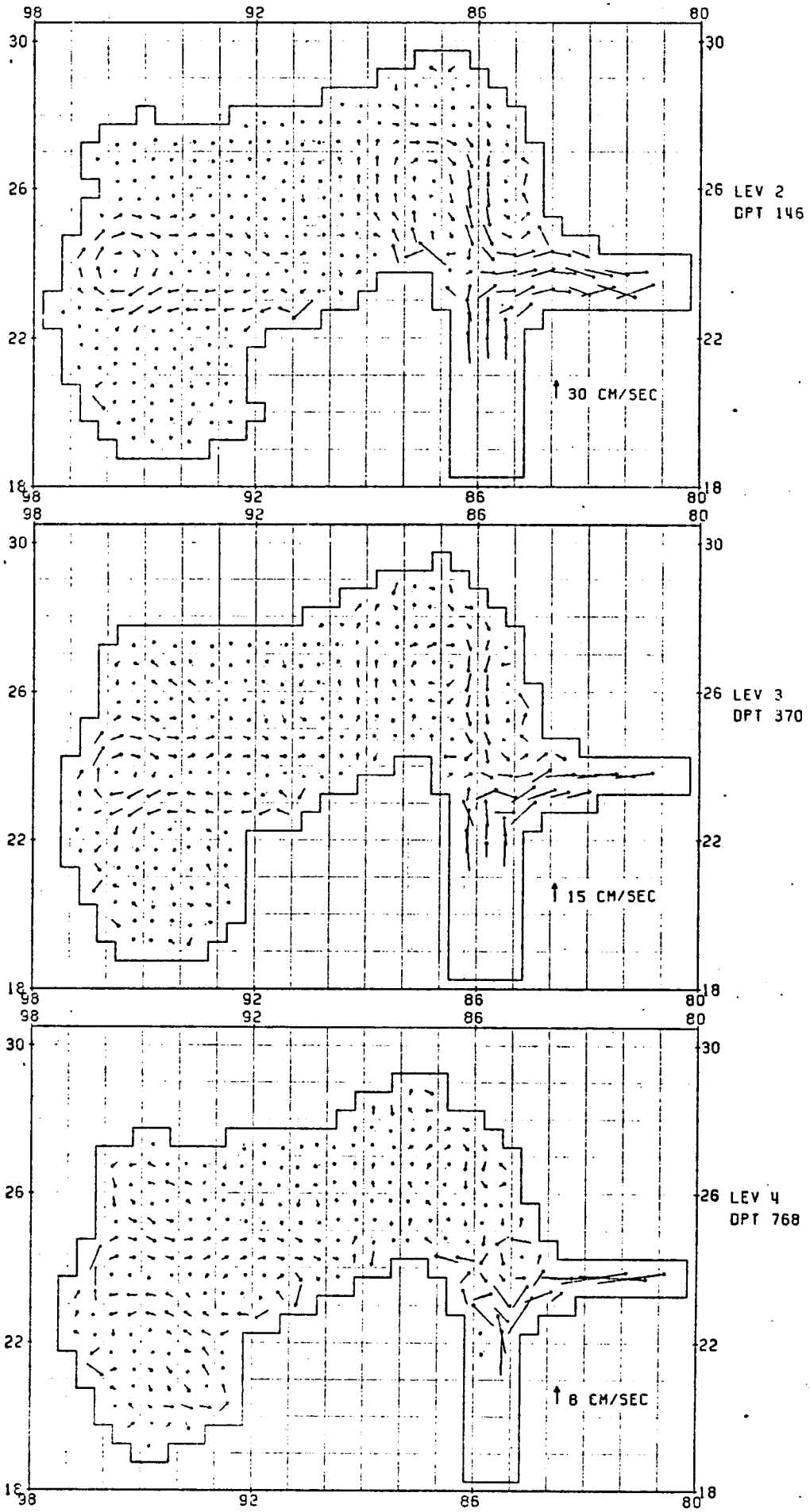

SYNOPTIC INCREMENT
AUGUST 1971

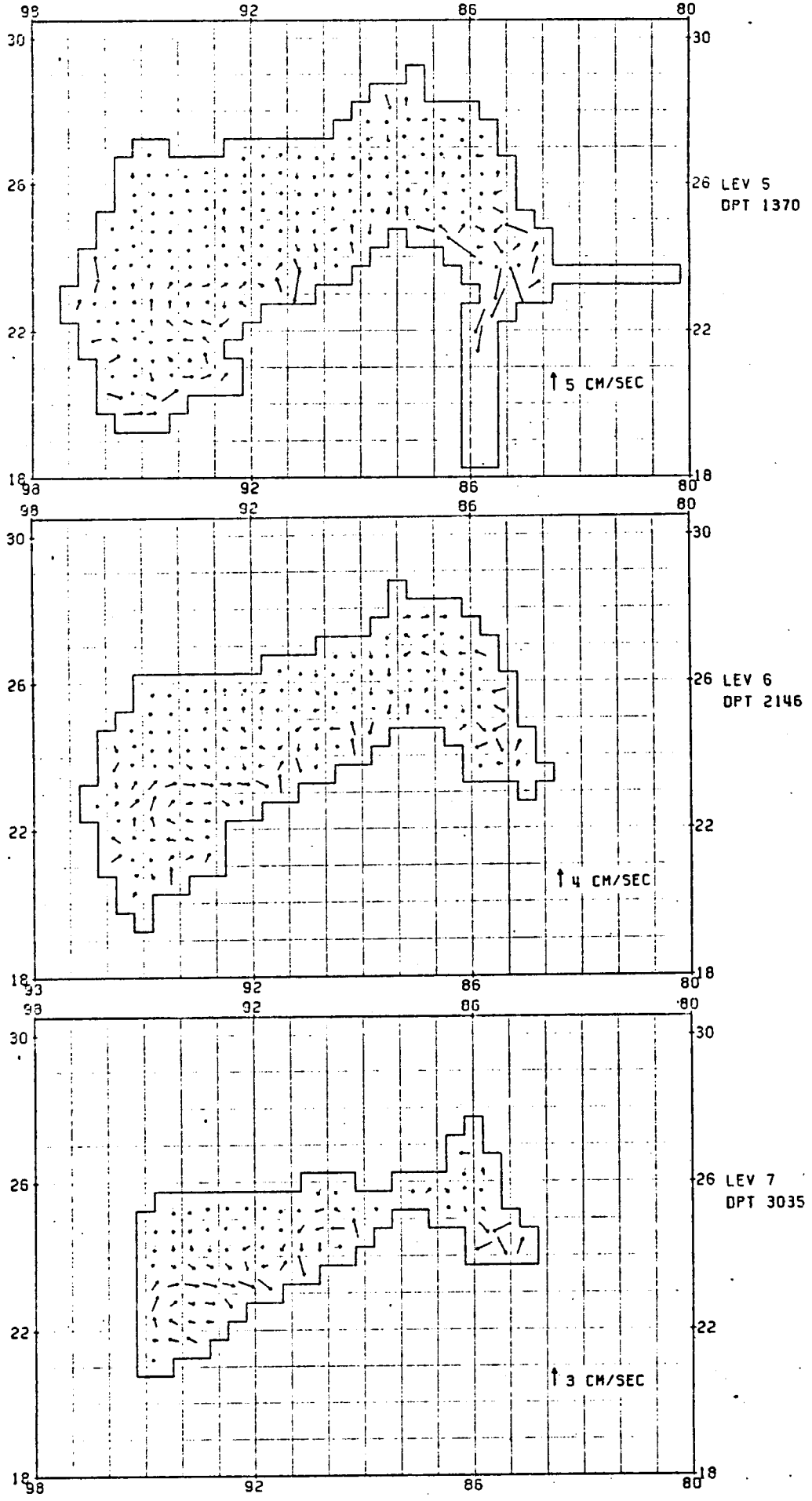

SYNOPTIC INCREMENT
AUGUST 1971

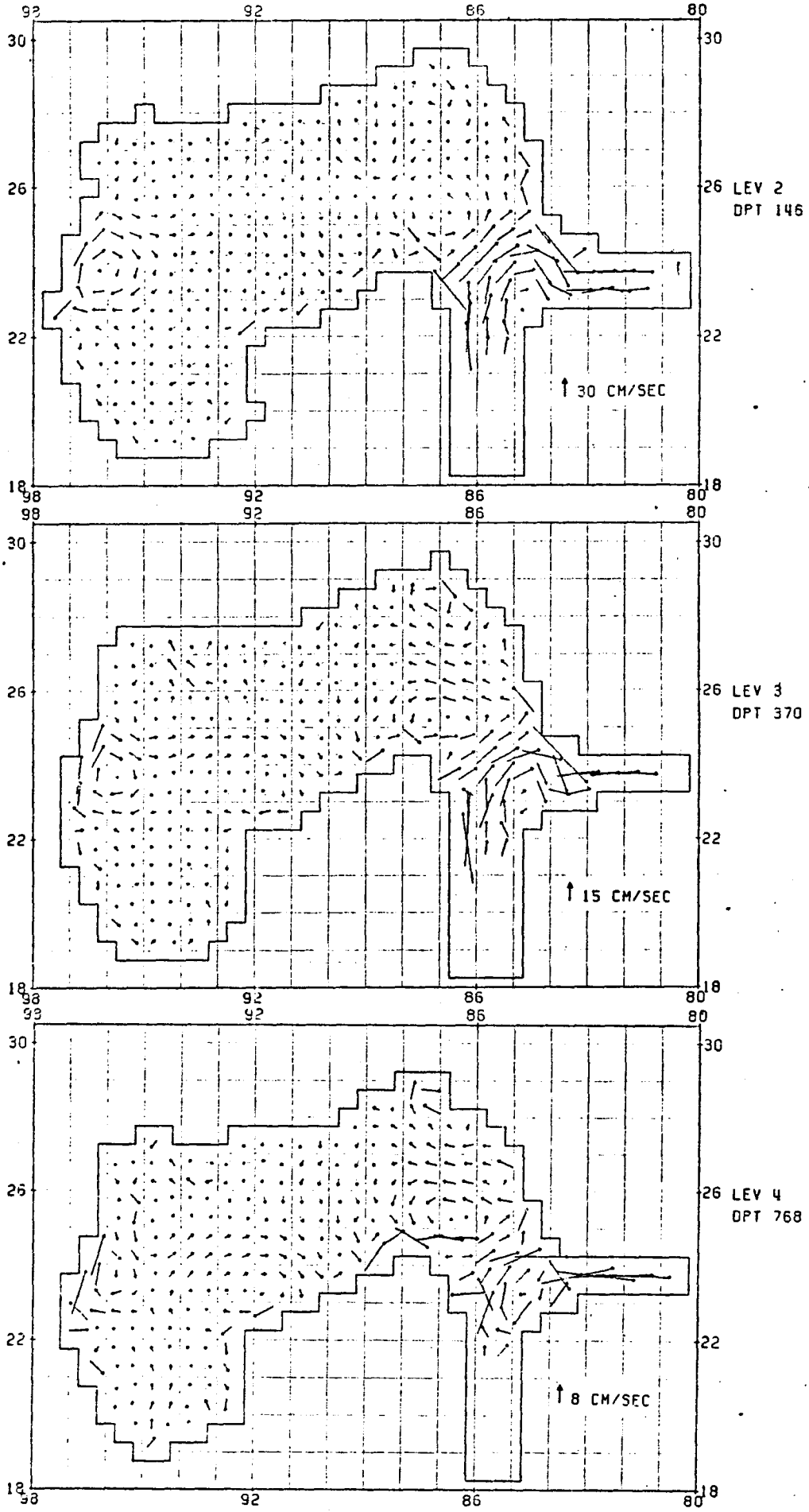

SYNOPTIC INCREMENT
JUNE 1975

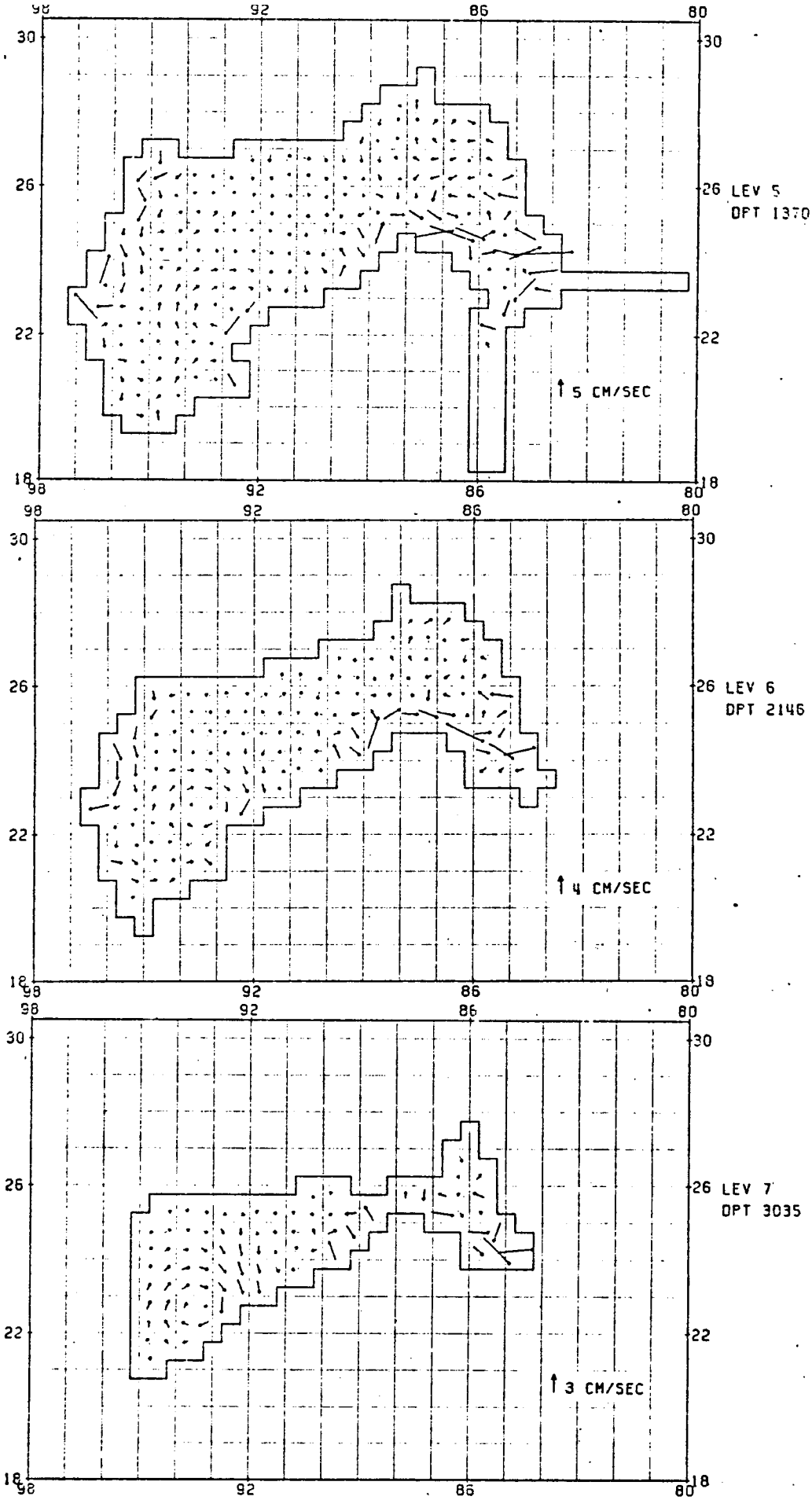

SYNOPTIC INCREMENT
JUNE 1975

APPENDIX II

Geostrophic Data and Computations

The three-month average, distribution of data and additional results of the geostrophic model computations are included in this Appendix. If data are missing at an interior point, an interpolation routine using the surrounding data points is used to fill-in the required value. In the Yucatan Straits and Straits of Florida, a subjective extrapolation is performed to provide missing data. The geostrophic velocities computed from these extrapolated values are given by arrows with lighter shafts.

Extrapolated data are indicated by hexagons on the dynamic height maps. These maps have been machine contoured.

Vertical sections for four representative transects of the Gulf are also included. Those sections which suggest strong subsurface velocity cores are suspect. These subsurface velocity maximums are probably artifacts of the data distribution and/or handling, rather than real features of the circulation.

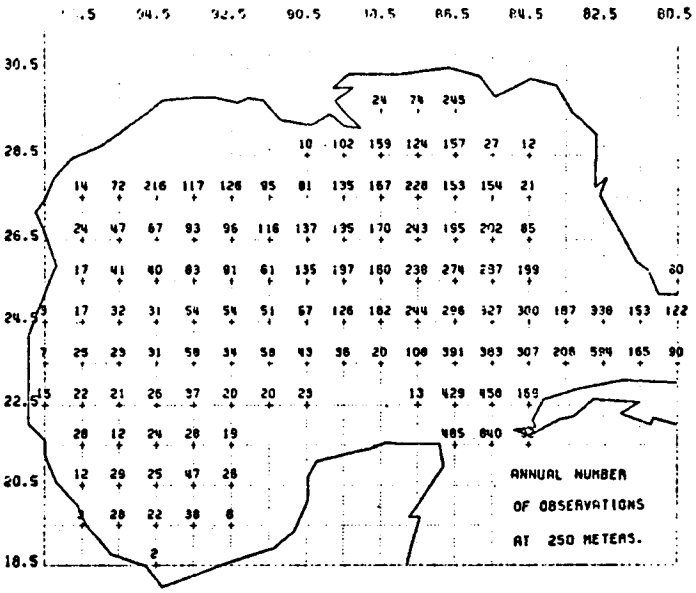

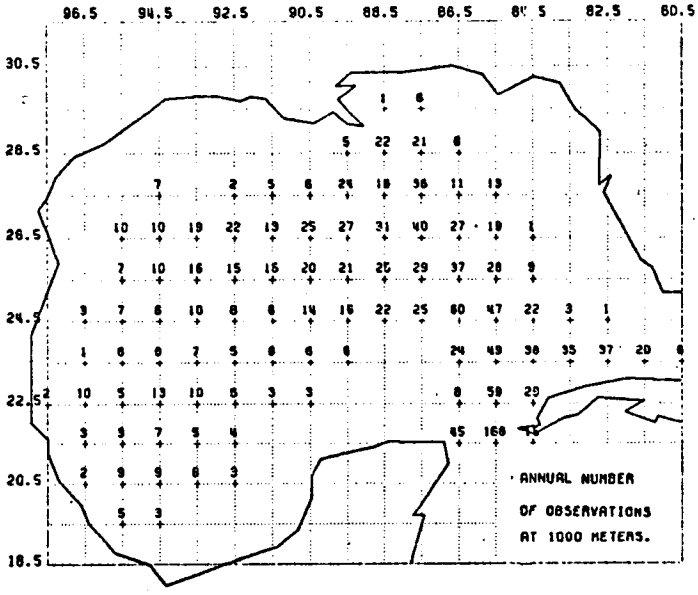

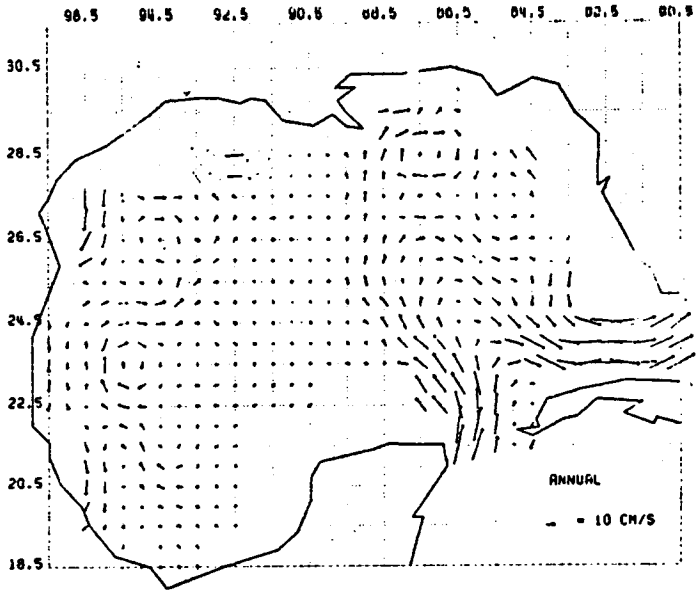

ANNUAL
GEOSTROPHIC VELOCITIES AT A DEPTH OF .0 METERS.
VELOCITIES ARE COMPUTED RELATIVE TO THE 250.0 M LEVEL.

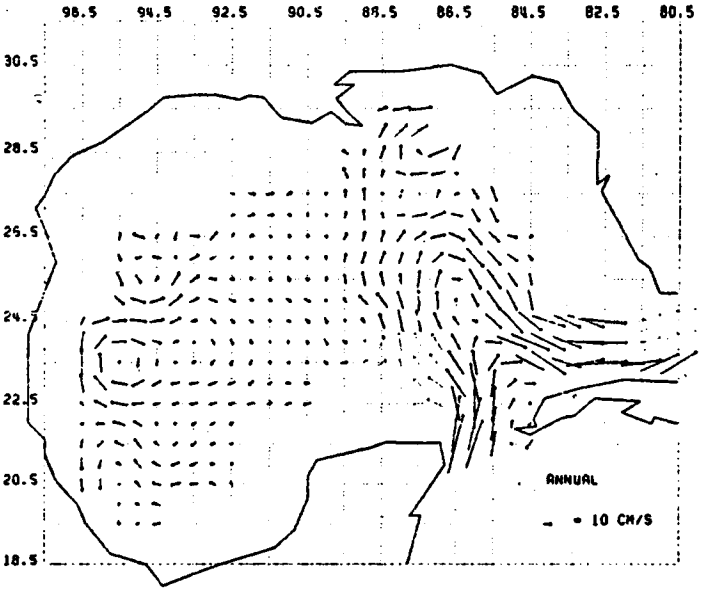

ANNUAL
GEOSTROPHIC VELOCITIES AT A DEPTH OF .0 METERS.
VELOCITIES ARE COMPUTED RELATIVE TO THE1000.0 M LEVEL.

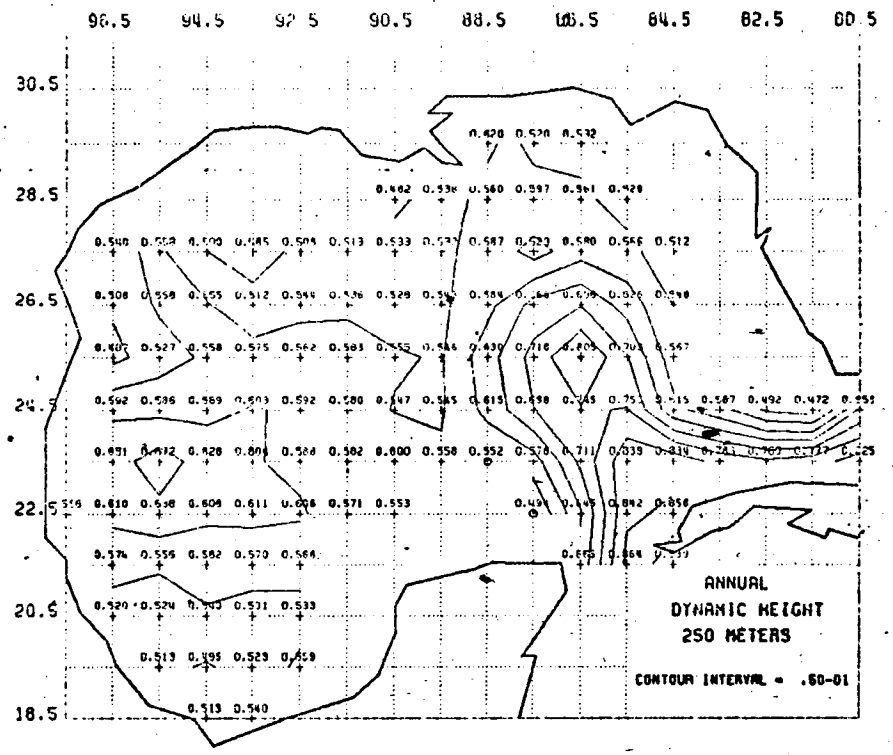
96.5
94.5
92.5
90.5
88.5
86.5
84.5
82.5
80.5
30.5
28.5
26.5
24.5
22.5
20.5
18.5
ANNUAL
DYNAMIC HEIGHT
250 METERS
CONTOUR INTERVAL = .60-01

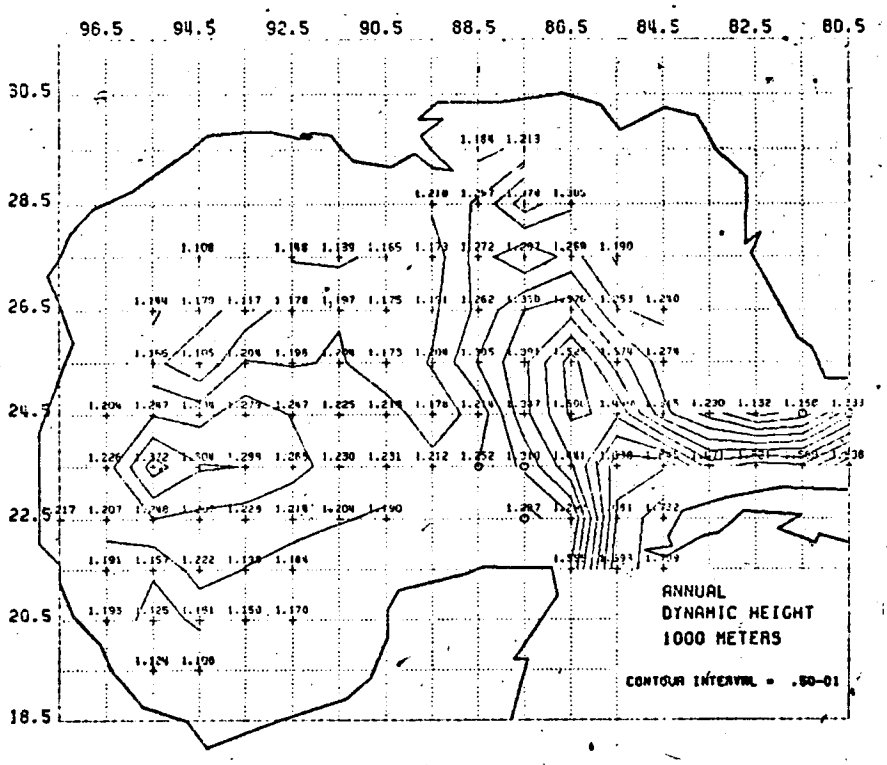
96.5
94.5
92.5
90.5
88.5
86.5
84.5
82.5
80.5
30.5
28.5
26.5
24.5
22.5
20.5
18.5
ANNUAL
DYNAMIC HEIGHT
1000 METERS
CONTOUR INTERVAL = .60-01

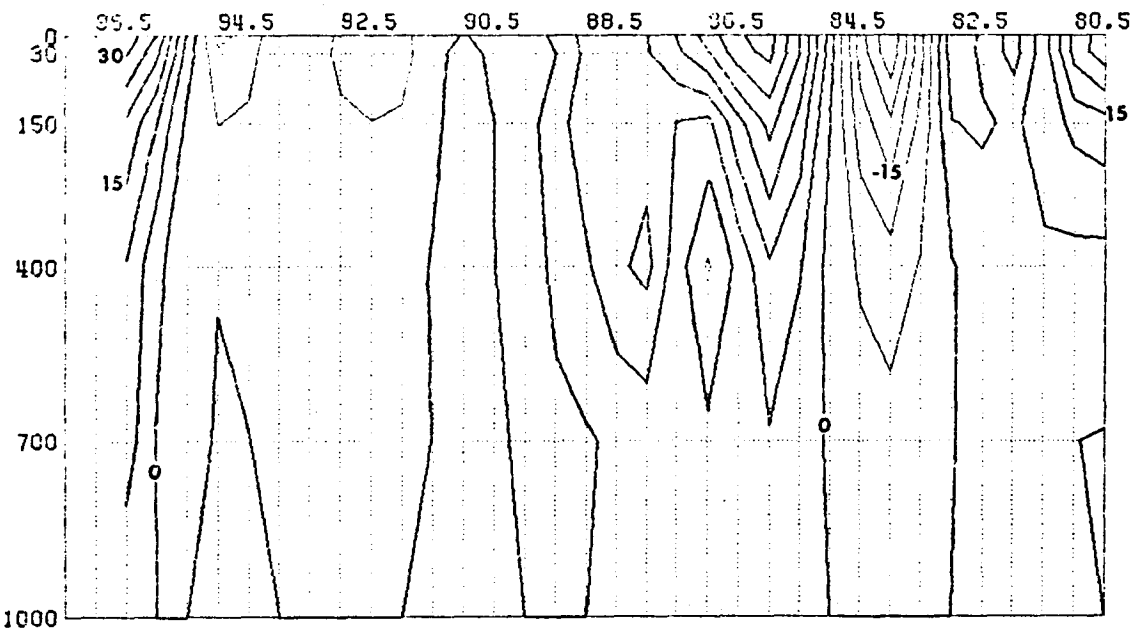

ANNUAL

E-W CROSS SECTION FOR V COMPONENT OF GEOSTROPHIC VELOCITY AT LATITUDE 23.5. VELOCITIES ARE COMPUTED RELATIVE TO 1000 M LEVEL. HEAVY LINES DENOTE NORTH VELOCITY. THE CONTOUR INTERVAL IS 5.0 CM/S.

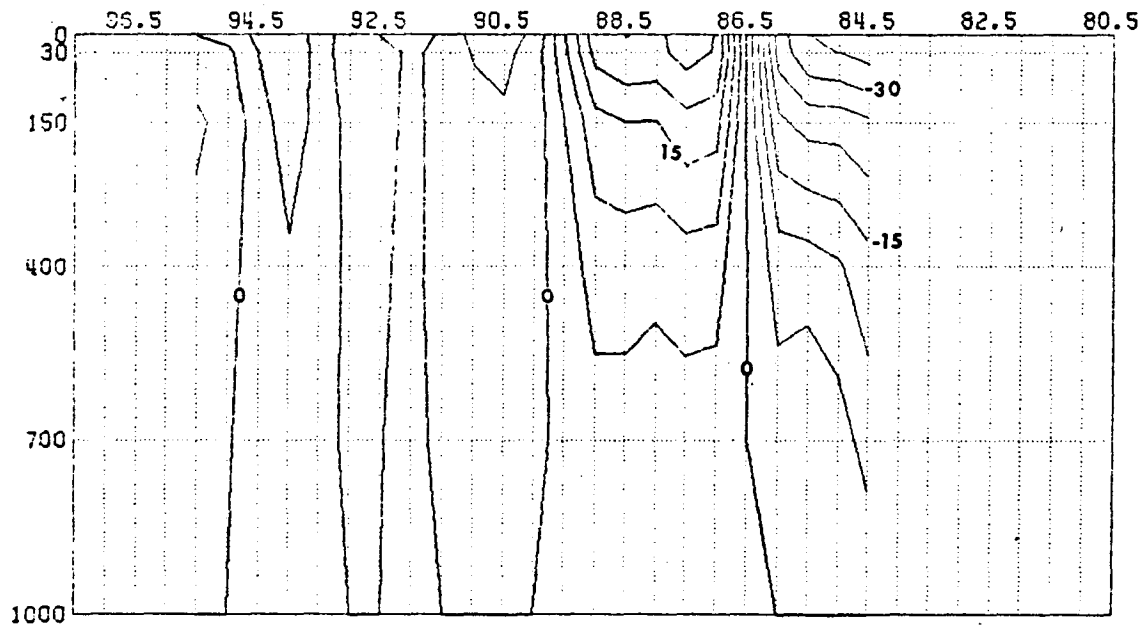

ANNUAL

E-W CROSS SECTION FOR V COMPONENT OF GEOSTROPHIC VELOCITY AT LATITUDE 25.5. VELOCITIES ARE COMPUTED RELATIVE TO 1000 M LEVEL. HEAVY LINES DENOTE NORTH VELOCITY. THE CONTOUR INTERVAL IS 5.0 CM/S.

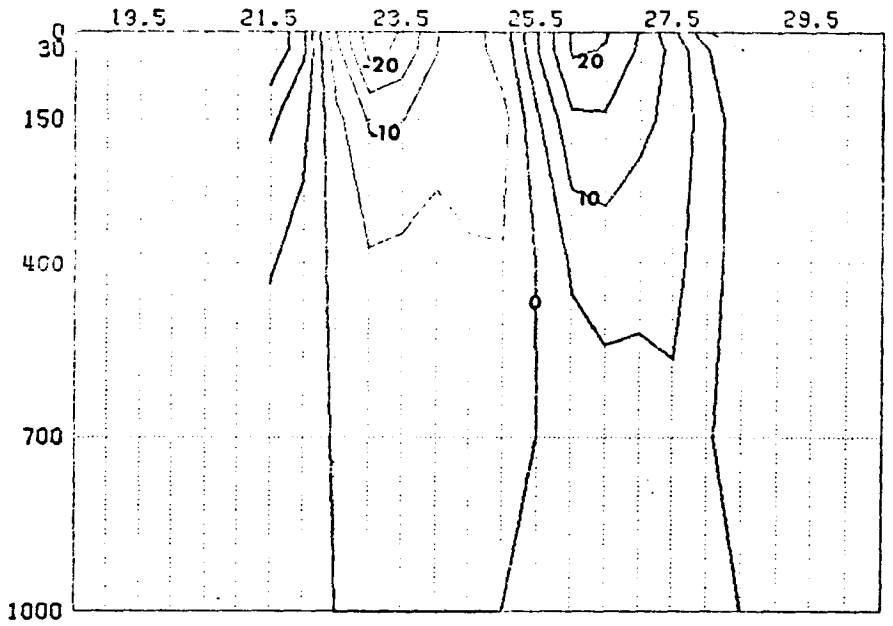

ANNUAL
N-S CROSS SECTION FOR U COMPONENT OF GEOSTROPHIC VELOCITY AT LONGITUDE 86.5. VELOCITIES ARE COMPUTED RELATIVE TO 1000 M LEVEL. HEAVY LINES DENOTE EAST VELOCITY. THE CONTOUR INTERVAL IS 5.0 CM/S.

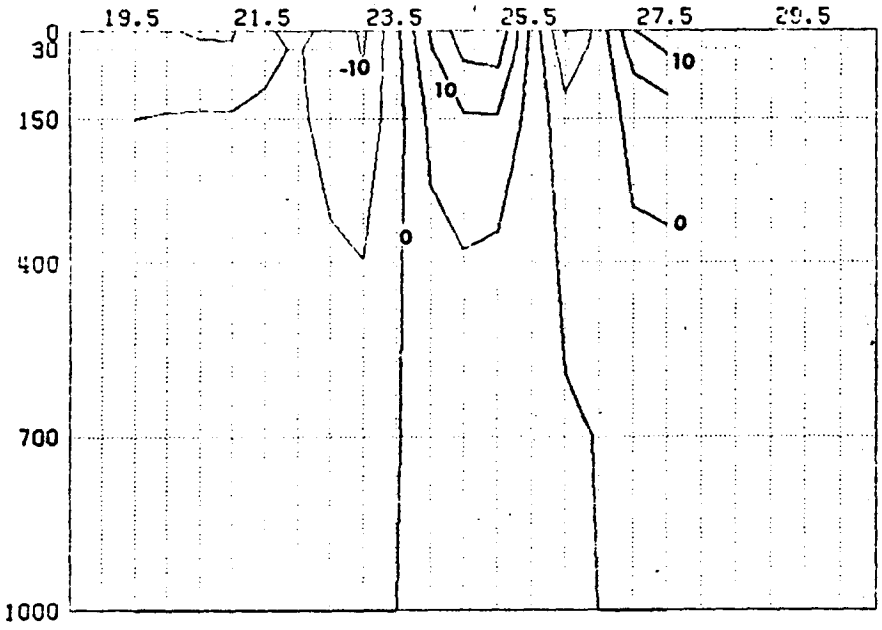

ANNUAL
N-S CROSS SECTION FOR U COMPONENT OF GEOSTROPHIC VELOCITY AT LONGITUDE 94.5. VELOCITIES ARE COMPUTED RELATIVE TO 1000 M LEVEL. HEAVY LINES DENOTE EAST VELOCITY. THE CONTOUR INTERVAL IS 5.0 CM/S.

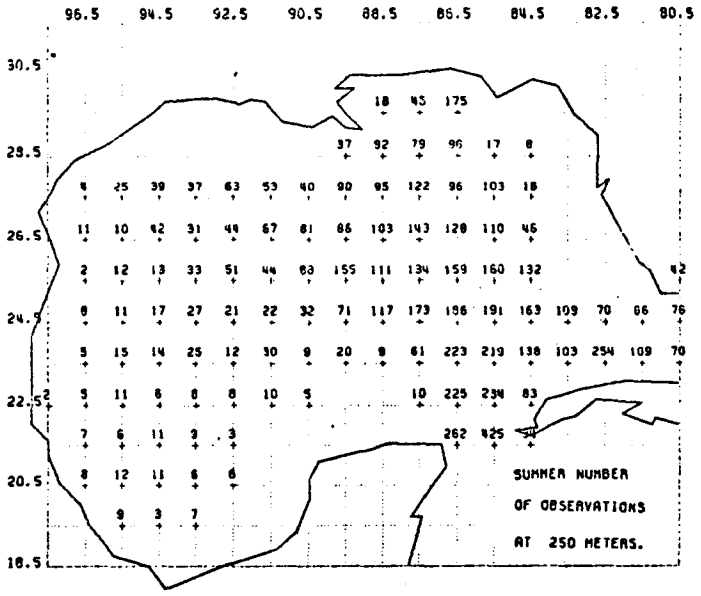

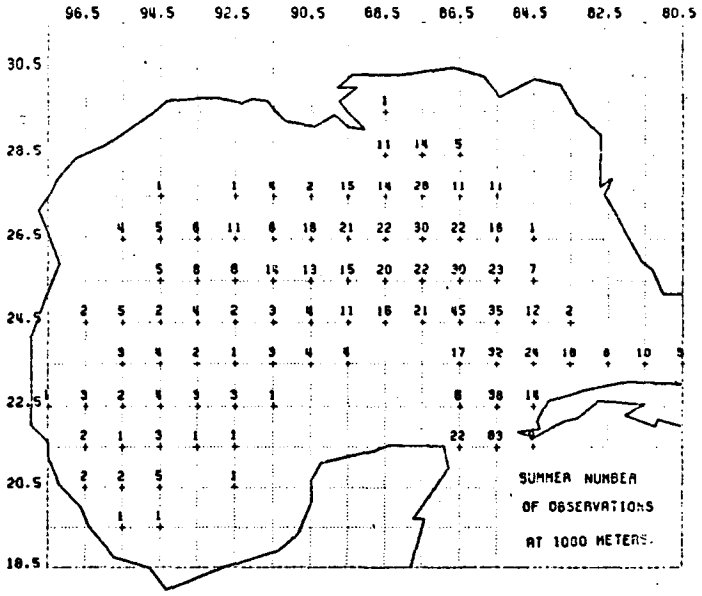

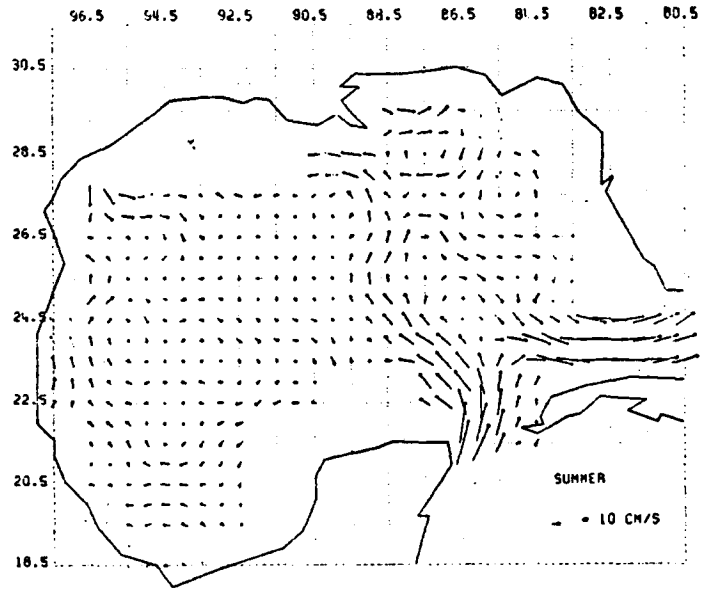

SUMMER
GEOSTROPHIC VELOCITIES AT A DEPTH OF .0 METERS.
VELOCITIES ARE COMPUTED RELATIVE TO THE 250.0 M LEVEL.

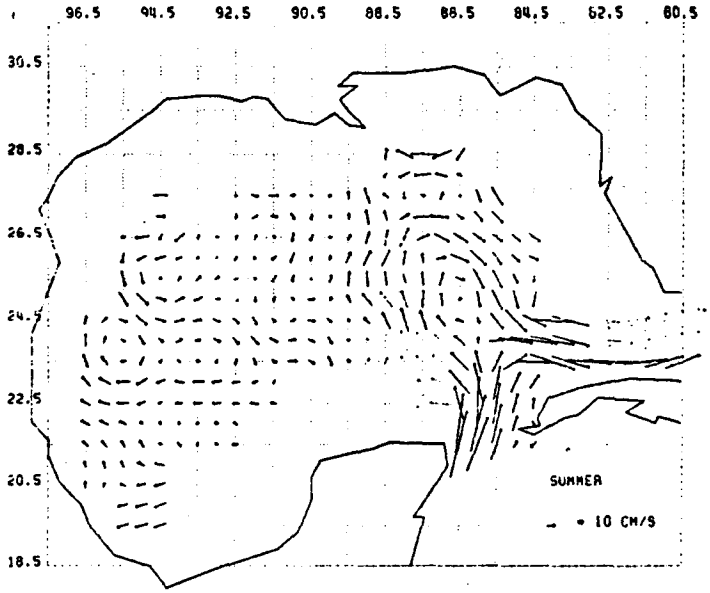

SUMMER
GEOSTROPHIC VELOCITIES AT A DEPTH OF .0 METERS.
VELOCITIES ARE COMPUTED RELATIVE TO THE 1000.0 M LEVEL.

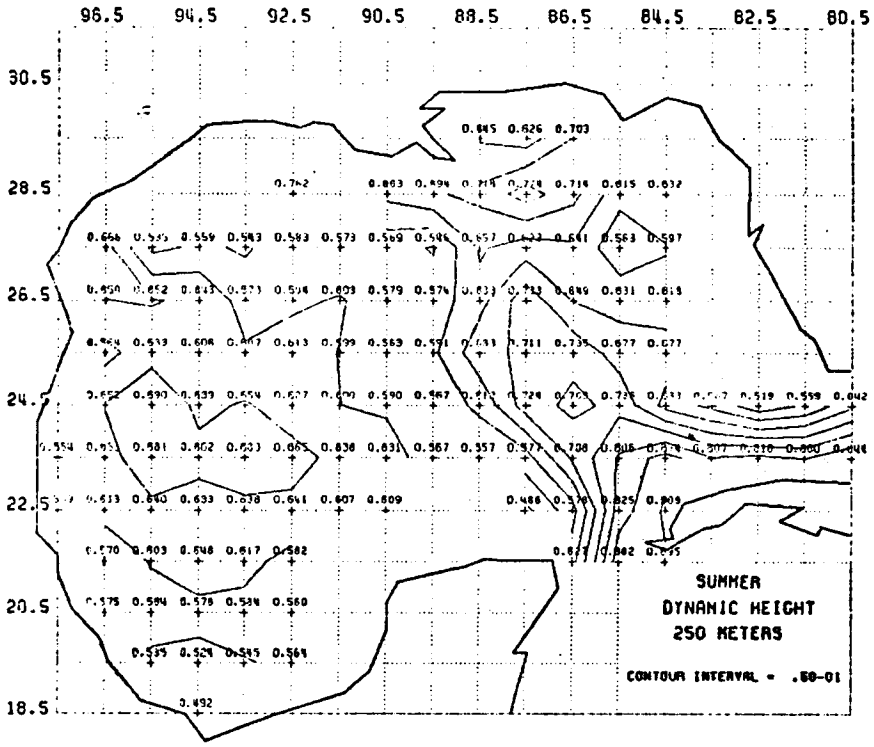
96.5
94.5
92.5
90.5
88.5
86.5
84.5
82.5
80.5
30.5
28.5
26.5
24.5
22.5
20.5
18.5
SUMMER
DYNAMIC HEIGHT
250 METERS
CONTOUR INTERVAL = .50-01

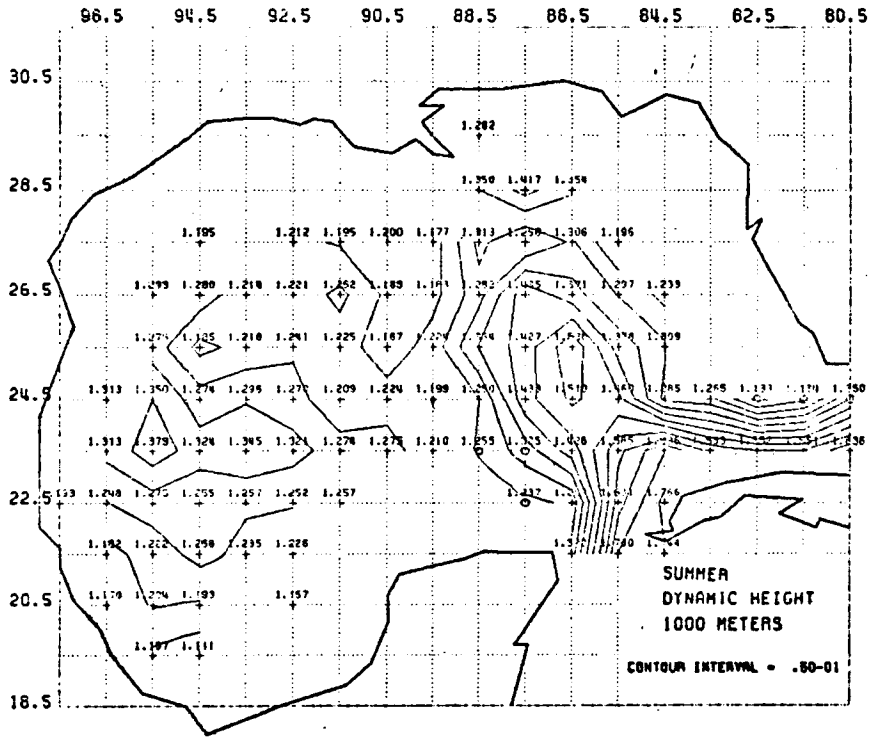
96.5
94.5
92.5
90.5
88.5
86.5
84.5
82.5
80.5
30.5
28.5
26.5
24.5
22.5
20.5
18.5
SUMMER
DYNAMIC HEIGHT
1000 METERS
CONTOUR INTERVAL = .50-01

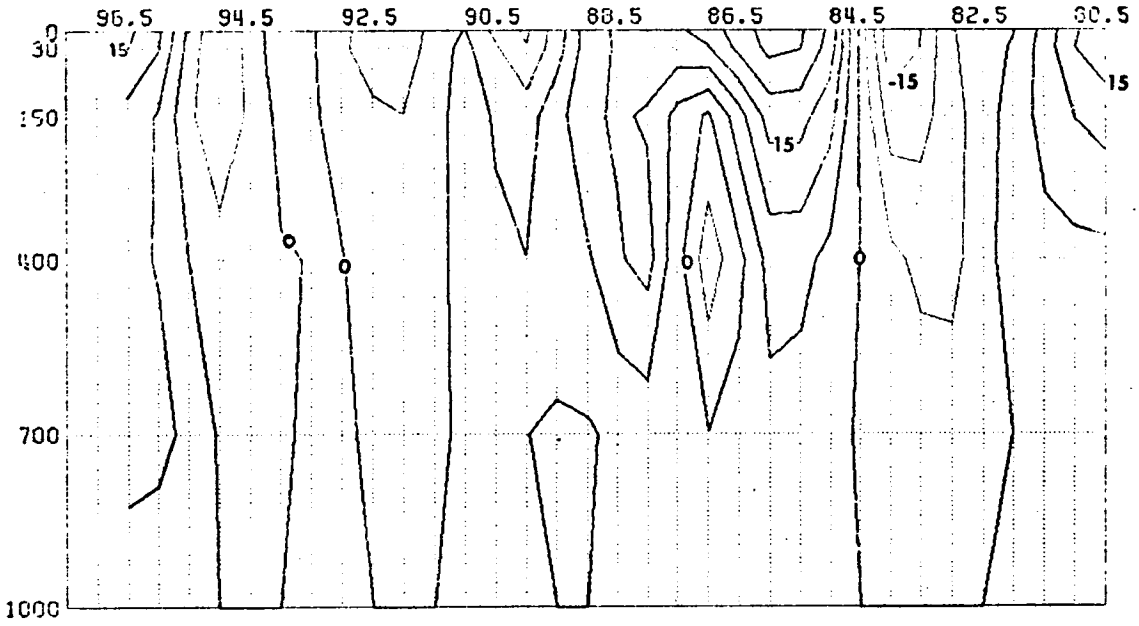

SUMMER

E-W CROSS SECTION FOR V COMPONENT OF GEOSTROPHIC VELOCITY AT LATITUDE 23.5. VELOCITIES ARE COMPUTED RELATIVE TO 1000 M LEVEL. HEAVY LINES DENOTE NORTH VELOCITY. THE CONTOUR INTERVAL IS 5.0 CM/S.

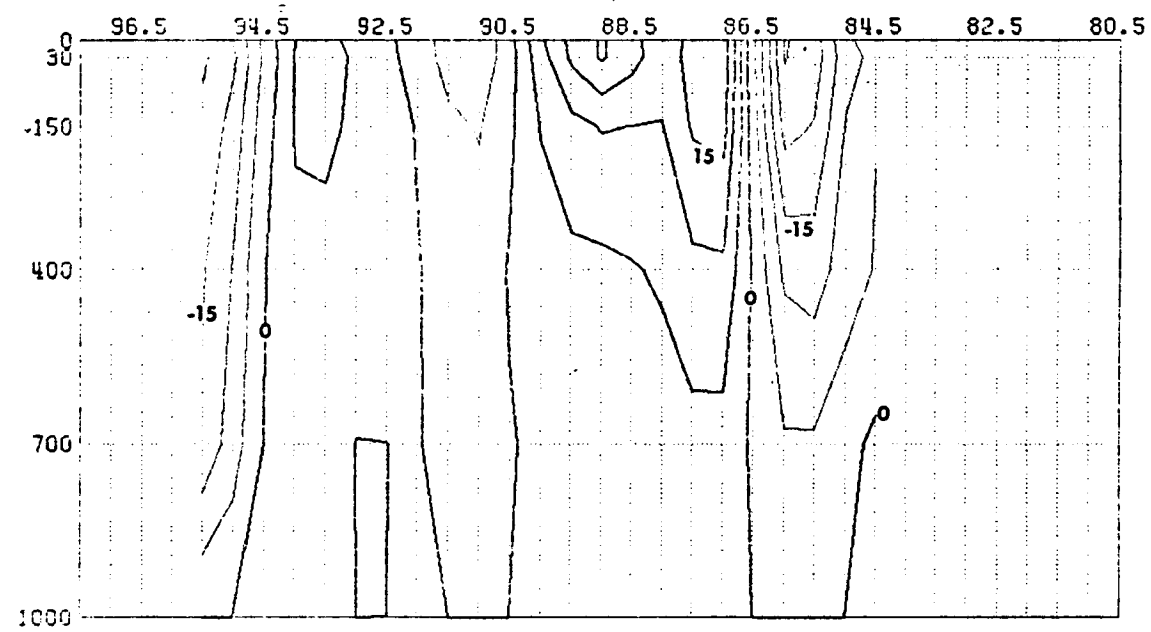

SUMMER

E-W CROSS SECTION FOR V COMPONENT OF GEOSTROPHIC VELOCITY AT LATITUDE 25.5. VELOCITIES ARE COMPUTED RELATIVE TO 1000 M LEVEL. HEAVY LINES DENOTE NORTH VELOCITY. THE CONTOUR INTERVAL IS 5.0 CM/S.

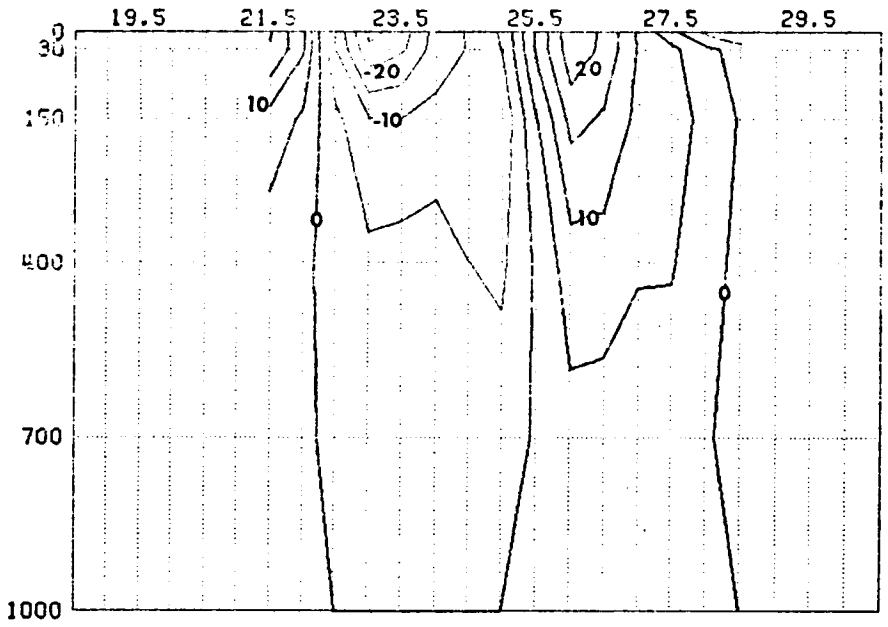

SUMMER

N-S CROSS SECTION FOR U COMPONENT OF GEOSTROPHIC VELOCITY AT LONGITUDE 86.5. VELOCITIES ARE COMPUTED RELATIVE TO 1000 M LEVEL. HEAVY LINES DENOTE EAST VELOCITY. THE CONTOUR INTERVAL IS 5.0 CM/S.

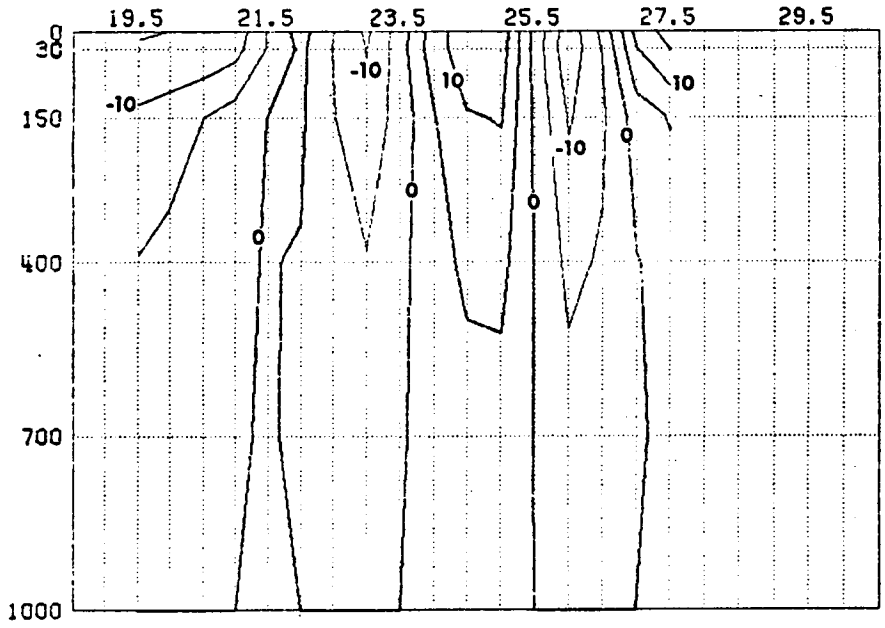

SUMMER

N-S CROSS SECTION FOR U COMPONENT OF GEOSTROPHIC VELOCITY AT LONGITUDE 94.5. VELOCITIES ARE COMPUTED RELATIVE TO 1000 M LEVEL. HEAVY LINES DENOTE EAST VELOCITY. THE CONTOUR INTERVAL IS 5.0 CM/S.

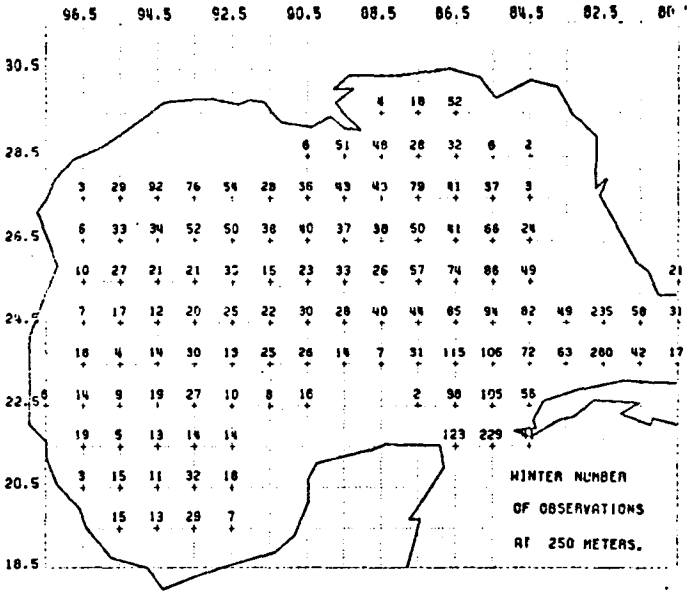

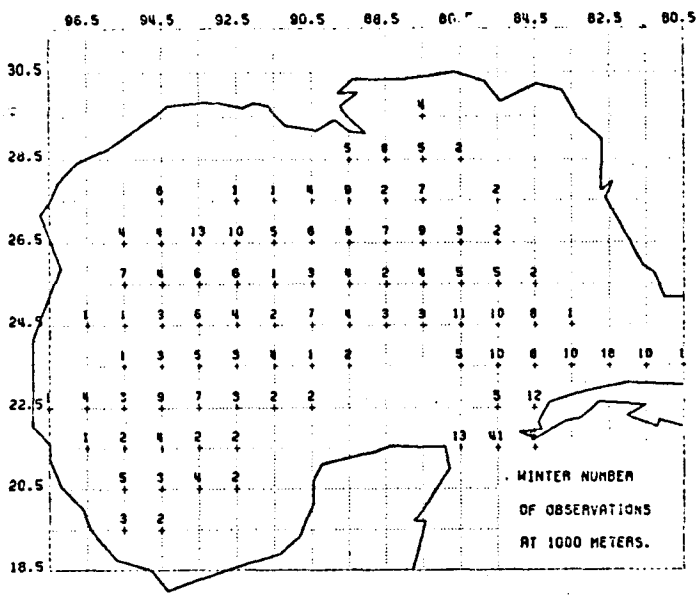

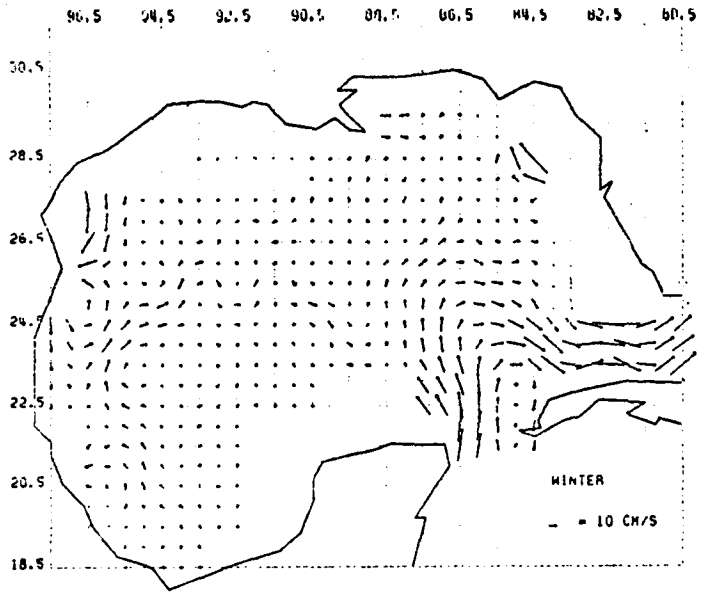

WINTER
GEOSTROPHIC VELOCITIES AT A DEPTH OF .0 METERS.
VELOCITIES ARE COMPUTED RELATIVE TO THE 250.0 M LEVEL.

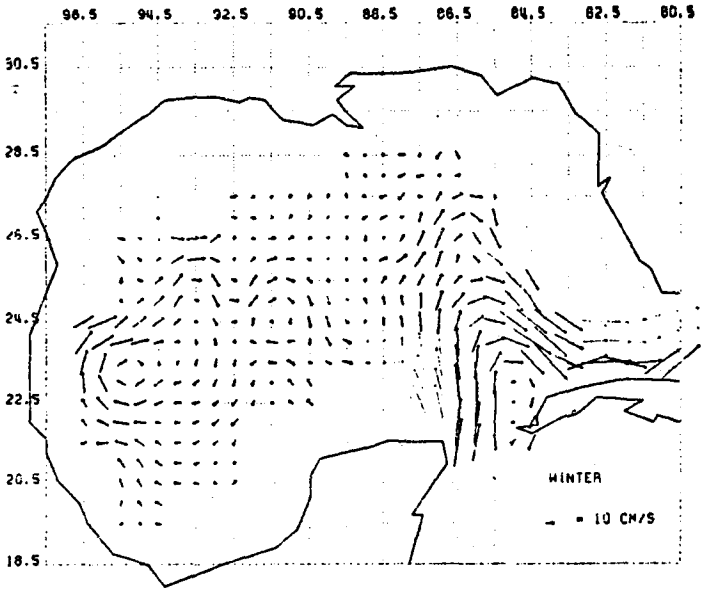

WINTER
GEOSTROPHIC VELOCITIES AT A DEPTH OF .0 METERS.
VELOCITIES ARE COMPUTED RELATIVE TO THE1000.0 M LEVEL.

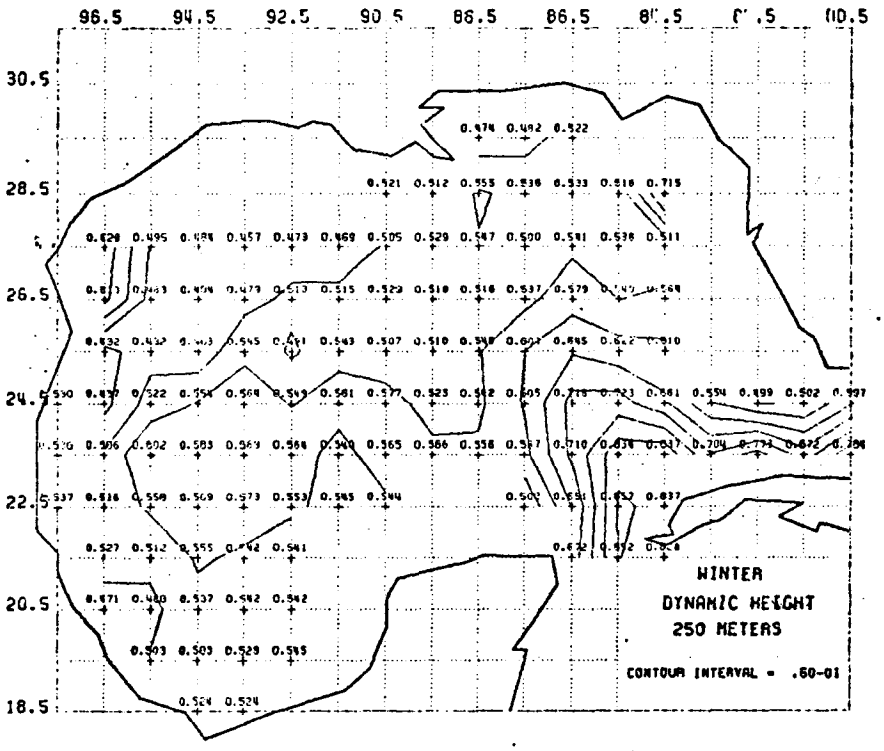
96.5
94.5
92.5
90.5
88.5
86.5
84.5
82.5
80.5
30.5
28.5
26.5
24.5
22.5
20.5
18.5
WINTER
DYNAMIC HEIGHT
250 METERS
CONTOUR INTERVAL = .60-01

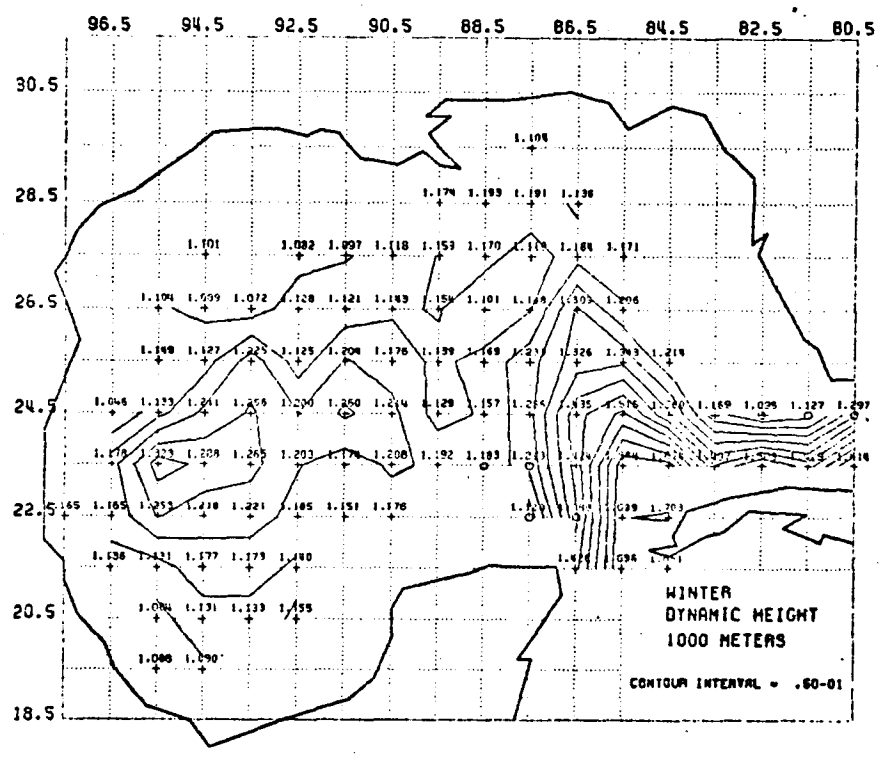
96.5
94.5
92.5
90.5
88.5
86.5
84.5
82.5
80.5
30.5
28.5
26.5
24.5
22.5
20.5
18.5
WINTER
DYNAMIC HEIGHT
1000 METERS
CONTOUR INTERVAL = .60-01

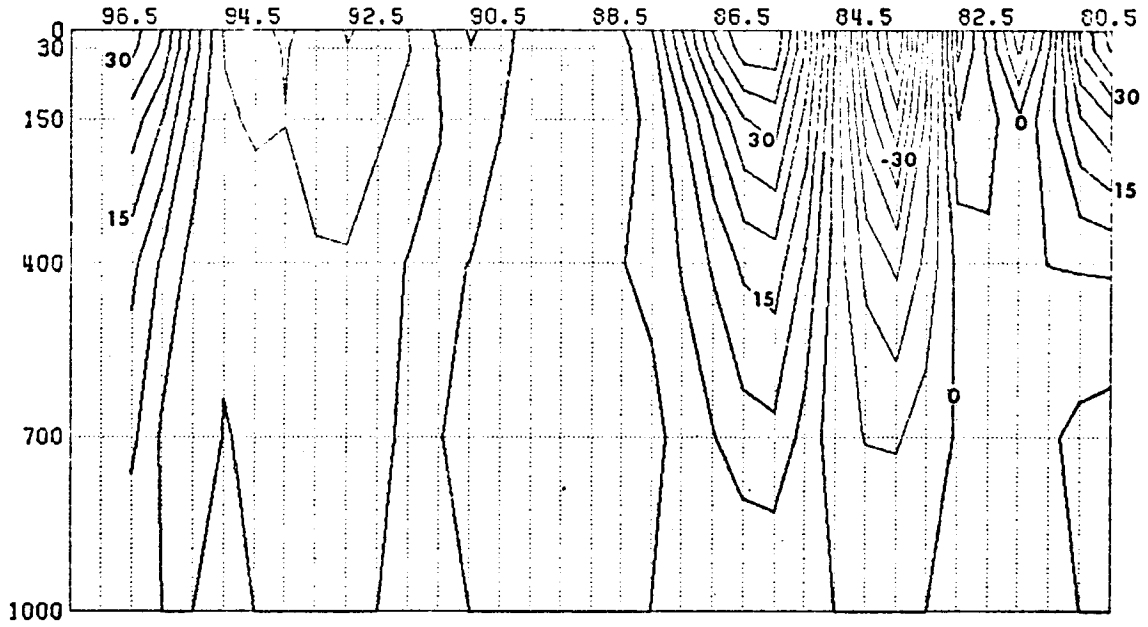

WINTER
E-W CROSS SECTION FOR V COMPONENT OF GEOSTROPHIC VELOCITY AT LATITUDE 23.5. VELOCITIES ARE COMPUTED RELATIVE TO 1000 M LEVEL. HEAVY LINES DENOTE NORTH VELOCITY. THE CONTOUR INTERVAL IS 5.0 CM/S.

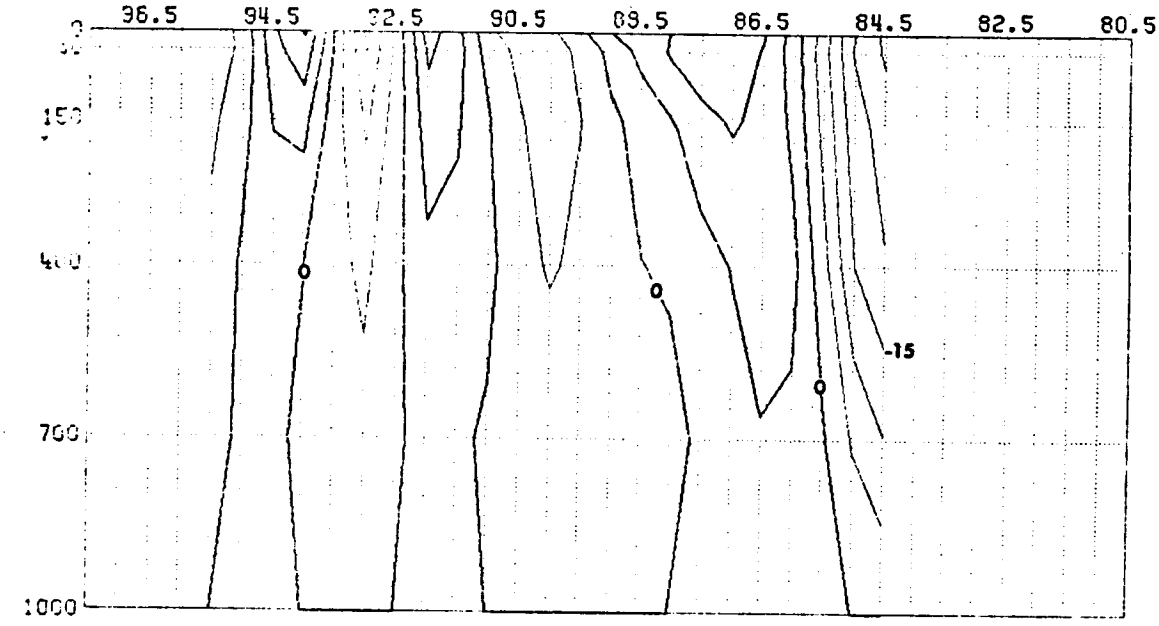

WINTER
E-W CROSS SECTION FOR V COMPONENT OF GEOSTROPHIC VELOCITY AT LATITUDE 25.5. VELOCITIES ARE COMPUTED RELATIVE TO 1000 M LEVEL. HEAVY LINES DENOTE NORTH VELOCITY. THE CONTOUR INTERVAL IS 5.0 CM/S.

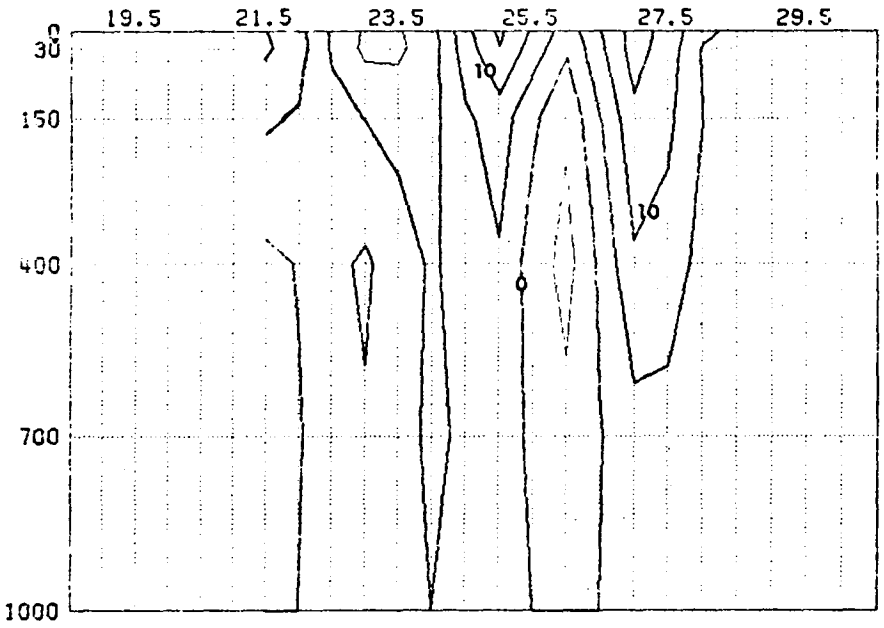

WINTER

N-S CROSS SECTION FOR U COMPONENT OF GEOSTROPHIC VELOCITY AT LONGITUDE 86.5. VELOCITIES ARE COMPUTED RELATIVE TO 1000 M LEVEL. HEAVY LINES DENOTE EAST VELOCITY. THE CONTOUR INTERVAL IS 5.0 CM/S.

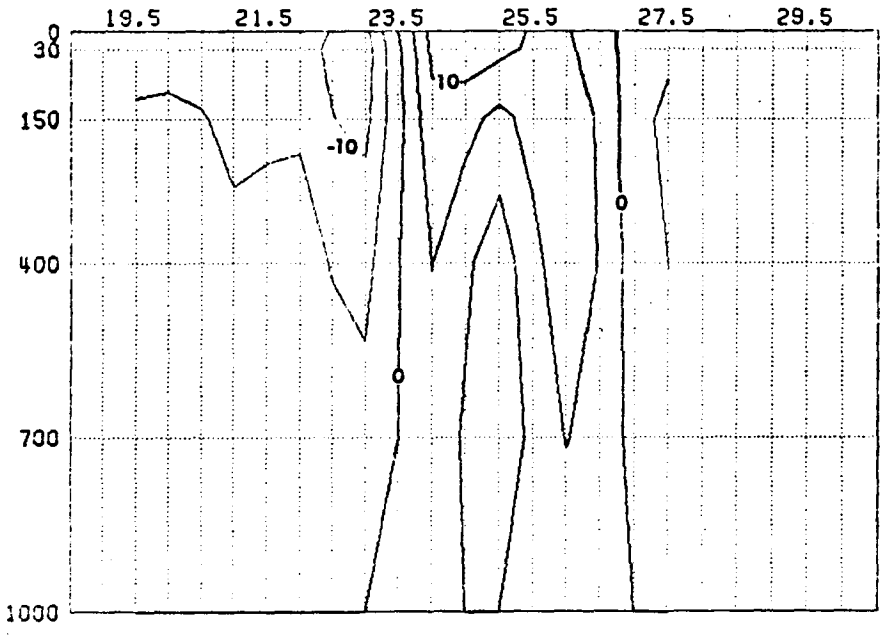

WINTER

N-S CROSS SECTION FOR U COMPONENT OF GEOSTROPHIC VELOCITY AT LONGITUDE 94.5. VELOCITIES ARE COMPUTED RELATIVE TO 1000 M LEVEL. HEAVY LINES DENOTE EAST VELOCITY. THE CONTOUR INTERVAL IS 5.0 CM/S.

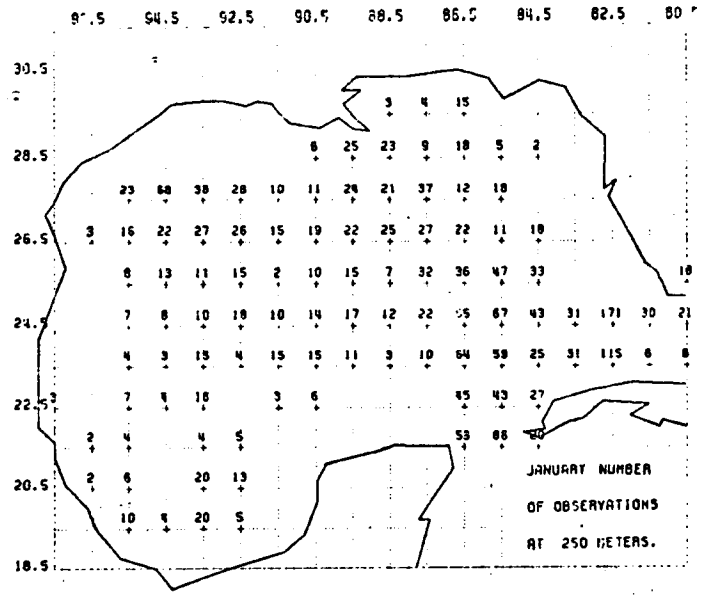

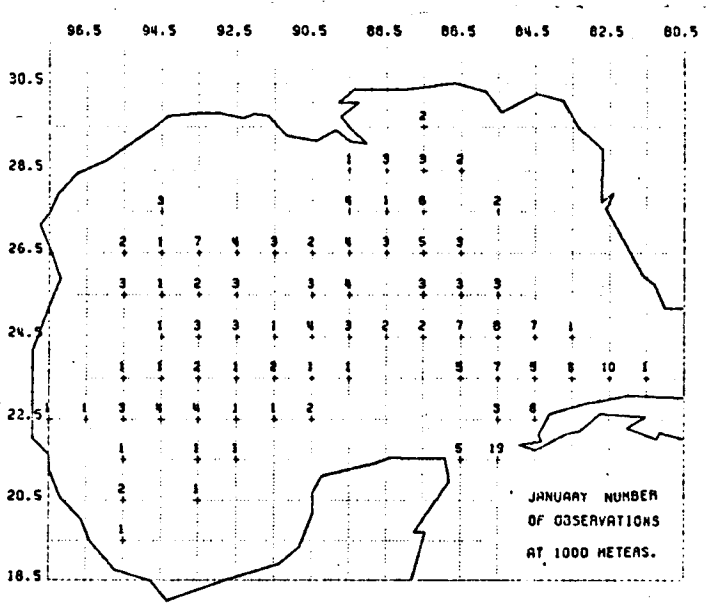

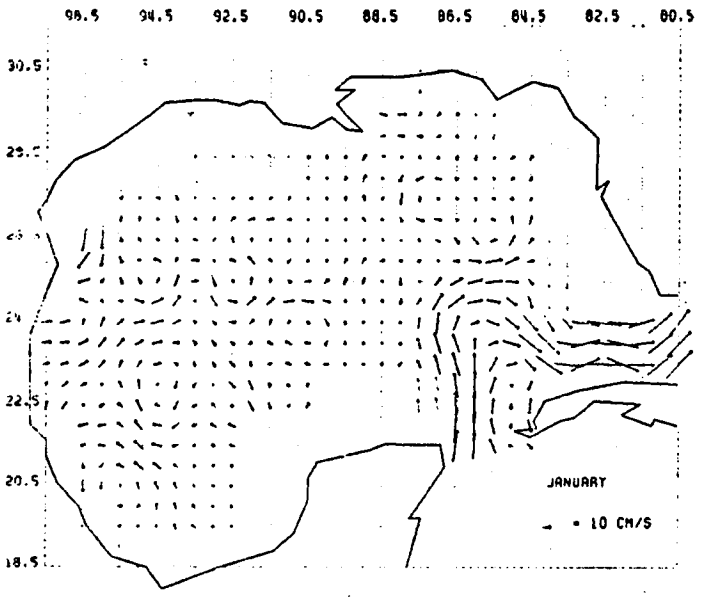

JANUARY
GEOSTROPHIC VELOCITIES AT A DEPTH OF .0 METERS.
VELOCITIES ARE COMPUTED RELATIVE TO THE 250.0 M LEVEL.

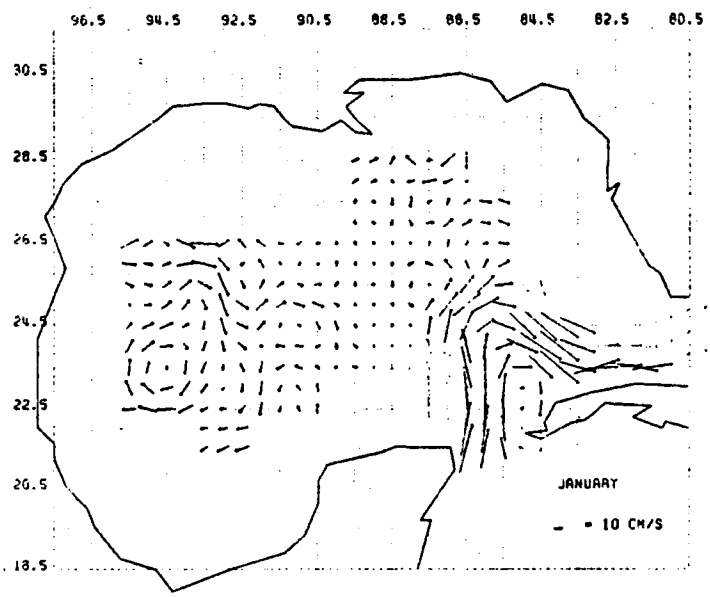

JANUARY
GEOSTROPHIC VELOCITIES AT A DEPTH OF .0 METERS.
VELOCITIES ARE COMPUTED RELATIVE TO THE1000.0 M LEVEL.

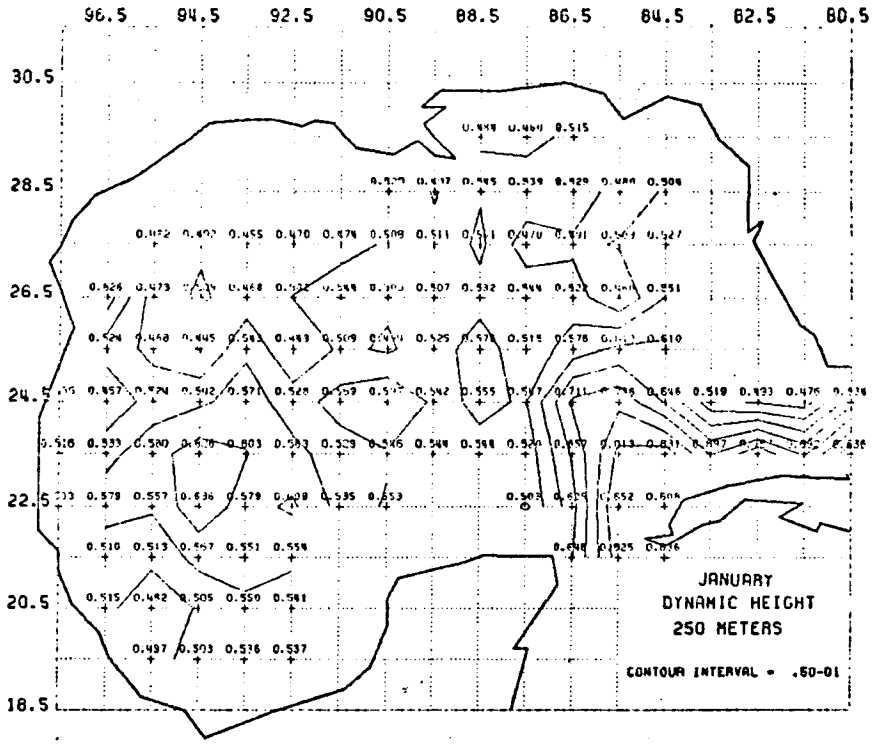
96.5
94.5
92.5
90.5
88.5
86.5
84.5
82.5
80.5
30.5
28.5
26.5
24.5
22.5
20.5
18.5
JANUARY
DYNAMIC HEIGHT
250 METERS
CONTOUR INTERVAL = .60-01

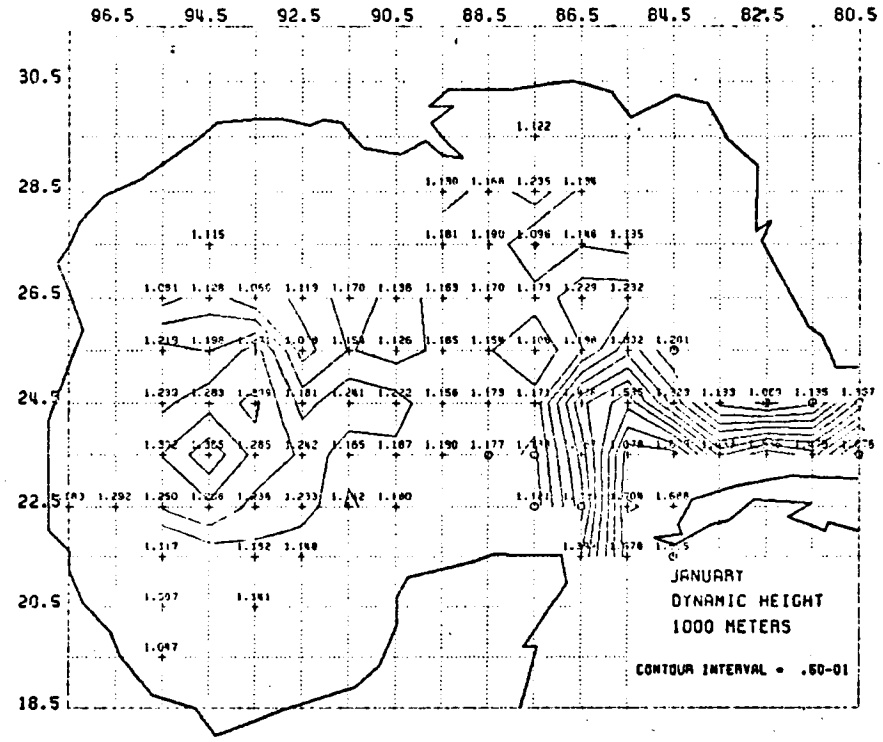
96.5
94.5
92.5
90.5
88.5
86.5
84.5
82.5
80.5
30.5
28.5
26.5
24.5
22.5
20.5
18.5
JANUARY
DYNAMIC HEIGHT
1000 METERS
CONTOUR INTERVAL = .60-01

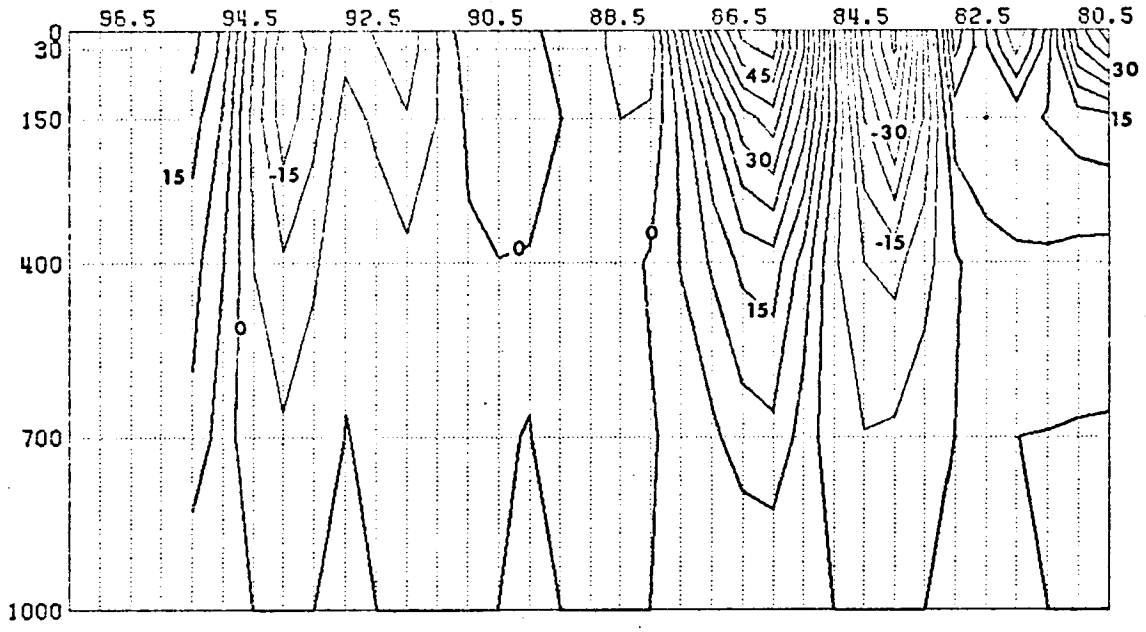

JANUARY

E-W CROSS SECTION FOR V COMPONENT OF GEOSTROPHIC VELOCITY AT LATITUDE 23.5. VELOCITIES ARE COMPUTED RELATIVE TO 1000 M LEVEL. HEAVY LINES DENOTE NORTH VELOCITY. THE CONTOUR INTERVAL IS 5.0 CM/S.

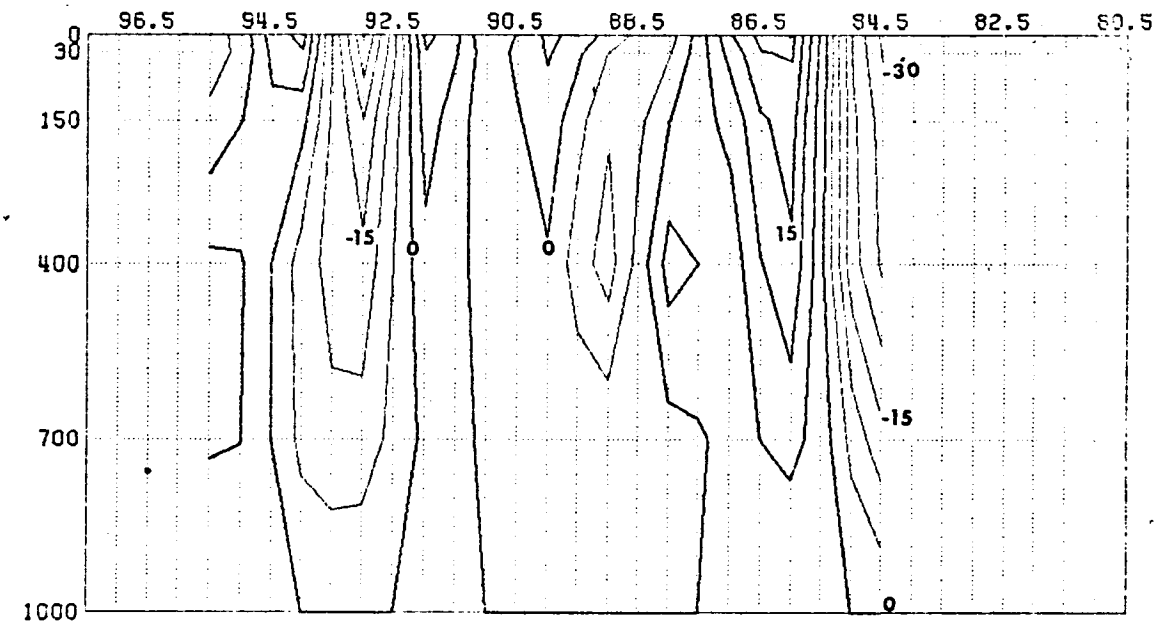

JANUARY

E-W CROSS SECTION FOR V COMPONENT OF GEOSTROPHIC VELOCITY AT LATITUDE 25.5. VELOCITIES ARE COMPUTED RELATIVE TO 1000 M LEVEL. HEAVY LINES DENOTE NORTH VELOCITY. THE CONTOUR INTERVAL IS 5.0 CM/S.

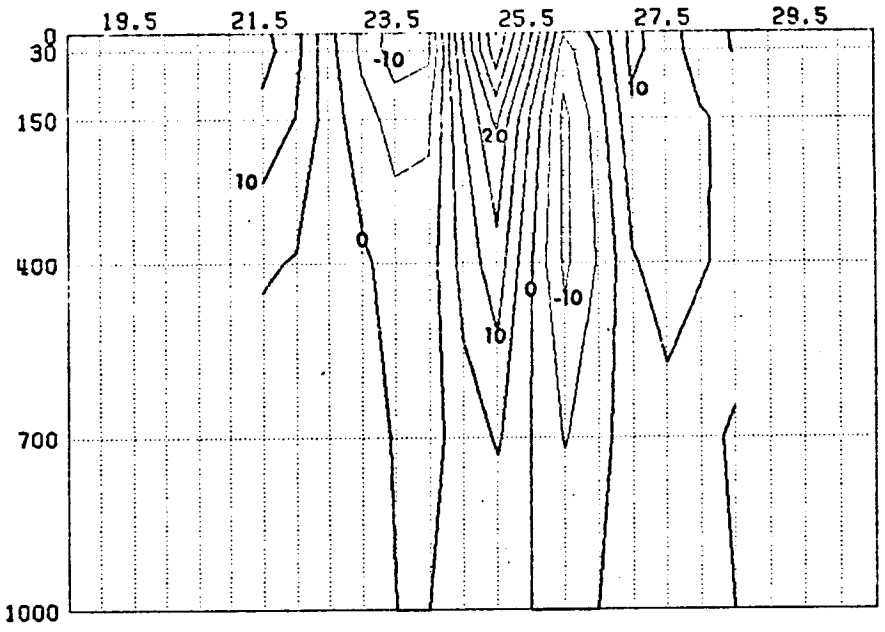

JANUARY

N-S CROSS SECTION FOR U COMPONENT OF GEOSTROPHIC VELOCITY AT LONGITUDE 86.5. VELOCITIES ARE COMPUTED RELATIVE TO 1000 M LEVEL. HEAVY LINES DENOTE EAST VELOCITY. THE CONTOUR INTERVAL IS 5.0 CM/S.

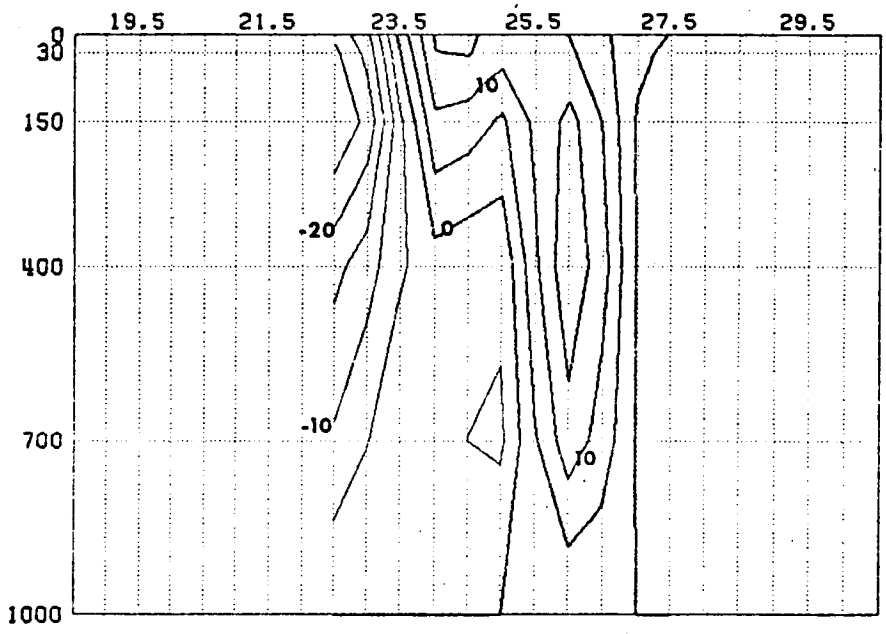

JANUARY

N-S CROSS SECTION FOR U COMPONENT OF GEOSTROPHIC VELOCITY AT LONGITUDE 94.5. VELOCITIES ARE COMPUTED RELATIVE TO 1000 M LEVEL. HEAVY LINES DENOTE EAST VELOCITY. THE CONTOUR INTERVAL IS 5.0 CM/S.

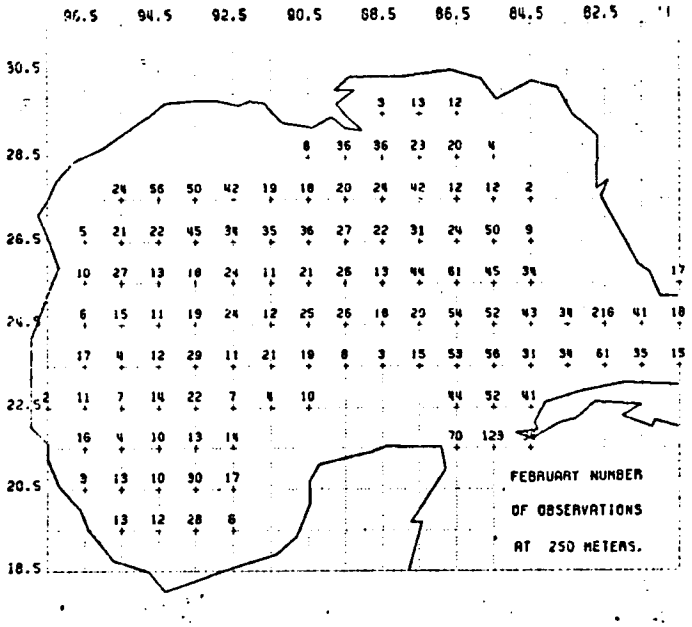

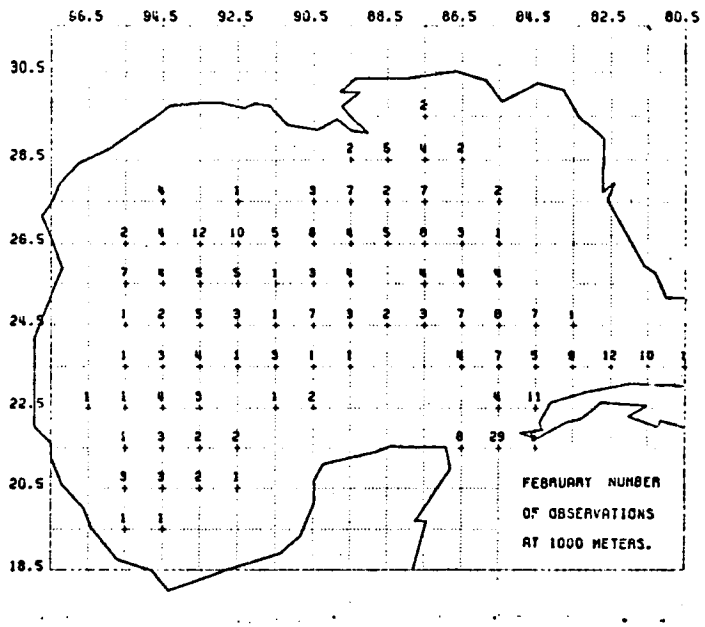

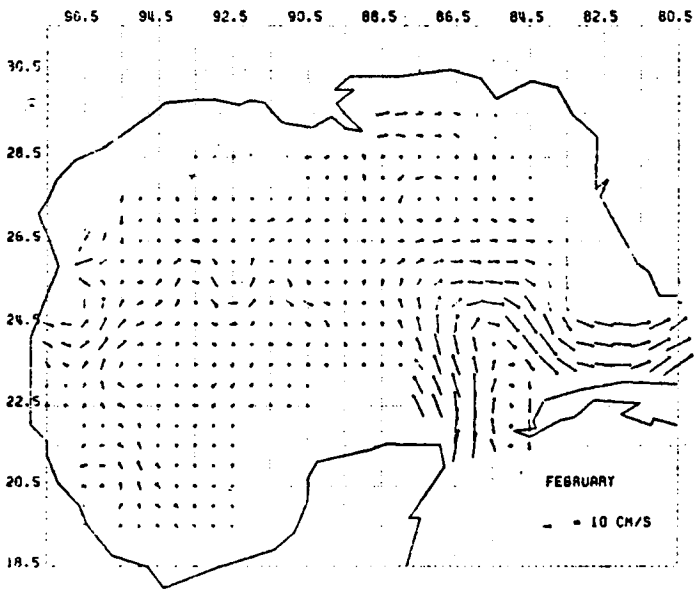

FEBRUARY
GEOSTROPHIC VELOCITIES AT A DEPTH OF .0 METERS.
VELOCITIES ARE COMPUTED RELATIVE TO THE 250.0 M LEVEL.

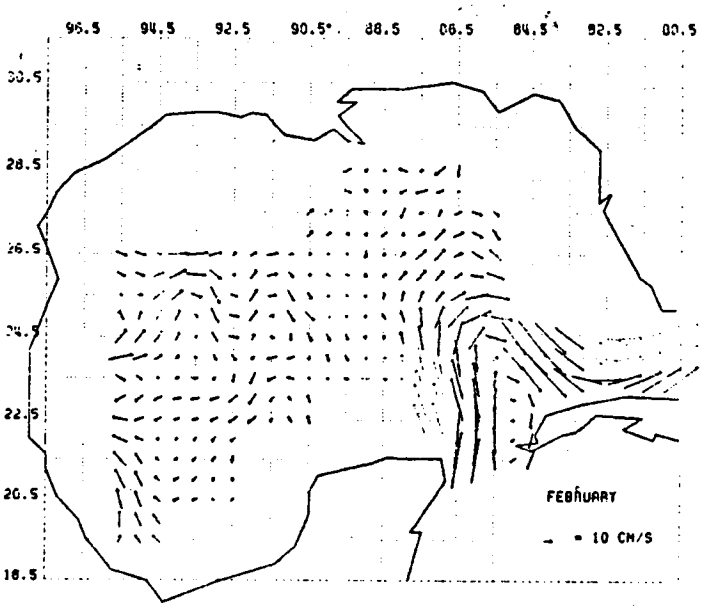

FEBRUARY
GEOSTROPHIC VELOCITIES AT A DEPTH OF .0 METERS.
VELOCITIES ARE COMPUTED RELATIVE TO THE1000.0 M LEVEL.

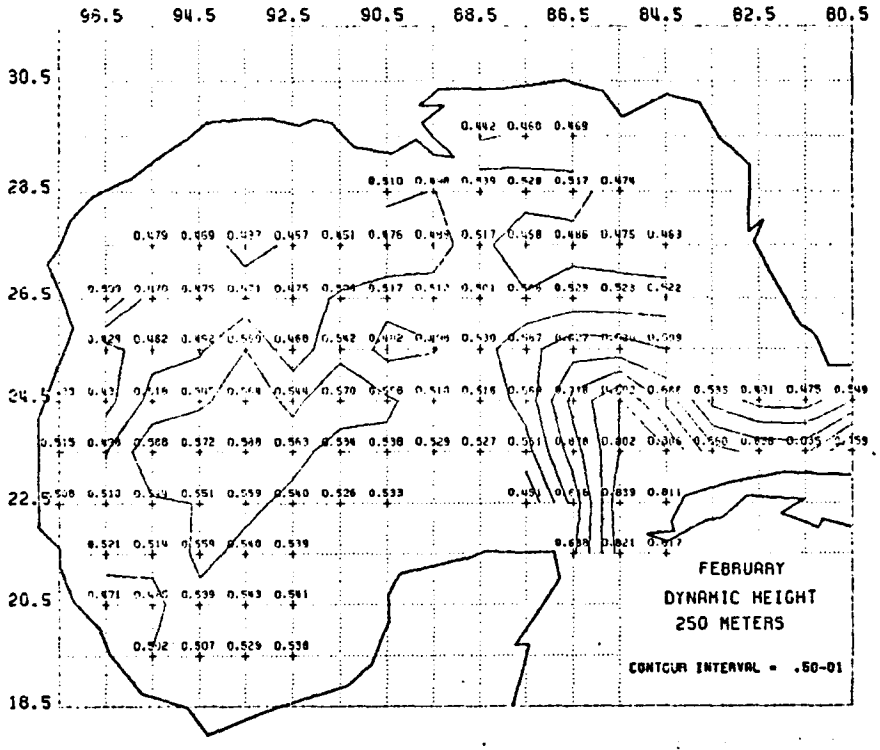
96.5
94.5
92.5
90.5
88.5
86.5
84.5
82.5
80.5
30.5
28.5
26.5
24.5
22.5
20.5
18.5
FEBRUARY
DYNAMIC HEIGHT
250 METERS
CONTOUR INTERVAL = .50-01

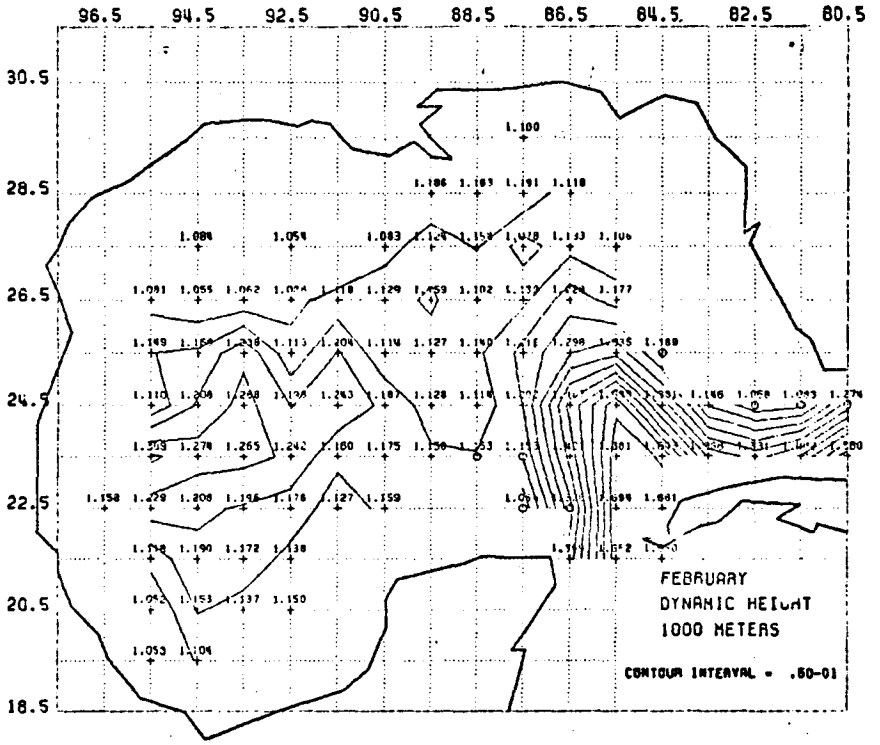
96.5
94.5
92.5
90.5
88.5
86.5
84.5
82.5
80.5
30.5
28.5
26.5
24.5
22.5
20.5
18.5
FEBRUARY
DYNAMIC HEIGHT
1000 METERS
CONTOUR INTERVAL = .50-01

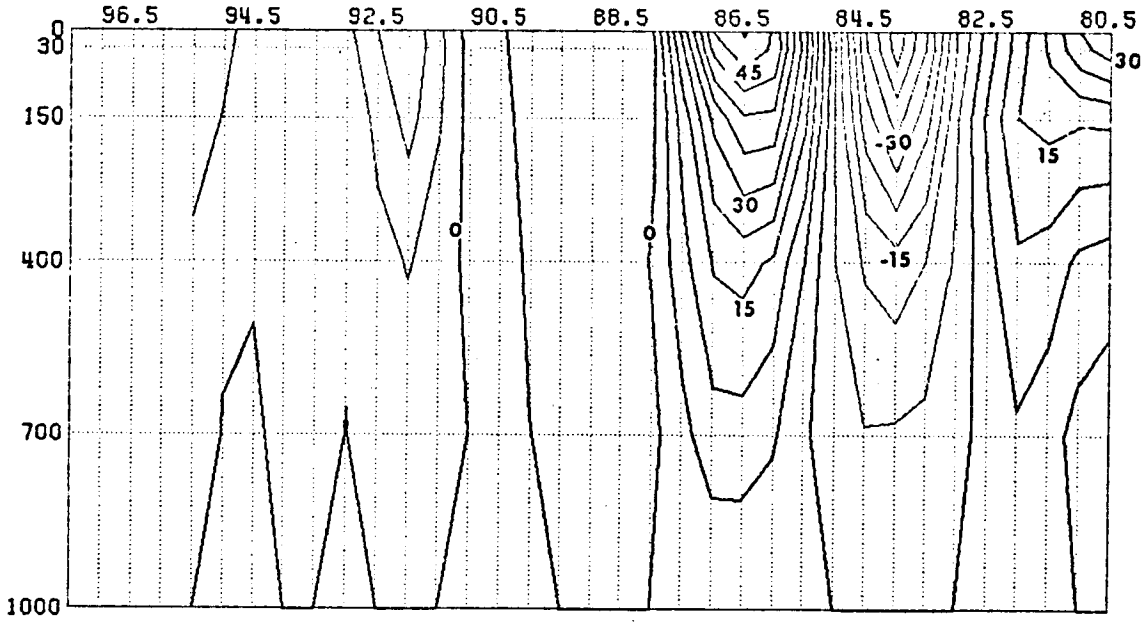

FEBRUARY

E-W CROSS SECTION FOR V COMPONENT OF GEOSTROPHIC VELOCITY AT LATITUDE 23.5. VELOCITIES ARE COMPUTED RELATIVE TO 1000 M LEVEL. HEAVY LINES DENOTE NORTH VELOCITY. THE CONTOUR INTERVAL IS 5.0 CM/S.

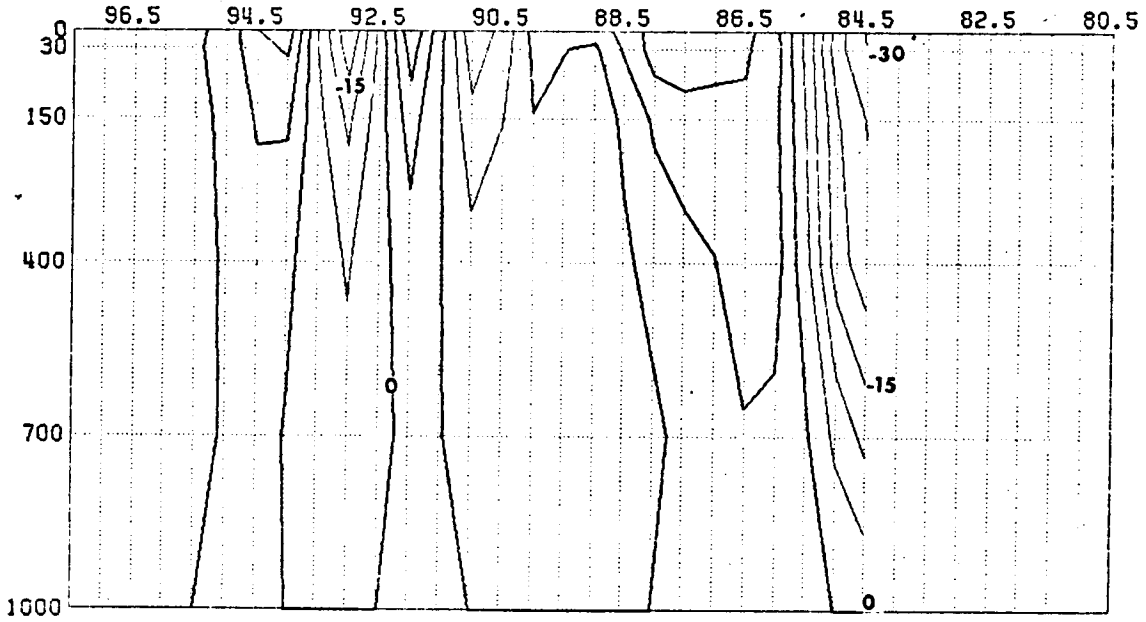

FEBRUARY

E-W CROSS SECTION FOR V COMPONENT OF GEOSTROPHIC VELOCITY AT LATITUDE 25.5. VELOCITIES ARE COMPUTED RELATIVE TO 1000 M LEVEL. HEAVY LINES DENOTE NORTH VELOCITY. THE CONTOUR INTERVAL IS 5.0 CM/S.

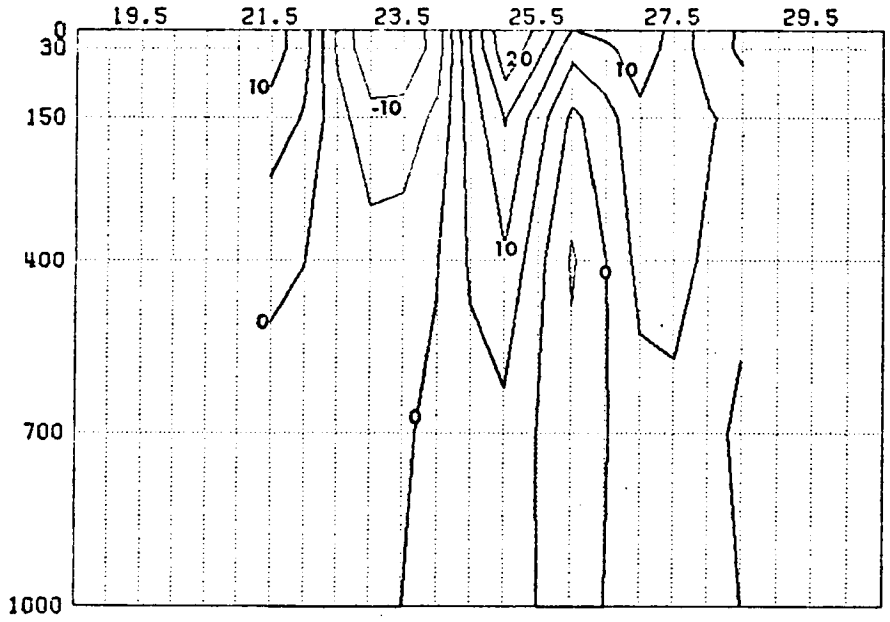

FEBRUARY

N-S CROSS SECTION FOR U COMPONENT OF GEOSTROPHIC VELOCITY AT LONGITUDE 86.5. VELOCITIES ARE COMPUTED RELATIVE TO 1000 M LEVEL. HEAVY LINES DENOTE EAST VELOCITY. THE CONTOUR INTERVAL IS 5.0 CM/S.

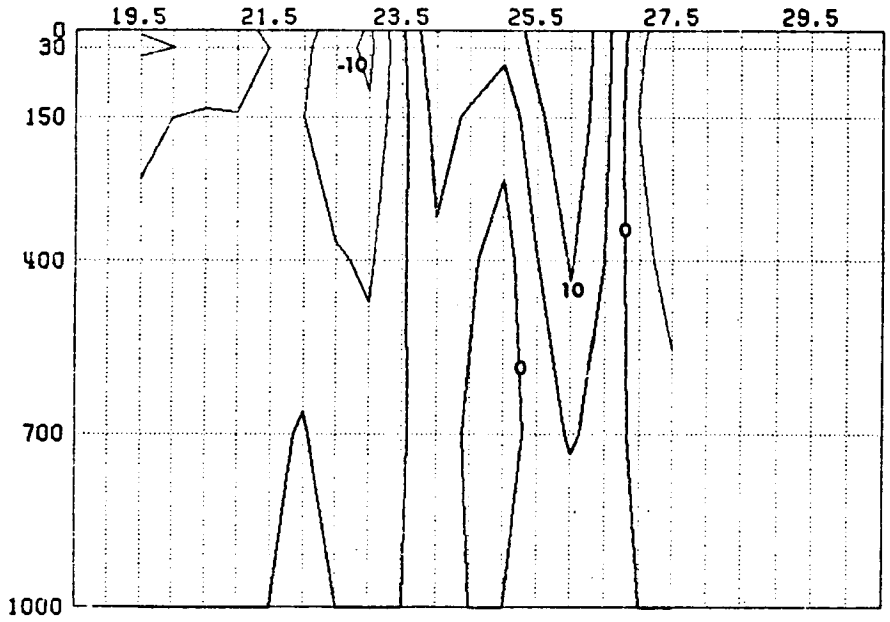

FEBRUARY

N-S CROSS SECTION FOR U COMPONENT OF GEOSTROPHIC VELOCITY AT LONGITUDE 94.5. VELOCITIES ARE COMPUTED RELATIVE TO 1000 M LEVEL. HEAVY LINES DENOTE EAST VELOCITY. THE CONTOUR INTERVAL IS 5.0 CM/S.

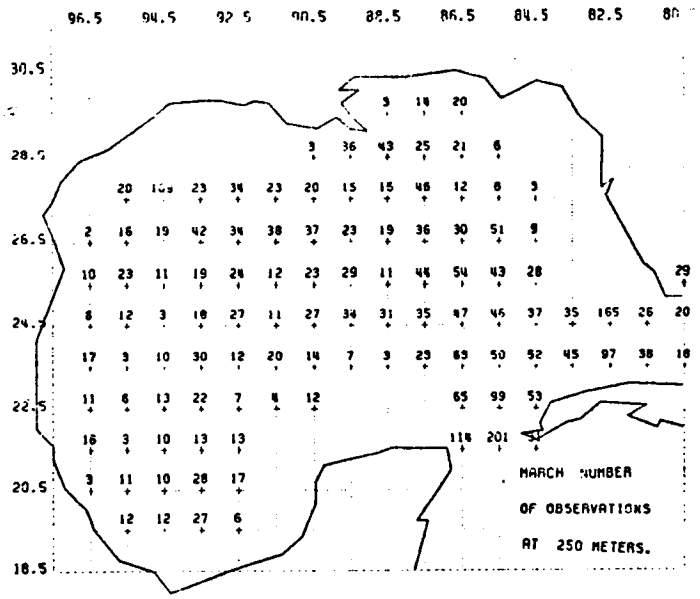

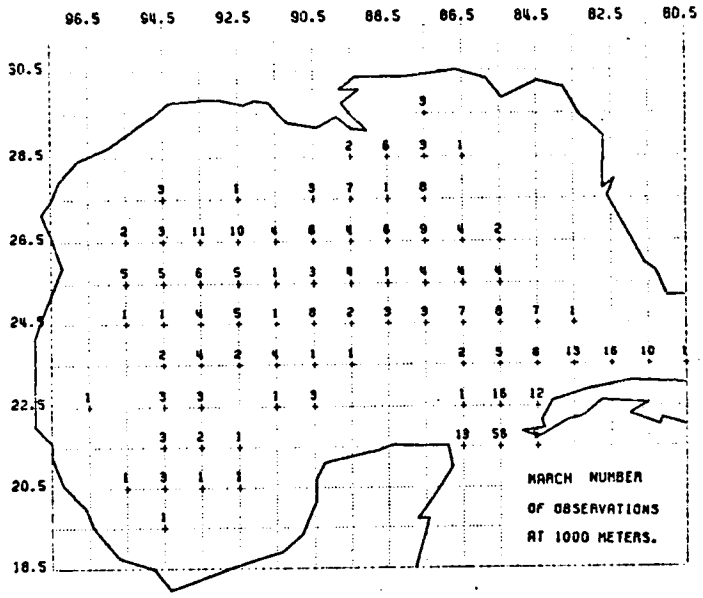

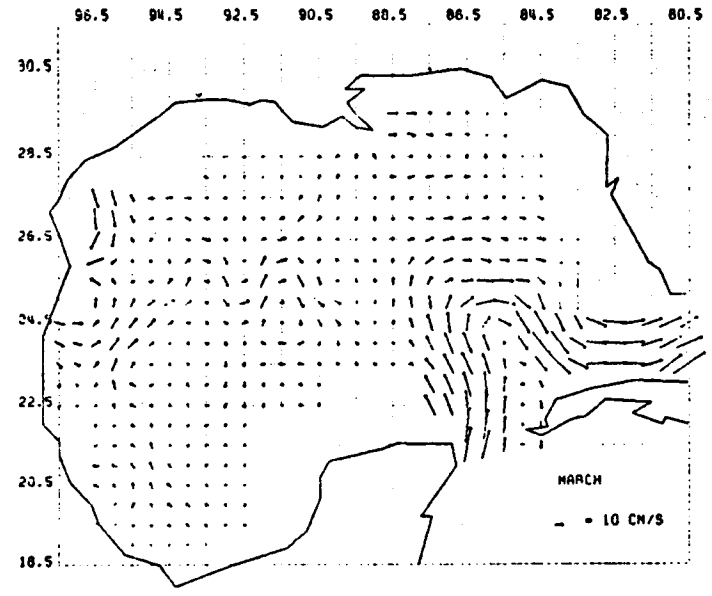

MARCH
GEOSTROPHIC VELOCITIES AT A DEPTH OF .0 METERS.
VELOCITIES ARE COMPUTED RELATIVE TO THE 250.0 M LEVEL.

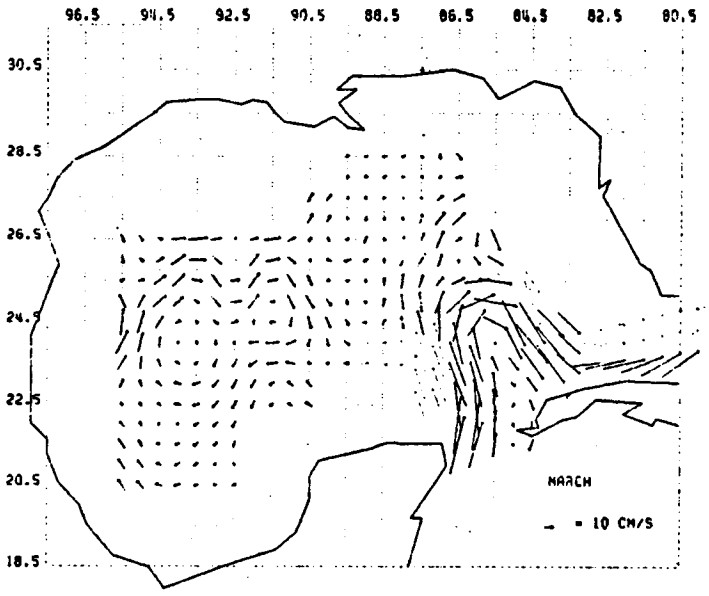

MARCH
GEOSTROPHIC VELOCITIES AT A DEPTH OF .0 METERS.
VELOCITIES ARE COMPUTED RELATIVE TO THE1000.0 M LEVEL.

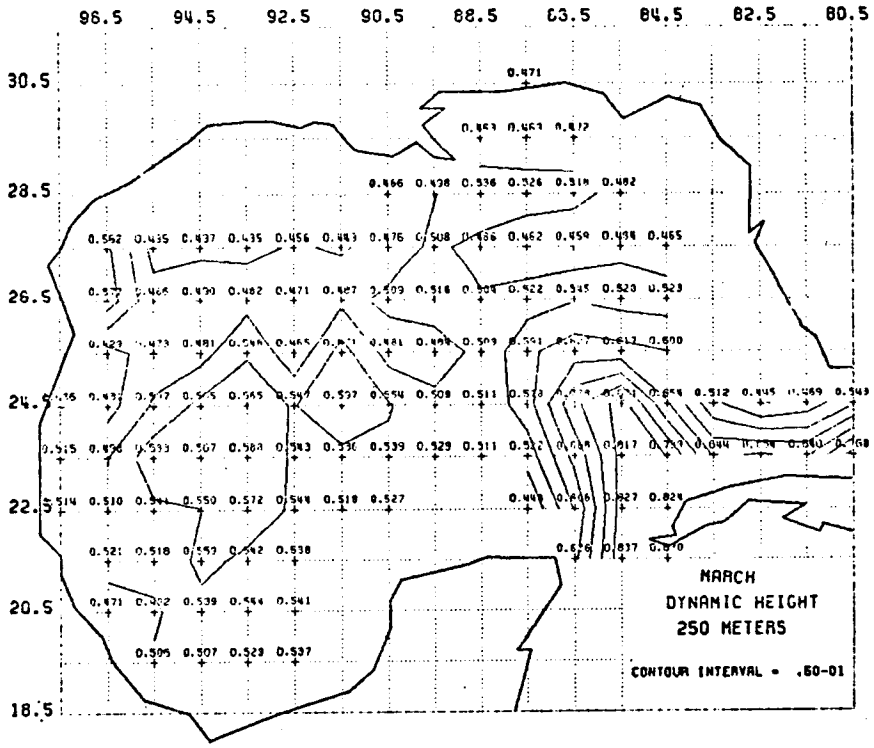
96.5
94.5
92.5
90.5
88.5
86.5
84.5
82.5
80.5
30.5
28.5
26.5
24.5
22.5
20.5
18.5
MARCH
DYNAMIC HEIGHT
250 METERS
CONTOUR INTERVAL = .60-01

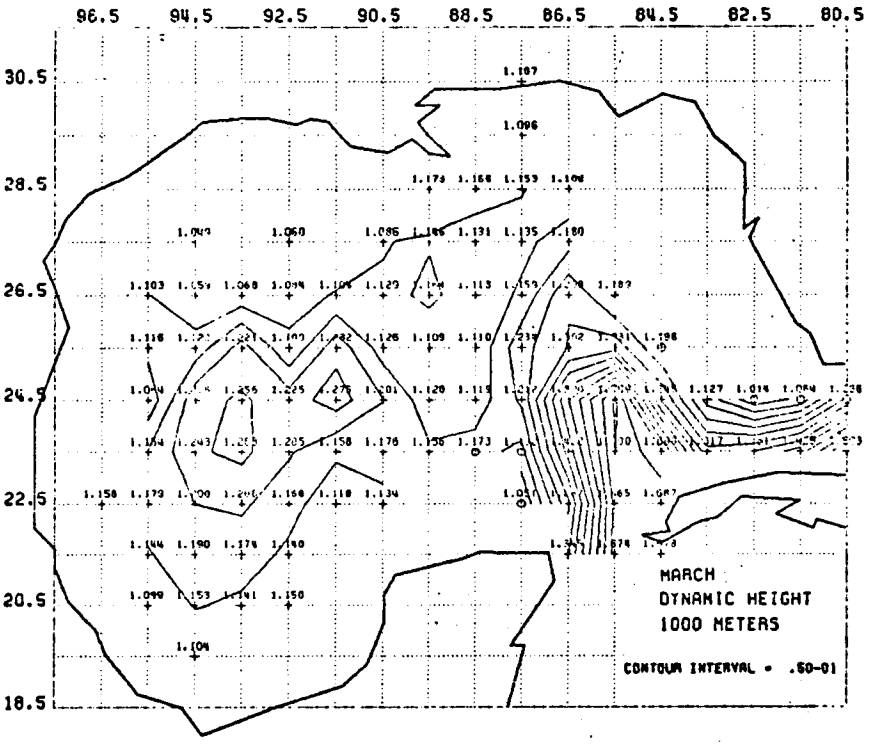
96.5
94.5
92.5
90.5
88.5
86.5
84.5
82.5
80.5
30.5
28.5
26.5
24.5
22.5
20.5
18.5
MARCH
DYNAMIC HEIGHT
1000 METERS
CONTOUR INTERVAL = .60-01

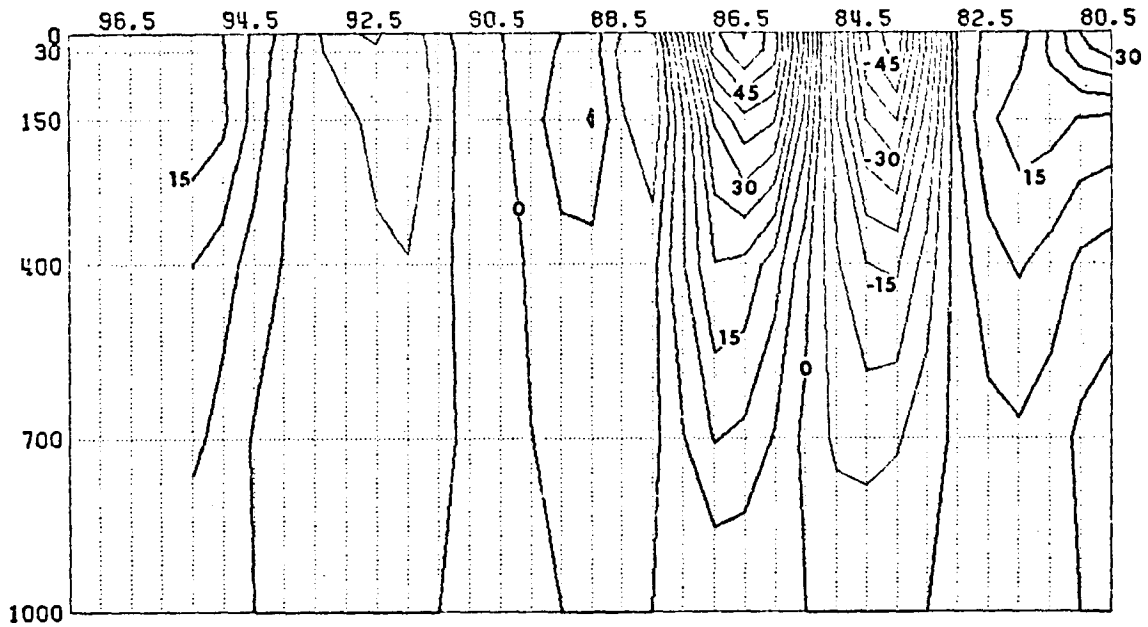

MARCH

E-W CROSS SECTION FOR V COMPONENT OF GEOSTROPHIC VELOCITY AT LATITUDE 23.5. VELOCITIES ARE COMPUTED RELATIVE TO 1000 M LEVEL. HEAVY LINES DENOTE NORTH VELOCITY. THE CONTOUR INTERVAL IS 5.0 CM/S.

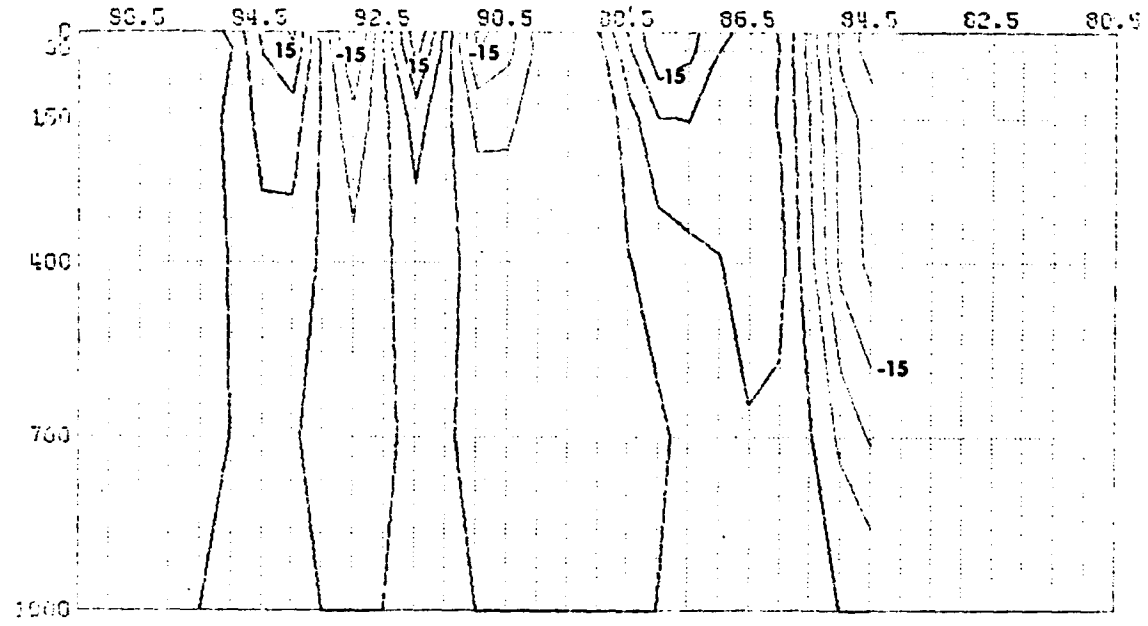

MARCH

E-W CROSS SECTION FOR V COMPONENT OF GEOSTROPHIC VELOCITY AT LATITUDE 25.5. VELOCITIES ARE COMPUTED RELATIVE TO 1000 M LEVEL. HEAVY LINES DENOTE NORTH VELOCITY. THE CONTOUR INTERVAL IS 5.0 CM/S.

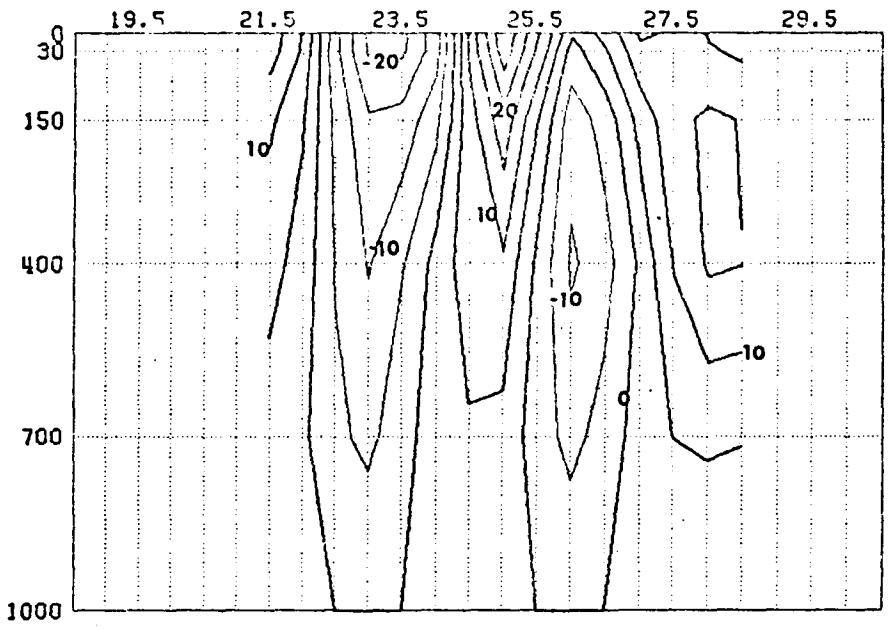

MARCH

N-S CROSS SECTION FOR U COMPONENT OF GEOSTROPHIC VELOCITY AT LONGITUDE 86.5. VELOCITIES ARE COMPUTED RELATIVE TO 1000 M LEVEL. HEAVY LINES DENOTE EAST VELOCITY. THE CONTOUR INTERVAL IS 5.0 CM/S.

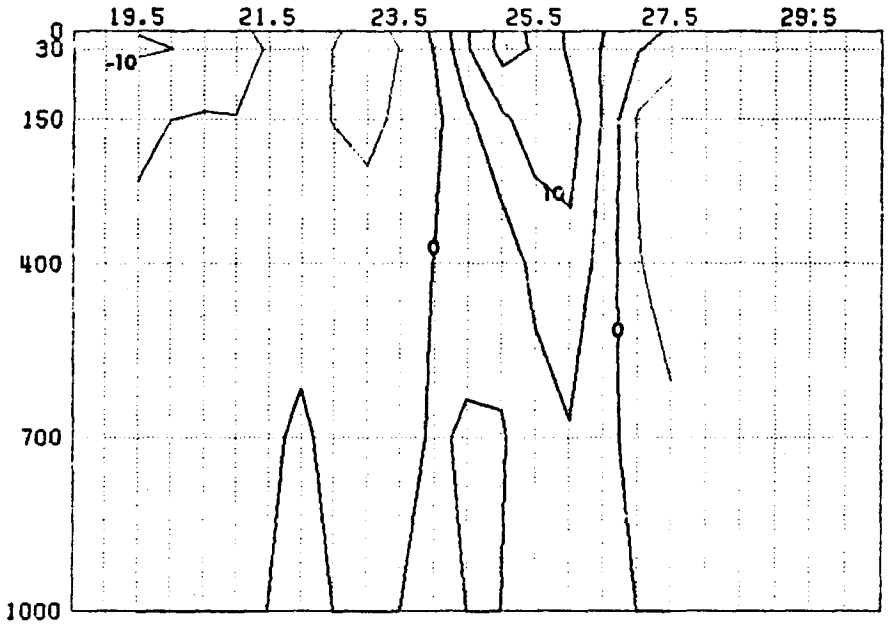

MARCH

N-S CROSS SECTION FOR U COMPONENT OF GEOSTROPHIC VELOCITY AT LONGITUDE 94.5. VELOCITIES ARE COMPUTED RELATIVE TO 1000 M LEVEL. HEAVY LINES DENOTE EAST VELOCITY. THE CONTOUR INTERVAL IS 5.0 CM/S.

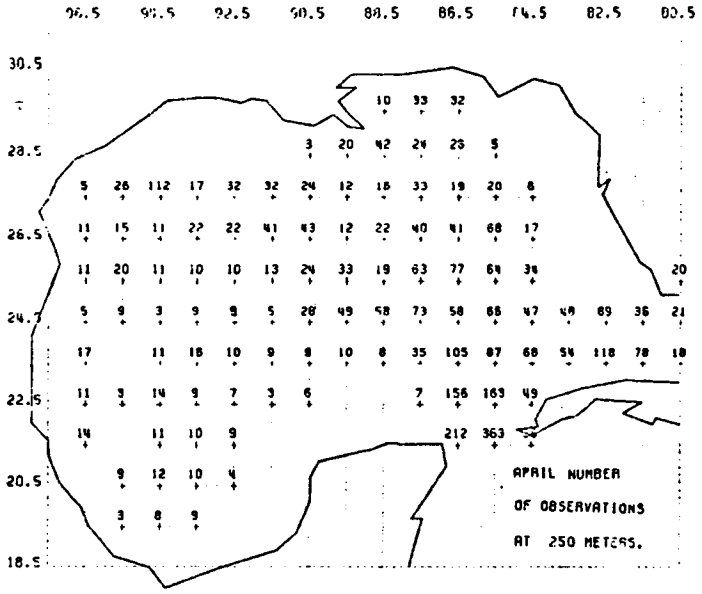

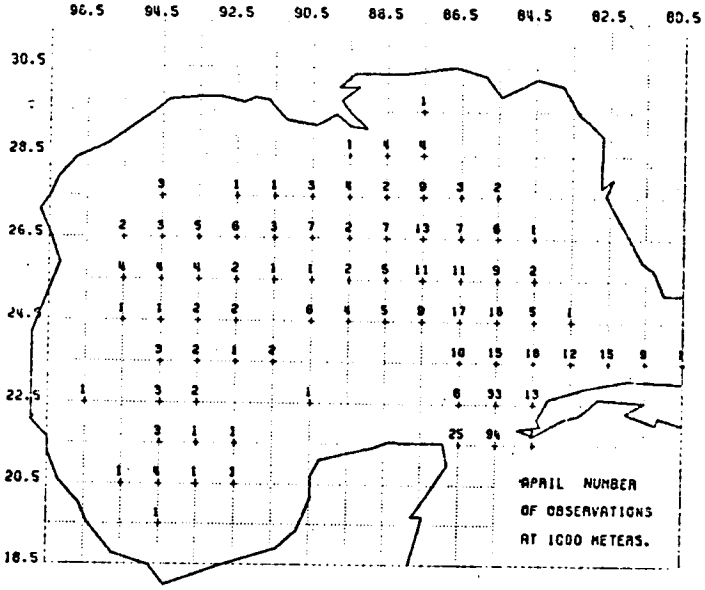

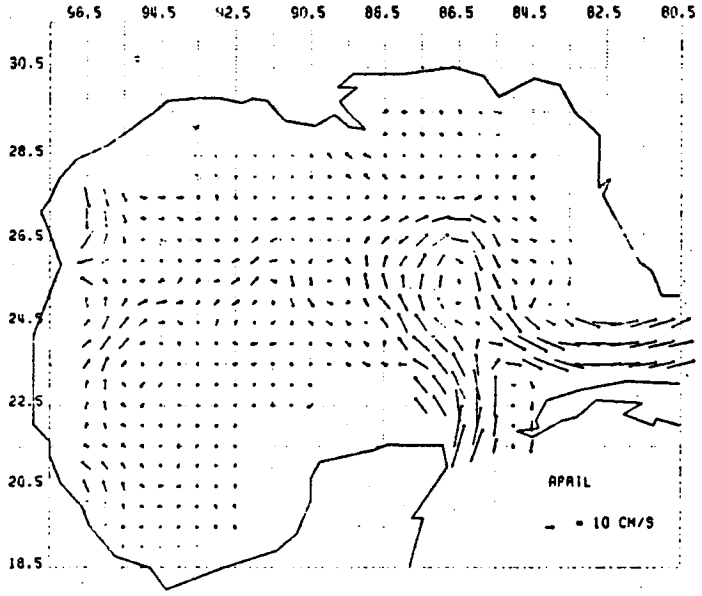

APRIL
GEOSTROPHIC VELOCITIES AT A DEPTH OF .0 METERS.
VELOCITIES ARE COMPUTED RELATIVE TO THE 250.0 M LEVEL.

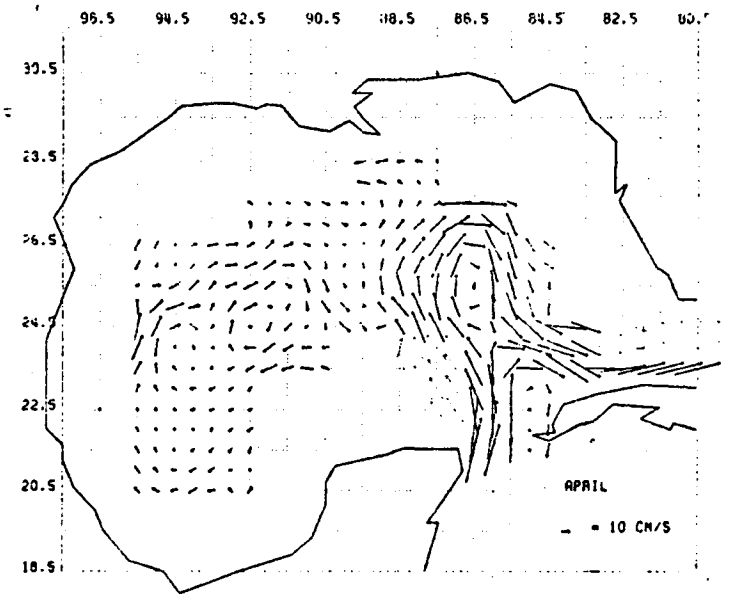

APRIL
GEOSTROPHIC VELOCITIES AT A DEPTH OF .0 METERS.
VELOCITIES ARE COMPUTED RELATIVE TO THE1000.0 M LEVEL.

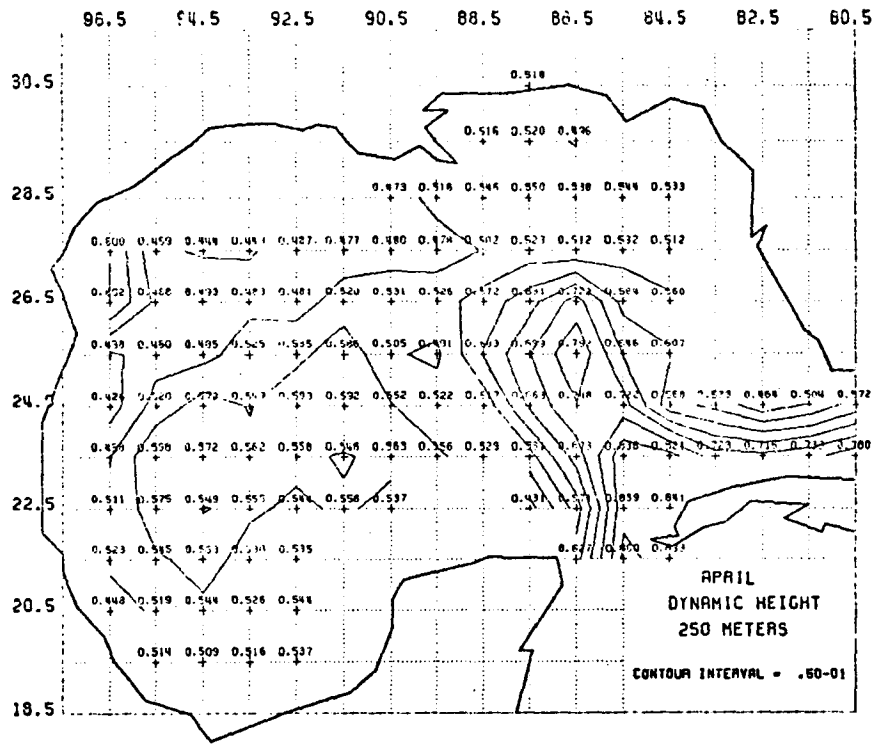
96.5
94.5
92.5
90.5
88.5
86.5
84.5
82.5
80.5
30.5
28.5
26.5
24.5
22.5
20.5
18.5
APRIL
DYNAMIC HEIGHT
250 METERS
CONTOUR INTERVAL = .60-01

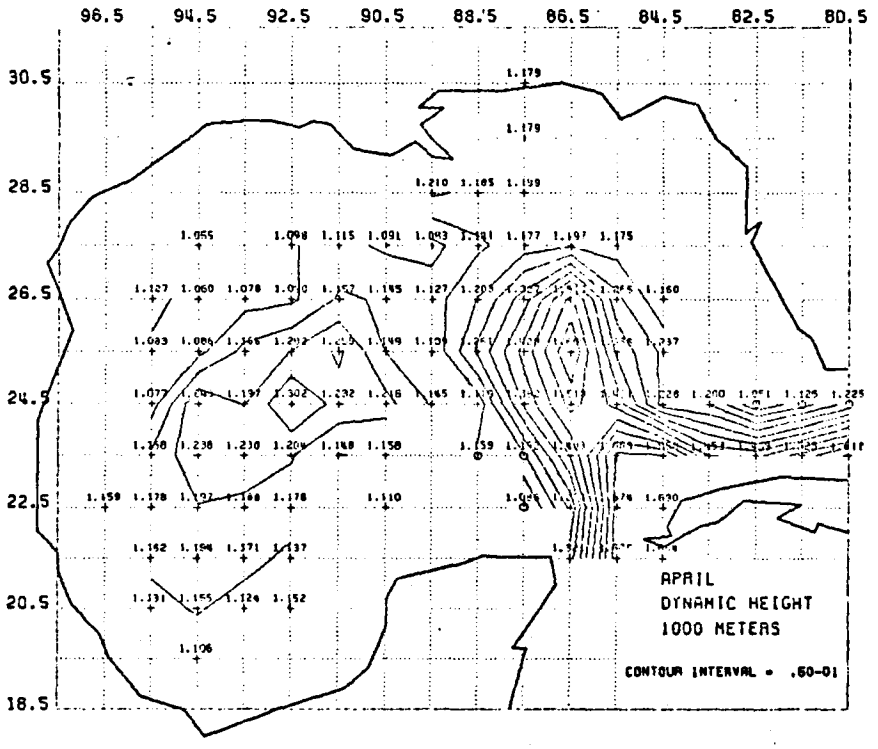
96.5
94.5
92.5
90.5
88.5
86.5
84.5
82.5
80.5
30.5
28.5
26.5
24.5
22.5
20.5
18.5
APRIL
DYNAMIC HEIGHT
1000 METERS
CONTOUR INTERVAL = .60-01

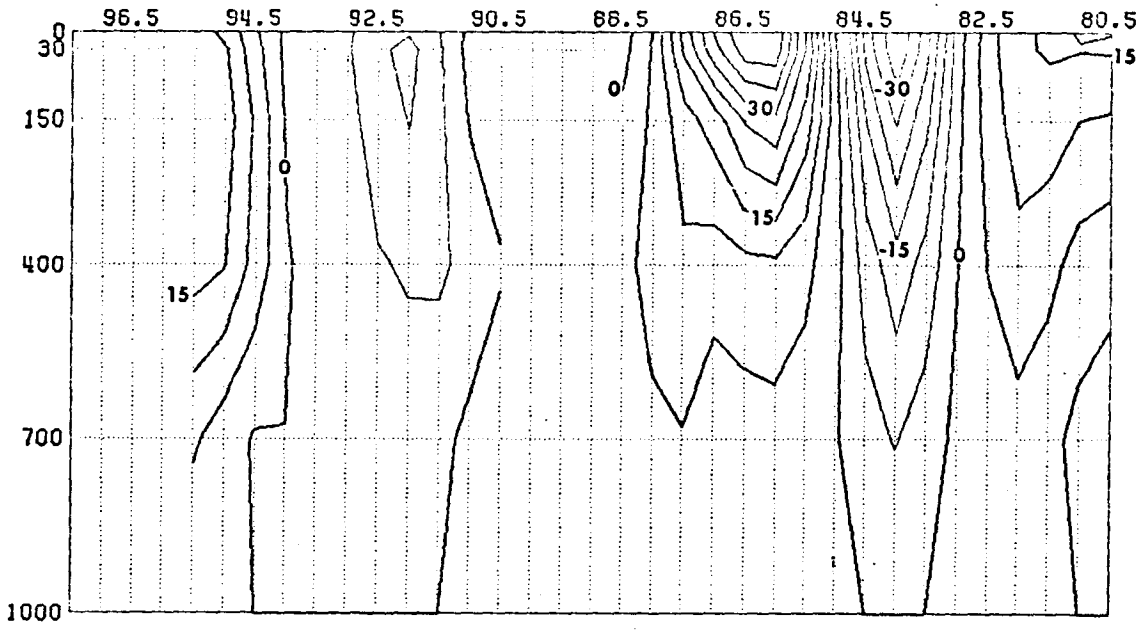

APRIL

E-W CROSS SECTION FOR V COMPONENT OF GEOSTROPHIC VELOCITY AT LATITUDE 23.5. VELOCITIES ARE COMPUTED RELATIVE TO 1000 M LEVEL. HEAVY LINES DENOTE NORTH VELOCITY. THE CONTOUR INTERVAL IS 5.0 CM/S.

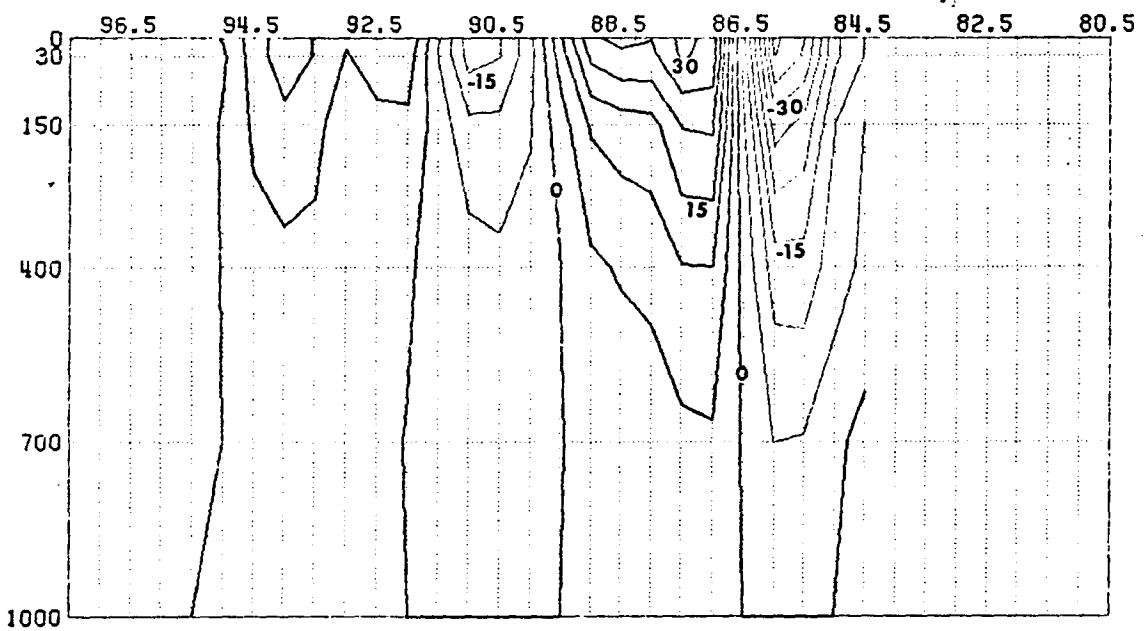

APRIL

E-W CROSS SECTION FOR V COMPONENT OF GEOSTROPHIC VELOCITY AT LATITUDE 25.5. VELOCITIES ARE COMPUTED RELATIVE TO 1000 M LEVEL. HEAVY LINES DENOTE NORTH VELOCITY. THE CONTOUR INTERVAL IS 5.0 CM/S.

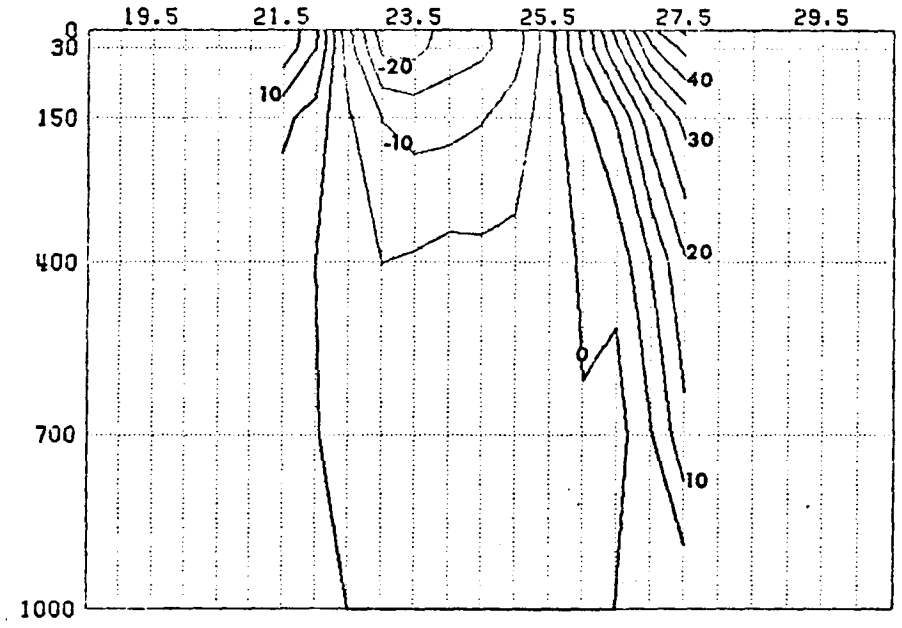

APRIL

N-S CROSS SECTION FOR U COMPONENT OF GEOSTROPHIC VELOCITY AT LONGITUDE 86.5. VELOCITIES ARE COMPUTED RELATIVE TO 1000 M LEVEL. HEAVY LINES DENOTE EAST VELOCITY. THE CONTOUR INTERVAL IS 5.0 CM/S.

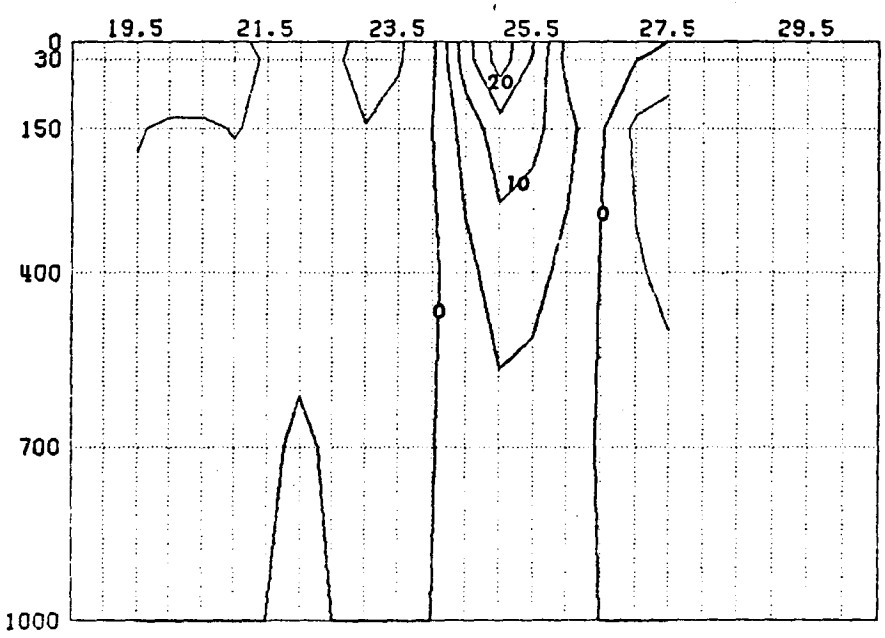

APRIL

N-S CROSS SECTION FOR U COMPONENT OF GEOSTROPHIC VELOCITY AT LONGITUDE 94.5. VELOCITIES ARE COMPUTED RELATIVE TO 1000 M LEVEL. HEAVY LINES DENOTE EAST VELOCITY. THE CONTOUR INTERVAL IS 5.0 CM/S.

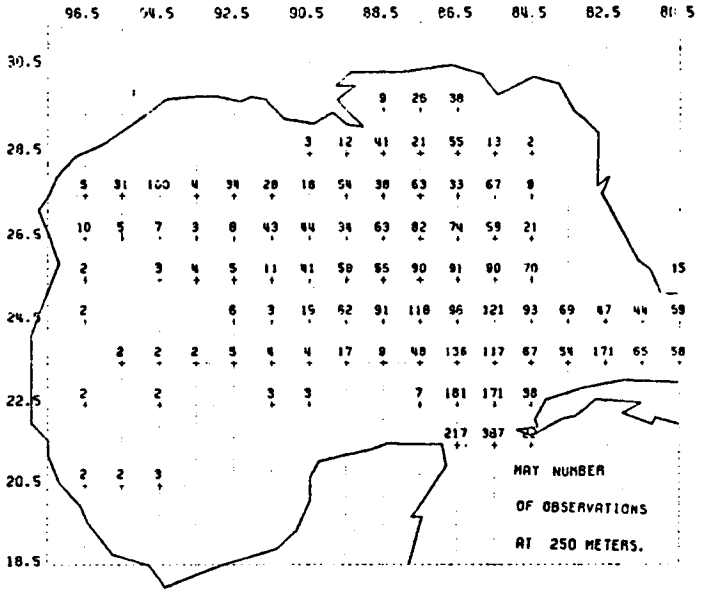

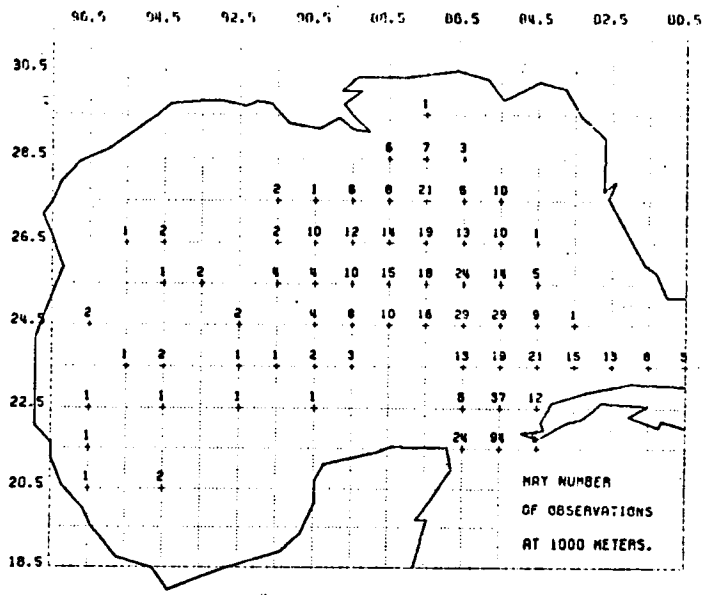

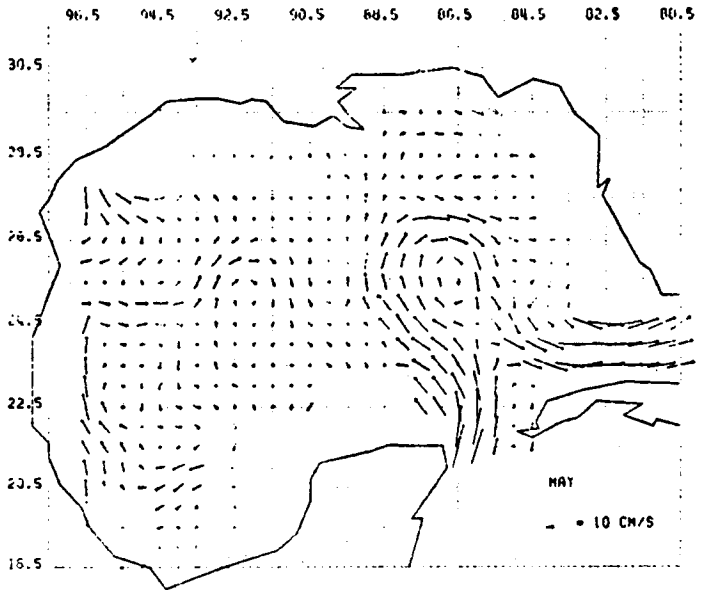

MAY
GEOSTROPHIC VELOCITIES AT A DEPTH OF .0 METERS.
VELOCITIES ARE COMPUTED RELATIVE TO THE 250.0 M LEVEL.

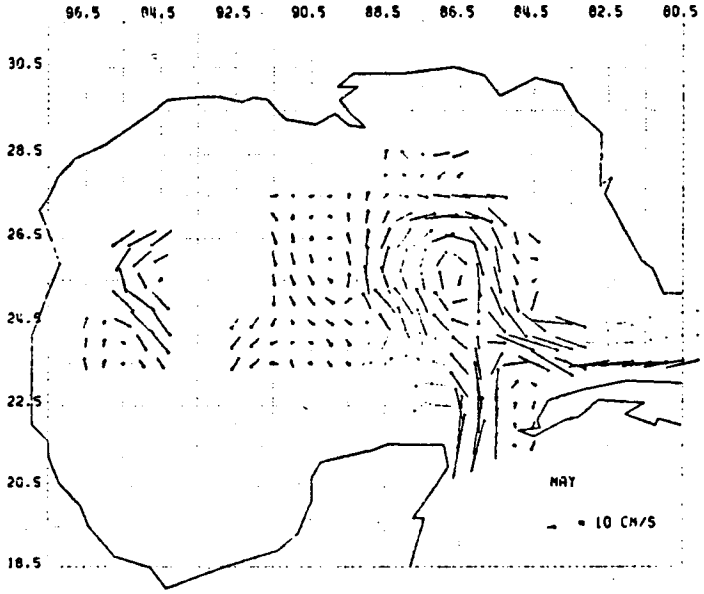

MAY
GEOSTROPHIC VELOCITIES AT A DEPTH OF .0 METERS.
VELOCITIES ARE COMPUTED RELATIVE TO THE1000.0 M LEVEL.

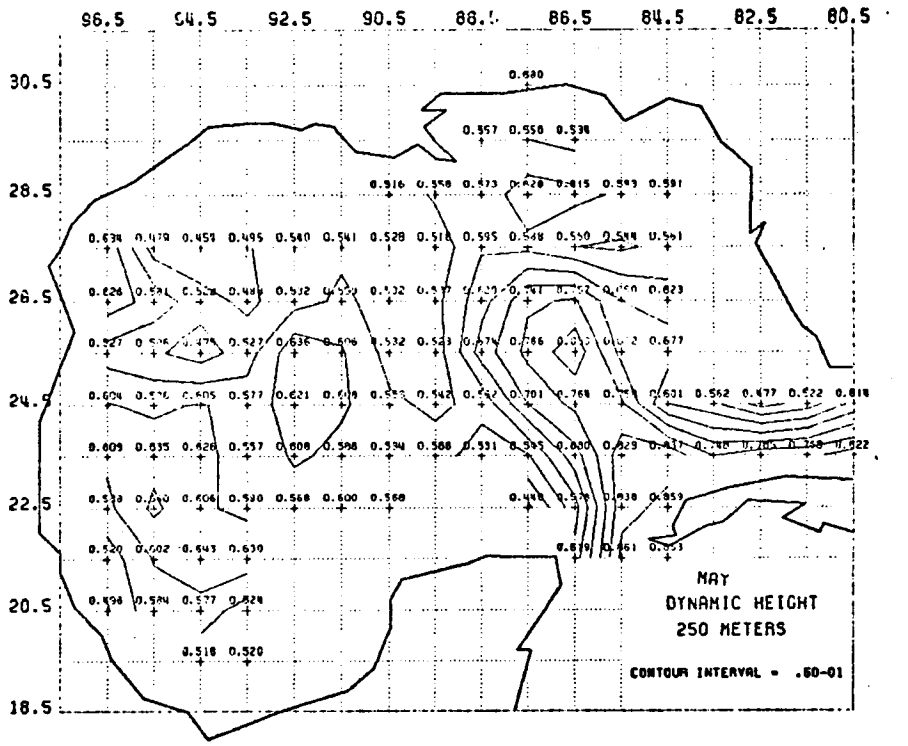
96.5
94.5
92.5
90.5
88.5
86.5
84.5
82.5
80.5
30.5
28.5
26.5
24.5
22.5
20.5
18.5
MAY
DYNAMIC HEIGHT
250 METERS
CONTOUR INTERVAL = .60-01

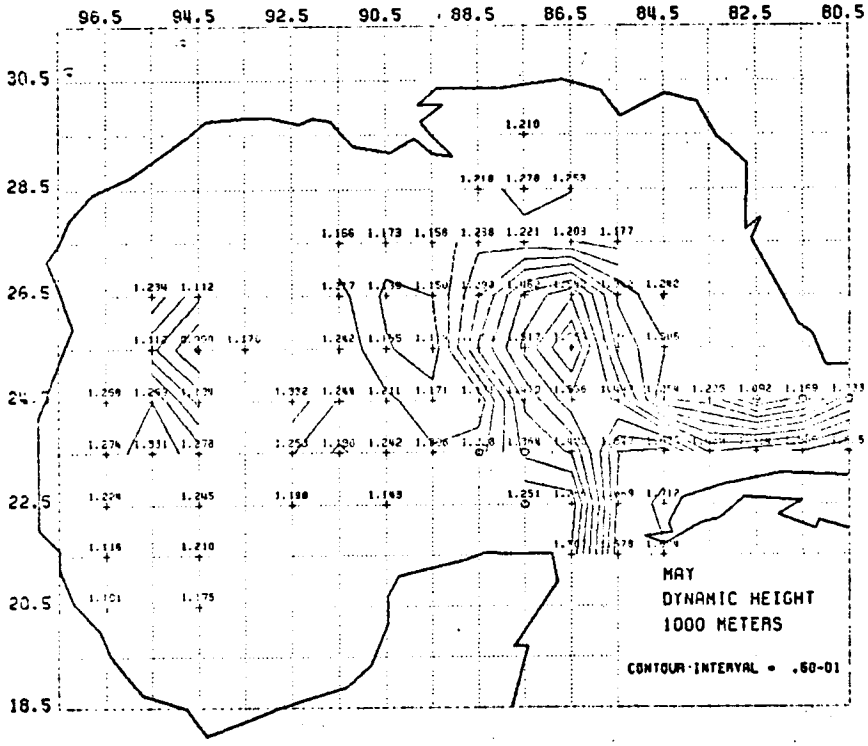
96.5
94.5
92.5
90.5
88.5
86.5
84.5
82.5
80.5
30.5
28.5
26.5
24.5
22.5
20.5
18.5
MAY
DYNAMIC HEIGHT
1000 METERS
CONTOUR INTERVAL = .60-01

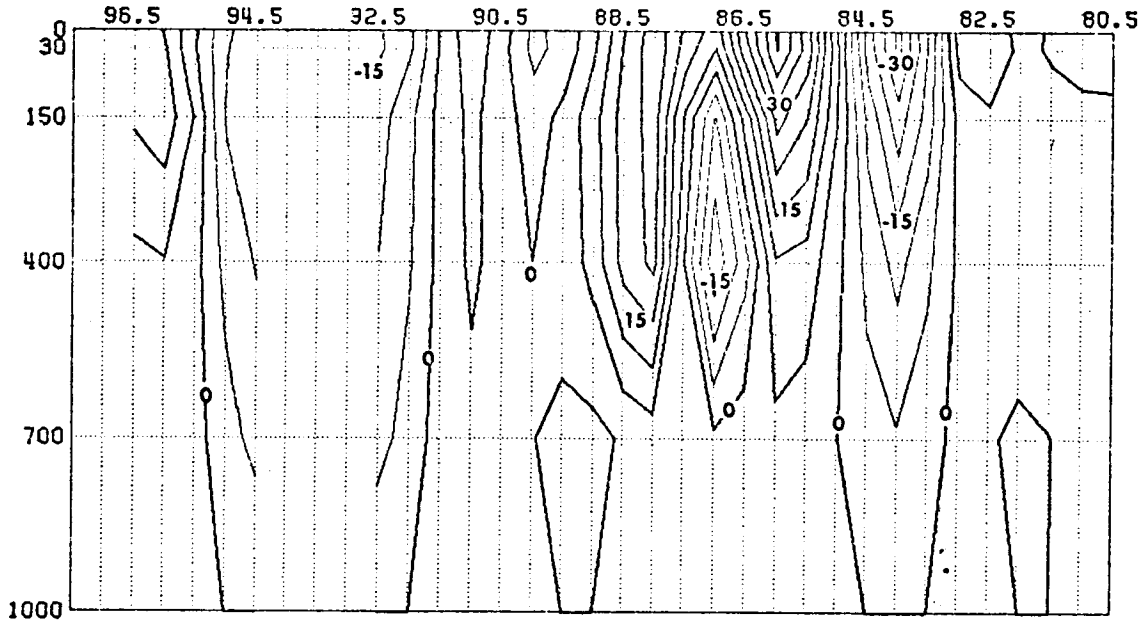

MAY

E-W CROSS SECTION FOR V COMPONENT OF GEOSTROPHIC VELOCITY AT LATITUDE 23.5. VELOCITIES ARE COMPUTED RELATIVE TO 1000 M LEVEL. HEAVY LINES DENOTE NORTH VELOCITY. THE CONTOUR INTERVAL IS 5.0 CM/S.

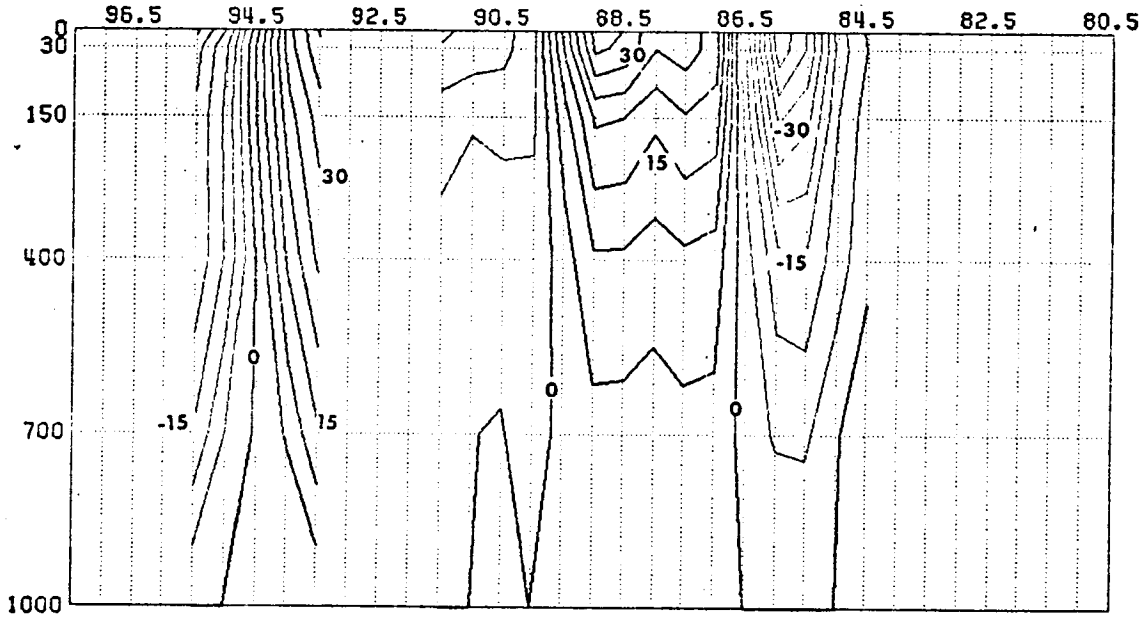

MAY

E-W CROSS SECTION FOR V COMPONENT OF GEOSTROPHIC VELOCITY AT LATITUDE 25.5. VELOCITIES ARE COMPUTED RELATIVE TO 1000 M LEVEL. HEAVY LINES DENOTE NORTH VELOCITY. THE CONTOUR INTERVAL IS 5.0 CM/S.

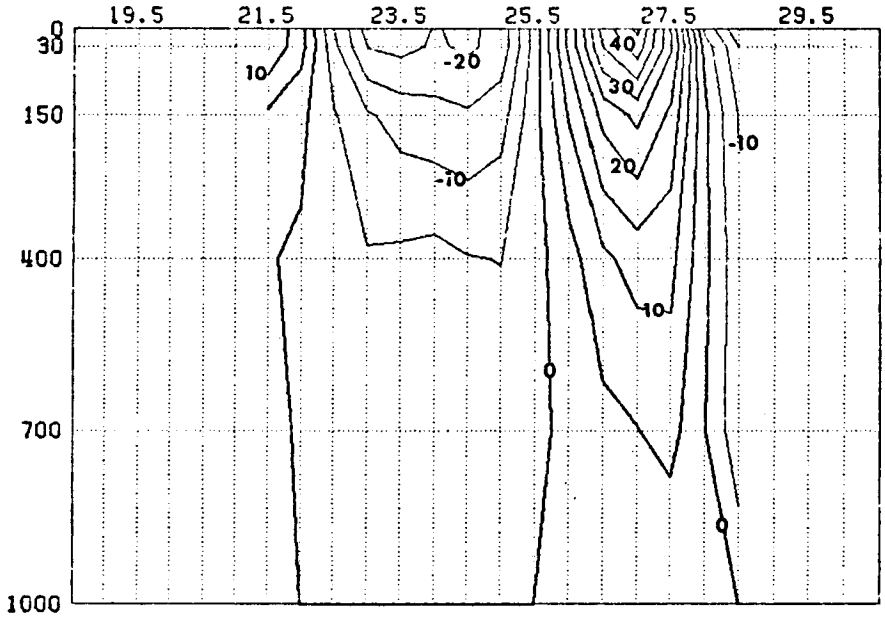

MAY

N-S CROSS SECTION FOR U COMPONENT OF GEOSTROPHIC VELOCITY AT LONGITUDE 86.5. VELOCITIES ARE COMPUTED RELATIVE TO 1000 M LEVEL. HEAVY LINES DENOTE EAST VELOCITY. THE CONTOUR INTERVAL IS 5.0 CM/S.

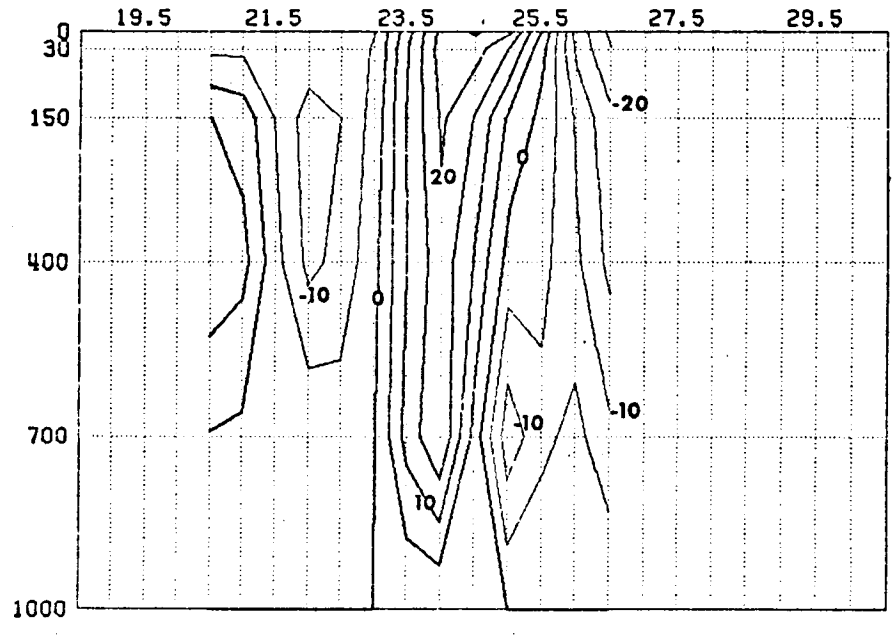

MAY

N-S CROSS SECTION FOR U COMPONENT OF GEOSTROPHIC VELOCITY AT LONGITUDE 94.5. VELOCITIES ARE COMPUTED RELATIVE TO 1000 M LEVEL. HEAVY LINES DENOTE EAST VELOCITY. THE CONTOUR INTERVAL IS 5.0 CM/S.

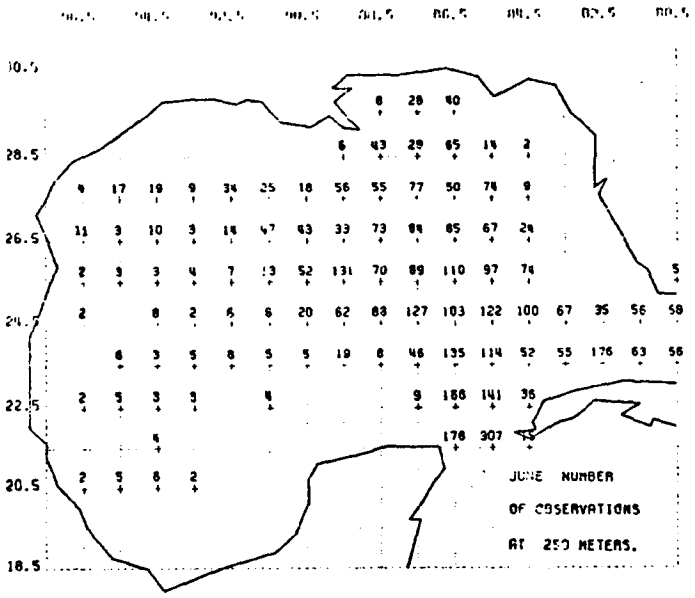

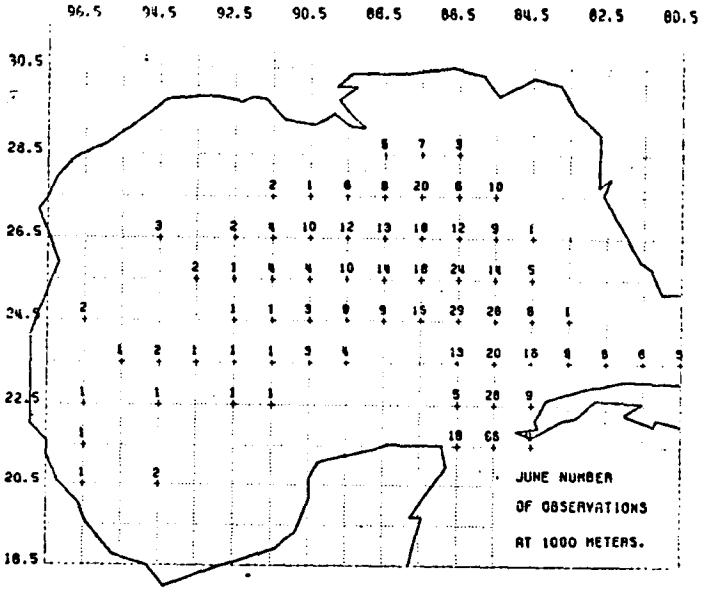

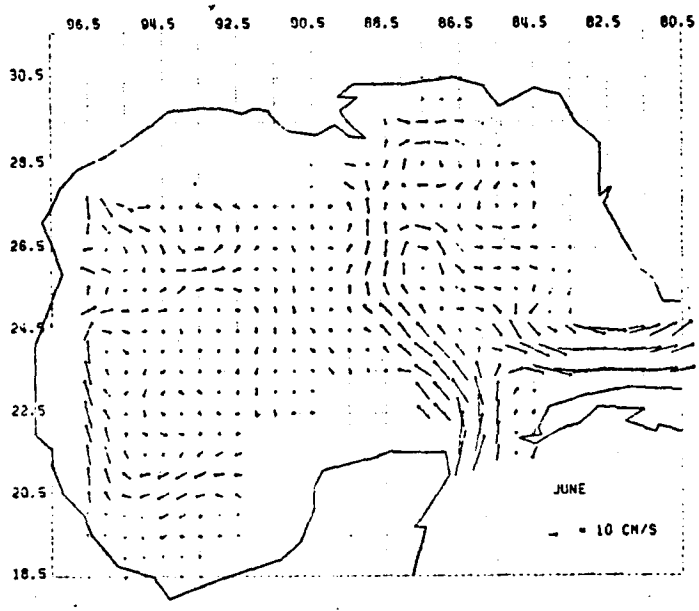

JUNE
GEOSTROPHIC VELOCITIES AT A DEPTH OF .0 METERS.
VELOCITIES ARE COMPUTED RELATIVE TO THE 250.0 M LEVEL.

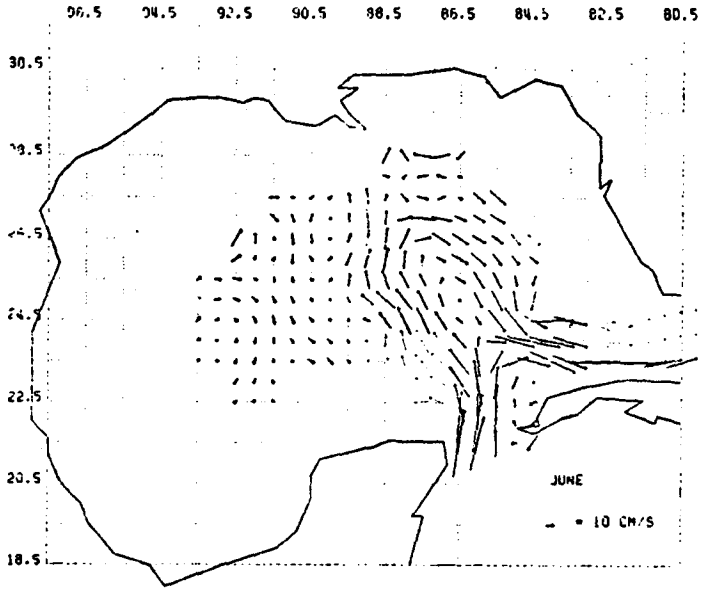

JUNE
GEOSTROPHIC VELOCITIES AT A DEPTH OF .0 METERS.
VELOCITIES ARE COMPUTED RELATIVE TO THE1000.0 M LEVEL.

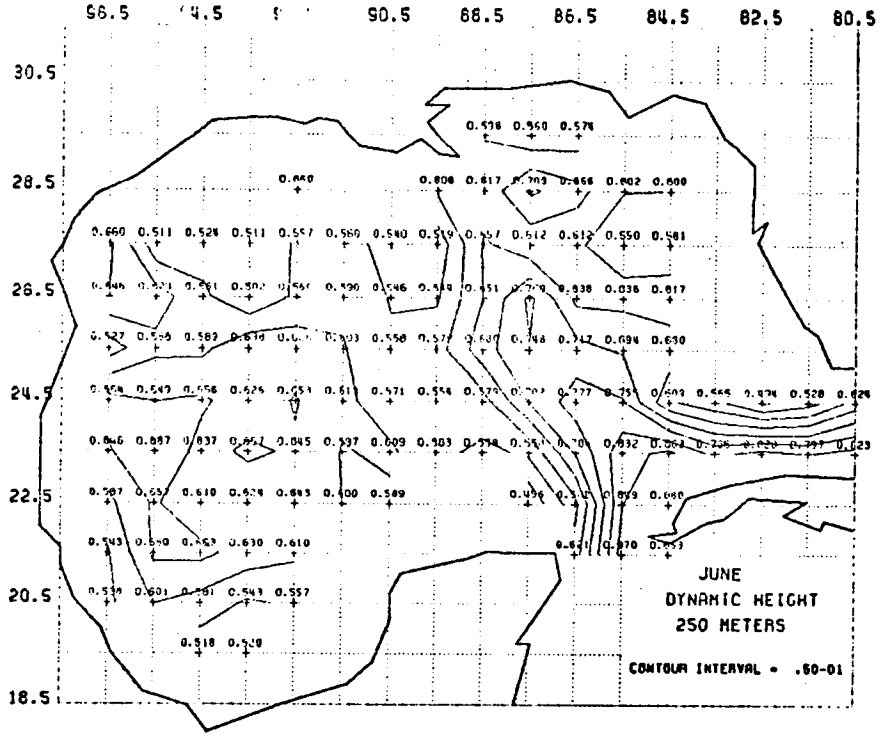
96.5
94.5
92.5
90.5
88.5
86.5
84.5
82.5
80.5
30.5
28.5
26.5
24.5
22.5
20.5
18.5
JUNE
DYNAMIC HEIGHT
250 METERS
CONTOUR INTERVAL = .50-01

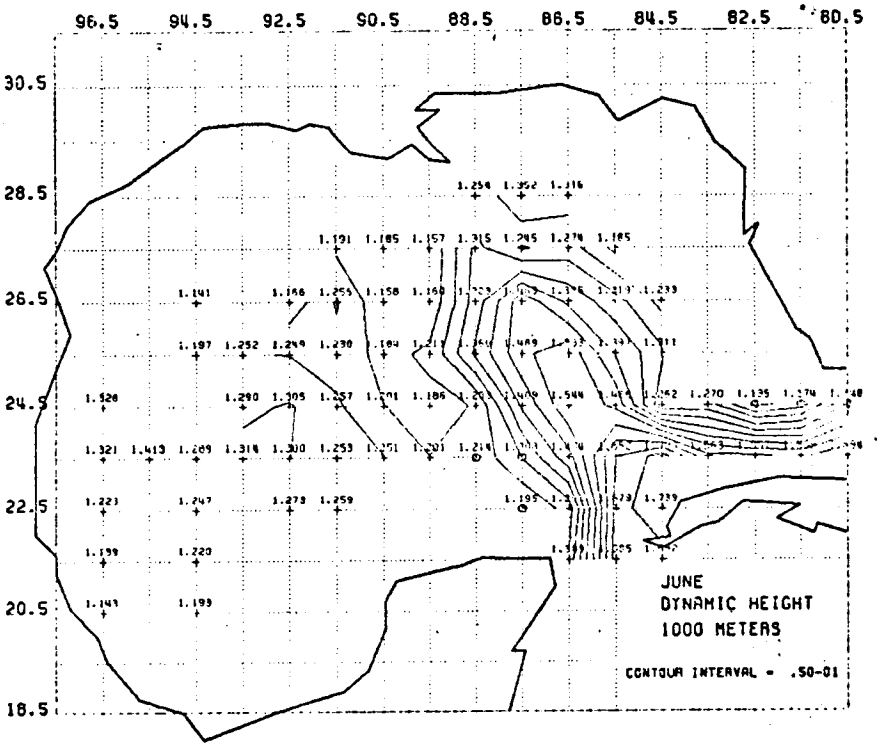
96.5
94.5
92.5
90.5
88.5
86.5
84.5
82.5
80.5
30.5
28.5
26.5
24.5
22.5
20.5
18.5
JUNE
DYNAMIC HEIGHT
1000 METERS
CONTOUR INTERVAL = .50-01

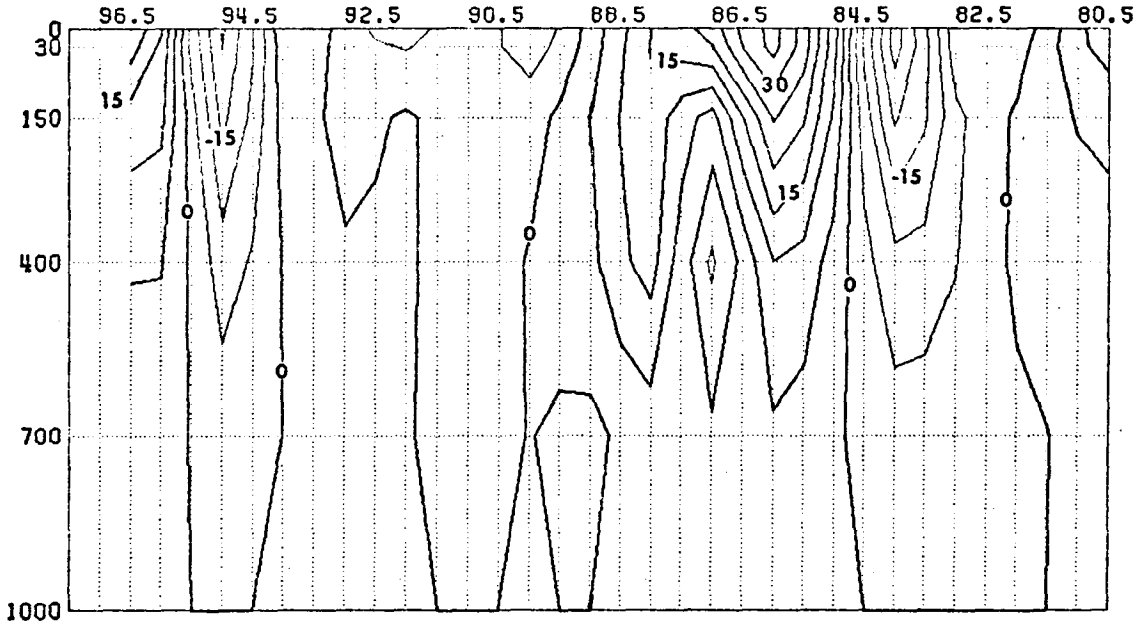

JUNE

E-W CROSS SECTION FOR V COMPONENT OF GEOSTROPHIC VELOCITY AT LATITUDE 23.5. VELOCITIES ARE COMPUTED RELATIVE TO 1000 M LEVEL. HEAVY LINES DENOTE NORTH VELOCITY. THE CONTOUR INTERVAL IS 5.0 CM/S.

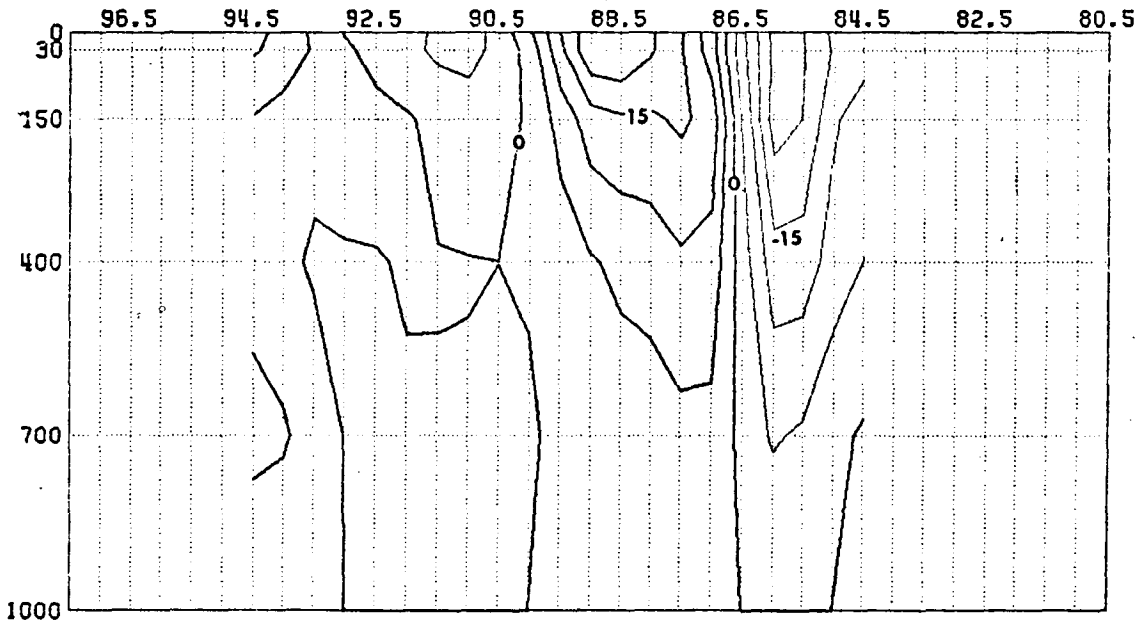

JUNE

E-W CROSS SECTION FOR V COMPONENT OF GEOSTROPHIC VELOCITY AT LATITUDE 25.5. VELOCITIES ARE COMPUTED RELATIVE TO 1000 M LEVEL. HEAVY LINES DENOTE NORTH VELOCITY. THE CONTOUR INTERVAL IS 5.0 CM/S.

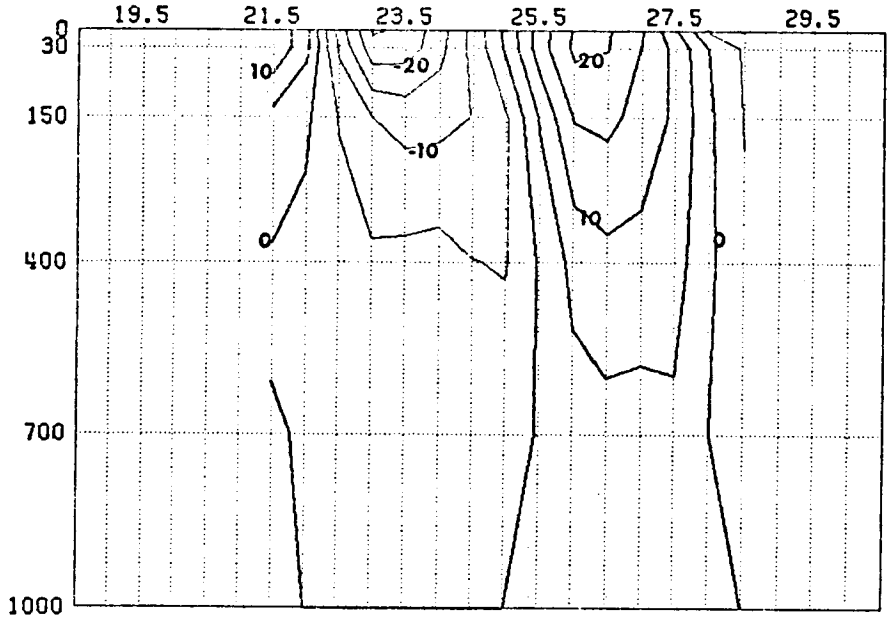

JUNE

N-S CROSS SECTION FOR U COMPONENT OF GEOSTROPHIC VELOCITY AT LONGITUDE 86.5. VELOCITIES ARE COMPUTED RELATIVE TO 1000 M LEVEL. HEAVY LINES DENOTE EAST VELOCITY. THE CONTOUR INTERVAL IS 5.0 CM/S.

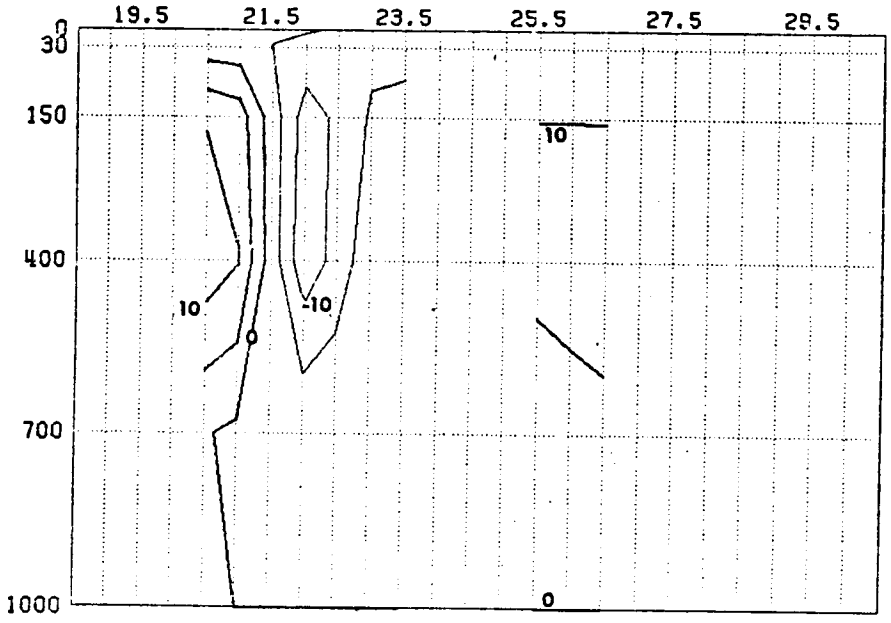

JUNE

N-S CROSS SECTION FOR U COMPONENT OF GEOSTROPHIC VELOCITY AT LONGITUDE 94.5. VELOCITIES ARE COMPUTED RELATIVE TO 1000 M LEVEL. HEAVY LINES DENOTE EAST VELOCITY. THE CONTOUR INTERVAL IS 5.0 CM/S.

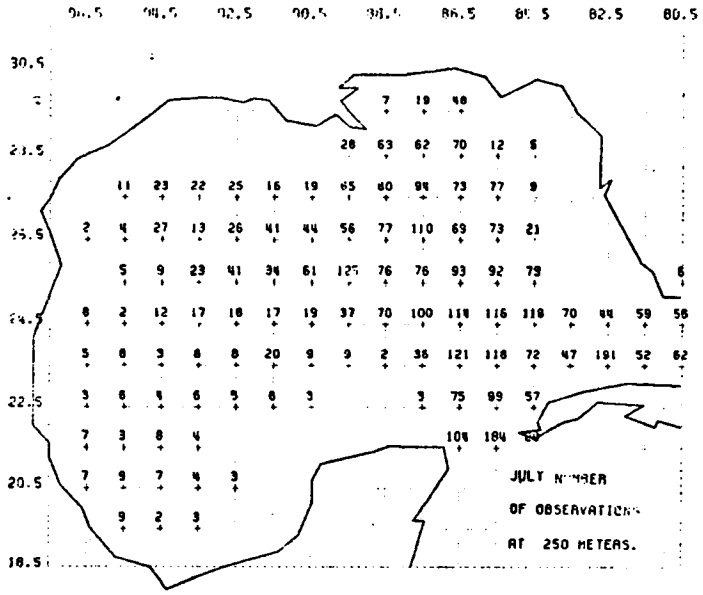

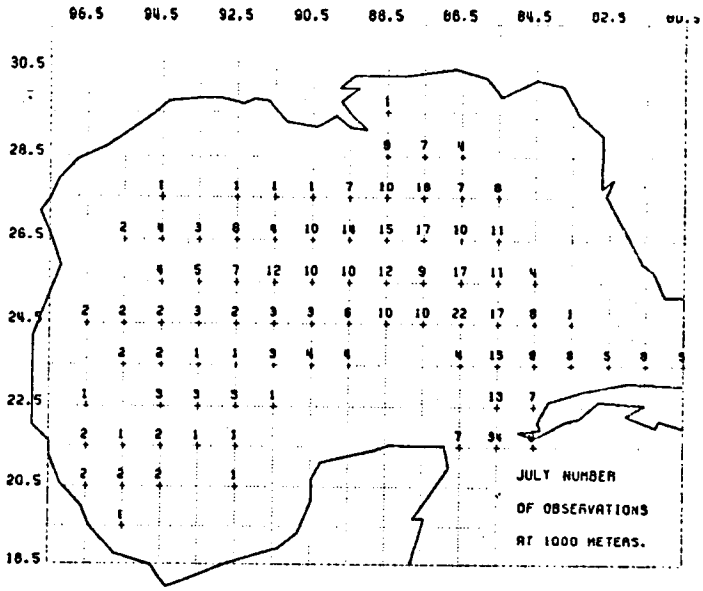

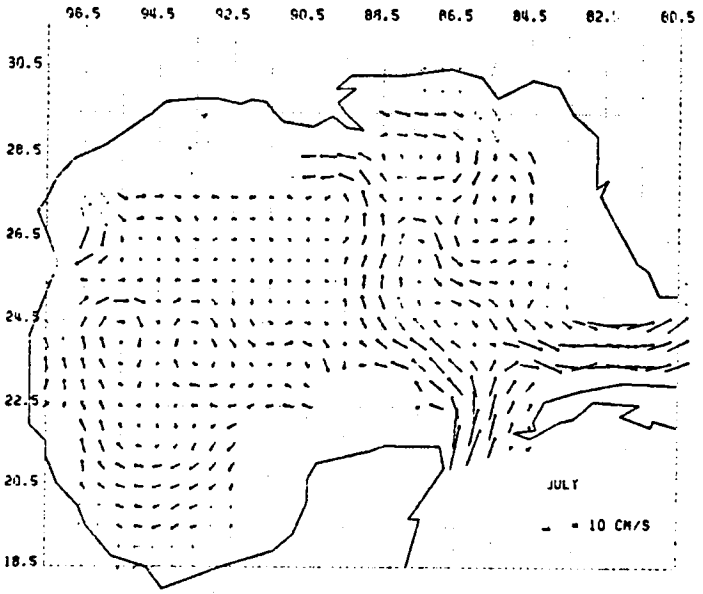

JULY
GEOSTROPHIC VELOCITIES AT A DEPTH OF .0 METERS.
VELOCITIES ARE COMPUTED RELATIVE TO THE 250.0 M LEVEL.

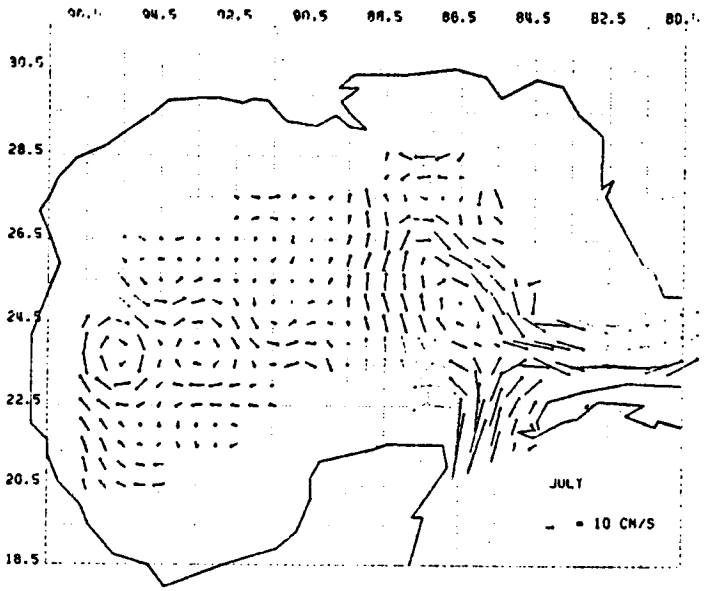

JULY
GEOSTROPHIC VELOCITIES AT A DEPTH OF .0 METERS.
VELOCITIES ARE COMPUTED RELATIVE TO THE1000.0 M LEVEL.

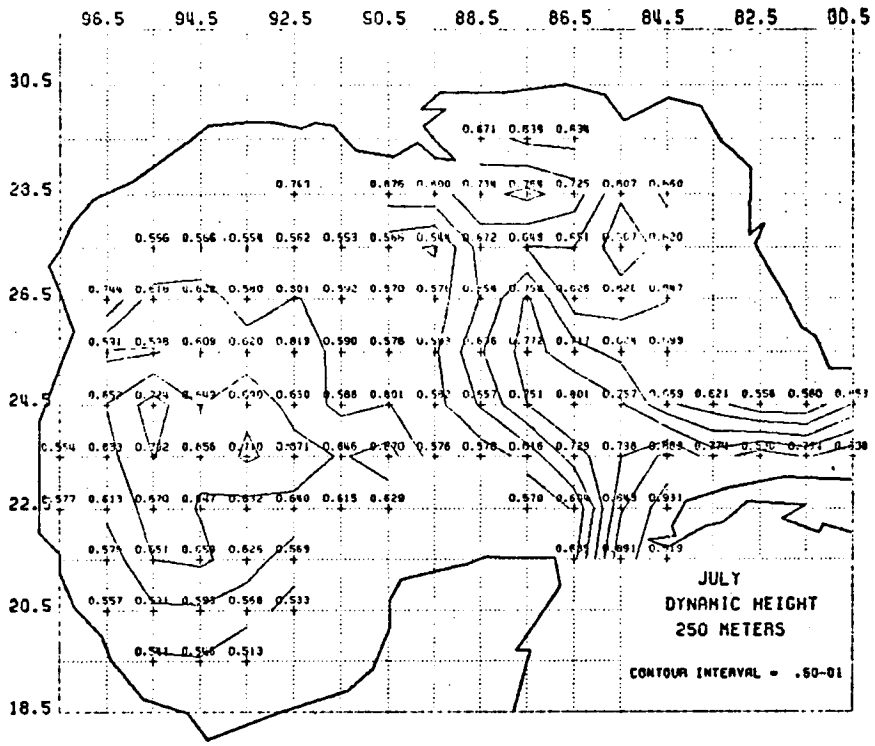
96.5
94.5
92.5
90.5
88.5
86.5
84.5
82.5
80.5
30.5
28.5
26.5
24.5
22.5
20.5
18.5
JULY
DYNAMIC HEIGHT
250 METERS
CONTOUR INTERVAL = .60-01

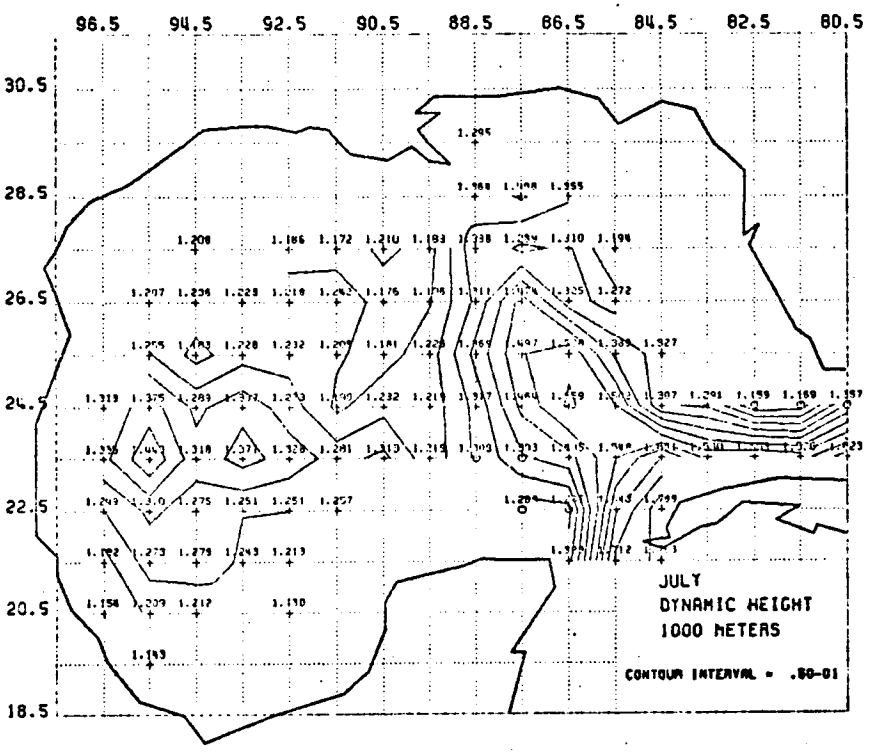
96.5
94.5
92.5
90.5
88.5
86.5
84.5
82.5
80.5
30.5
28.5
26.5
24.5
22.5
20.5
18.5
JULY
DYNAMIC HEIGHT
1000 METERS
CONTOUR INTERVAL = .60-01

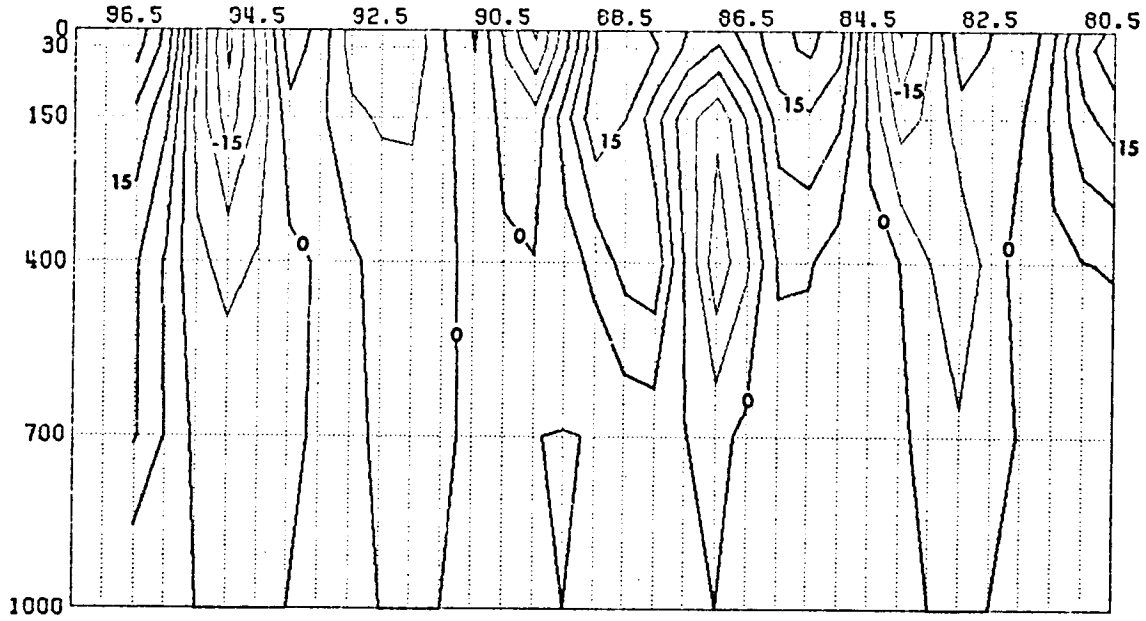

JULY
E-W CROSS SECTION FOR V COMPONENT OF GEOSTROPHIC VELOCITY AT LATITUDE 23.5. VELOCITIES ARE COMPUTED RELATIVE TO 1000 M LEVEL. HEAVY LINES DENOTE NORTH VELOCITY. THE CONTOUR INTERVAL IS 5.0 CM/S.

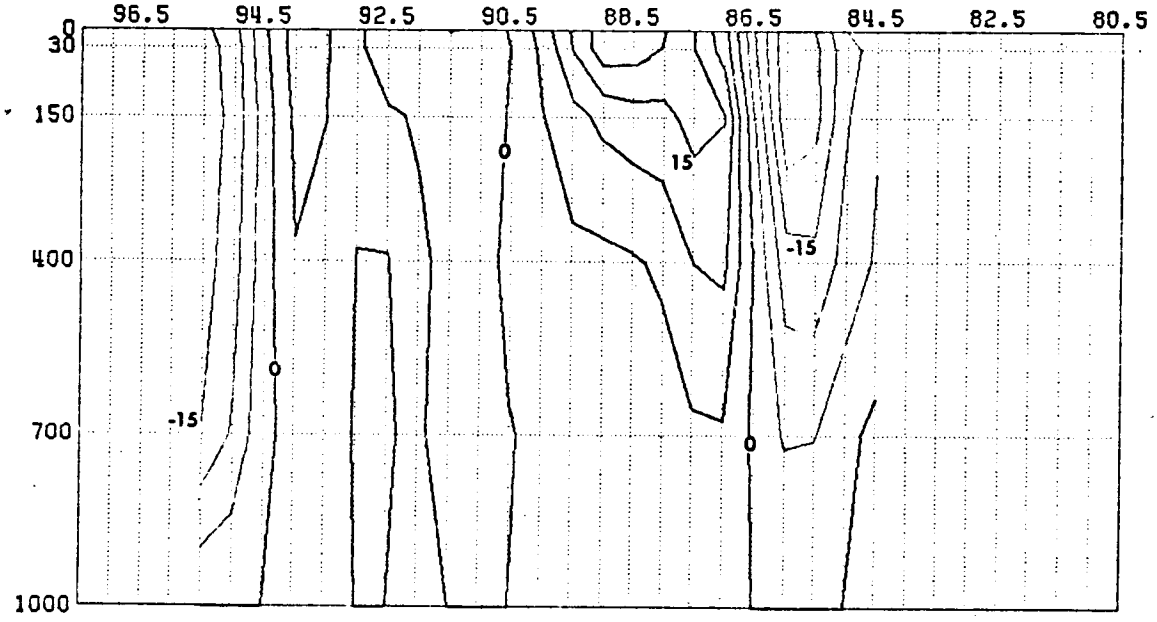

JULY
E-W CROSS SECTION FOR V COMPONENT OF GEOSTROPHIC VELOCITY AT LATITUDE 25.5. VELOCITIES ARE COMPUTED RELATIVE TO 1000 M LEVEL. HEAVY LINES DENOTE NORTH VELOCITY. THE CONTOUR INTERVAL IS 5.0 CM/S.

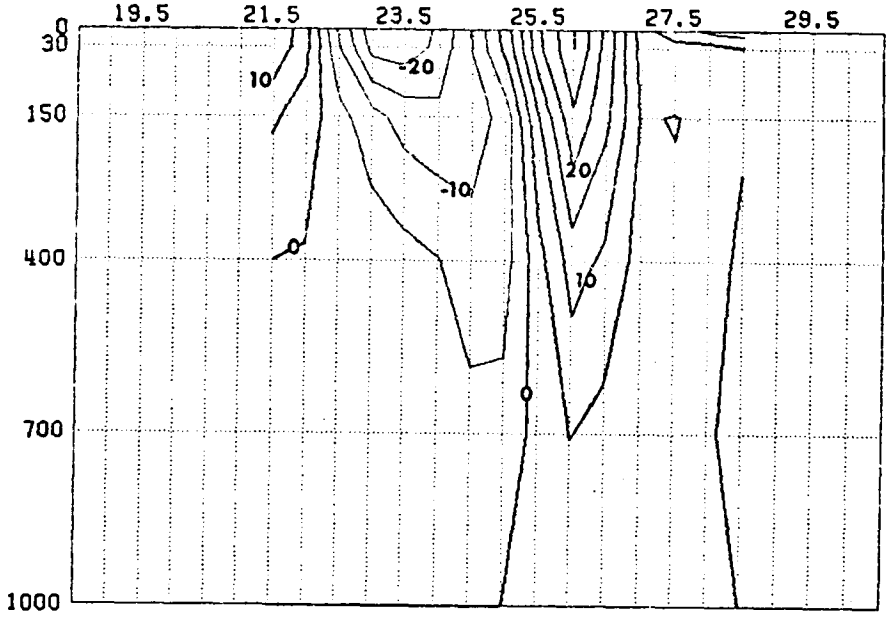

JULY

N-S CROSS SECTION FOR U COMPONENT OF GEOSTROPHIC VELOCITY AT LONGITUDE 86.5. VELOCITIES ARE COMPUTED RELATIVE TO 1000 M LEVEL. HEAVY LINES DENOTE EAST VELOCITY. THE CONTOUR INTERVAL IS 5.0 CM/S.

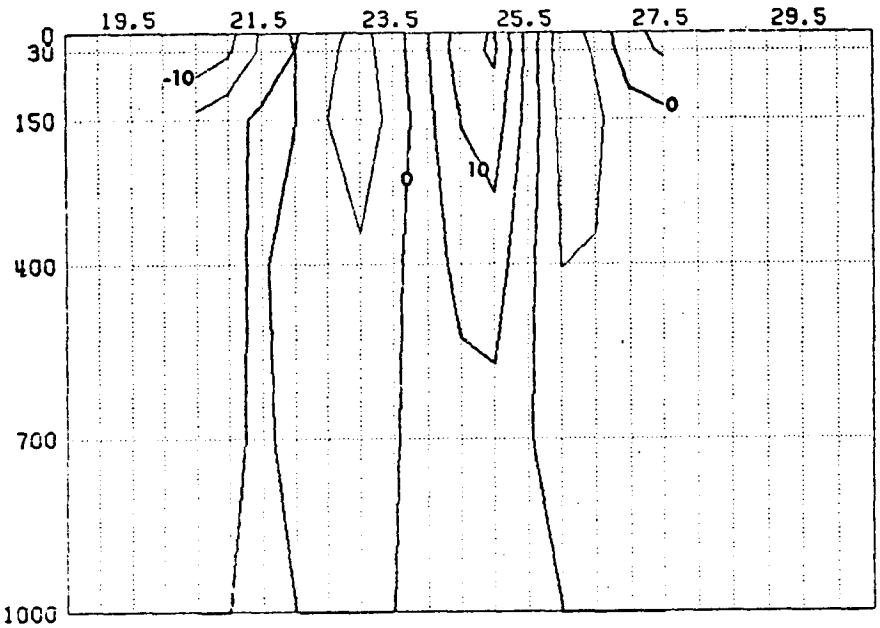

JULY

N-S CROSS SECTION FOR U COMPONENT OF GEOSTROPHIC VELOCITY AT LONGITUDE 84.5. VELOCITIES ARE COMPUTED RELATIVE TO 1000 M LEVEL. HEAVY LINES DENOTE EAST VELOCITY. THE CONTOUR INTERVAL IS 5.0 CM/S.

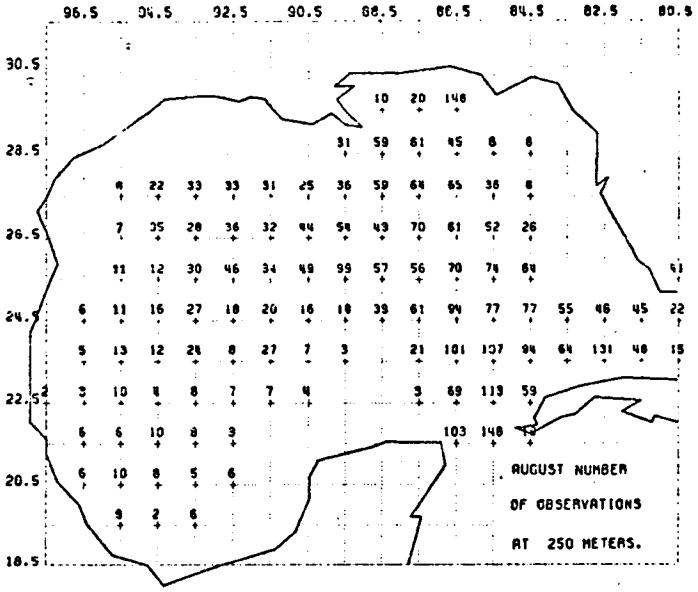

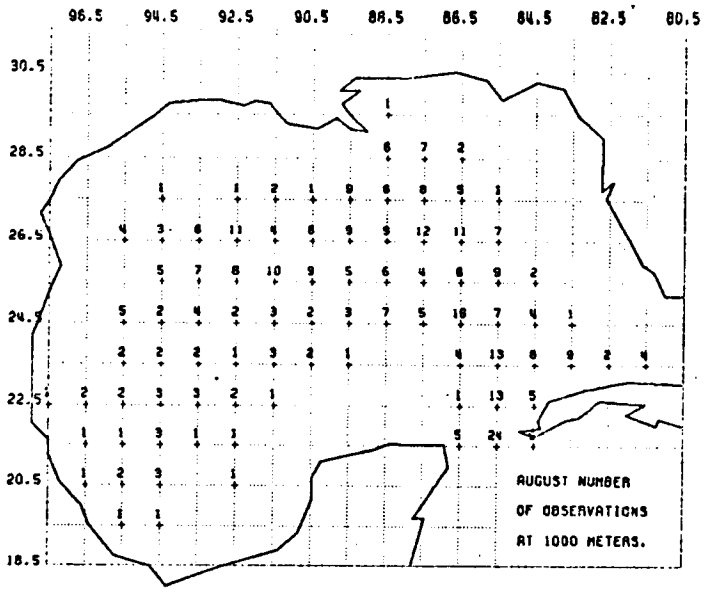

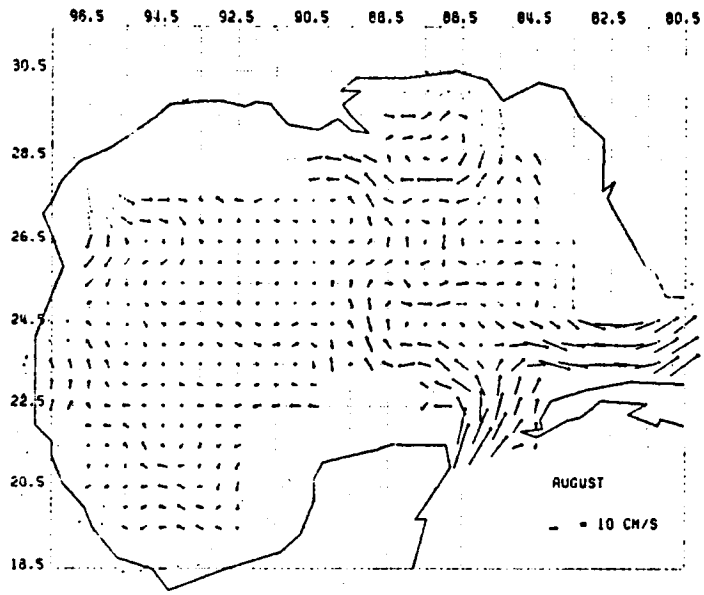

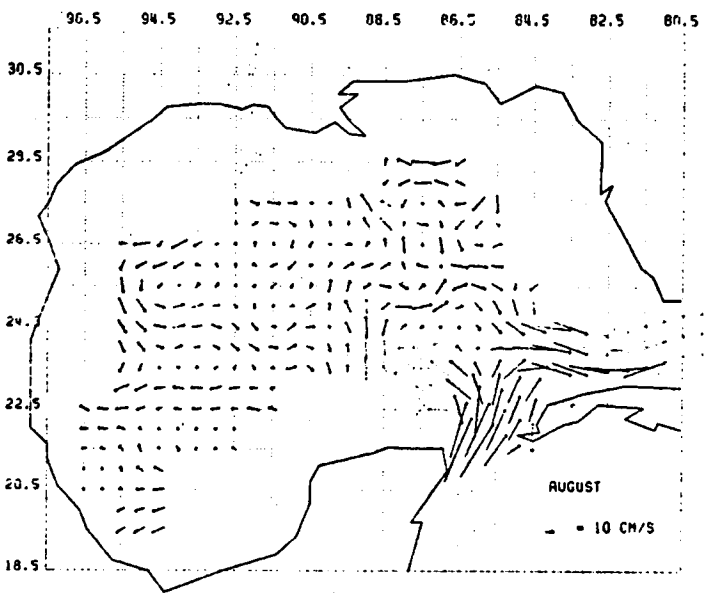

AUGUST
GEOSTROPHIC VELOCITIES AT A DEPTH OF .0 METERS.
VELOCITIES ARE COMPUTED RELATIVE TO THE 250.0 M LEVEL.

AUGUST
GEOSTROPHIC VELOCITIES AT A DEPTH OF .0 METERS.
VELOCITIES ARE COMPUTED RELATIVE TO THE1000.0 M LEVEL.

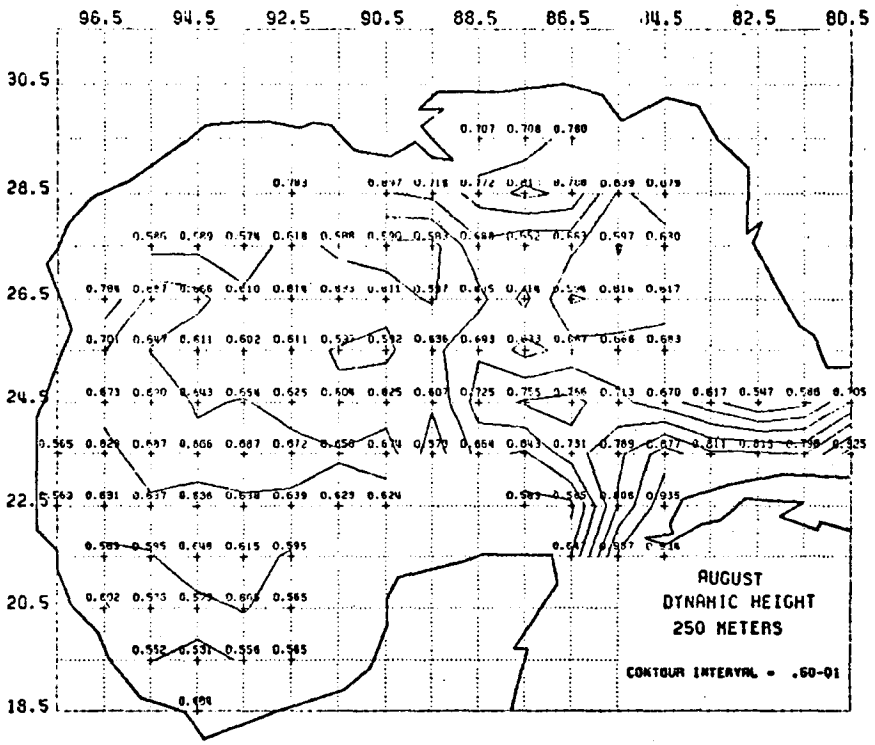
96.5
94.5
92.5
90.5
88.5
86.5
84.5
82.5
80.5
30.5
28.5
26.5
24.5
22.5
20.5
18.5
AUGUST
DYNAMIC HEIGHT
250 METERS
CONTOUR INTERVAL = .60-01

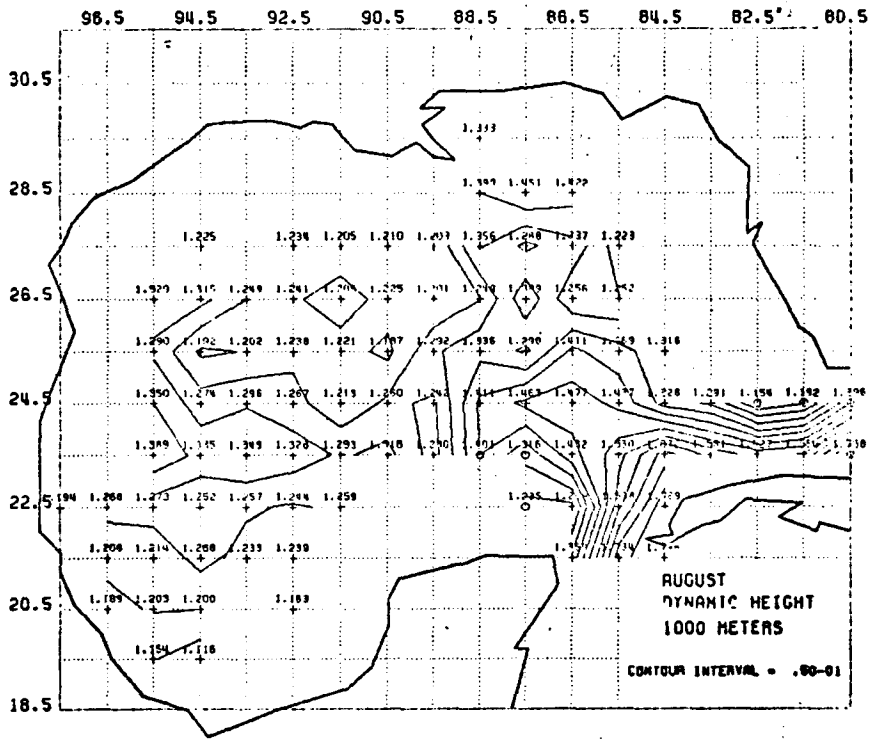
96.5
94.5
92.5
90.5
88.5
86.5
84.5
82.5
80.5
30.5
28.5
26.5
24.5
22.5
20.5
18.5
AUGUST
DYNAMIC HEIGHT
1000 METERS
CONTOUR INTERVAL = .60-01

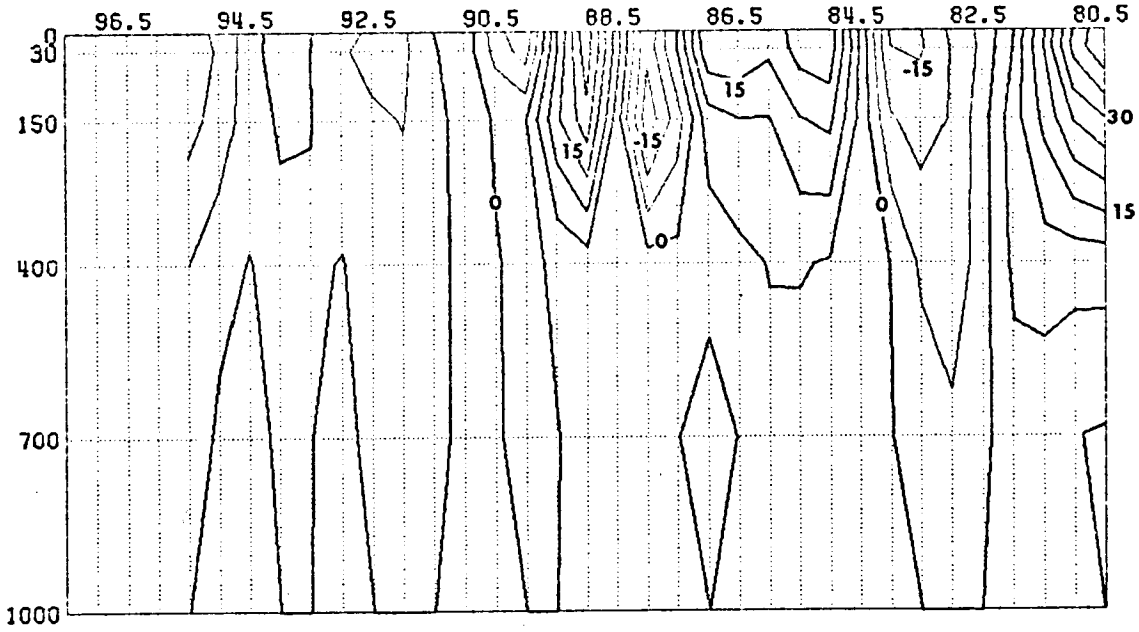

FIG. AUGUST
E-W CROSS SECTION FOR V COMPONENT OF GEOSTROPHIC VELOCITY AT LATITUDE 23.5. VELOCITIES ARE COMPUTED RELATIVE TO 1000 M LEVEL. HEAVY LINES DENOTE NORTH VELOCITY. THE CONTOUR INTERVAL IS 5.0 CM/S.

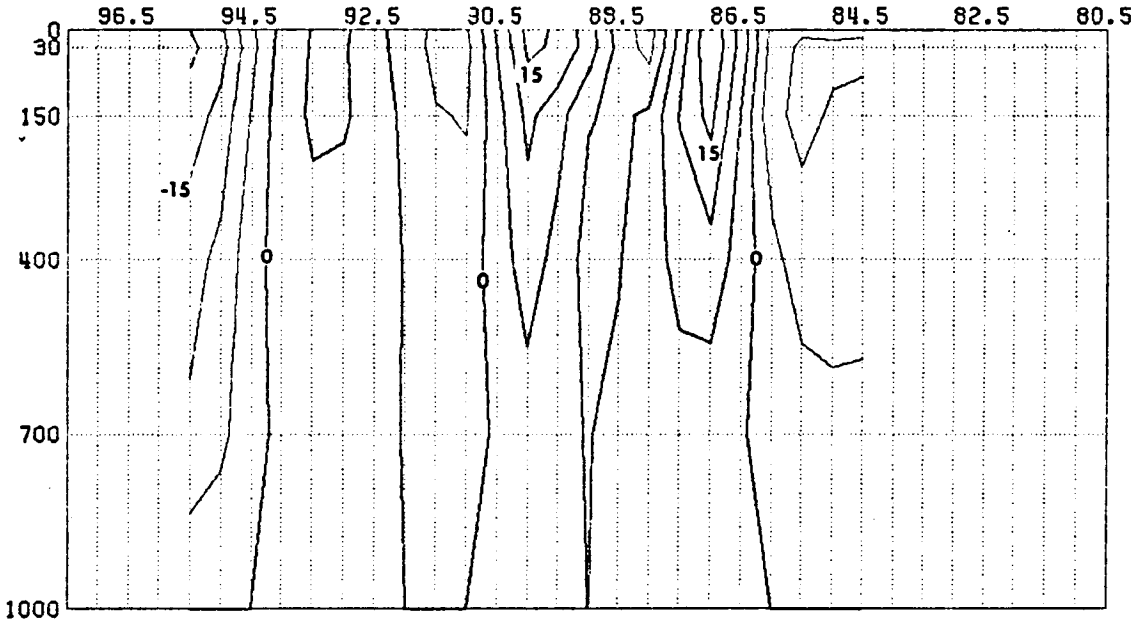

AUGUST
E-W CROSS SECTION FOR V COMPONENT OF GEOSTROPHIC VELOCITY AT LATITUDE 25.5. VELOCITIES ARE COMPUTED RELATIVE TO 1000 M LEVEL. HEAVY LINES DENOTE NORTH VELOCITY. THE CONTOUR INTERVAL IS 5.0 CM/S.

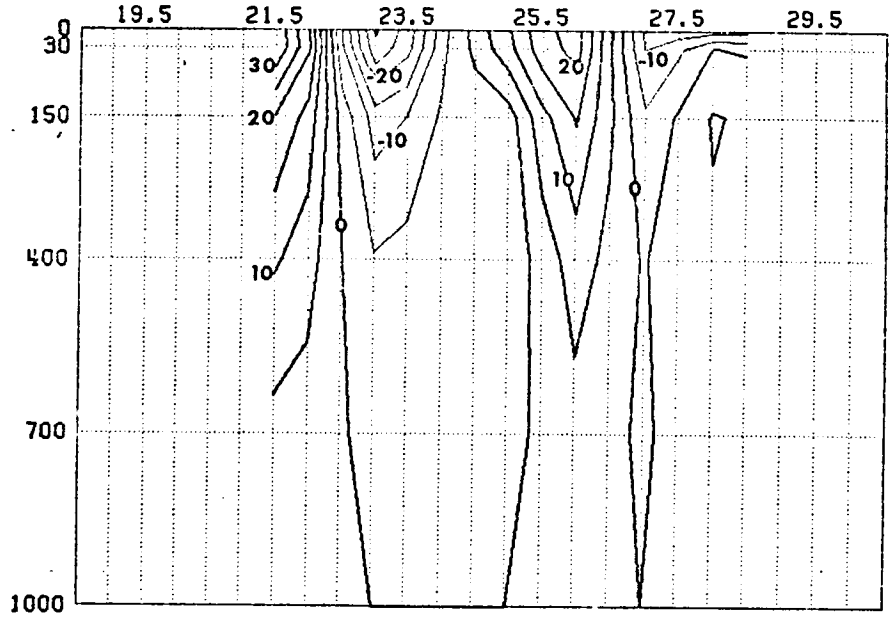

FIG. AUGUST
N-S CROSS SECTION FOR U COMPONENT OF GEOSTROPHIC VELOCITY AT LONGITUDE 86.5. VELOCITIES ARE COMPUTED RELATIVE TO 1000 M LEVEL. HEAVY LINES DENOTE EAST VELOCITY. THE CONTOUR INTERVAL IS 5.0 CM/S.

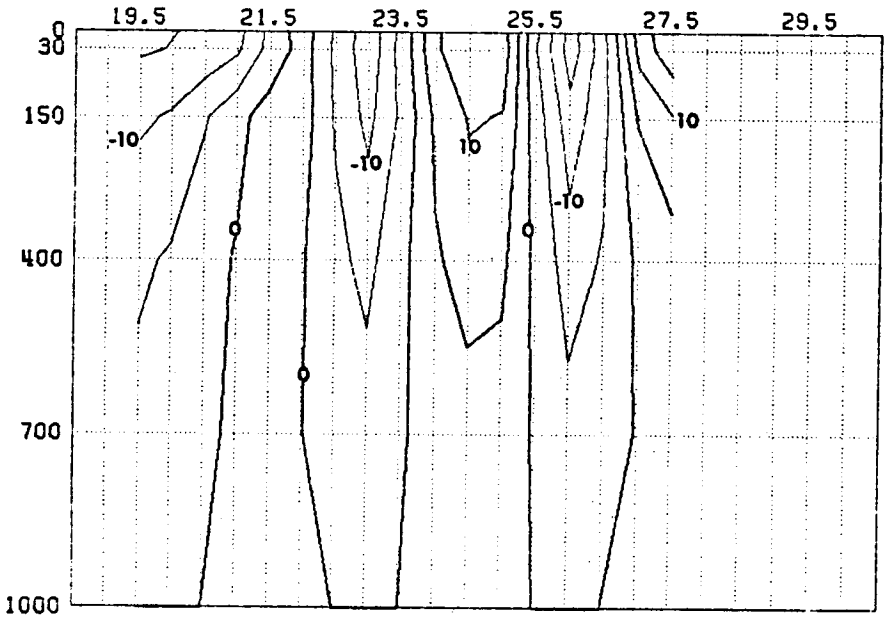

AUGUST
N-S CROSS SECTION FOR U COMPONENT OF GEOSTROPHIC VELOCITY AT LONGITUDE 84.5. VELOCITIES ARE COMPUTED RELATIVE TO 1000 M LEVEL. HEAVY LINES DENOTE EAST VELOCITY. THE CONTOUR INTERVAL IS 5.0 CM/S.

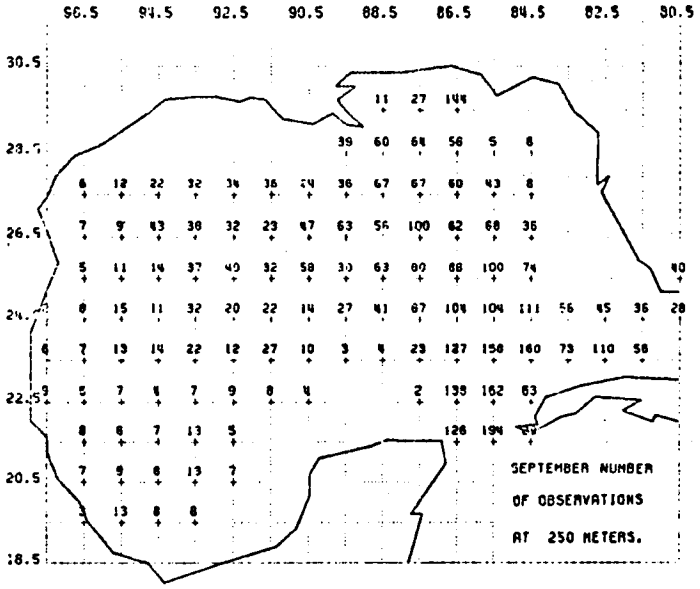

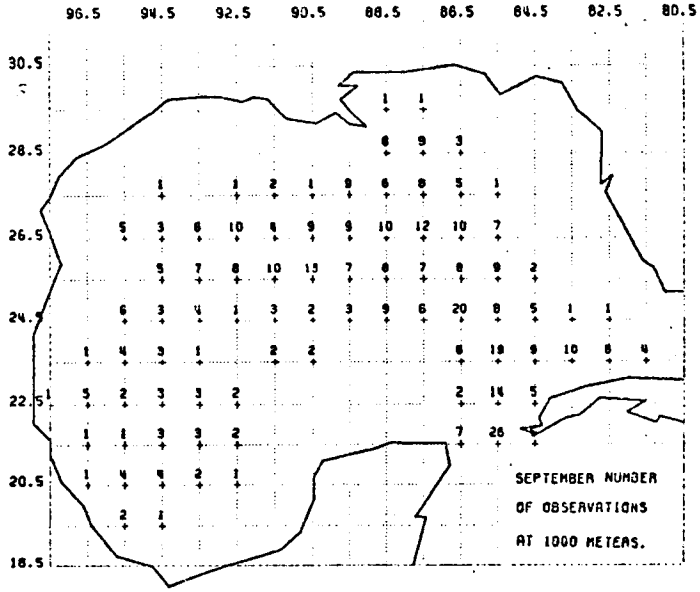

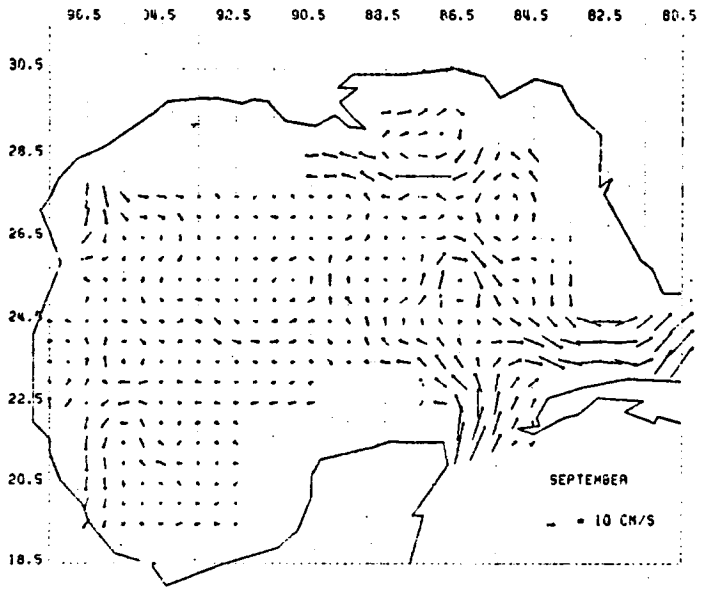

SEPTEMBER
GEOSTROPHIC VELOCITIES AT A DEPTH OF .0 METERS.
VELOCITIES ARE COMPUTED RELATIVE TO THE 250.0 M LEVEL.

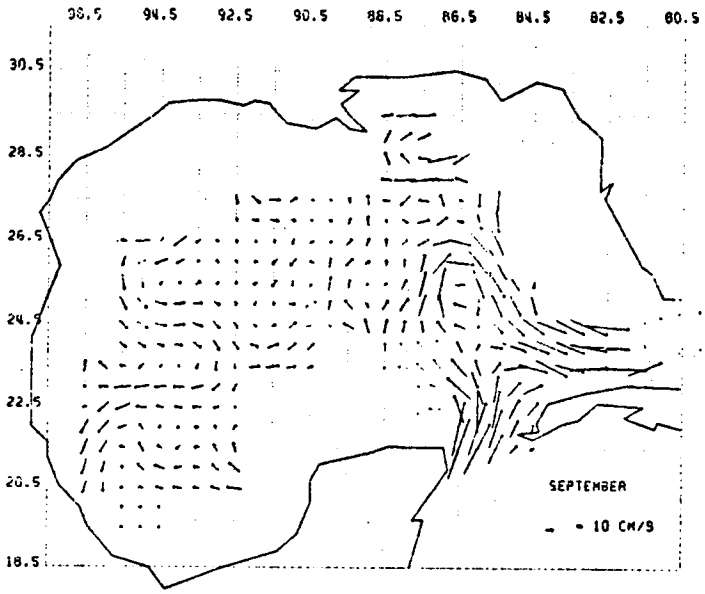

SEPTEMBER
GEOSTROPHIC VELOCITIES AT A DEPTH OF .0 METERS.
VELOCITIES ARE COMPUTED RELATIVE TO THE1000.0 M LEVEL.

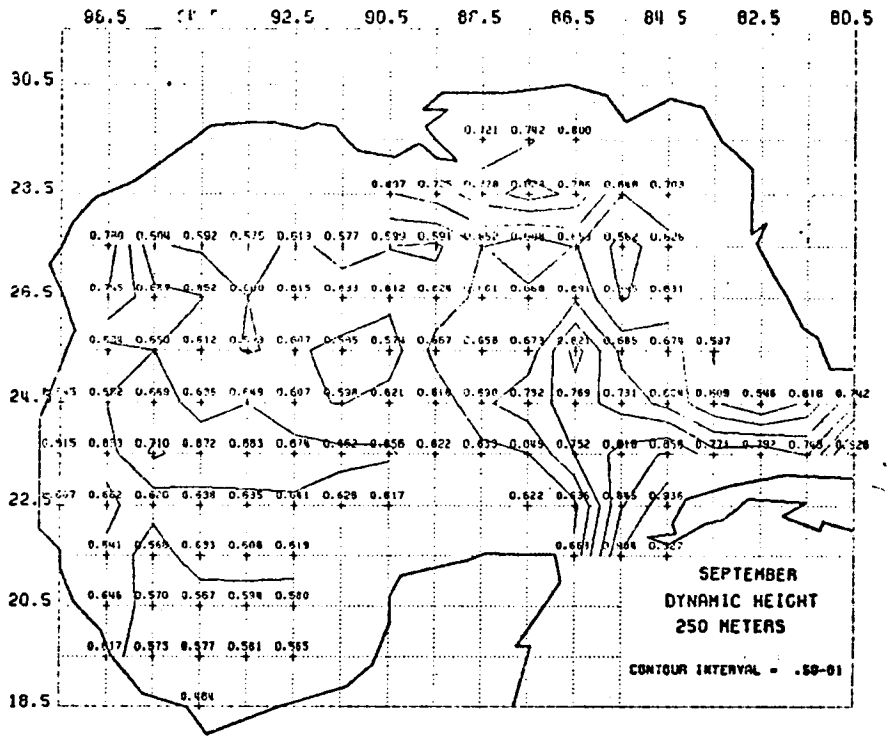
96.5
92.5
90.5
88.5
86.5
84.5
82.5
80.5
30.5
28.5
26.5
24.5
22.5
20.5
18.5
SEPTEMBER
DYNAMIC HEIGHT
250 METERS
CONTOUR INTERVAL = .50-01

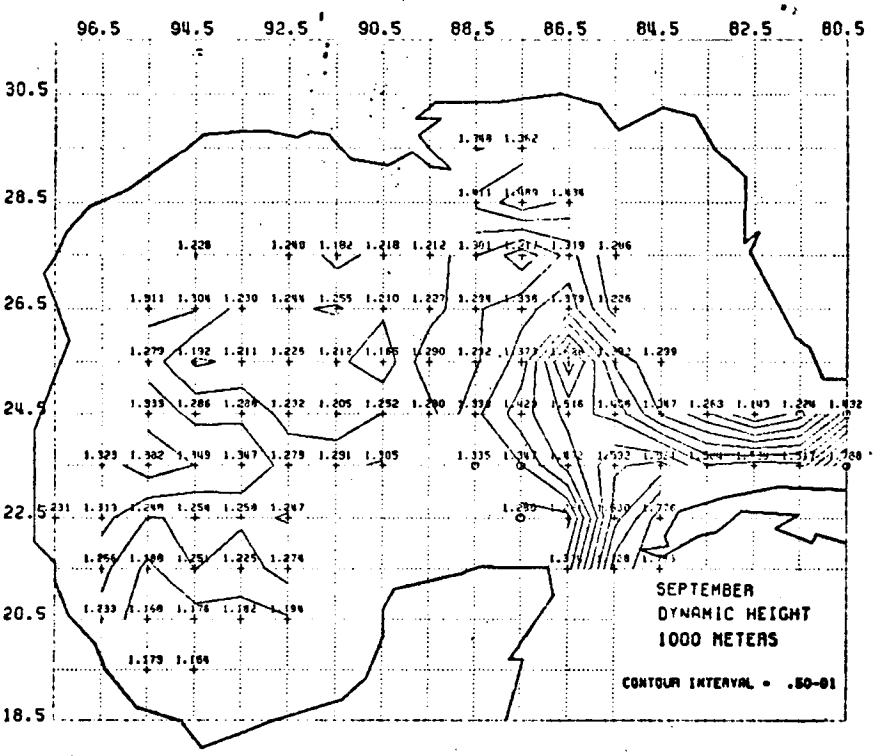
96.5
94.5
92.5
90.5
88.5
86.5
84.5
82.5
80.5
30.5
28.5
26.5
24.5
22.5
20.5
18.5
SEPTEMBER
DYNAMIC HEIGHT
1000 METERS
CONTOUR INTERVAL = .50-01

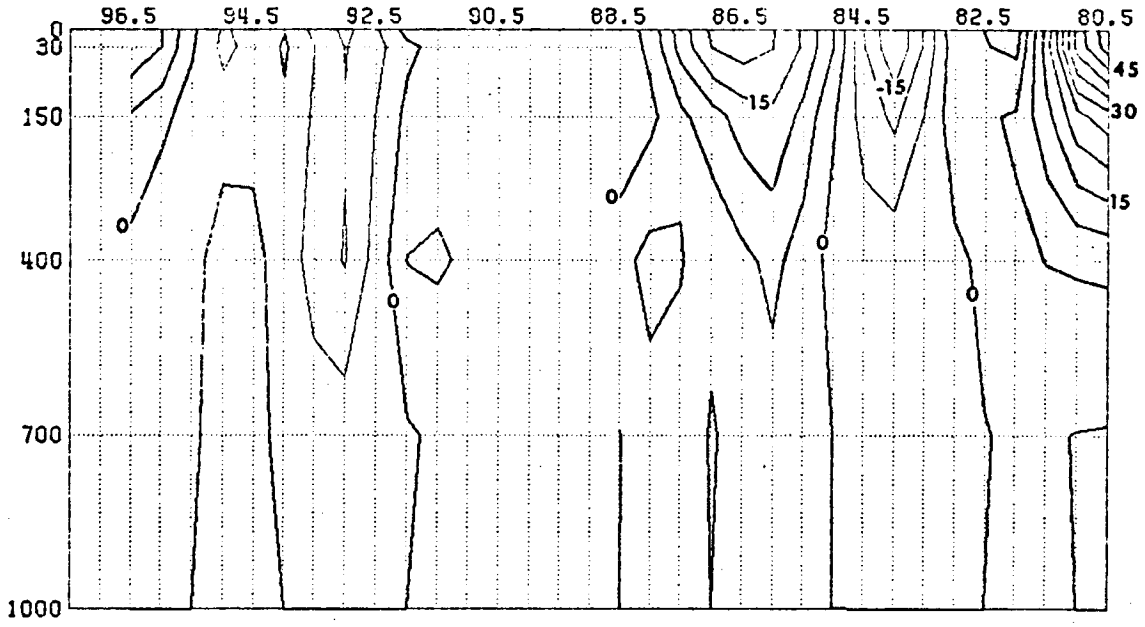

SEPTEMBER

E-W CROSS SECTION FOR V COMPONENT OF GEOSTROPHIC VELOCITY AT LATITUDE 23.5. VELOCITIES ARE COMPUTED RELATIVE TO 1000 M LEVEL. HEAVY LINES DENOTE NORTH VELOCITY. THE CONTOUR INTERVAL IS 5.0 CM/S.

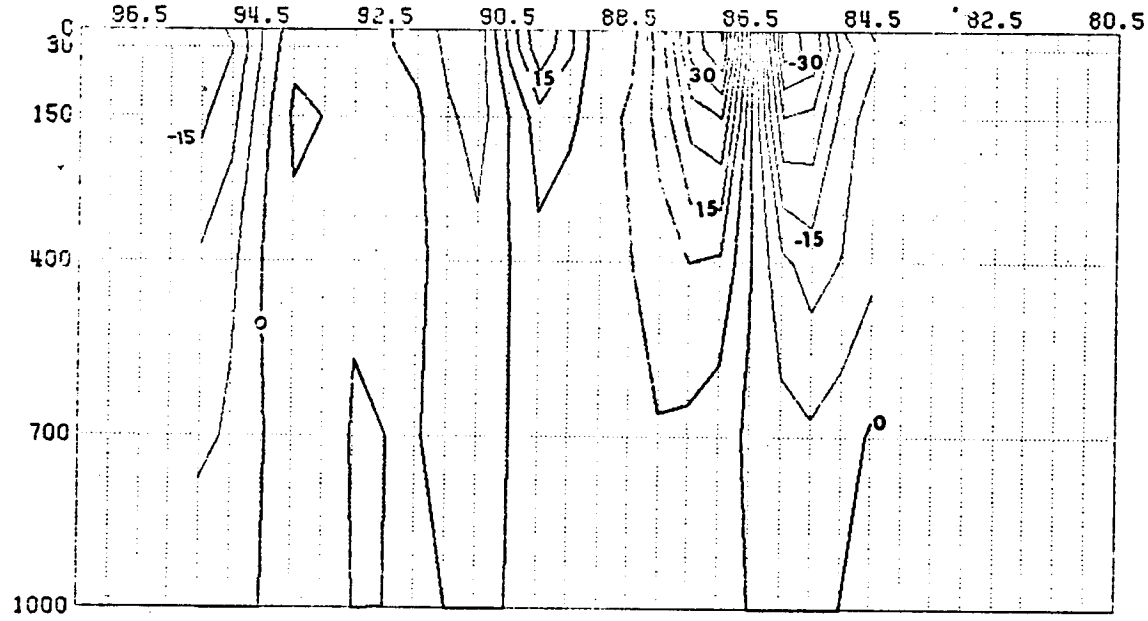

SEPTEMBER

E-W CROSS SECTION FOR V COMPONENT OF GEOSTROPHIC VELOCITY AT LATITUDE 25.5. VELOCITIES ARE COMPUTED RELATIVE TO 1000 M LEVEL. HEAVY LINES DENOTE NORTH VELOCITY. THE CONTOUR INTERVAL IS 5.0 CM/S.

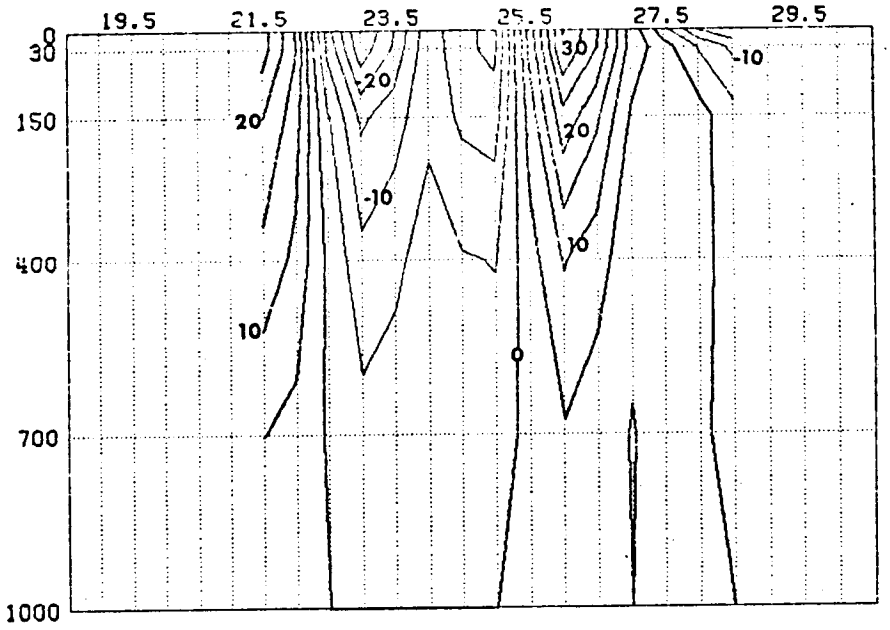

SEPTEMBER

N-S CROSS SECTION FOR U COMPONENT OF GEOSTROPHIC VELOCITY AT LONGITUDE 86.5. VELOCITIES ARE COMPUTED RELATIVE TO 1000 M LEVEL. HEAVY LINES DENOTE EAST VELOCITY. THE CONTOUR INTERVAL IS 5.0 CM/S.

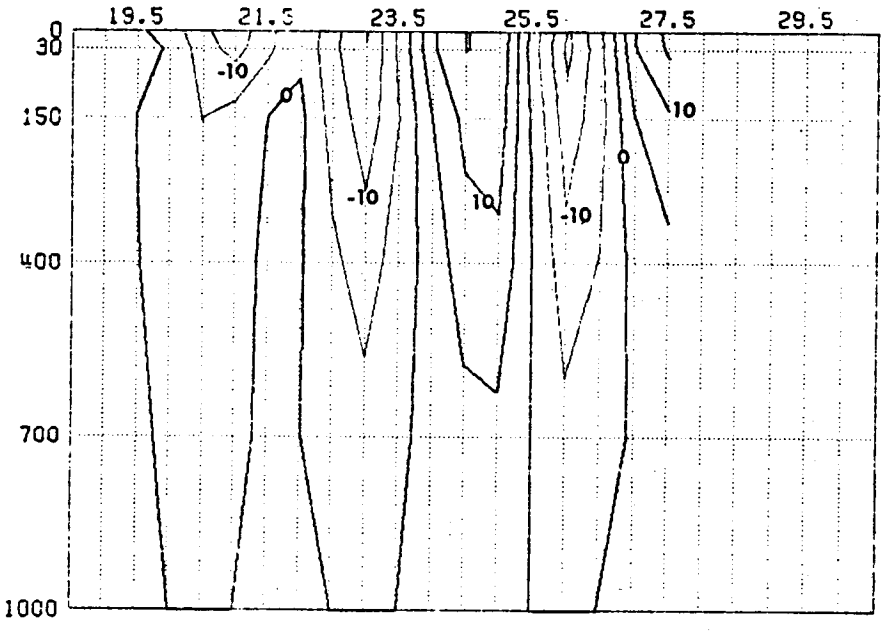

SEPTEMBER

N-S CROSS SECTION FOR U COMPONENT OF GEOSTROPHIC VELOCITY AT LONGITUDE 94.5. VELOCITIES ARE COMPUTED RELATIVE TO 1000 M LEVEL. HEAVY LINES DENOTE EAST VELOCITY. THE CONTOUR INTERVAL IS 5.0 CM/S.

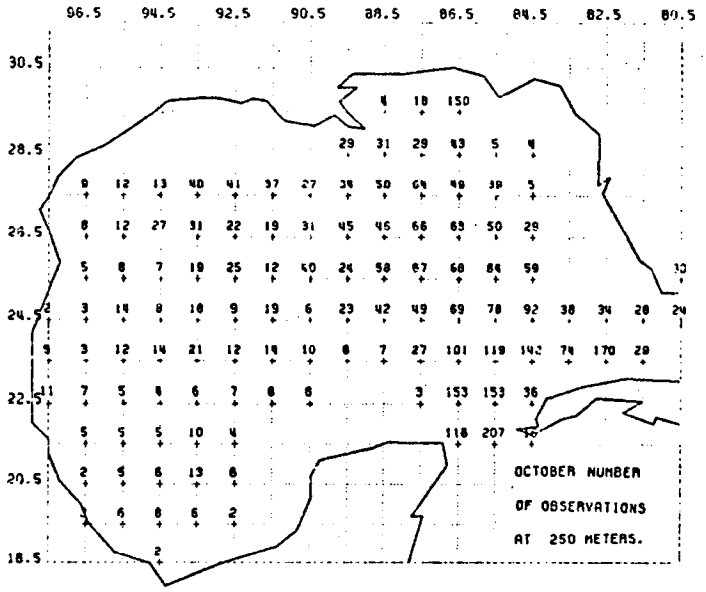

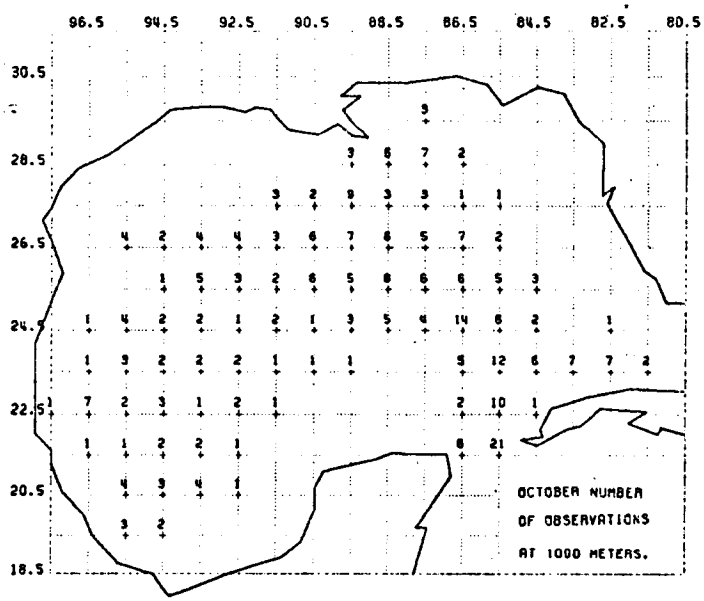

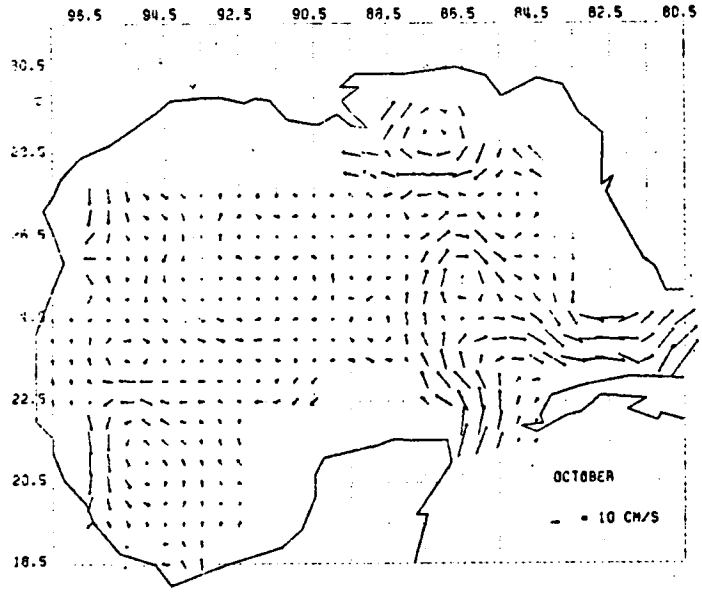

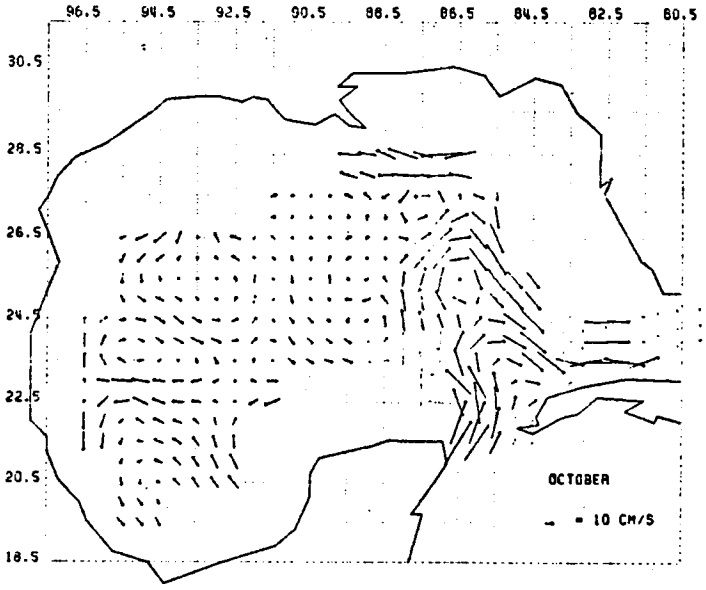

OCTOBER
GEOSTROPHIC VELOCITIES AT A DEPTH OF .0 METERS.
VELOCITIES ARE COMPUTED RELATIVE TO THE 250.0 M LEVEL.

OCTOBER
GEOSTROPHIC VELOCITIES AT A DEPTH OF .0 METERS.
VELOCITIES ARE COMPUTED RELATIVE TO THE1000.0 M LEVEL.

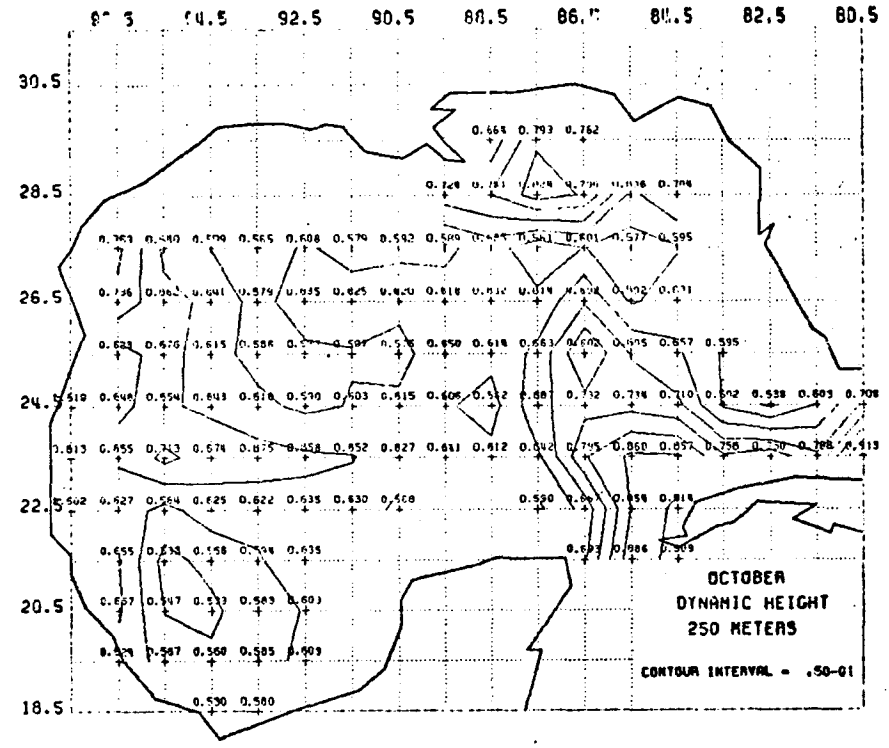
98.5
94.5
92.5
90.5
88.5
86.5
84.5
82.5
80.5
30.5
28.5
26.5
24.5
22.5
20.5
18.5
OCTOBER
DYNAMIC HEIGHT
250 METERS
CONTOUR INTERVAL = .50-01

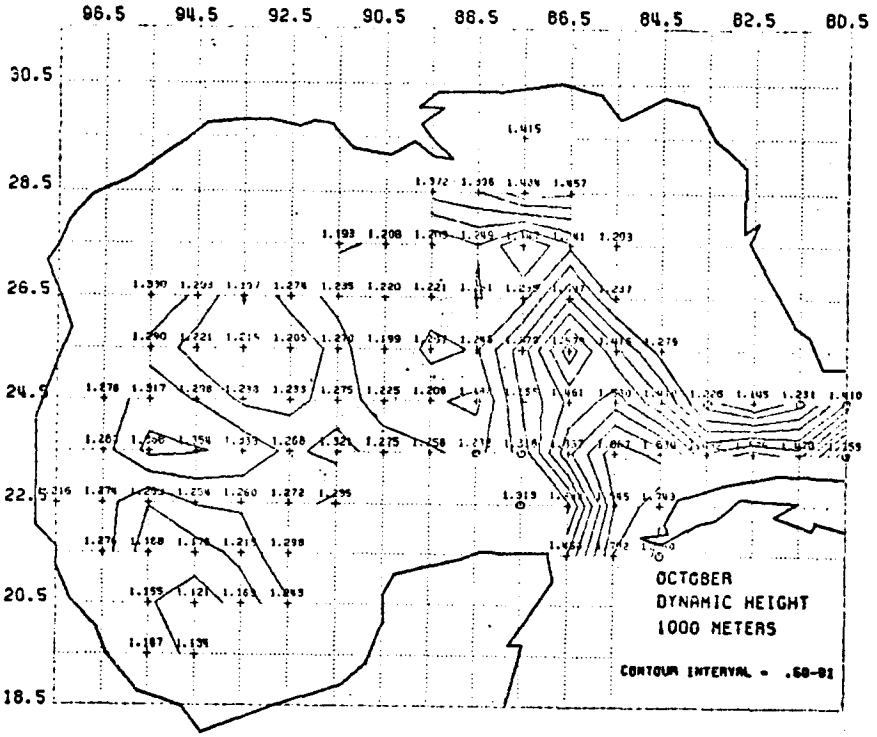
96.5
94.5
92.5
90.5
88.5
86.5
84.5
82.5
80.5
30.5
28.5
26.5
24.5
22.5
20.5
18.5
OCTOBER
DYNAMIC HEIGHT
1000 METERS
CONTOUR INTERVAL = .50-01

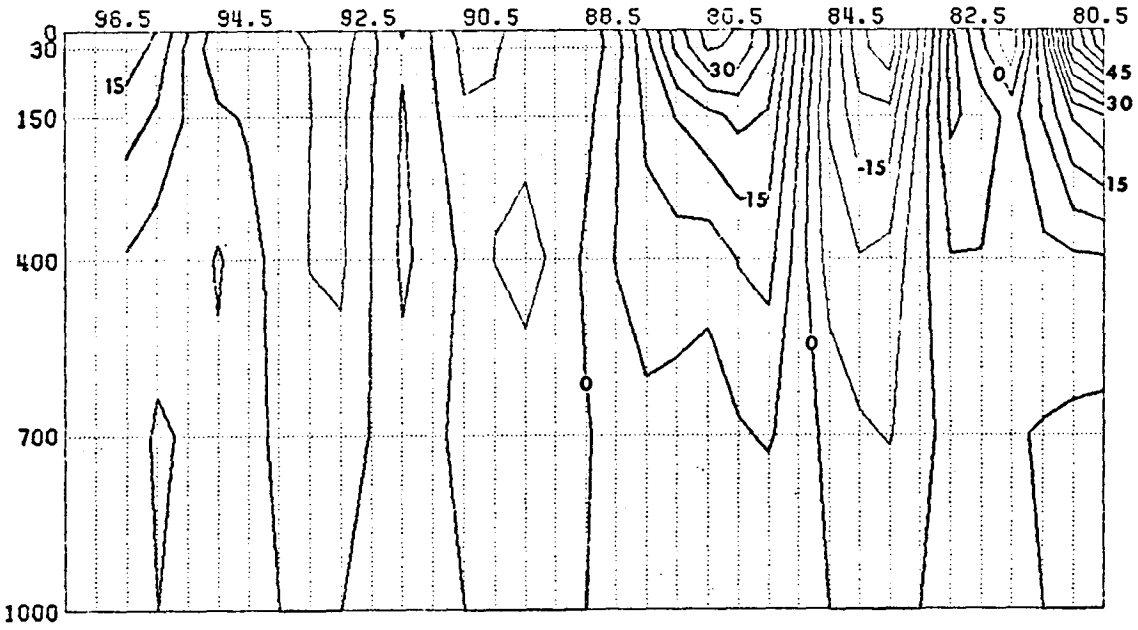

OCTOBER

E-W CROSS SECTION FOR V COMPONENT OF GEOSTROPHIC VELOCITY AT LATITUDE 23.5. VELOCITIES ARE COMPUTED RELATIVE TO 1000 M LEVEL. HEAVY LINES DENOTE NORTH VELOCITY. THE CONTOUR INTERVAL IS 5.0 CM/S.

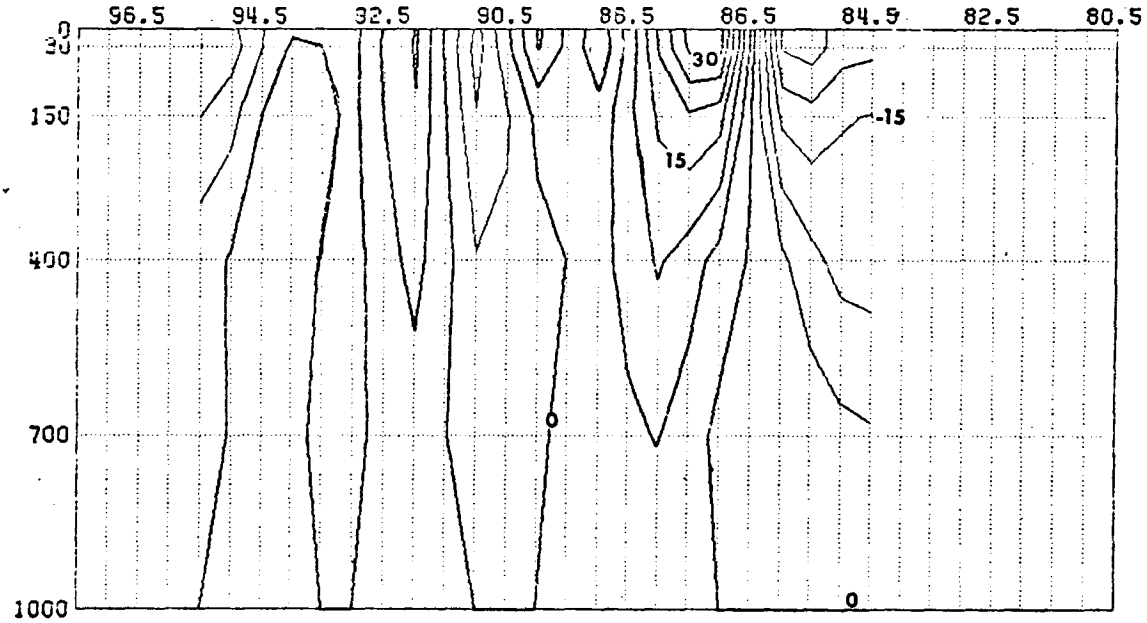

OCTOBER

E-W CROSS SECTION FOR V COMPONENT OF GEOSTROPHIC VELOCITY AT LATITUDE 25.5. VELOCITIES ARE COMPUTED RELATIVE TO 1000 M LEVEL. HEAVY LINES DENOTE NORTH VELOCITY. THE CONTOUR INTERVAL IS 5.0 CM/S.

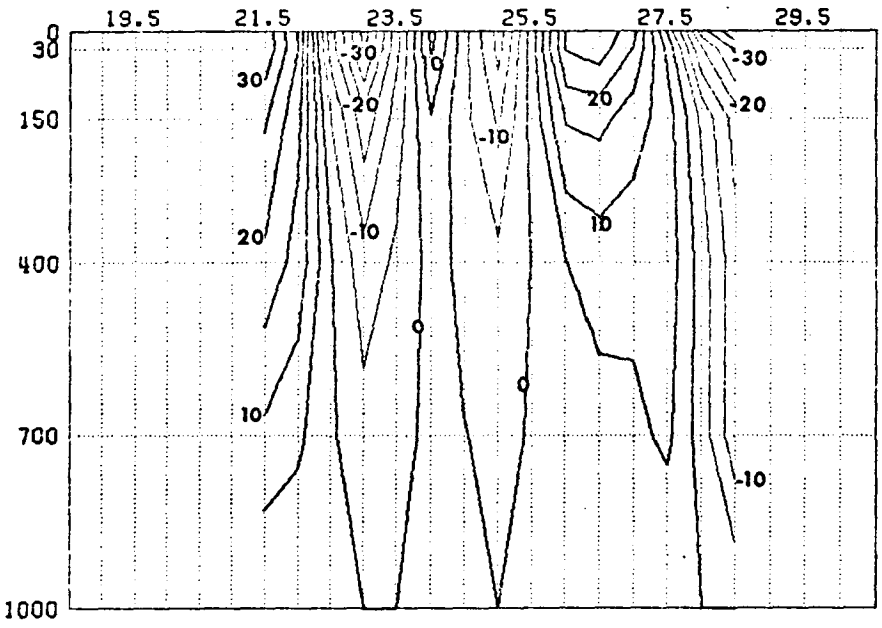

OCTOBER

N-S CROSS SECTION FOR U COMPONENT OF GEOSTROPHIC VELOCITY AT LONGITUDE 86.5. VELOCITIES ARE COMPUTED RELATIVE TO 1000 M LEVEL. HEAVY LINES DENOTE EAST VELOCITY. THE CONTOUR INTERVAL IS 5.0 CM/S.

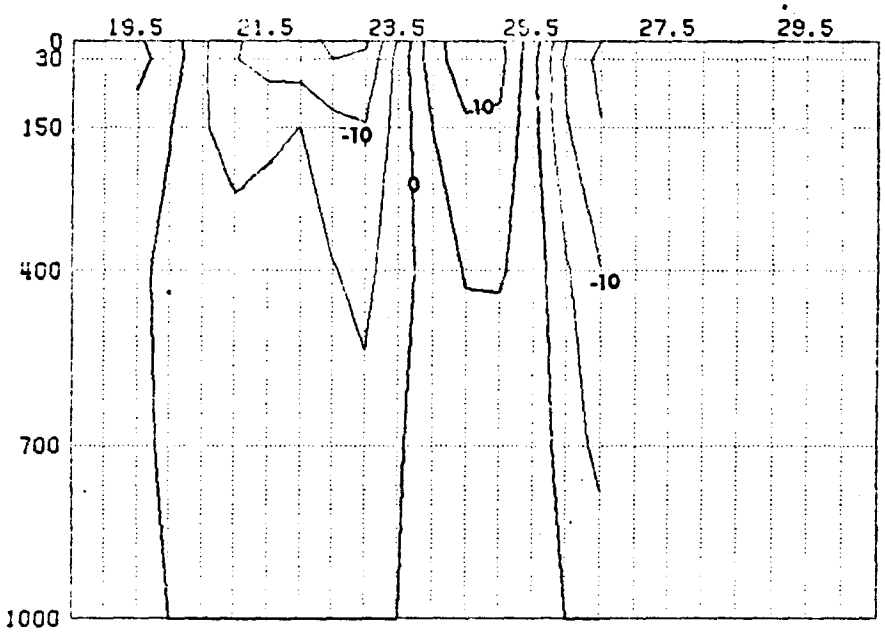

OCTOBER

N-S CROSS SECTION FOR U COMPONENT OF GEOSTROPHIC VELOCITY AT LONGITUDE 94.5. VELOCITIES ARE COMPUTED RELATIVE TO 1000 M LEVEL. HEAVY LINES DENOTE EAST VELOCITY. THE CONTOUR INTERVAL IS 5.0 CM/S.

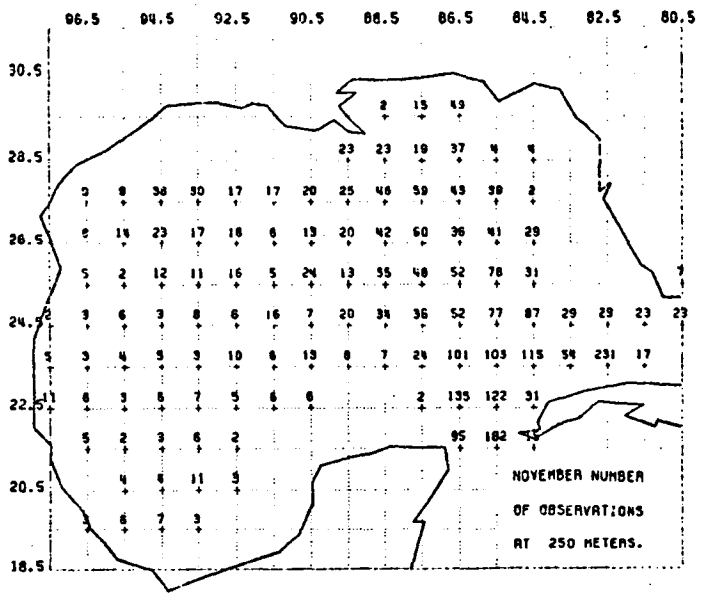

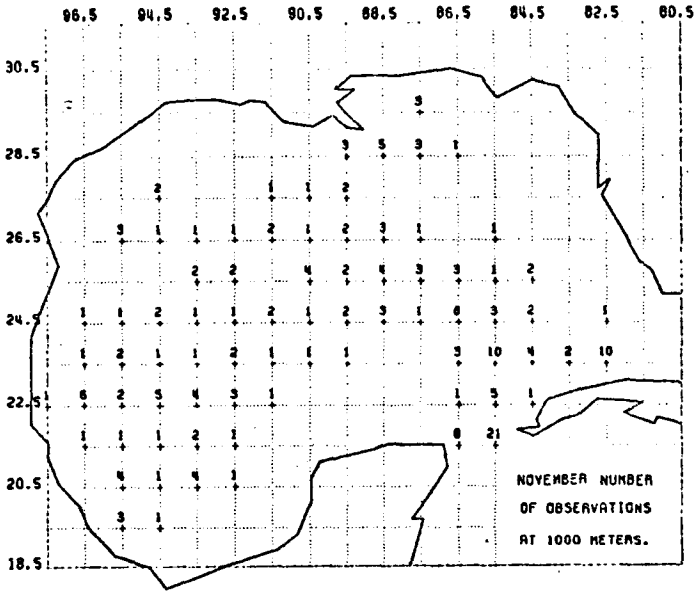

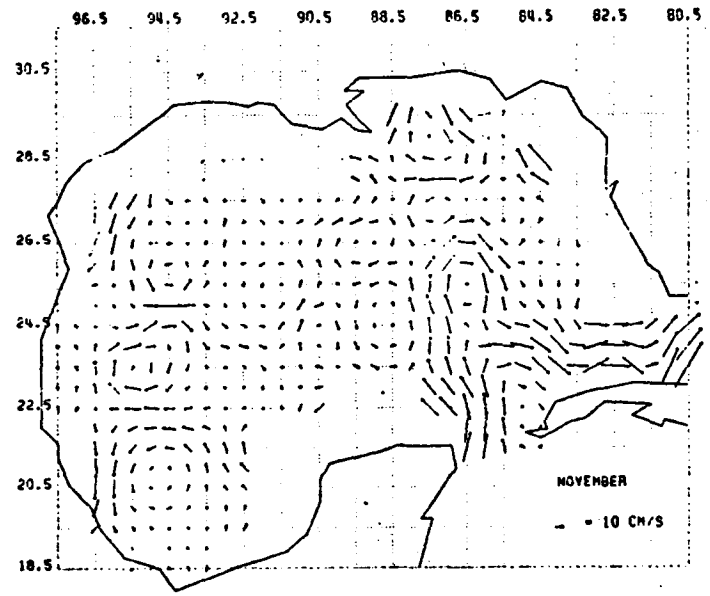

NOVEMBER
GEOSTROPHIC VELOCITIES AT A DEPTH OF .0 METERS.
VELOCITIES ARE COMPUTED RELATIVE TO THE 250.0 M LEVEL.

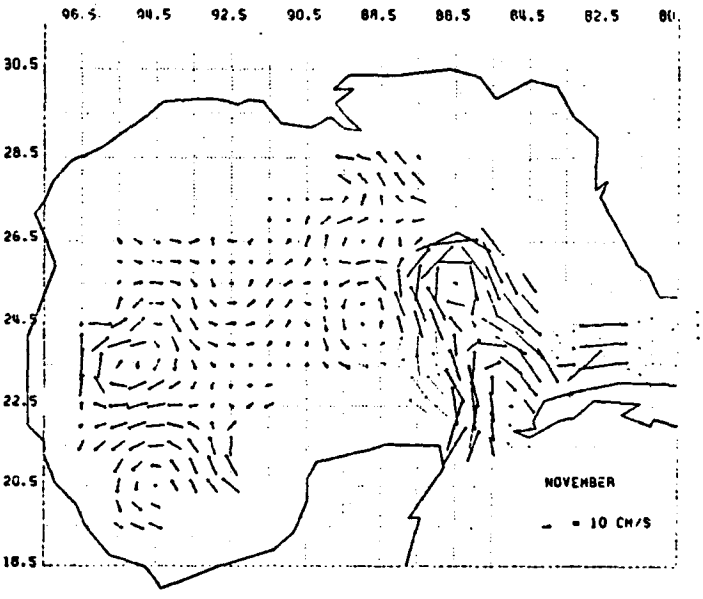

NOVEMBER
GEOSTROPHIC VELOCITIES AT A DEPTH OF .0 METERS.
VELOCITIES ARE COMPUTED RELATIVE TO THE1000.0 M LEVEL.

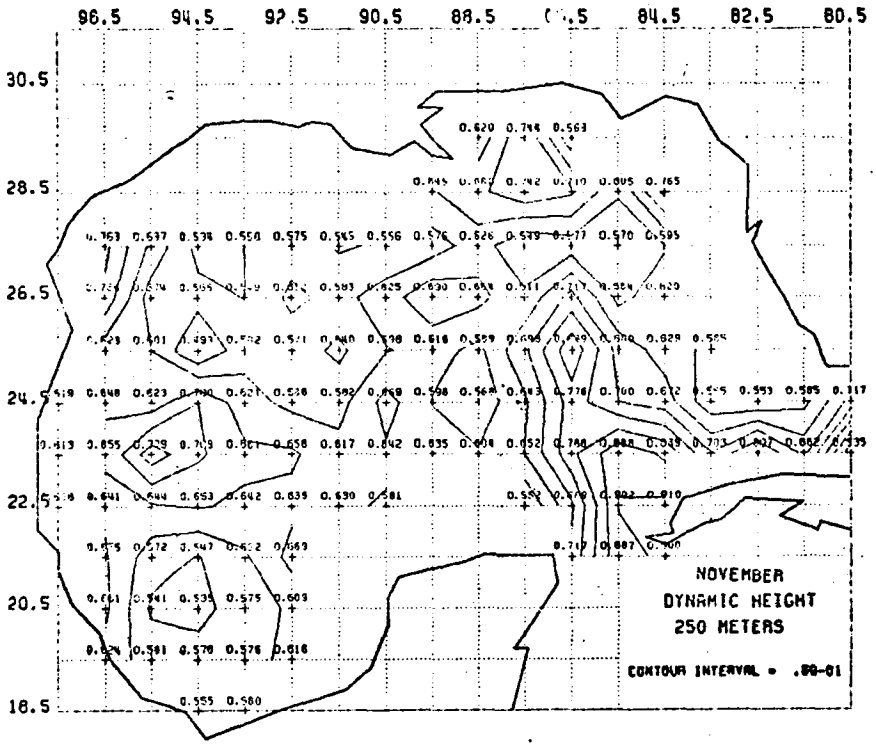
96.5
94.5
92.5
90.5
88.5
84.5
82.5
80.5
30.5
28.5
26.5
24.5
22.5
20.5
18.5
NOVEMBER
DYNAMIC HEIGHT
250 METERS
CONTOUR INTERVAL = .00-01

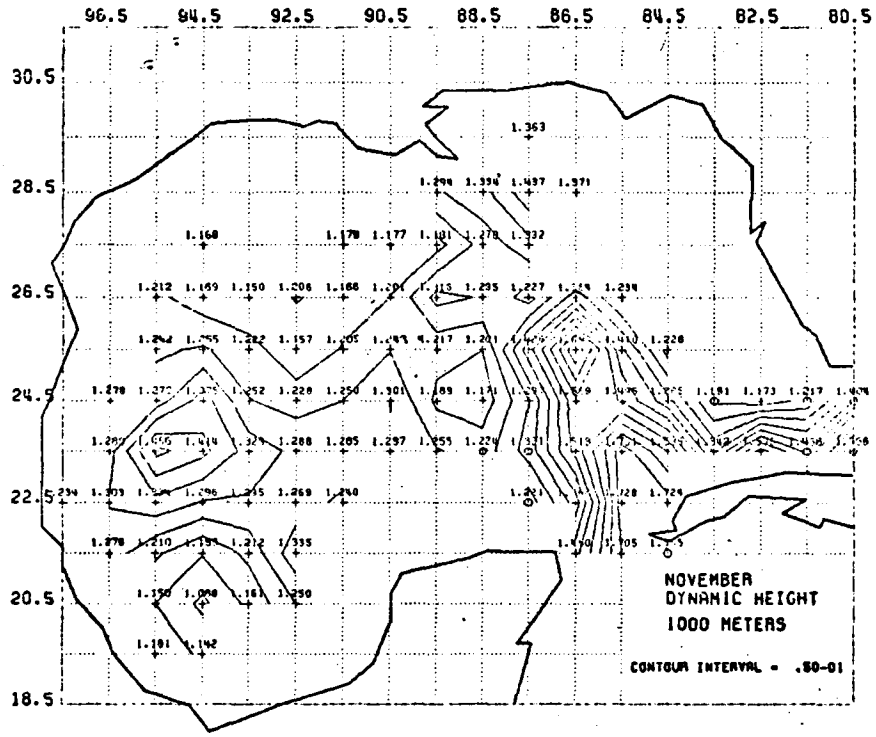
96.5
94.5
92.5
90.5
88.5
86.5
84.5
82.5
80.5
30.5
28.5
26.5
24.5
22.5
20.5
18.5
NOVEMBER
DYNAMIC HEIGHT
1000 METERS
CONTOUR INTERVAL = .00-01

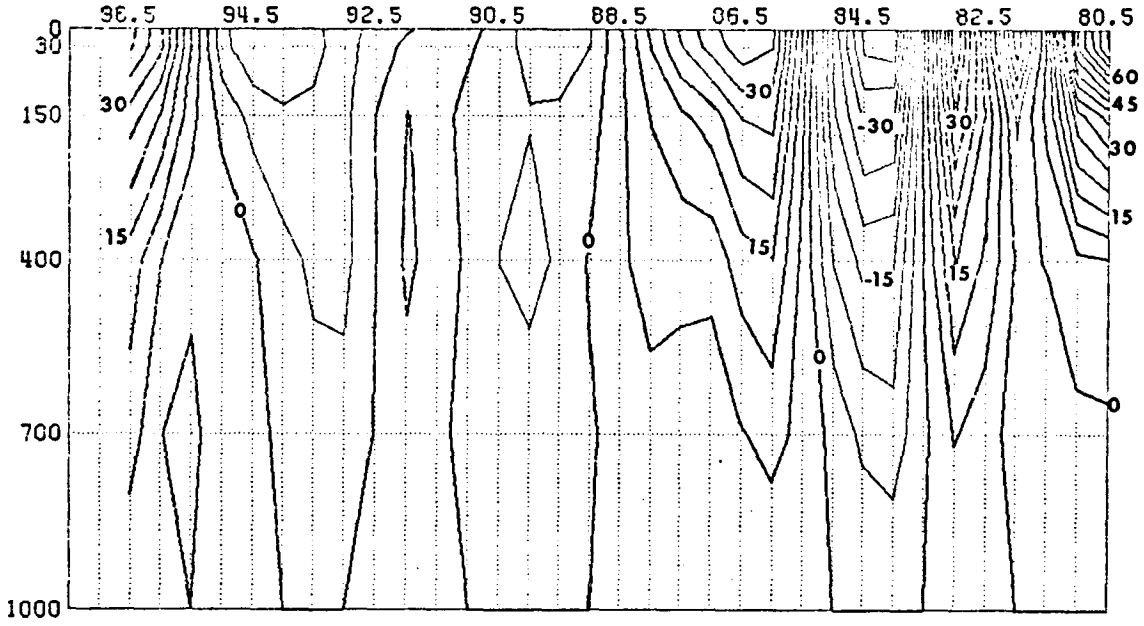

NOVEMBER

E-W CROSS SECTION FOR V COMPONENT OF GEOSTROPHIC VELOCITY AT LATITUDE 23.5. VELOCITIES ARE COMPUTED RELATIVE TO 1000 M LEVEL. HEAVY LINES DENOTE NORTH VELOCITY. THE CONTOUR INTERVAL IS 5.0 CM/S.

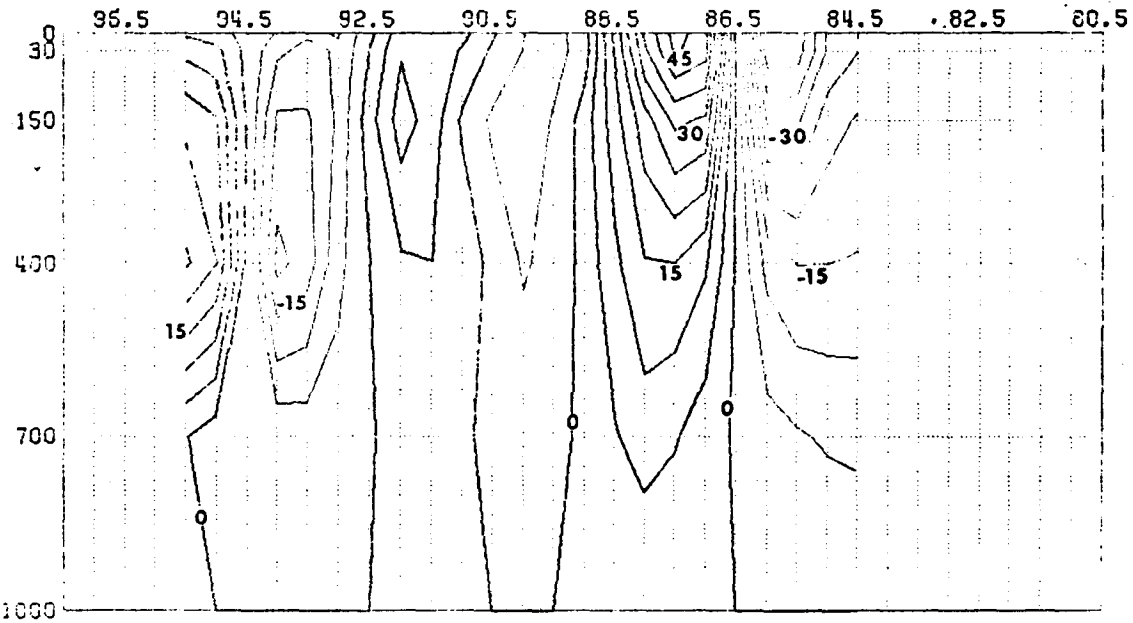

NOVEMBER

E-W CROSS SECTION FOR V COMPONENT OF GEOSTROPHIC VELOCITY AT LATITUDE 25.5. VELOCITIES ARE COMPUTED RELATIVE TO 1000 M LEVEL. HEAVY LINES DENOTE NORTH VELOCITY. THE CONTOUR INTERVAL IS 5.0 CM/S.

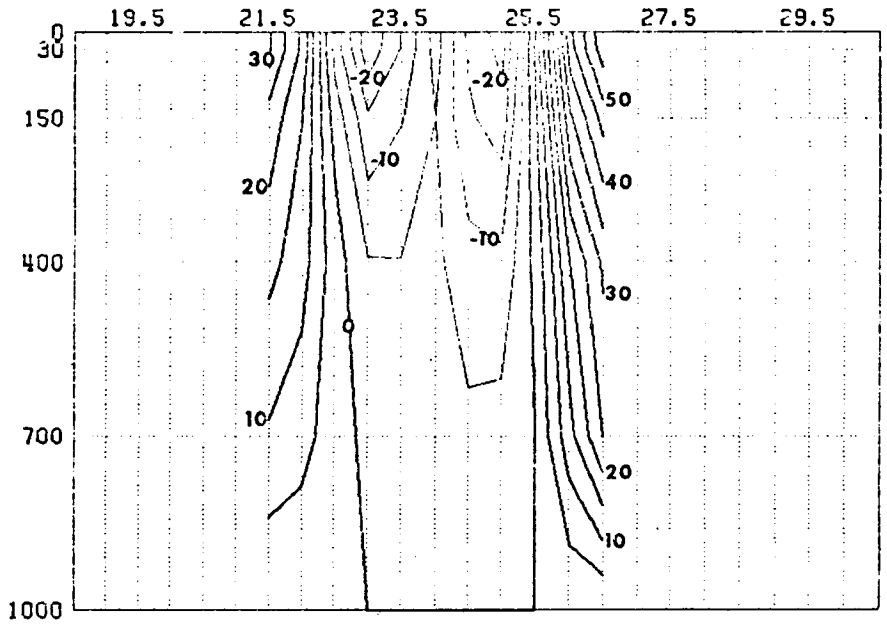

NOVEMBER

N-S CROSS SECTION FOR U COMPONENT OF GEOSTROPHIC VELOCITY AT LONGITUDE 86.5. VELOCITIES ARE COMPUTED RELATIVE TO 1000 M LEVEL. HEAVY LINES DENOTE EAST VELOCITY. THE CONTOUR INTERVAL IS 5.0 CM/S.

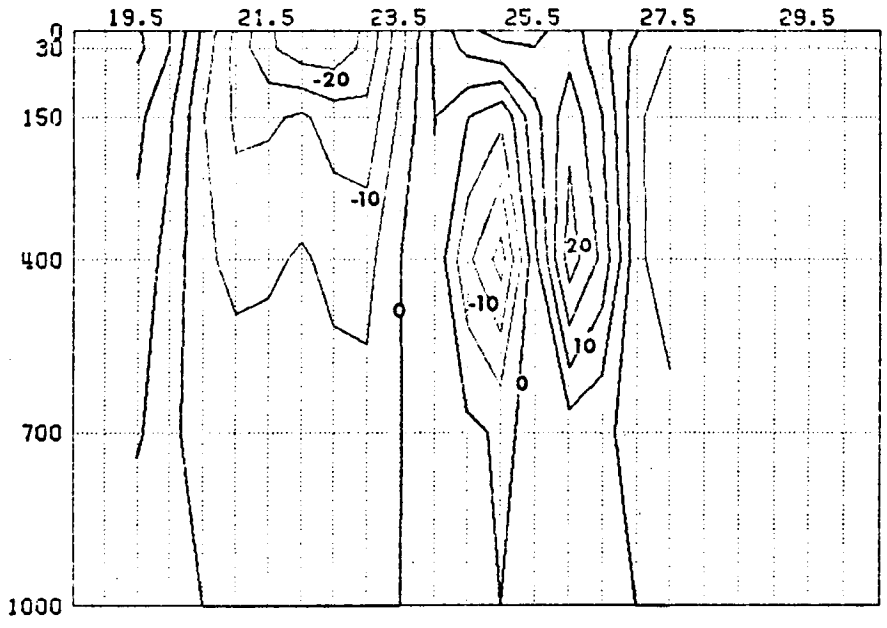

NOVEMBER

N-S CROSS SECTION FOR U COMPONENT OF GEOSTROPHIC VELOCITY AT LONGITUDE 94.5. VELOCITIES ARE COMPUTED RELATIVE TO 1000 M LEVEL. HEAVY LINES DENOTE EAST VELOCITY. THE CONTOUR INTERVAL IS 5.0 CM/S.

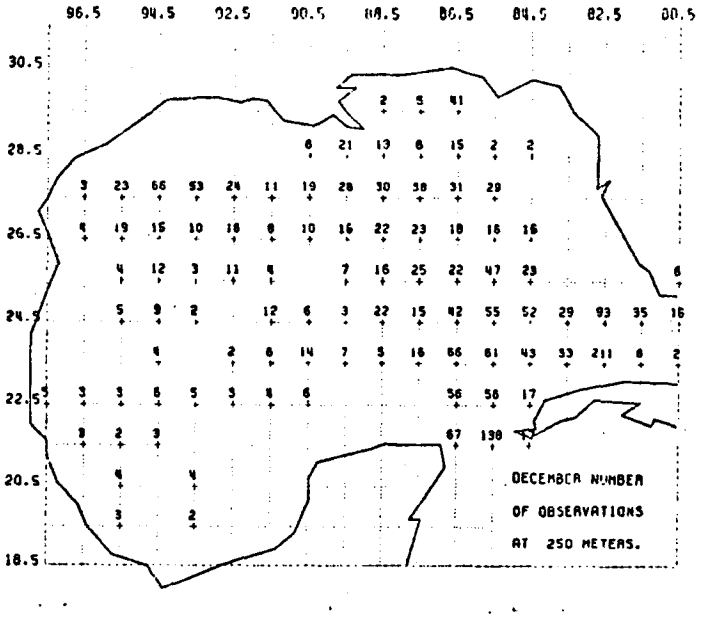

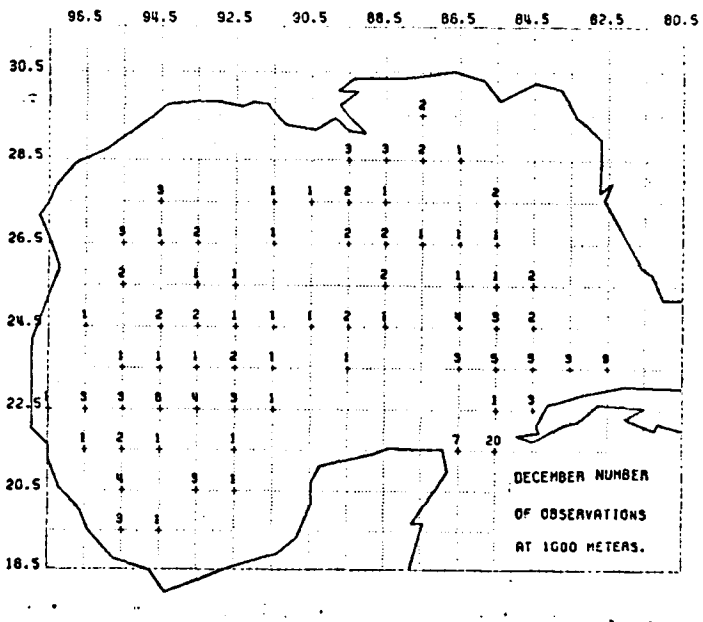

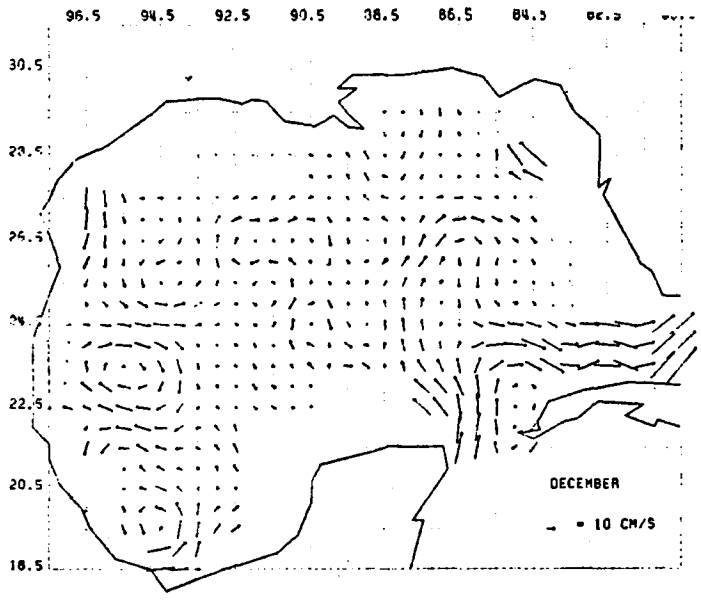

DECEMBER
GEOSTROPHIC VELOCITIES AT A DEPTH OF .0 METERS.
VELOCITIES ARE COMPUTED RELATIVE TO THE 250.0 M LEVEL.

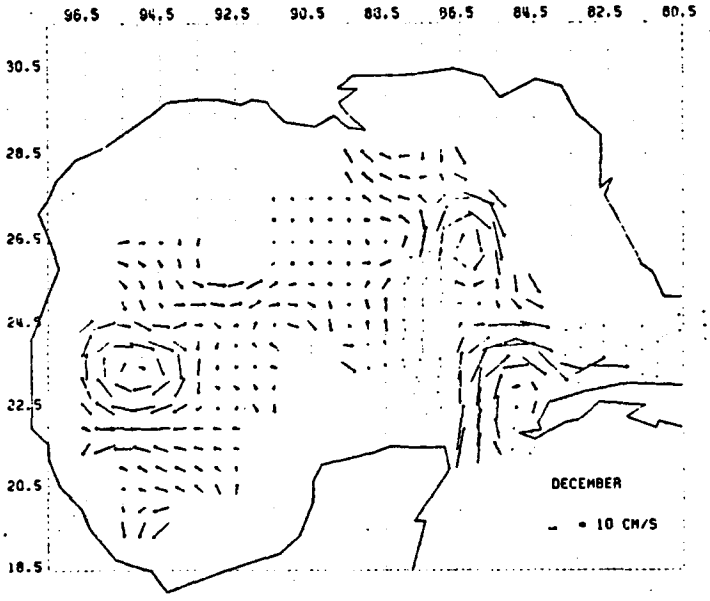

DECEMBER
GEOSTROPHIC VELOCITIES AT A DEPTH OF .0 METERS.
VELOCITIES ARE COMPUTED RELATIVE TO THE1000.0 M LEVEL.

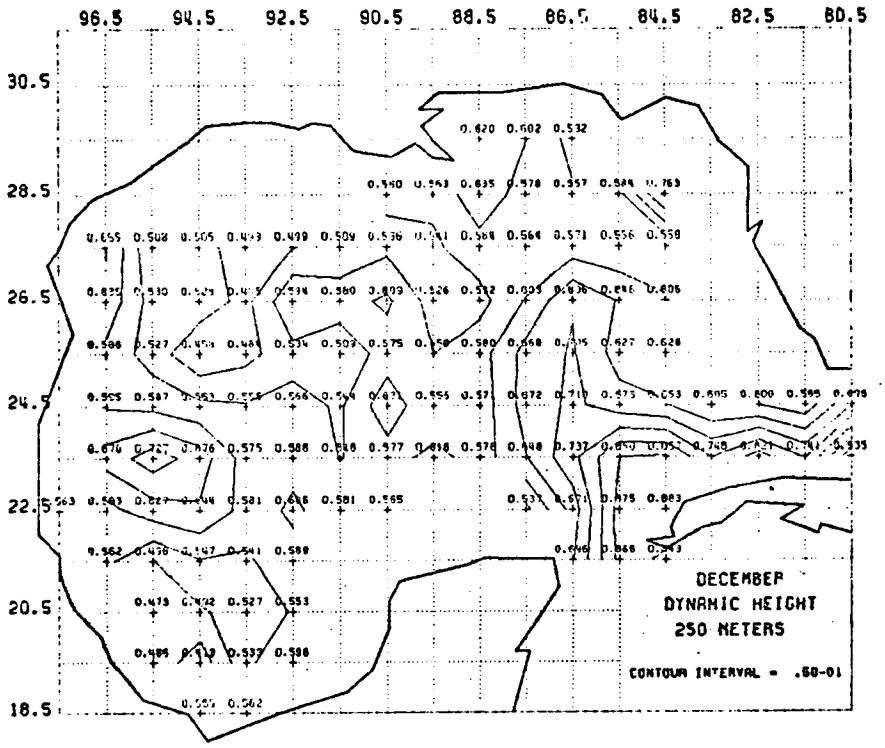
96.5
94.5
92.5
90.5
88.5
86.5
84.5
82.5
80.5
30.5
28.5
26.5
24.5
22.5
20.5
18.5
DECEMBER
DYNAMIC HEIGHT
250 METERS
CONTOUR INTERVAL = .60-01

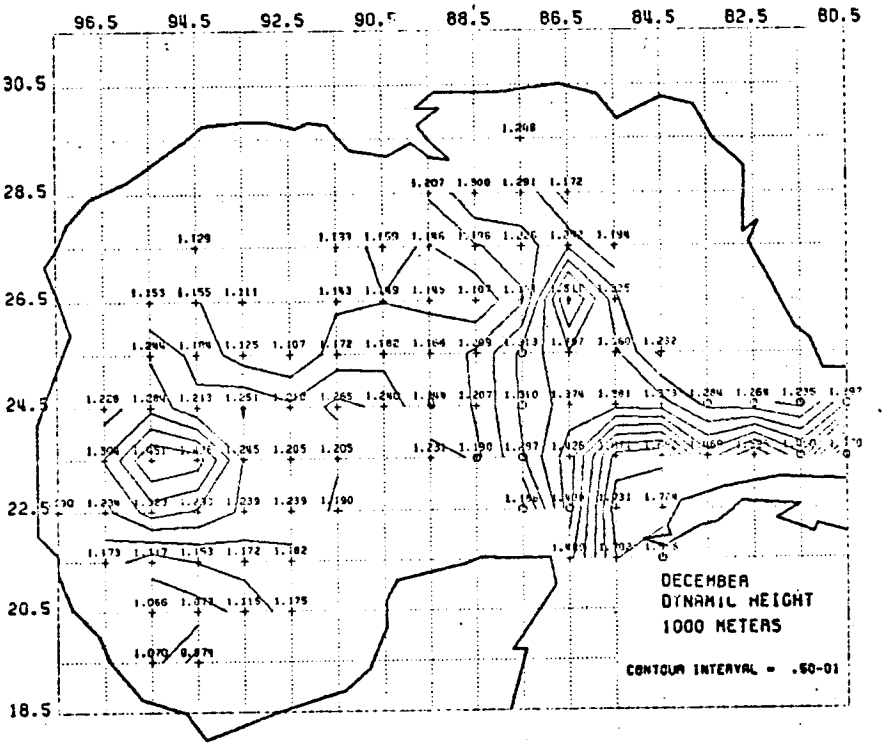
96.5
94.5
92.5
88.5
86.5
84.5
82.5
80.5
30.5
28.5
26.5
24.5
22.5
20.5
18.5
DECEMBER
DYNAMIC HEIGHT
1000 METERS
CONTOUR INTERVAL = .60-01

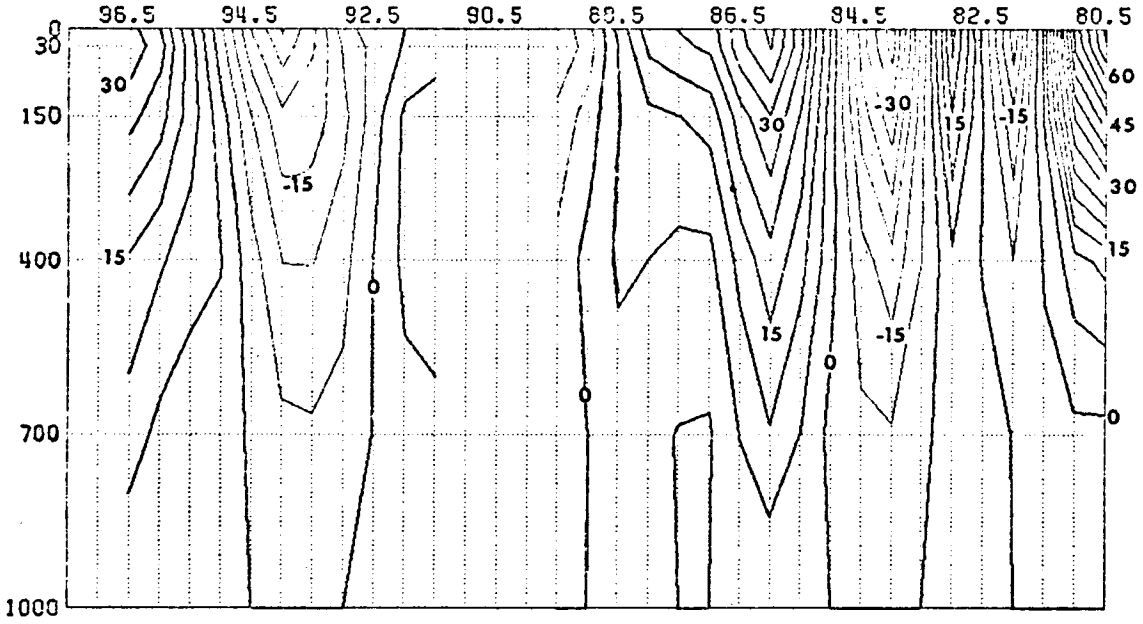

DECEMBER

E-W CROSS SECTION FOR V COMPONENT OF GEOSTROPHIC VELOCITY AT LATITUDE 23.5. VELOCITIES ARE COMPUTED RELATIVE TO 1000 M LEVEL. HEAVY LINES DENOTE NORTH VELOCITY. THE CONTOUR INTERVAL IS 5.0 CM/S.

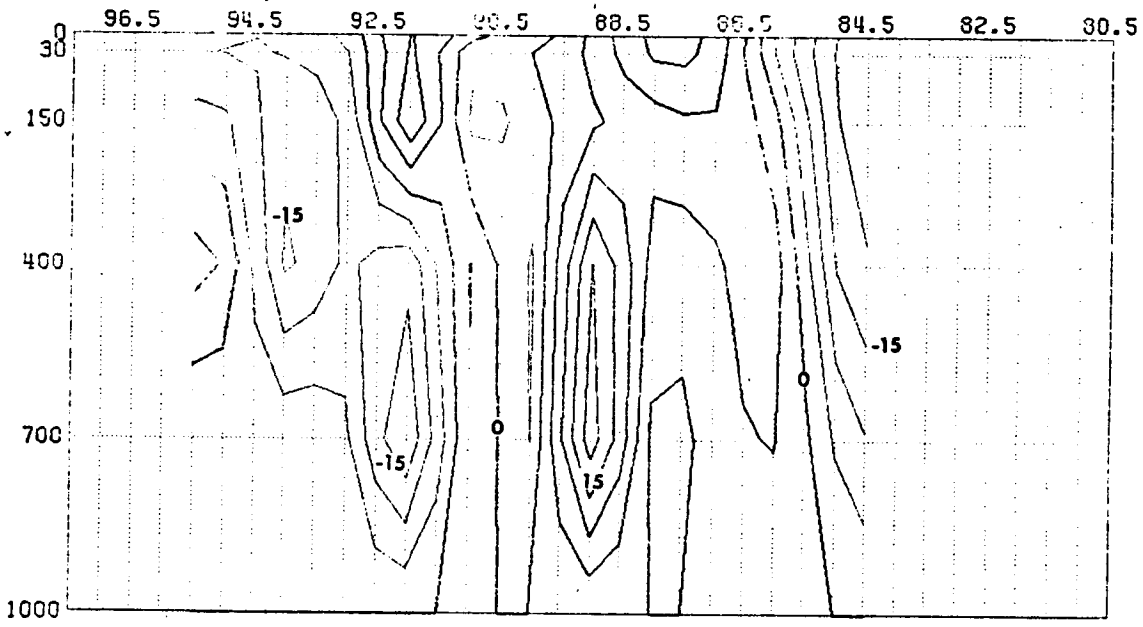

DECEMBER

E-W CROSS SECTION FOR V COMPONENT OF GEOSTROPHIC VELOCITY AT LATITUDE 25.5. VELOCITIES ARE COMPUTED RELATIVE TO 1000 M LEVEL. HEAVY LINES DENOTE NORTH VELOCITY. THE CONTOUR INTERVAL IS 5.0 CM/S.

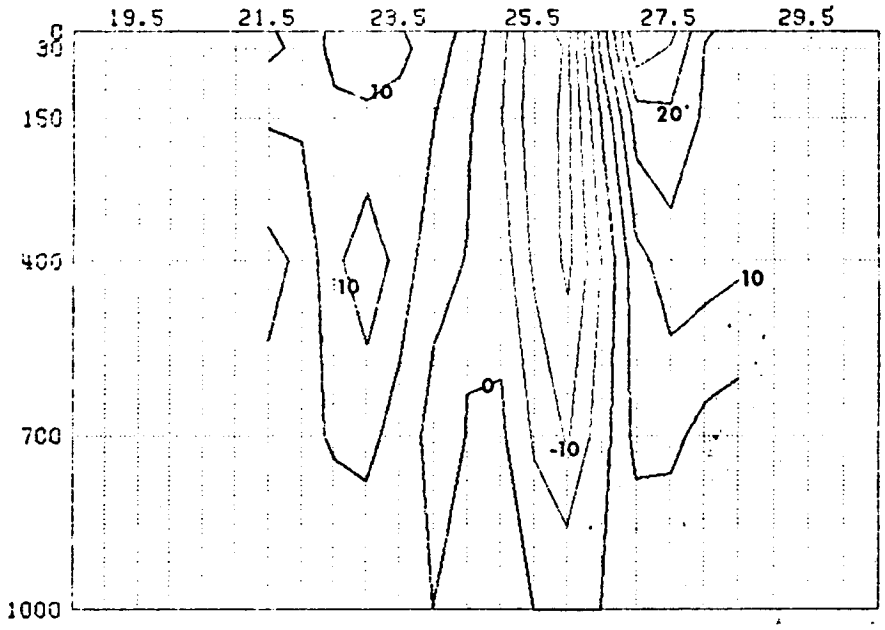

DECEMBER

N-S CROSS SECTION FOR U COMPONENT OF GEOSTROPHIC VELOCITY AT LONGITUDE 86.5. VELOCITIES ARE COMPUTED RELATIVE TO 1000 M LEVEL. HEAVY LINES DENOTE EAST VELOCITY. THE CONTOUR INTERVAL IS 5.0 CM/S.

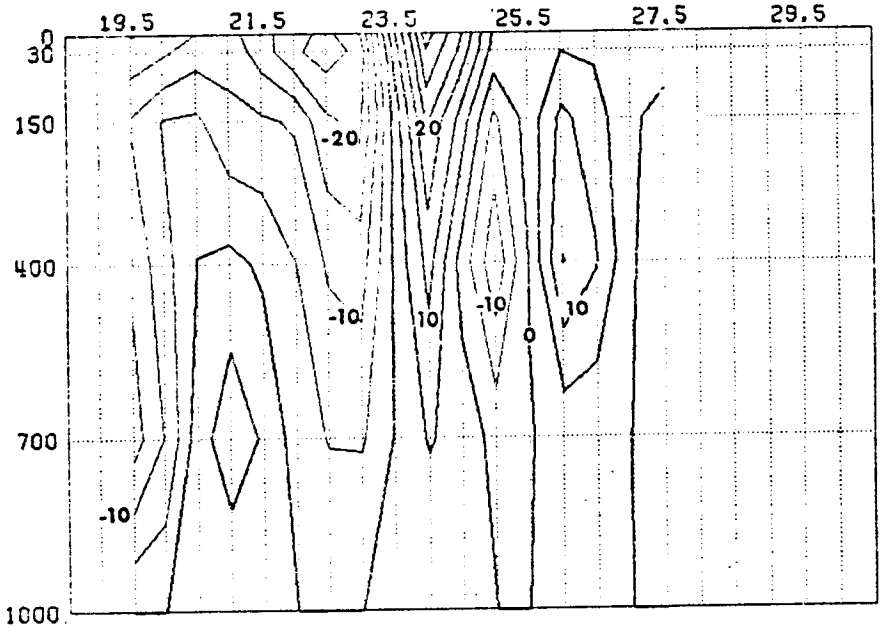

DECEMBER

N-S CROSS SECTION FOR U COMPONENT OF GEOSTROPHIC VELOCITY AT LONGITUDE 86.5. VELOCITIES ARE COMPUTED RELATIVE TO 1000 M LEVEL. HEAVY LINES DENOTE EAST VELOCITY. THE CONTOUR INTERVAL IS 5.0 CM/S.

The Department of the Interior Mission

As the Nation's principal conservation agency, the Department of the Interior has responsibility for most of our nationally owned public lands and natural resources. This includes fostering sound use of our land and water resources; protecting our fish, wildlife, and biological diversity; preserving the environmental and cultural values of our national parks and historical places; and providing for the enjoyment of life through outdoor recreation. The Department assesses our energy and mineral resources and works to ensure that their development is in the best interests of all our people by encouraging stewardship and citizen participation in their care. The Department also has a major responsibility for American Indian reservation communities and for people who live in island territories under U.S. administration.

The Minerals Management Service Mission

As a bureau of the Department of the Interior, the Minerals Management Service's (MMS) primary responsibilities are to manage the mineral resources located on the Nation's Outer Continental Shelf (OCS), collect revenue from the Federal OCS and onshore Federal and Indian lands, and distribute those revenues.

Moreover, in working to meet its responsibilities, the **Offshore Minerals Management Program** administers the OCS competitive leasing program and oversees the safe and environmentally sound exploration and production of our Nation's offshore natural gas, oil and other mineral resources. The MMS **Minerals Revenue Management** meets its responsibilities by ensuring the efficient, timely and accurate collection and disbursement of revenue from mineral leasing and production due to Indian tribes and allottees, States and the U.S. Treasury.

The MMS strives to fulfill its responsibilities through the general guiding principles of: (1) being responsive to the public's concerns and interests by maintaining a dialogue with all potentially affected parties and (2) carrying out its programs with an emphasis on working to enhance the quality of life for all Americans by lending MMS assistance and expertise to economic development and environmental protection.